DTE Hydrology

Final Report

Deliverable D7.1

ESA Contract 4000129870/19/I-NB

Project reference: DTE Hydrology_D7.1

Issue: 2.0

16/03/22

This page has been intentionally left blank

Change Record

Date	Issue	Section	Page	Comment
16/03/22	2.0			Final version

Control Document

Process	Name	Date
Written by:	Luca Brocca, Christian Massari, Angelica Tarpanelli, Luca Ciabatta, Jacopo Dari and Sara Modanesi (CNR-IRPI), Lorenzo Alfieri, Francesco Avanzi, Fabio Delogu and Simone Gabellani (CIMA), Dominik Rains and Diego Miralles (UGent), Mariette Vreugdenhil, Wolfgang Wagner and Raphael Quast (TUWien), Alessio Domeneghetti (UNIBO), Christian Briese, Philipp Stranner and Sean Hoyal (EODC).	16/03/2022
Checked by	Luca Brocca (CNR-IRPI)	16/03/2022

	Signature	Date
For DTE Hydrology team	Luca Brocca	16/03/2022

Table of contents

4D DTE Hydrology underlying data reconstruction

1. Introduction

1.1. The DTE Hydrology Project

The objective of DTE Hydrology is to develop and demonstrate a prototype of Digital Twin Earth with focus on water cycle and hydrological processes and their impacts. In DTE Hydrology we aim to highlight the huge potential of high-resolution ESA satellite products for describing the water cycle, for predicting hydrology extremes (floods, landslides and drought) and for monitoring and managing water resources.

The activity comprises four sequential steps: 1) building the 4D DTE Hydrology dataset, a high resolution (1 km, sub-daily, 2015-2019) EO-based dataset, also integrating in situ observations, 2) develop a high resolution modelling system ingesting the 4D DTE Hydrology dataset and able to provide a 4D reconstruction of the water cycle, 3) integrating the modelling system in the cloud-based DTE Hydrology simulation and visualization tool, and 4) exploiting the DTE Hydrology tool to develop user-oriented case studies focusing on flood and landslide risk, and water resources management.

The area of focus of DTE Hydrology is the Po River Basin (northern Italy). In this area high quality ground observations are available, which are useful to calibrate and test the modelling system. Floods and landslides occur in the area due to the complex topography and meteorological conditions. The large agricultural area in the Po River Valley ("Pianura Padana") makes water resources management fundamental, as crop production is largely dependent on rainfall and on water availability from the Po River.

DTE Hydrology builds on the expertise of the consortium members. Within the project EO datasets of rainfall, soil moisture, evaporation, river discharge, snow depth and land cover will be used. Soil moisture, rainfall, snow depth and evaporation datasets are provided by partners with well-established algorithms from satellite observations, TU Wien, CNR-IRPI, CIMA and UGent respectively. Expertise in hydrological and hydraulic modelling at high resolution is brought in by CNR-IRPI, CIMA and UNIBO. High performance computing is pivotal in DTE Hydrology and is managed and hosted by EODC. Outreach and visualization of the project outcomes is done by CNR-IRPI, CIMA, EODC and UNIBO.

1.2. Scope of this Report

This report provides the first technical document of DTE Hydrology and focuses on the EO-based dataset. For each dataset used in DTE Hydrology an overview of the algorithmic developments and data format is described. All the products have been stored in the DTE Hydrology data repository that can be accessed from the project website at https://osf.io/yh8uv/.

1.3. Applicable Documents

Not available

1.4. Reference Documents

RD-01 DTE Hydrology Technical Proposal - V1.0

1.5. Document Organisation

The document is organized according to variables, where each variable comprises one section: Section 2 - Rainfall, Section 3 - Soil moisture, Section 4: Evaporation, Section 5 - River discharge, Section 6 - Snow Depth, Section 7 - Land cover and Section 8 - Irrigation. The sections are subdivided in subsections describing the "Algorithm baseline and DTE Hydrology improvements" and "Product description".

2. Rainfall

The accuracy of measurements is increasingly becoming a factor of major importance in all applications of meteorology and hydrology, whose recent advances showed the need for a better precision in real-time measurement of precipitation, for example, for operational river flow and flash flood forecasting.

Precipitation is a highly variable atmospheric variable and this makes it difficult to provide accurate spatial and quantitative description of rainfall. Rain gauges may provide good local quantitative rainfall estimates but can lack an accurate description of the rainfall spatial distribution (SEVRUK, 2002) Weather radars are directly sensitive to precipitation elements (rain drops) and hence are a valuable tool in precipitation observation. However, their application for accurate precipitation estimation with good spatial description is hampered by technical problems (absorption of the radar signal in precipitation elements, calibration difficulties, the formation or evaporation of precipitation below the radar beam. Radar provides better spatial (although biased) representation than a rain gauge network, but a much poorer quantitative estimate (Zrnic,1999). Over the past three decades the estimation of rainfall from satellites has seen considerable improvements. The Global Precipitation Measurement (GPM) mission (HOU ET AL., 2014), launched by NASA and JAXA (Japan Aerospace Exploration Agency) in coordination with the Goddard Earth Sciences Data and Information Services Center (GES DISC) introduced a new concept for rainfall retrieval based on a multi-sensor integration. Within GPM, multiple observations from different instruments (microwaves and infrared) are intercalibrated, merged and interpolated with the GPM Combined Core Instrument product to produce half-hourly precipitation estimates on a 0.1∘ regular grid over the 60∘ N–S domain through the Integrated Multi-Satellite Retrievals for GPM (IMERG; HUFFMAN ET AL., 2018).

Recent studies have also proposed to use satellite soil moisture observations for correcting SPPs (BROCCA ET AL. 2014, MASSARI ET AL. 2020). The underlying idea is that soil moisture can be used as a trace of precipitation, as after a rain event it can persist from a few hours to several days. In other words, soil moisture is informative of the amount of water stored in the soil after a rainfall event, which can be exploited to retrieve information on the fallen precipitation. On this basis, the SM2RAIN method developed by Brocca et al. (2014) inverts the soil water budget equation and uses two consecutive soil moisture measurements for estimating the precipitation fallen within the interval between two satellite overpasses. Based on soil moisture, SM2RAIN rainfall estimates can exploit high-resolution SAR observations derived from Sentinel-1 satellites to provide satellite-based rainfall at 1 km spatial resolution (never achieved before).

In summary, direct and indirect measurements of precipitation also cover a range of scales, from point raingauge observations to spatially aggregated radar and satellite observations. Available data sources tend to trade off accuracy and spatial coverage. Rain gauges and radar provide the best description of actual rainfall but have the most limited coverage. Satellite-based rainfall are normally less accurate especially over challenging areas but provide broad and continuous coverage as well as precious information of the rainfall spatial distribution at the cost of a coarse spatial resolution at least with coarse scale sensors.

Moreover, the type of measurements deserving greater credibility depends on many factors which span from the land cover conditions, type of storm, rain gauge spatial distribution, topography etc… Since each type of rainfall measurements technique has distinct advantages and limitations, it is reasonable to combine different types of measurements so as to take maximum advantage of all available sources of information.

2.1. Algorithm baseline and DTE Hydrology improvements

The algorithm used within DTE Hydrology merges the information from three basic independent sources of precipitation estimates: rain gauges, meteorological radar and satellite observations derived from the classical state-of-the-art products (i.e., GPM IMERG) and from soil moisture (i.e., SM2RAIN applied to ASCAT and Sentinel-1). Each estimate is affected by biases and by errors of different sources and nature. Given the independent nature of the sources of errors and their different spatial and temporal resolution we will rely on different techniques, namely, i) the Triple Collocation Analysis for error characterization (MASSARI ET AL. 2017, CHEN ET AL. 2021), and ii) the Bayesian combination (MAZZETTI AND TODINI, 2004) that allows for the substantial elimination of the bias and the reduction of the variance of the estimation errors, thus increasing the reliability of the precipitation estimates. The Bayesian combination was applied here only to the combination of an already merged rainfall-radar product known as the rainfall-radar product is MCM (Modified Conditional Merging) and satellite-based rainfall estimates derived from IMERG-GPM Late Run and SM2RAIN-ASCAT (next release will incorporate explicitly a 1km product obtained from the application of SM2RAIN to Sentinel-1 soil moisture). While it is still possible to rely upon Bayesian combination for merging radar and rain gauges, the existence of a very good merged rainfall radar product, allowed us to skip this step.

In particular we use the following scheme (see Figure 1):

1) we upscaled all products at the 10 km-scale and daily and applied Triple Collocation analysis to provide information about the product error variances.
2) We used these variances to merge rainfall estimates derived from SM2RAIN-ASCAT and GPM-IMERG-rainfall observations at daily time scale and 10 km sampling.
3) The obtained product was then downscaled via a Kalman Smoother applied in time to hourly time scale as to obtain sub-daily rainfall merged IMERG-LR-SM2RAIN-ASCAT at 10 km
4) We then merged this product via the Bayesian combination with MCM transferring the information at the 10 km scale to the 1 km scale.

In the following we provide the main technical details of Triple Collocation analysis and notion of Bayesian combination. For further details the reader is referred to the relevant publications.

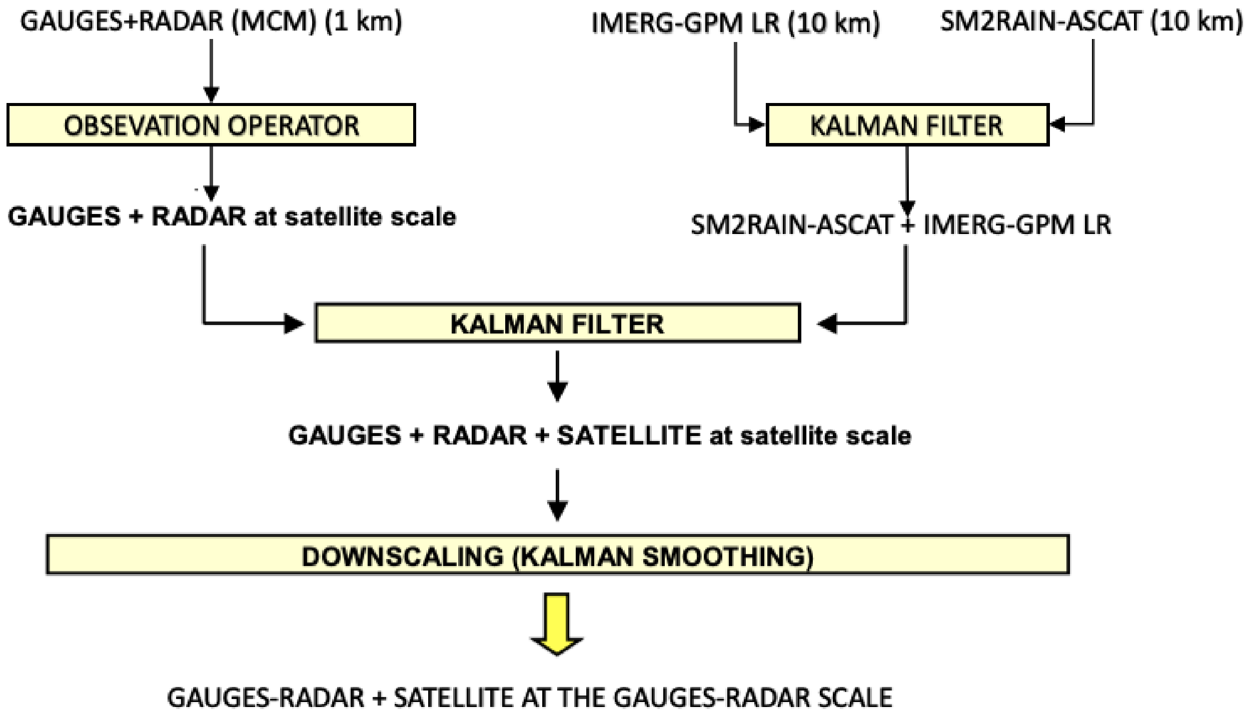

Figure 1: scheme for the merging of the Gauges+Radar with satellite rainfall estimates from GPM Early Run and SM2RAIN-ASCAT.

2.1.1. Triple Collocation analysis

Triple collocation (TC) method permits the assessment of uncertainties of three different products against an unknown true reference. Here a brief explanation of the theory behind the method is presented. For further information about the technique applied to the rainfall estimates, the reader is referred to MASSARI ET AL. (2017) and FAN ET AL. (2021).

Each measure related to a quantity is characterized by both a random and a systematic error:

$$X = \alpha_X + \beta_X\theta + \varepsilon_X$$

where θ is the measure, X is the unknown truth, ε_X the random error and α_X and β_X are the additive and multiplicative component of the systematic error, respectively. Taking into consideration three different datasets whose errors are uncorrelated, the random error of each dataset should be Gaussian distributed with zero mean. The error variance of each dataset can therefore be written as (MCCOLL ET AL., 2014):

$$\sigma_\varepsilon = \begin{bmatrix} \sqrt{Q_{11} - {Q_{12}Q_{13}}/{Q_{23}}} \\ \sqrt{Q_{22} - {Q_{12}Q_{23}}/{Q_{13}}} \\ \sqrt{Q_{33} - {Q_{13}Q_{23}}/{Q_{12}}} \end{bmatrix}$$

where Q_{ij} is the covariance between the dataset *i* and *j*.

2.1.2. Bayesian combination

From a Bayesian point of view, the algorithm of the gauges plus radar and satellite Bayesian combination can be seen as a data assimilation algorithm. Rainfall measurements provided by the different measuring devices, each one with its own particular dynamics and error characteristics, supply information that can be combined on the basis of the local relative uncertainty. If the characteristics of the noise are known (in this particular case we used information derived from Triple Collocation analysis), every source of rainfall will benefit from the merging with the other. For this reason, a combination involving rain gauges-radar and satellite measurements can provide the best information on rainfall fields. Let us assume that our precipitation measurement network covering space Ω consists of two rainfall sources: a rain gauge plus radar product and the satellite (Figure 2). The first problem to be solved is to make comparable the two estimates. This is done by building an observation operator that upscale raingauge+radar information to the satellite scale. The two estimates are then comparable and it is reasonable to assume that they are independent estimates of the same unknown quantity and Kalman Filter approach is taken to find the a posteriori estimates by combining the a priori estimates provided by the radar plus rain gages and the satellite rainfall estimates in a Bayesian framework.

The up-scaling and the Bayesian combination with satellite estimates lead to an optimal rainfall estimate at the satellite scale. As the spatial resolution of the satellite pixels is too coarse for hydrological applications, thus it is necessary to move the results of the Bayesian combination from the satellite scale to the raingauge+radar scale. The coarse-to-fine step, namely the downscaling, is performed through the application of a Kalman fixed-interval smoother (Chen and Yu, 2003).

For further details on the equations the reader is referred to Mazzetti and Todini (2004).

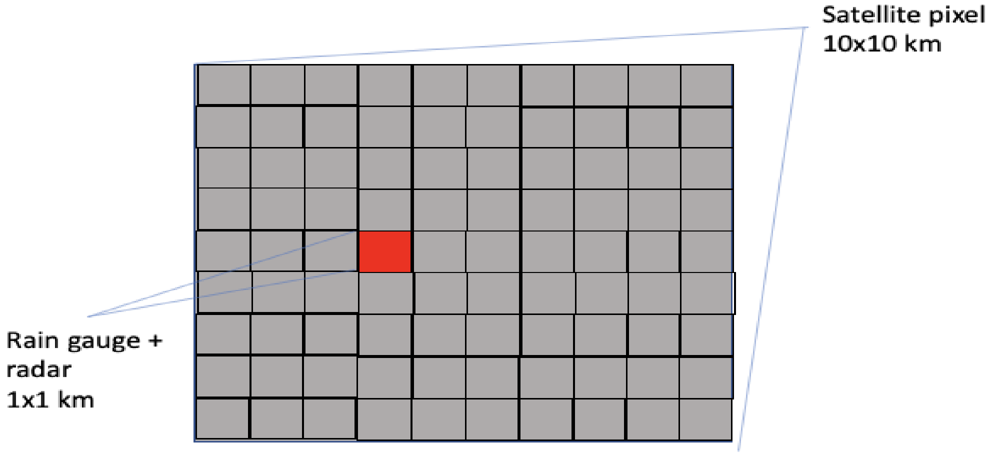

Figure 2: satellite and radar plus rain gage grids comparison within the domani Ω.

2.2.Product description

Based on the methods described above we have produced a demo version of two hourly-based products:

- A 10-km spatially-sampled version based on the combination of SM2RAIN-ASCAT with GPM IMERG-Late Run;
- A 1-km spatially-sampled version based on the combination of SM2RAIN-ASCAT, GPM IMERG-Late Run and radar plus rain gauges product (MCM).

The maps of the yearly average rainfall for the period 2016-2019 are shown below:

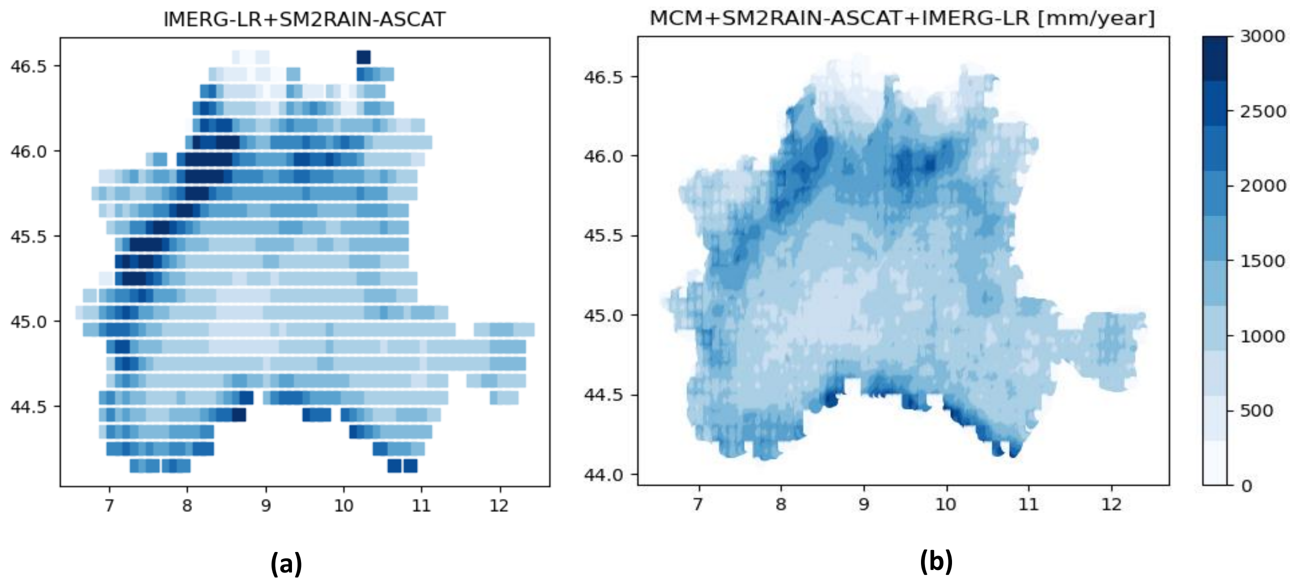

Figure 3: Annual average rainfall obtained by (a) a 10-km spatially-sampled version based on the combination of SM2RAIN-ASCAT with GPM IMERG-LR and (b) a 1-km spatially-sampled version based on the combination of SM2RAIN-ASCAT, GPM IMERG-LR and Radar plus rain gauges product (MCM).

3. Evaporation

Terrestrial evaporation is an essential component of the climate system that links water and energy cycles. By doing so, it regulates the interaction between land and atmosphere through multiple feedbacks on climate, shaping local precipitation, cloudiness and temperature. Bearing in mind this crucial importance, the monitoring of continental-to-global magnitude and variability of evaporation has been given a lot of attention over the past years. However, hydrological and agricultural applications, from catchment-to-regional scales, require estimates of terrestrial evaporation at high spatial resolutions of a maximum one kilometer. In situ measurements do not meet these requirements due to their sparse distribution and point nature, and current large-scale satellite data-based products do not have the adequate high spatial resolution.

3.1. Algorithm baseline and DTE Hydrology improvements

The Global Land Evaporation Amsterdam Model (GLEAM) is a state-of-art method dedicated to the retrieval of terrestrial evaporation and all its components (i.e. transpiration, bare soil evaporation and interception loss), together with root-zone soil moisture – see MIRALLES ET AL (2011A), MARTENS ET AL. (2017). GLEAM combines global satellite observations of meteorological variables (precipitation, near-surface net radiation and air temperature) and surface characteristics (soil and vegetation water content and snow water equivalents) that are informative of the evaporation process. Since its publication in 2011, the model has been widely applied at coarse resolution to analyse trends in the water cycle, study land–atmospheric feedbacks, and benchmark climate models. Advantages of GLEAM over analogous methods are the explicit estimation of root-zone soil moisture data, and the detailed calculation of rainfall interception (MARTENS ET AL., 2017). Traditionally used for global studies, GLEAM is in the present being adapted to work at higher resolutions (e.g. MARTENS ET AL., 2018).

Figure 4 shows a schematic overview of the main GLEAM components, i.e. the potential evaporation, interception, soil moisture and stress modules, from which actual evaporation is computed.

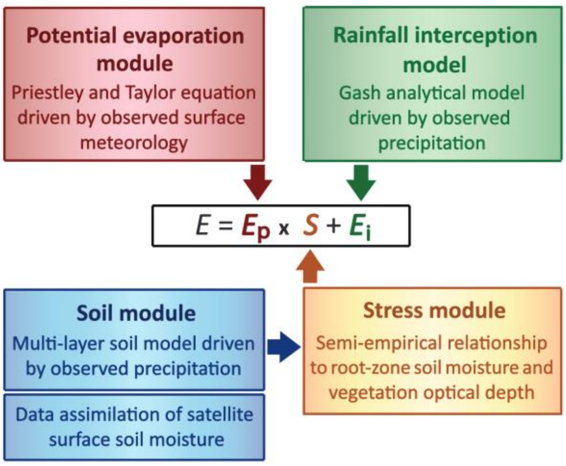

Figure 4: Schematic overview of the main components of GLEAM.

DTE Hydrology is an ideal test case for the new Python implementation of GLEAM, which contains numerous improvements in terms of code base and performance that enable the efficient generation of high-resolution estimates across large regions such as the Po basin. Furthermore, the updated GLEAM version includes a number of algorithmic improvements and optimisations.

3.2.Product description

GLEAM output for the Po basin is provided on a 0.01°x0.01° grid for pixel averaged variables as well per vegetation fraction. Each pixel is populated by a certain percentage of bare soil, herbaceous vegetation and tall vegetation, for which the calculations are performed separately. GLEAM variables of interest within DTE Hydrology are actual evaporation as well as potential evaporation, both over land as well as for lakes. GLEAM requires a number of input variables which have a large impact on the quality and spatial variability of the output. For the land surface representation of the initial Po basin we used MOD44B continuous vegetation fields and 3D Soil Hydraulic Database of Europe at 1 km (**Tóth et al., 2017**). For the time being, downscaled ERA-5 atmospheric forcing is used to drive the model, including precipitation, net radiation, air temperature. Vegetation Optical Depth from microwave observations acts as a phenology descriptor. For the purpose of consistency and increased accuracy, the products from DTE Hydrology will be incorporated in future dataset updates, i.e. high-resolution precipitation input, soil moisture (to be assimilated), snow depth and land use, making the ERA-5 forcings no longer necessary.

4. Soil Moisture

Soil moisture plays a crucial role in the water cycle, controlling evaporation, infiltration and runoff. Because of this, and its role in the carbon and energy cycles, it has been named an essential climate variable and of great interest in the last decades. Highly variable over space and time, remote sensing of soil moisture is the most reliable method to obtain spatial and temporal resolution and coverage needed for hydrological applications. Since the 1970's radiometers observe Earth's surface and global soil moisture products are available going back to 1978 (**Dorigo et al., 2017**). Since 2001, active microwave systems, such as scatterometers on-board ERS and Metop ASCAT provide backscatter data that can be used to retrieve soil moisture operationally (e.g. **Wagner et al., 1999**). In the last decades, Synthetic Aperture Radar systems have gained traction as a source of data for soil moisture retrieval. Although the drawback was often the low temporal resolution. ESA's Sentinel-1 satellite series provides backscatter observations with a temporal resolution of 1-4 days over Europe. However, with an observation every 4 days, temporal resolution over some areas is still relatively low to capture highly dynamics processes which drive soil moisture. Therefore, coarse scale resolution satellites, with the benefit of high temporal resolution in the order of daily observations, can still provide valuable information on changes in soil moisture.

For DTE Hydrology the strength of both high spatial resolution EO data and high temporal resolution EO data is used to provide two soil moisture products:

- Surface soil moisture from Sentinel-1 observations
- Soil Water Index from Sentinel-1 and Metop ASCAT observations.

Both products are described in detail in the following sections.

4.1.RT1

4.1.1. Algorithm baseline and DTE Hydrology improvements

The RT1 model (QUAST ET AL. 2019) is based on a first-order expansion of the radiative transfer equation, describing the scattering behaviour of a rough soil surface covered by a vegetation layer. Using the assumption that only single-scattering events within the vegetation-canopy add a significant contribution to the measured signal, the backscattering-coefficient σ^0can be expanded as:

$$\sigma^0 = \gamma^2 \sigma^0{}_{bare\ soil} + \sigma^0{}_{vegetation} + \sigma^0{}_{interaction}$$

Where $\sigma^0{}_{bare\ soil}$is the contribution from the bare soil surface, $\gamma^2 = e^{-2\tau/cos(\theta)}$ is the two-way attenuation coefficient $\sigma^0{}_{vegetation}$is the direct-scattering contribution from the vegetation-layer and $\sigma^0{}_{interaction}$represents radiation that has been scattered once within the vegetation-layer and once by the soil-surface (or vice-versa). In order to describe a large variety of soil- and vegetation characteristics while maintaining a reasonable mathematical complexity suitable for processing large amounts of data, the scattering behaviour of both the soil-surface and the vegetation-layer is described by means of parametric scattering distribution functions.

The parameters of the selected functional descriptions as well as the radiative-transfer parameters “single-scattering albedo” ω and “optical depth” $\tau$are evaluated by utilizing a non-linear least squares fitting procedure that attempts to optimize the difference between (incidence-angle dependent) measured- and modelled σ^0over the whole timeseries.

The number of parameters (e.g. the complexity in describing the properties of soil- and vegetation) that have to be evaluated for each pixel individually must be carefully selected with respect to the utilized σ^0data to avoid ambiguities in the obtained parametrizations. Furthermore, the model complexity must be chosen in conjunction with the available computational resources to ensure achievable processing times.

The primary challenge within the DTE Hydrology project therefore was the adaption of existing RT1 algorithms to cope with the large amounts of data (~268 000 pixels over a time-period from 2016-2019) as well as the adjustments of retrieval methods and predefined model-parameters to deal with the subtleties of Sentinel-1 data characteristics (coarse temporal sampling ~6 days, only one incidence-angle per observation, inhomogeneous coverage due to orbit geometries, etc.).

Since only a single measurement is available for each timestamp, an unambiguous separation of long-term seasonalities of soil- and vegetation scattering contributions from the co-polarized σ^0 data alone is not directly possible. Therefore, the seasonality of the vegetation-coverage has been modelled by assuming a linear relationship between the “optical depth” τ and the Leaf Area Index (LAI) timeseries provided by ERA5-Land.

Due to the fact that the Sentinel-1 σ^0 data exhibits a bias with respect to individual satellite orbits that can not be fully accounted for via the modelled incidence-angle dependency of the RT1 model, an averaging procedure with respect to the satellite-orbits is applied to the final retrievals to reduce the high-frequency "sawtooth"-like soil-moisture variations that are introduced by the orbit-differences in σ^0 between two consecutive observations.

Figure 5 shows an example of the DTE Hydrology S1 RT1 hemispherical reflectance factor for the Po River Basin for August, 2018.

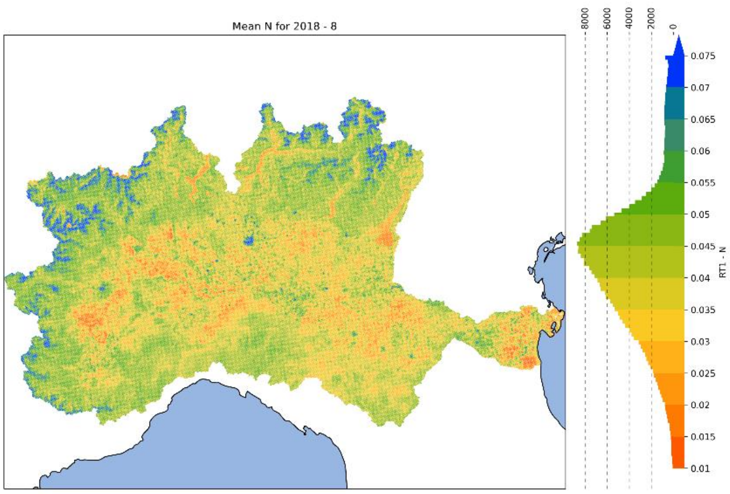

Figure 5: Hemispherical reflectance factor from the DTE Hydrology S1 RT1 product over the Po valley basin for August 2018.

4.1.2. Product description

The retrievals have been performed using the RT1 v1.3 python module [DOI: 10.5281/zenodo.4552262].

Results are provided as a single NetCDF file with the following characteristics:

Dimensions:

- date: (2088 unique entries ranging from 3.1.2016 to 30.12.2019
- ID: (281804 unique site-IDs) with the following naming-convention:

  {subgrid-id and spatial-sampling }_{ Equi7 tile ID }_{row}_{column}

Variables:

- x, y: Equi7Grid coordinates
- lat, lon: Latitude, Longitude
- N: RT1 (nadir) hemispherical reflectance factor (proportional to soil-moisture)
- Nmean: orbit-averaged RT1 (nadir) hemispherical reflectance factor
- Nmean_80D: orbit-averaged RT1 (nadir) hemispherical reflectance factor with 80 daily rolling mean removed

4.2. DIREX SCATSAR

4.2.1. Algorithm baseline and DTE Hydrology improvements

Root-zone soil moisture from EO data can be obtained through the so-called Soil Water Index approach. The SWI estimates the water content of the soil profile from the local history of the surface layer water content (obtained with EO). The approach is a simple two-layer water balance model consisting of the top layer (SL) and profile layer (PL). PL serves as a reservoir, which is affected only by the SL, which is connected to the atmosphere. Events fill the reservoir, with recent events having more impact, accounted for by the exponential weighting function over time. Infiltration time is controlled by the so-called T-value, with higher T-values representing deeper depths. The SWI is formulated as:

$$SWI_T\,(t_n) = \frac{\sum_i^n SSM(t_i)e^{\frac{-(t_n-t_i)}{T}}}{\sum_i^n e^{\frac{-(t_n-t_i)}{T}}}\; for\ t_i \leq t_n$$

where t_n is the observation time of the current SSM measurement and t_i are the observation times of the previous SSM measurements. All SSM observations prior to t_n are exponentially weighted, and the T-value controls the decrease of weight over time. An extensive description of SWI is given in ALBERGEL ET AL. (2008).

The DIREX SCATSAR Soil Water Index (SWI) product available in DTE Hydrology builds on the SCATSAR SWI product available through the Copernicus Global Land Service. Sentinel-1 surface soil moisture and ASCAT surface soil moisture are combined through the calculation of the Soil Water Index. The CGLS product is described in detail in BAUER-MARSCHALLINGER ET AL. (2018), but a short overview is given here.

The SCATSAR algorithm uses a fused data cube of ASCAT and Sentinel-1 SSM data and consists of two components, the offline parameter calculation, and the near-real-time SWI retrieval using incoming SSM and calculated parameters.

First data cubes are processed. Here, coarse spatial resolution ASCAT SSM is sampled to the EQUI7Grid at the spatial sampling of Sentinel-1, i.e. 500m. Oversampling is done using a radial basis interpolation using a “thin_plate”-function.

The offline parameters, matching parameters, weighting functions and correlation layer are calculated offline using a Sentinel-1 and ASCAT SSM data archive. The first parameters make sure systematic biases between the Sentinel-1 and ASCAT are removed using CDF matching. The weighting functions account for the quality of the ASCAT and Sentinel-1 data, currently giving more weight to the ASCAT product. The correlation layer makes sure SWI is only calculated when ASCAT and Sentinel-1 SSM describe the same SSM process, i.e. where the correlation between the coarse spatial resolution ASCAT and fine spatial resolution Sentinel-1 is high.

In the second component the SWI is calculated. The oversampled ASCAT data is matched to the Sentinel-1 SSM data using the CDF matching parameters. Then SWI is calculated using the Recursive Weighted Temporal Filtering method (ALBERGEL ET AL., 2008). The final SWI is using the correlation layer, calculated in the offline parameter generation.

Within DTE Hydrology two innovations within the production of high resolution SWI are made, related to the ASCAT SSM product. ASCAT SSM is detrended to account for increasing backscatter as a result of land cover change and increasing RFI. Furthermore, vegetation parameterization is improved as described by HAHN ET AL. (2020). The cross-over angles in the TU Wien change detection algorithm for Metop ASCAT (contained in the

WAter Retrieval Package WARP), control the strength of the vegetation correction, with lower cross over angles leading to stronger correction. The common cross over angles are 25 and 40 degrees, defined by WAGNER ET AL. (1999). PFEIL ET AL. (2019) and HAHN ET AL. (2020) revisited the cross-over angles, and found that cross-over angles of 10 and 30 degrees provided better soil moisture estimates over Austria. This was attributed to the stronger correction, which benefited the soil moisture, especially in spring and summer. For the DTE Hydrology SWI product, cross-over angles of 10 and 30 degrees are used.

Secondly, downscaling of the ASCAT SSM is not done using a radial basis interpolation but based on temporal stability concept. Since backscatter is linearly related to surface soil moisture, high-resolution Sentinel-1 backscatter data from a local high-resolution pixel is related to neighbouring 12.5 km pixels. This results in multiple correlation coefficients for each local pixel, providing information about directional dependencies. The correlation coefficients are then used to downscale coarse scale ASCAT surface soil moisture by calculating a weighted average from different directions for each local pixel.

Figure 6 shows an example of the DTE Hydrology DIREX SAR SWI (T=5) for the Po River Basin for August 1, 2018.

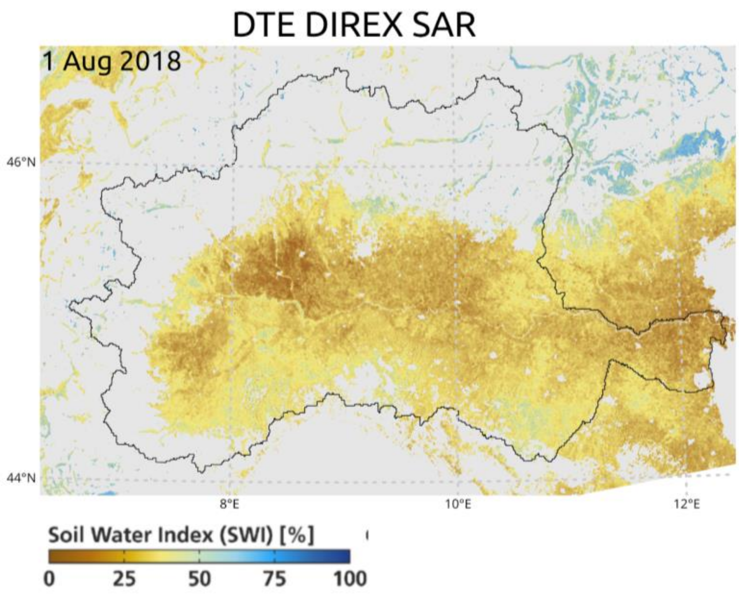

Figure 6: Soil Water Index from the DTE Hydrology DIREX SAR product over the Po valley basin for August 1st 2018.

4.2.2. Product description

The DIREX SCATSAR product is available at 500m sampling in the EQUI7Grid for two tiles covering the Po river basin. The projection can be adjusted to the needs in DTE Hydrology. Soil Water Index is provided for several T-values: 2, 5, 10, 15, 20, 40, 60 and 100. Data is stored per EQUI7 tile. Filename convention is as follows:

MYYYYMMDD_HHMMSS--_SWI-----_SCATSAR-55VV-_---_C0423_EU500M_E***N***T6.nc

<MYYYYMMDD> gives the processing line (Master or Development) and the temporal location of the file. YYYY, MM, DD, HH, MM and SS denote the year, the month, the day, the hour, the minutes and the seconds, respectively. Note that HHMMSS is always 0000 (0h UTC).

<E***N***T6> gives the EQUI7 tile number of the tile.

The products are provided as netCDF4 format with metadata according to the Climate and Forecast conventions the corresponding metadata file in XML format conforming to INSPIRE metadata guidelines.

Each netCDF4 data file contains the following variables:

- Three coordinate variables and associated dimensions:
  - Latitude: (lat) and longitude (lon)
  - Time
- A variable “crs” describing the grid mapping (coordinate reference system)
- Eight (8) SWI values, one per T-value: SWI_002 (for T=2), SWI_005 (T=5) and so on.
- Eight (8) Quality flags (QFLAG), also one per T-value: QFLAG_002, QGLAG_005 etc.

The netCDF files contain a number of metadata attributes at the global and variable level:

Attribute	Description	Example
conventions	Version of the CF-Conventions used	CF-1.6
copyright	Copyright notice, to be used when referring to the data source of this product in publications	TU Wien 2020
history	Describes the lineage	2020-12-19 -- SCATSAR-SWI NRT Production
long_name	Extended product name	Scatterometer - Synthetic Aperture Radar - Soil Water Index
orbit_type	Orbit type of the orbiting platform(s)	LEO
pixel_size	Size of a single pixel (in square)	500.0 metres
platform	Name(s) of the orbiting platform(s) used. One of “Metop A”, “Metop B” and “Metop A+B”	Metop A+B+C & Sentinel-1A+B
processing_level	Product processing level	L3
processing_mode	Processing mode used when generating the product. One of Near-Real Time, Consolidated, Offline or Reprocessing	Near Real Time
product_version	Version of the product (VM.m.r)	V1.0.1
sensor	Name(s) of the sensor(s) used	ASCAT + CSAR
source	The method of production of the original data	Derived from EO radar observations
time_coverage_start	Start date and time of the temporal coverage of the input data.	
title	A description of the contents of the file	SCATSAR-SWI NRT Product

Attribute	Description	Example
_FillValue	Single value used to represent missing or undefined data and to pre-fill memory space in case a nonwritten part of data is read back.	255
unit	Units of the variable's content, taken from Unidata'sudunits library	%
fill_value	Single value used to represent missing or undefined data and to pre-fill memory space in case a nonwritten part of data is read back.	255
missing_value	Single value used to represent missing or undefined data, for applications following older versions of the standards.	255
scale_factor	Multiplication factor for the variable's contents that must be applied in order to obtain the real values.	0.5
add_offset	Single value that must be added in order to obtain real values.	0
long_name	A descriptive name that indicates a variable's content. This name is not standardized.	Soil Water Index
Class	Dataset type	DATA
grid_mapping	Reference to the grid mapping variable	azimuthal_equidistant
coordinates	References the coordinate variables	time y x
valid_range	Smallest and largest values for the variable. Missing data is to be represented by one or several values outside of this range.	[0 200]

5. River discharge

5.1. Algorithm baseline and DTE Hydrology improvements

The river discharge product is derived by the integration of data from two satellite sensors: altimeters and multispectral sensor. Based on the traditional definition of river discharge as the product of river flow area and velocity, the two satellite sensors are used to define the two quantities, respectively. Once known the survey of the cross-section geometry, the flow area is calculated as a function of the water level derived by satellite altimetry, whereas the flow velocity, traditionally measured through specific instruments installed in-situ (current meter, Acoustic doppler current profiler, velocimeter), is here a proxy coming from the reflectance measured by the Near Infrared signal of the multispectral sensor (Tarpanelli et al., 2015). In the following, the two processes separately and the final algorithm for the river discharge estimation are described separately.

5.1.1. Algorithm baseline for altimetry processing

The method to construct water level time series from multi-mission altimetry data is here resumed:

- First, data from different satellite missions are processed to derive water levels with respect to the EGM 2008 geoid model, through the retracking correction based on a primary peak sub-waveform retracker (JAIN ET AL., 2015).
- The data over the river are masked out using the occurrence product from the Global Surface Water Explorer (PEKEL ET AL., 2016).
- A state space model is carried out to merge data from different satellite missions. Indeed, the altimetry missions cross the river at different locations and at different time. In order to obtain a higher temporal resolution of the water level time series (the repeat time of the satellite ranges from 10 days for the Jason and 35 days for SARAL/AltiKa), data from different missions must be combined. The model represents the water level as a function of time and distance, taking into account the topographic component and the amplitude of the water level that may vary along the river according to the river width and bathymetry profile. The approach guarantees a time series with a temporal resolution up to 3 days that can be efficiently used to reproduce water level time series also in medium sized basin (Nielsen et al., submitted).

The altimetry data from the following products are collected:

- Baseline-C/Baseline D Level 1b for Cryosat-2
- Baseline-3, LAN, Enhanced_measurement for Sentinel-3
- Geophysical Data Record (GDR) for Altika
- Cryosat-2 data are downloaded from ESA website (ftp://science-pds.cryosat.esa.int/) for the year 2016 -2019. Based on the available mode over the study areas, LRM, SAR and SARIn are collected and processed.
- Sentinel-3 data are downloaded from the scihub platform (https://scihub.copernicus.eu/) for the period 2016 – 2019.
- Altika data are downloaded from Aviso website (https://www.aviso.altimetry.fr/data/data-access/ftp.html) for the period 2016 – 2019.

The water mask used for selecting altimetry measurements is provided by the Global Surface Water - Data Access (https://global-surface-water.appspot.com/download), selecting the occurrence product.

5.1.2. Algorithm baseline for NIR band processing

While for the river water level, the measurement is provided directly by the altimeter, for the velocity measurement, the process is more complex (TARPANELLI ET AL., 2013). In detail, this measurement depends on the physical process whereby the passive response of the reflectance signal coming from the soil is different from those coming from the water. This difference is the key parameter to identify a change in the land area nearby the river channel, that is demonstrated to be strongly correlated with river discharge. The increasing of the river discharge produces an increase of water surface width, and the area close to the river becomes wetter, changing its reflectance response. For an area near the river that is not affected by water, the reflectance remains almost constant (except for changes in vegetation cover) and its ratio with the reflectance of the wetted area can more accurately determine the estimation of changes in hydrological forcing, than the wet area alone. Indeed, due to the variations of water volume during flood events, the reflectance of a wet pixel decreases, while the reflectance of a dry pixel remains fairly constant. Consequently, in case of flooding the reflectance ratio between the dry pixel (called calibration pixel, C) and the wet pixel (called measurements pixel, M) is sensitive to the increase of water in the wet pixel and, hence, is directly correlated to the increasing of river discharge.

In the study of **Tarpanelli et al. (2013)**, where the main process is described, the reflectance ratio C/M has been extracted from a temporal series of eight years of almost daily images of MODIS over four stations along the Po River. Successively, a multi-mission method has been proposed (**Tarpanelli et al., 2020**) through the integration of MODIS from Terra and Aqua and OLCI data from Sentinel-3A and 3B. Despite the passive nature of the sensors that do not observe during cloudy sky, the results underlined the capability of the approach to obtain one measurement every 1.77 days on average. Starting from these outcomes, DTE Hydrology will consider this combined product along with the first attempt to englobe Sentinel-2 data as well. On this respect the following products are collected:

- MODIS datasets, Version 6, tile h18v04, are collected from the USGS website (https://search.earthdata.nasa.gov/). The product is MOD09GQ.006 TERRA and MYD09GQ.006 AQUA Surface Reflectance Daily Global 250 m;
- OLCI data over the region between latitude 44.771 and 45.205 and between longitude 9.562 and 11.901 are extracted from the overpasses of Sentinel-3A and Sentinel-3B through the Copernicus Open Access Hub website (https://scihub.copernicus.eu/);
- Sentinel-2 MSI Level-1C Top of Atmosphere Reflectance and Level-2A Surface Reflectance are not collected, but directly used on Google Earth Engine Platform (GEE).

5.1.3. Algorithm baseline for river discharge

According the base hydraulic definition, river discharge, Q [m^3/s] is given by the product:

$$Q = v \cdot A$$

in which A [m^2] is the cross-sectional area of flow that can be written as a function of water stage h, in the form:

$$A = ah^b = a(H - H_0)^b$$

where H [m] is the water level derived by altimetry, H_0 [m] the null-discharge elevation (bottom of the cross-section). a [m^{2-b}] and b [-] are parameters related to the surface width and the shape of the section (Neal et al., 2015) and in case of the Po River with geometry known, they are calibrated with ground observations. The flow velocity, v, is found correlated with the reflectance ratio C/M [-] according a relationship assumed in the form:

$$v = m\left(\frac{C}{M}\right)^f$$

in which m [m/s] and f [-] are empirical parameters of the regression.

The parameters of the equation are calibrated separately for each site by minimization of Nash-Sutcliffe efficiency, *NSE*, calculated between the simulated and the ground observed discharges.

5.2.Product description

The discharge product to be released in the DTE Hydrology includes time series of river discharge (date, discharge values) calculated in the period January 2016 - December 2019 for five in situ stations along the Po River: Piacenza, Cremona, Borgoforte, Sermide and Pontelagoscuro. The time series have a frequency consistent with the frequency of the multi-mission approaches: for altimetry is 3 days and for multispectral sensors is 1.77 days.

The water level derived by altimetry (Sentinel-3A and 3B and Cryosat-2) is released as a product in DTE Hydrology to be used as auxiliary data for the hydraulic modelling testing and calibration. The water level product includes date, water level value, longitude and latitude of each measurement. The product is spatially distributed according to the satellite tracks along the river stretch from Piacenza to Pontelagoscuro in the period January 2016 - December 2019.

6. Snow depth

6.1.Algorithm baseline and DTE Hydrology improvements

Snow-depth data were obtained from the Sentinel-1-based product proposed by **Lievens et al. (2019)**. These maps are likely one of the most resolved EO-based snow-depth products available on the market, with promising skills in capturing processes that are essential to snow modelling (e.g., slope-scale snow accumulation). The mapping algorithm is based on a change-detection approach and has been shown to provide reasonable performances across the whole northern Hemisphere. Available data cover the period September 2016 - April 2020.

6.2.Product description

The data product comes at 1-km spatial resolution and (nominal) daily granularity and is available through the public repository of the C-SNOW project (https://ees.kuleuven.be/project/c-snow/index.html). The data is provided as NetCDF containing snow depth [m], latitude, longitude coordinates [degree], and product flags for quality control.

7. Land use

7.1.Description

For DTE Hydrology three land cover products are resampled to the same spatial sampling of 500 m:

1. Copernicus Global Land Service Land Cover product is available at a 100m sampling on a yearly basis since 2015.
2. CCI Land Cover maps (1992-2015) and continuation in C3S Land Cover maps (2016-2019) are available at 300msampling on a yearly basis. The maps are based on Medium Resolution Imaging Spectrometer (MERIS, Advanced Very-High-Resolution Radiometer (AVHRR), SPOT_Vegetation (SPOT-VGT) and PROBA-Vegetation (PROBA-V) and Sentinel-3 OLCI time series.

3. CORINE Land cover data set. CORINE is based on LANDSAT-5/7/8, SPOT-4/5, IRS P6, RapidEye and Sentinel-2. Maps are available at a min mapping unit of 25 hectares for 1990, 2000, 2006, 2012 and 2018.

7.2.Product description

All datasets are available as TIFF files, covering the Po valley basin, with 500m sampling. For CGLS and CCI datasets yearly data is available from 2016-2019. For CORINE only 2018 is available.

8. Irrigation

In DTE Hydrology we will use the results of Irrigation+ as soon they will be delivered.

9. References

Albergel, Clément, Christoph Rüdiger, Thierry Pellarin, Jean-Christophe Calvet, Noureddine Fritz, Francis Froissard, David Suquia, Alain Petitpa, Bruno Piguet, and Eric Marti .(2008). From Near-Surface to Root-Zone Soil Moisture Using an Exponential Filter: An Assessment of the Method Based on in-Situ Observations and Model Simulations. Hydrology and Earth System Sciences Discussions 12: 1323–37.

Brocca, L., Ciabatta, L., Massari, C., Moramarco, T., Hahn, S., Hasenauer, S., Kidd, R., Dorigo, W., Wagner, W., Levizzani, V. (2014a). Soil as a natural rain gauge: estimating global rainfall from satellite soil moisture data. Journal of Geophysical Research, 119(9), 5128–5141. Doi: 10.1002/2014JD021489

Chen, F., Crow, W. T., Ciabatta, L., Filippucci, P., Panegrossi, G., Marra, A. C., ... & Massari, C. (2021). Enhanced large-scale validation of satellite-based land rainfall products. Journal of Hydrometeorology, 22(2), 245-257.

Chen, G., & Yu, X. (Eds.). (2003). Chaos control: theory and applications (Vol. 292). Springer Science & Business Media.

Dorigo, Wouter, Wolfgang Wagner, Clement Albergel, Franziska Albrecht, Gianpaolo Balsamo, Luca Brocca, Daniel Chung, Martin Ertl, Matthias Forkel, and Alexander Gruber (2017). ESA CCI Soil Moisture for Improved Earth System Understanding: State-of-the Art and Future Directions. Remote Sensing of Environment 203: 185–215.

Hahn, S., W. Wagner, S. C. Steele-Dunne, M. Vreugdenhil, and T. Melzer (2020). Improving ASCAT Soil Moisture Retrievals With an Enhanced Spatially Variable Vegetation Parameterization. IEEE Transactions on Geoscience and Remote Sensing, 1–16. https://doi.org/10.1109/TGRS.2020.3041340.

Hou, A. Y., Kakar, R. K., Neeck, S., Azarbarzin, A. A., Kummerow, C. D., Kojima, M., Oki, R., Nakamura, K., Iguchi, T. (2014). The global precipitation measurement mission. Bulletin of the American Meteorological Society, 95 (5), 701–722. Doi: 10.1175/BAMS-D-13-00164.1

Huffman, G. J., Bolvin, D. T., Braithwaite, D., Hsu, K., Joyce, R., Xie, P., & Yoo, S. H. (2015). NASA global precipitation measurement (GPM) integrated multi-satellite retrievals for GPM (IMERG). Algorithm Theoretical Basis Document (ATBD) Version, 4, 26.

Jain, M., Andersen, O. B., Dall, J., & Stenseng, L. (2015). Sea surface height determination in the Arctic using Cryosat-2 SAR data from primary peak empirical retrackers. Advances in Space Research, 55(1), 40–50. Doi:10.1016/j.asr.2014.09.006

Lievens, H., Demuzere, M., Marshall, H.-P., Reichle, R.H., Brucker, L., Brangers, I., Rosnay, P. de, Dumont, M., Girotto, M., Immerzeel, W.W., Jonas, T., Kim, E.J., Koch, I., Marty, C., Saloranta, T., Schöber, J., Lannoy, G.J.M.D., (2019). Snow depth variability in the Northern Hemisphere mountains observed from space. Nat Commun 10, 1–12. https://doi.org/10.1038/s41467-019-12566-y

Martens, Brecht, Diego G. Miralles, Hans Lievens, Robin van der Schalie, Richard AM De Jeu, Diego Fernández-Prieto, Hylke E. Beck, Wouter A. Dorigo, and Niko EC Verhoest (2017). GLEAM v3: Satellite-based land evaporation and root-zone soil moisture. Geoscientific Model Development 10, no. 5: 1903-1925.

Massari, C., Brocca, L., Pellarin, T., Abramowitz, G., Filippucci, P., Ciabatta, L., Maggioni, V., Kerr, Y., Fernández-Prieto, D. (2020). A daily/25km short-latency rainfall product for data scarce regions based on the integration of the GPM IMERG Early Run with multiple satellite soil moisture products. Hydrology and Earth System Sciences, 24, 2687–2710. Doi: 10.5194/hess-24-2687-2020

Massari, C., Crow, W., Brocca, L. (2017). An assessment of the performance of global rainfall estimates without ground-based observations. Hydrology and Earth System Sciences, 21, 4347–4361. Doi: 10.5194/hess-21-4347-2017

Mazzetti, C.; Todini, E. Combining raingages and radar precipitation measurements using a Bayesian approach. In: geoENV IV—Geostatistics for Environmental Applications. Springer, Dordrecht, 2004. p. 401-412.

McColl, K. A., Vogelzang, J., Konings, A. G., Entekhabi, D., Piles, M., Stoffelen, A. (2014). Extended triple collocation: Estimating errors and correlation coefficients with respect to an unknown target. Geophysical Research Letters, 41, 6229–6236. Doi: 10.1002/2014GL061322

Miralles, D. G., R. A. M. De Jeu, J. H. Gash, T. R. H. Holmes, and A. J. Dolman (2011). Magnitude and variability of land evaporation and its components at the global scale. Hydrology and Earth System Sciences 15, no. 3: 967-981.

Nielsen K., Zakharova E., Tarpanelli A., Andersen O.B., Benveniste J. (…) River levels from multi mission altimetry, a statistical approach. Under Review on Remote Sensing of Environment.

Pekel J. F., Cottam A., Gorelick N., Belward A. S. (2016) High-resolution mapping of global surface water and its long-term changes. Nature, 540(7633), 418-422. Doi:10.1038/nature20584

Pfeil, Isabella, Mariette Vreugdenhil, Sebastian Hahn, Wolfgang Wagner, Peter Strauss, and Günter Blöschl (2018). Improving the Seasonal Representation of ASCAT Soil Moisture and Vegetation Dynamics in a Temperate Climate. Remote Sensing 10 (11): 1788. https://doi.org/10.3390/rs10111788.

Quast, Raphael; Albergel, Clément; Calvet, Jean-Christophe; Wagner, Wolfgang (2019). A Generic First-Order Radiative Transfer Modelling Approach for the Inversion of Soil and Vegetation Parameters from Scatterometer Observations. Remote Sens. 11, no. 3: 285. https://doi.org/10.3390/rs11030285

Sevruk, B. (2002). WMO questionnaire on recording precipitation gauges: state-of-the-art. Water science and technology, 45(2), 139-145.

Tarpanelli A., Brocca L., Barbetta S., Faruolo M., Lacava T., Moramarco T. (2015) Coupling MODIS and radar altimetry data for discharge estimation in poorly gauged river basin. IEEE Journal of Selected Topics in Applied Earth Observations and Remote Sensing, 8(1), 141-148. http://dx.doi.org/10.1109/JSTARS.2014.2320582.

Tarpanelli A., Brocca L., Lacava T., Melone F., Moramarco T., Faruolo M., Pergola N., Tramutoli V. (2013) Toward the estimation of river discharge variations using MODIS data in ungauged basins. Remote Sensing of Environment, 136, 47–55. Doi:10.1016/j.rse.2013.04.010

Tarpanelli A., Iodice F., Brocca L., Restano M., Benveniste J. (2020). River flow monitoring by Sentinel-3 OLCI and MODIS: comparison and combination. Remote Sensing, 12(23), 3867. https://doi.org/10.3390/rs12233867

Tóth, Brigitta, Melanie Weynants, László Pásztor, and Tomislav Hengl (2017). 3D soil hydraulic database of Europe at 250 m resolution. *Hydrological Processes* 31, no. 14: 2662-2666.

Wagner, Wolfgang, Guido Lemoine, and Helmut Rott (1999). A Method for Estimating Soil Moisture from ERS Scatterometer and Soil Data. Remote Sensing of Environment 70 (2): 191–207. https://doi.org/10.1016/S0034-4257(99)00036-X.

Zrnic, D. S., & Ryzhkov, A. V. (1999). Polarimetry for weather surveillance radars. Bulletin of the American Meteorological Society, 80(3), 389-406.

Technical Note 2: DTE-Hydrology consistent end-to-end integrated framework description and validation

1. Introduction

1.1. The DTE Hydrology Project

The objective of DTE Hydrology is to develop and demonstrate a prototype of Digital Twin Earth with focus on water cycle and hydrological processes and their impacts. In DTE Hydrology we aim to highlight the huge potential of high-resolution ESA satellite products for describing the water cycle, for predicting hydrology extremes (floods, landslides and drought) and for monitoring and managing water resources.

The activity comprises four sequential steps: 1) building the 4D DTE Hydrology dataset, a high resolution (1 km, hourly, 2016-2019) EO-based dataset, also integrating in situ observations, 2) develop a high resolution modelling system ingesting the 4D DTE Hydrology dataset and able to provide a 4D reconstruction of the water cycle, 3) integrating the modelling system in the cloud-based DTE Hydrology simulation and visualization tool, and 4) exploiting the DTE Hydrology tool to develop user-oriented case studies focusing on flood and landslide risk, and water resources management.

The area of focus of DTE Hydrology is the Po River Basin (northern Italy). In this area high quality ground observations are available, which are useful to calibrate and test the modelling system. Floods and landslides occur in the area due to the complex topography and meteorological conditions. The large agricultural area in the Po River Valley ("Pianura Padana") makes water resources management fundamental, as crop production is largely dependent on rainfall and on water availability from the Po River.

DTE Hydrology builds on the expertise of the consortium members. Within the project EO datasets of rainfall, soil moisture, evaporation, river discharge, snow depth and land cover will be used. Soil moisture, rainfall, snow depth and evaporation datasets are provided by partners with well-established algorithms from satellite observations, TU Wien, CNR-IRPI, CIMA and UGent respectively. Expertise in hydrological and hydraulic modelling at high resolution is brought in by CNR-IRPI, CIMA and UNIBO. High performance computing is pivotal in DTE Hydrology and is managed and hosted by EODC. Outreach and visualization of the project outcomes is done by CNR-IRPI, CIMA, EODC and UNIBO.

1.2. Scope of this Report

This report describes the activities concluded for WP100 (assessment of satellite products, 4D DTE Hydrology dataset) and currently being performed in WP200 and WP400.

The current version of the document is a snapshot of the activities at the end of March 2021, corresponding to the Mid-Term Review Meeting, while the complete version will be submitted by the end of June 2021. The assessment of satellite products is completed. However, output of the hydrological modelling activities will be used as input by the other models (see **Figure 1**). Hence, simulation results are here reported only for hydrological modelling, while for the other models (hydraulic and landslides) we report the main methodological features. The definition of case studies for WP400 is also reported (needed for setting up the modelling system).

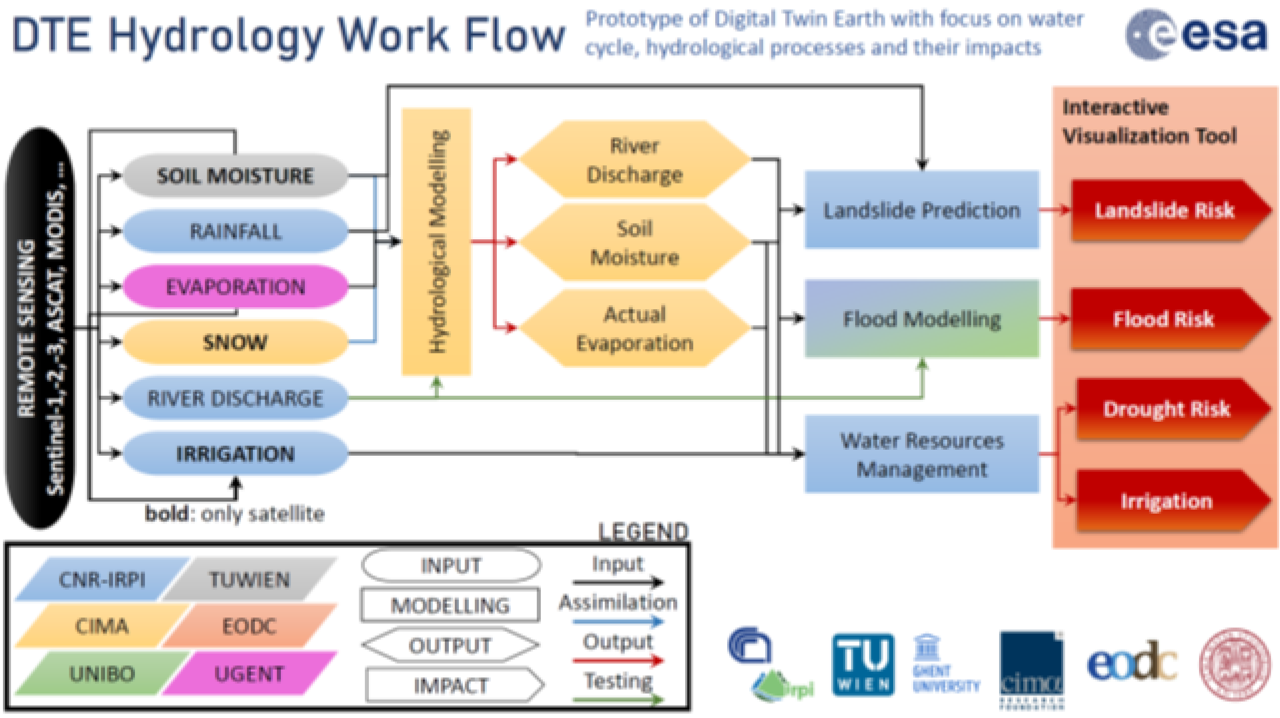

Figure 1: Work flow of DTE Hydrology project.

1.3. Applicable Documents

Not available.

1.4. Reference Documents

RD-01 DTE Hydrology Technical Proposal - V1.0

RD-02 Deliverable D1.1: 4D DTE Hydrology underlying data reconstruction

RD-03 Deliverable D1.2: DTE Hydrology data set

RD-04 Progress report October 2020-January 2021

1.5. Document Organisation

The document is organized in four sections: Section 2 - Satellite product assessment, Section 3 - Modelling system, Section 4 - DTE Hydrology case studies, and Section 5 - DTE Hydrology Prototype description. The sections are subdivided in subsections describing the different satellite products and modelling approaches.

2. Satellite products assessment

2.1. Precipitation

The satellite precipitation product developed within DTE Hydrology (DTE Hydrology 1-km 1-hourly, DTE 1km from here onward) is based on the integration of multiple precipitation products, namely, SM2RAIN-ASCAT (**Brocca et al., 2019**), IMERG-LR and S1-based rainfall estimates (**Massari et al., 2017; 2019; 2020**).

Within this report we assessed DTE 1km the integrated rain gauges and radar measurements from the MCM product developed by CIMA Research Foundation. DTE 1km is further cross validated by using hydrological simulations (**Brocca et al., 2020; Camici et al., 2020**) obtained with Continuum and MISDc hydrological models.

Figure 2 plots the spatial distribution of the mean annual precipitation over the study area. It can be seen that the pattern of the precipitation is very similar and quantitatively consistent. However, the two products have some bias which results in lower rainfall accumulation for DTE 1km (see **Figure 3**) with a mean annual bias of 29 mm.

Figure 4 shows the hourly and monthly Pearson correlation coefficient between the DTE 1km and MCM. Daily Pearson correlation is reported in **Figure 5** along with the value obtained for SM2RAIN-ASCAT, SM2RAIN-S1 and IMERG-LR. Considering the different scales of calculation of the correlation (10 km for SM2RAIN-ASCAT and IMERG and 1 km for DTE 1km) which should favor coarse scale products the developed DTE 1km provides instead a significant improvement with respect to the baseline products reaching a median daily correlation of 0.734. The correlation patterns show an overall deterioration of the correlation over the Alps and in general over mountainous regions which are guided by all the parent products. It is interesting to note that the generally lower performance of SM2RAIN-S1 does not significantly impact the correlation pattern of DTE 1km suggesting the optimality of the integration technique.

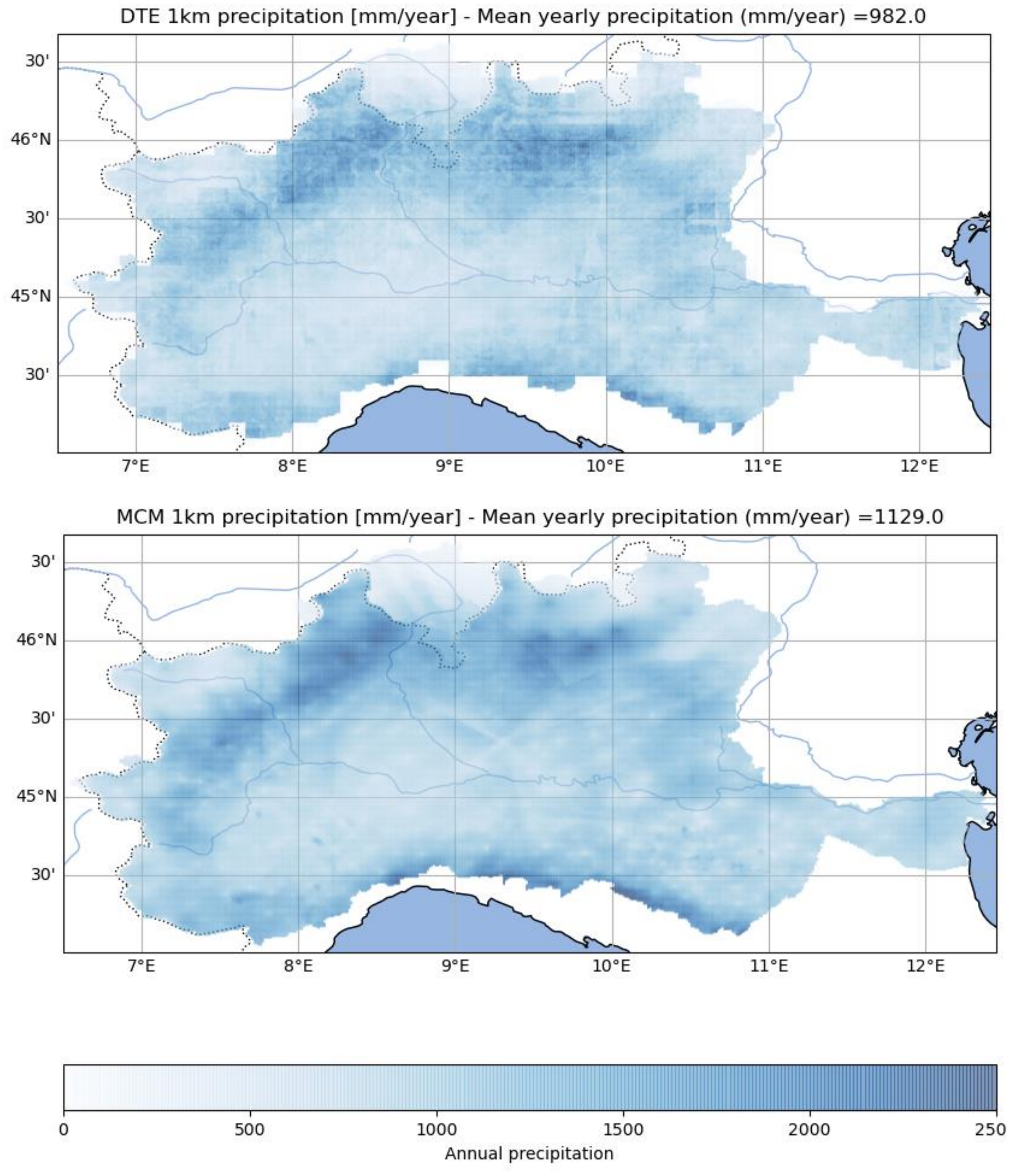

Figure 2*:* Mean annual precipitation accumulation of DTE 1km precipitation product (top) and the MCM (bottom).

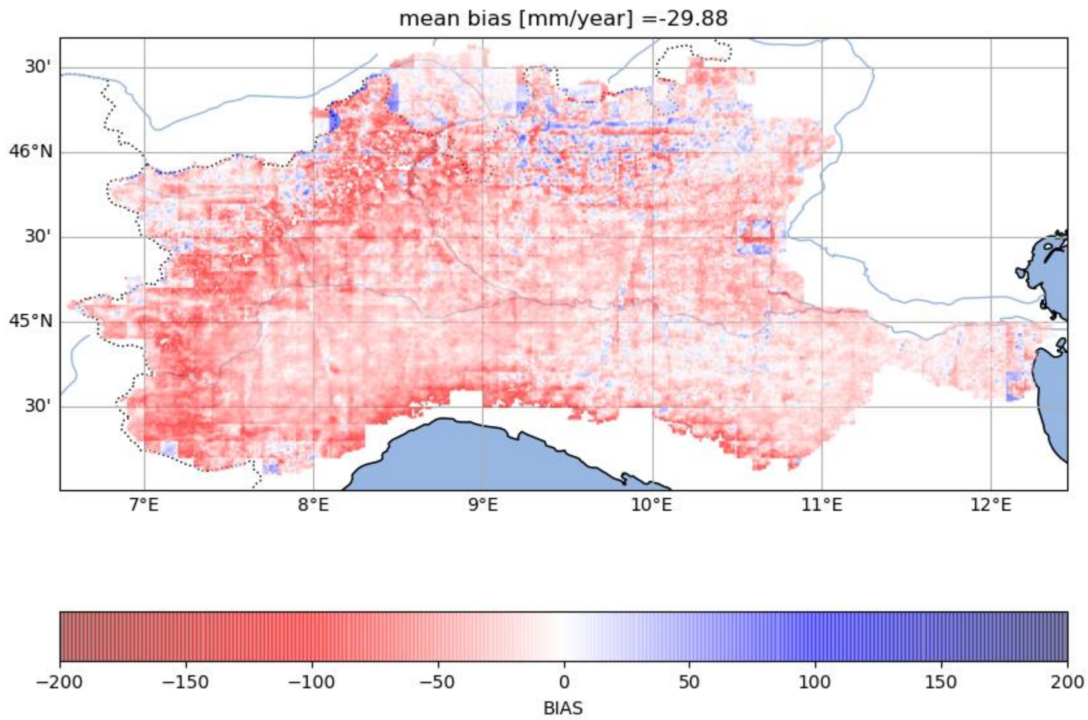

Figure 3*:* Mean annual bias between DTE 1km and MCM.

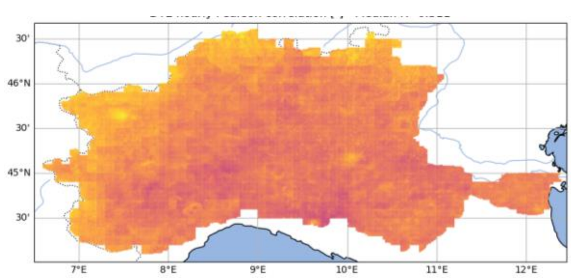

(a) DTE 1km/hourly hourly correlation R(median) = 0.311

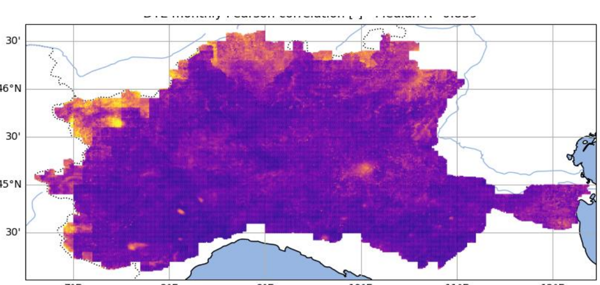

(b) DTE 1km/hourly monthly correlation R(median) = 0.839

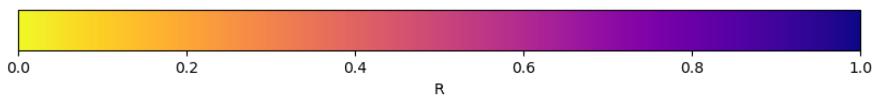

Figure 4*:* Hourly (a), daily(b) and monthly(c) Pearson correlation coefficient between DTE Hydrology 1 km precipitation products and the MCM product.

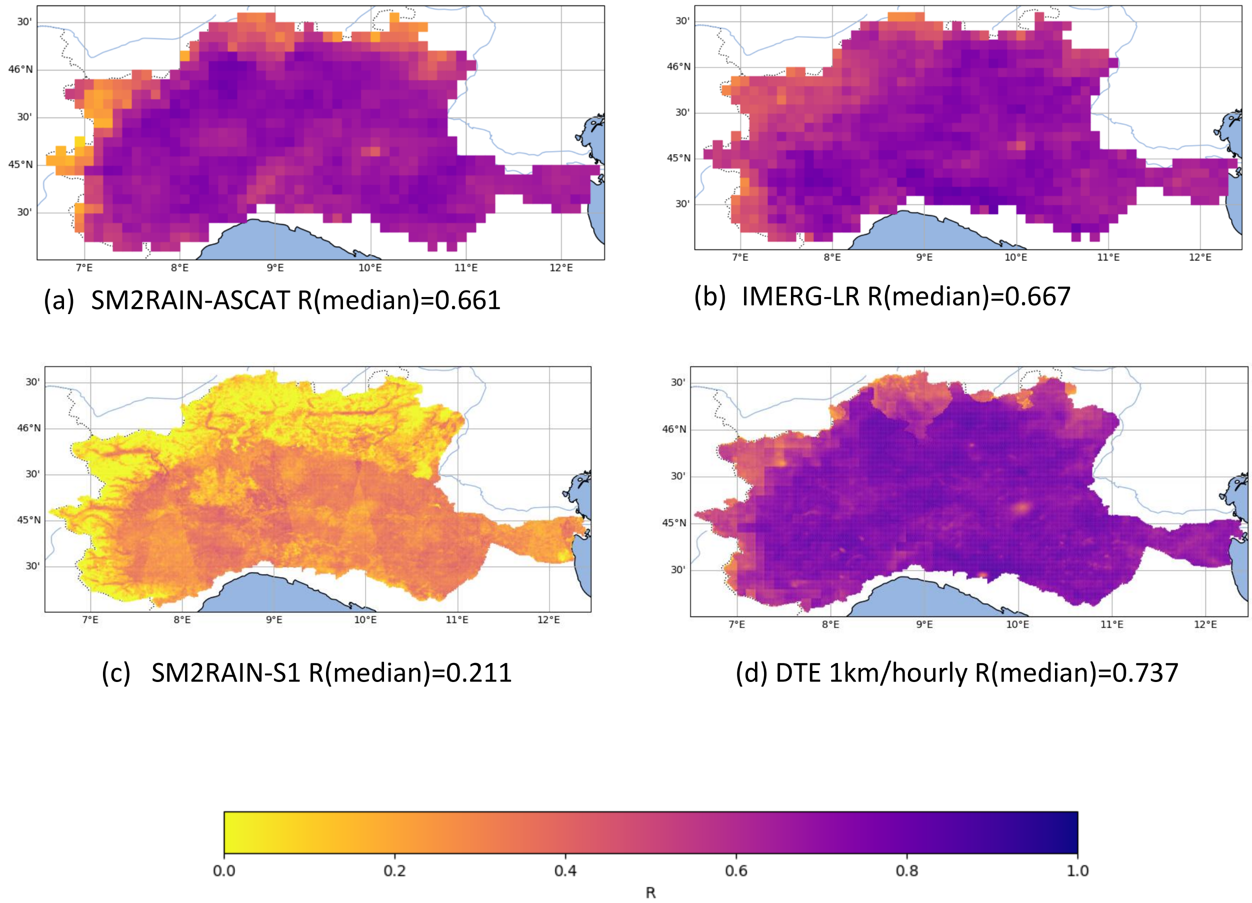

Figure 5*:* Daily Pearson correlation coefficient between (a) SM2RAIN-ASCAT, (b) IMERG-LR, SM2RAIN-S1 (c) and DTE Hydrology 1 km (d) and MCM.

2.2. Evaporation

The Global Land Evaporation Amsterdam Model (GLEAM) has been adapted to the requirements of the high-resolution 1km runs by incorporating land surface information suitable for representing the spatial heterogeneity of the Po river basin (see **Figure 6**). Furthermore, the model and input data were adapted to also compute evaporation for lakes (in its standard implementation GLEAM only computes evaporation for water bodies if the pixel is also covered by a fraction of land).

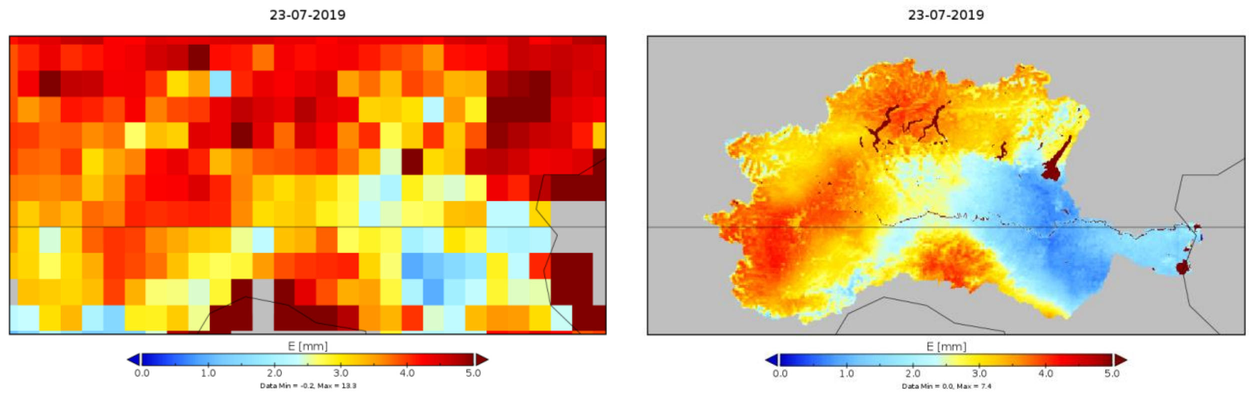

Figure 6*:* Evaporation across the Po river basin on 23th July 2019 with GLEAM v35b at the global 0.25 resolution (left) and the high-resolution simulations at 1 km (right).

The availability of local in situ data for the time period of interest (2016–2019) from FLUXNET towers is very limited. We therefore mostly infer the capability of GLEAM to provide realistic evaporation estimates from other validation studies. The good performance of GLEAM for global simulations (spanning 1980–2014) is for instance shown by **Martens et al., 2017**, with an average R of 0.78 and 0.80 (depending on the algorithm version). Among the existing global evaporation datasets, those based on the Priestley and Taylor equation (like GLEAM) typically show a better agreement against in situ observations (**Miralles et al., 2016**).The capability of GLEAM to also provide realistic spatial-temporal patterns of evaporation at a high spatial resolution (100m) has been demonstrated by **Martens et al., 2017** over The Netherlands, Flanders, and western Germany for the period 2013–2017 with the per-site correlation coefficient against in situ data ranging from 0.65 to 0.95. Ongoing work on providing pan-European evaporation data at 1 km resolution, using similar input data to the preliminary version used in DTE–Hydrology, equally shows a good agreement between modelled evaporation and in situ measurements with correlations mostly in between 0.70 and 0.85 for 2018 across 33 FLUXNET sites (**Rains et al., in prep.**).

The evaporation estimates from the GLEAM Po river basin simulations and from FLUXNET measurements for two Italian sites, namely IT-Sr2 and IT-Tor, within or adjacent to the study area are shown in **Figure 7**.

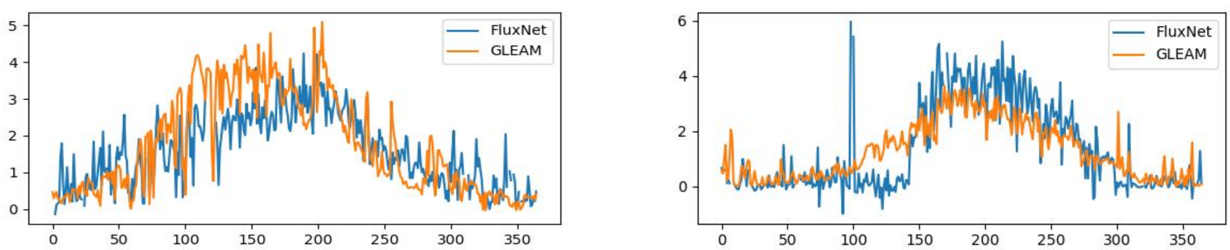

Figure 7*:* Daily evaporation from the FLUXNET sites IT-SR2 (left) and IT-Tor (right) and GLEAM for 2018. Pearson's correlation R is 0.78 and 0.83 respectively.

During the following steps of DTE–Hydrology, the evaporation in GLEAM will be calculated using the precipitation (Section 2.1), soil moisture (Section 2.3) and snow cover (Section 2.5) that are being internally produced within the project framework. A final update to the simulations will incorporate the assimilation of surface soil moisture retrieved from Sentinel-1 (**Rains et al., in review**), as well as 1km net-radiation forcing based on Sentinel 3 land surface temperatures. The latter is being developed in a parallel project, ET–Sense, funded by the Belgian Science Policy Office (BELSPO).

2.3. Soil moisture

The satellite soil moisture retrievals have been adjusted to achieve the best performance over the Po River Basin. Surface Soil Moisture (SSM) and Soil Water Index (SWI) retrievals have been evaluated with respect to the ERA5-Land "soil water volume in the first layer" (swvl1) (**Munoz-Sabater et al., 2021**) as well as in-situ Soil Moisture (SM) observations from the Oltrepo station with a measurement depth of 10 cm. Three products are compared, the original Copernicus Global Land Service SCATSAR SWI, and the two products developed for DTE Hydrology, the DIREX SAR SWI product and RT1 SSM product. For the validation all observations are masked for frozen soils and snow cover, using ERA5-Land. Furthermore, the datasets are temporally matched to the lowest temporal resolution product, and scaled to either ERA5-Land swvl1 or the in-situ SM. Pearson R correlation and unbiased Root Mean Square Difference are calculated between the satellite products and reference products.

Figure 8 shows the resulting Pearson correlation between SCATSAR, DIREX SAR and RT1 retrievals and ERA5-Land swvl1. The rectangular artefacts visible in the images stem from the fact that the spatial resolution of the comparison-dataset is 9 km while the satellite-based products are provided with a spatial sampling of 500 m. The CGLS SCATSAR and DIREXSAR SWI products are masked for complex terrain in the processing chain. For completeness the RT1 comparison is shown both masked with the CGLS masking and unmasked.

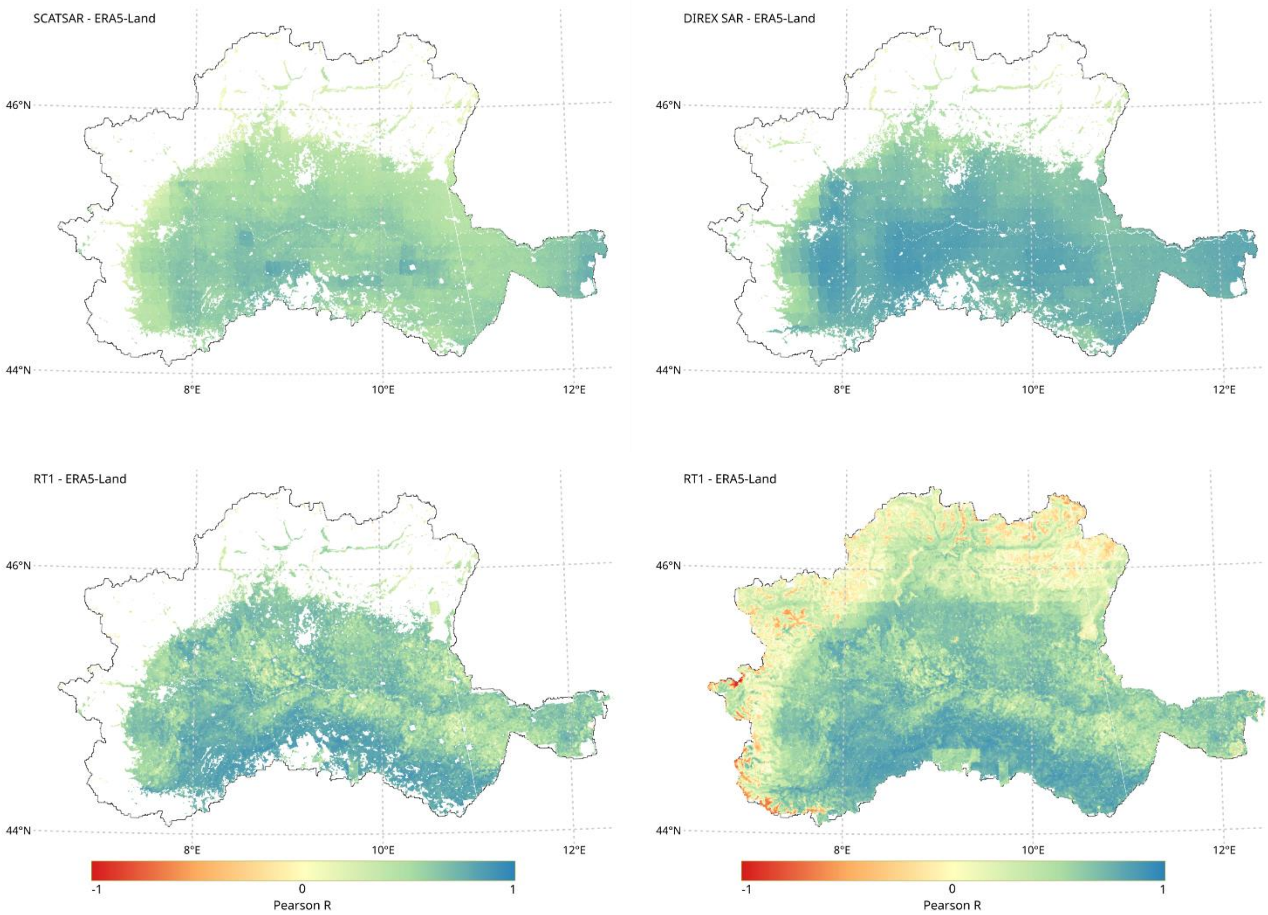

Figure 8*:* Spatial maps of Pearson R correlation coefficient between SCATSAR SWI (top), DIREX SAR SWI (middle) and RT1 SSM (bottom) and ERA5-Land swvl1.

It can be seen that for all three products a good agreement in temporal dynamics is obtained in the expected areas, such as regions with moderately dense vegetation-coverage and low topographic complexity. Mountainous areas as well as urban areas and regions of rice growth, i.e. flooded agricultural fields, show low or negative correlations. The advantage of the RT1 product is that the temporal dynamics stem from Sentinel-1 only, whereas in the SWI products the temporal dynamics are strongly driven by coarse-resolution ASCAT observations, which are hence representative for a larger area. This is clear in **Figure 8**, where small scale variations in correlation coefficient are present between RT1 and ERA5-Land, which are not visible in the SWI products. The trade-off is that RT1 SSM shows slightly lower correlations than the two SWI products. This can be a result of the lower temporal resolution of Sentinel-1 compared to the combined ASCAT and Sentinel-1 products or the noisy character of Sentinel-1 observations. Therefore, depending on the application, either the DIREX SAR SWI or RT1 SSM is the best product to use.

The DIREX SAR SWI can be directly compared to the SCATSAR SWI product, as it has the exact same amount of observations. **Figure 9** shows the difference in correlation coefficient between the two satellite-based products and ERA5-Land. It is clear that the DIREX SAR improves soil moisture retrievals when compared to ERA5-Land soil moisture. Especially over agricultural areas improvements are large. A direct comparison between the two SWI products and RT1 SM is not possible on account of the different temporal resolution of

RT1 SM, which is based only on Sentinel-1 observations, and the SWI products, which are based on ASCAT and Sentinel-1 observations.

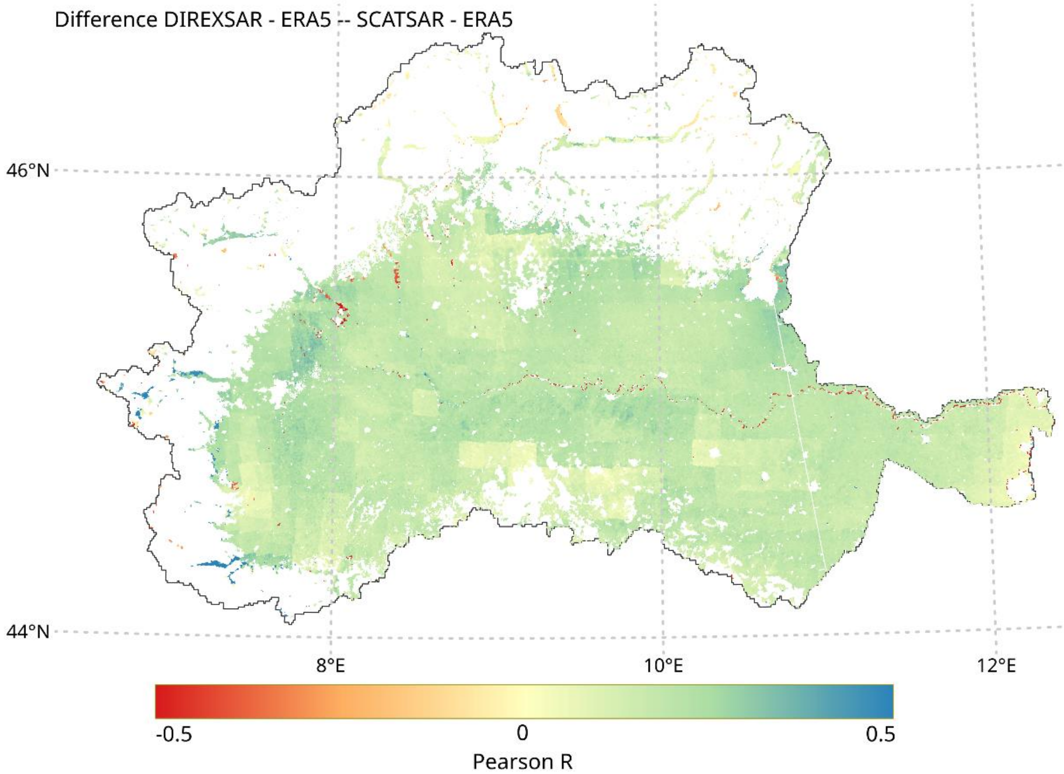

Figure 9*:* Difference in Pearson R correlation coefficient SCATSAR SWI and DIREX SAR SWI when compared to ERA5-Land swvl1.

Figure 10 shows the time series of the SCATSAR SWI, DIREX SAR SWI and RT1 SSM with respect to in situ SM in Oltrepo. Again, results of SCATSAR SWI and DIREX SAR SWI can be compared directly, and a significant increase in temporal correlation (from 0.74 to 0.81) and unbiased Root Mean Square Difference (uRMSD, from 0.057 to 0.047) can be observed for DIREX SAR SWI. When investigating the time series, it shows that the SCATSAR SWI has a dry bias in spring, which is smaller, or even not present in the DIREX SAR SWI. The improvements in SWI are mainly due to the improved capturing of these seasonal dynamics in DIREX SAR SWI. This is confirmed in the comparison of anomalies (calculated using a climatology calculated over the four years of data) between the satellite products and in situ SM (**Figure 11**). The temporal correlation of anomalies does not improve for DIREX SAR SWI compared to SCATSAR SWI.

The RT1 SSM shows lower temporal correlation and uRMSD, although it needs to be noted that a temporal correlation of 0.69 is high for Sentinel-1 only SSM retrievals compared to other Sentinel-1 products (e.g. Bauer-Marschallinger et al., 2019). From the timeseries it can be observed that mainly in summer the RT1 SSM shows large variations, i.e. a dry bias in early July, followed by a strong increase and wet bias in August, which are not observed in in situ soil moisture. This can be the result of the vegetation parameterization applied in RT1 and is subject of further research.

Overall, it can be concluded that the two products developed for DTE Hydrology show improvements compared to existing SSM and SWI products. The DIREX SAR SWI product especially improves the seasonal representation of soil moisture dynamics.

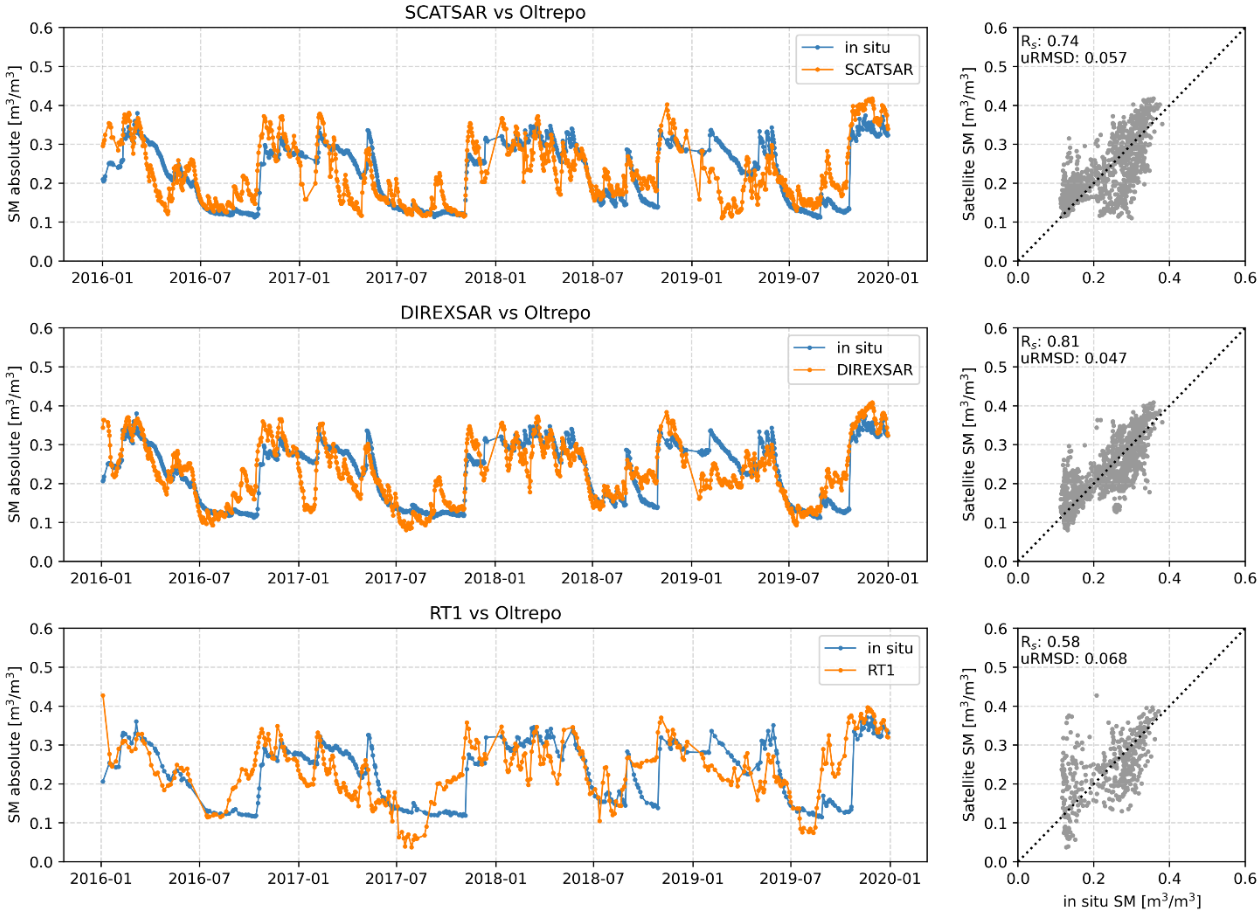

Figure 10*:* Time series of absolute SCATSAR SWI (top), DIREX SAR SWI (middle) and RT1 SSM (bottom) compared to in situ SM in Oltrepo.

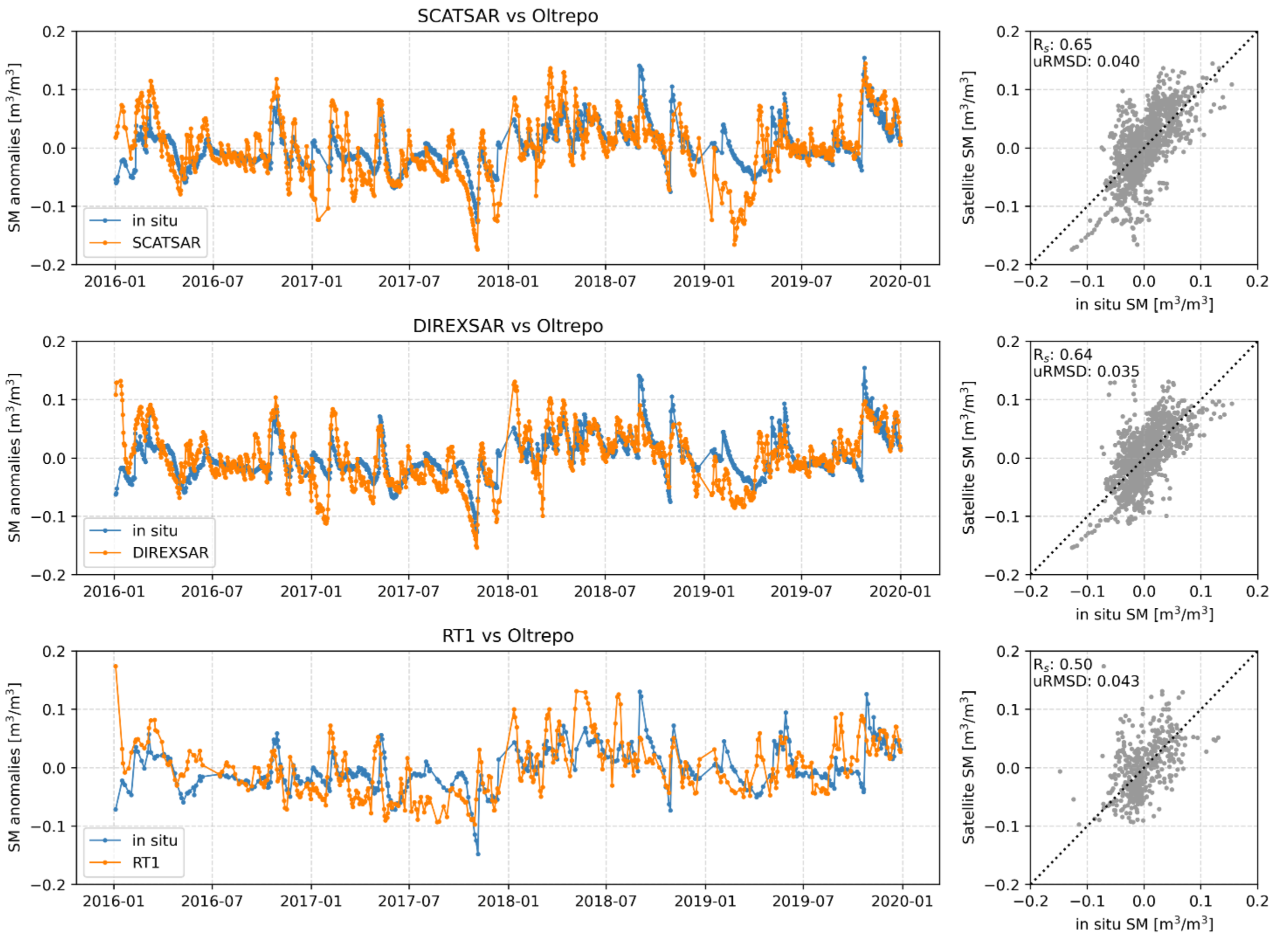

Figure 11*:* Time series of anomalies of SCATSAR SWI (top), DIREX SAR SWI (middle) and RT1 SSM (bottom) compared to in situ SM in Oltrepo.

2.4. River discharge

The evaluation of the discharge product cannot prescind to the evaluation of the water level derived by altimetry series and flow velocity derived by Near Infrared (NIR) band sensors. Therefore, in the following the validation for every product is carried out. Specifically, for the altimetry and the velocity product, the performances are calculated in terms of Pearson correlation, *R*, Root Mean Square Error, *RMSE*, and Nash Sutcliffe Efficiency, *NSE*. For the river discharge, two additional metrics are considered: Relative *RMSE*, *rRMSE*, calculated as the *RMSE* divided by the mean of the observations, and the Kling-Gupta Efficiency, *KGE*.

The validation of the water level time series is carried out by comparing the water levels derived by satellite altimetry versus those observed at five gauged stations along the Po River. The river model developed to integrate altimetry multi-mission data allows to derive the water level time series along all the river. Therefore, a direct comparison between the satellite and the ground observations is feasible exactly at the in-situ stations, where the water level is continuously monitored. **Figure 12** shows the comparison between satellite-derived and ground observed water levels for all the selected stations in terms of temporal series and scatter plot. The errors in the measurements of water level are resumed in **Table 1**. The time series derived from the satellite agree with those observed on the ground in almost all stations: the dynamics of the river are well reproduced and the points are mostly located on the bisector of the scatter plots. The good evaluation of the altimetric series is also confirmed by the performance indices in **Table 1**. At the Piacenza station, the performances are lower than the others, probably due to the disconnection related to the Isola Serafini dam, which is located 40 km downstream of Piacenza. Here, the multi-mission approach uses fewer satellite tracks with consequent missing peaks and lower temporal resolution (8.6 days compared to the 2.9 days for the other stations).

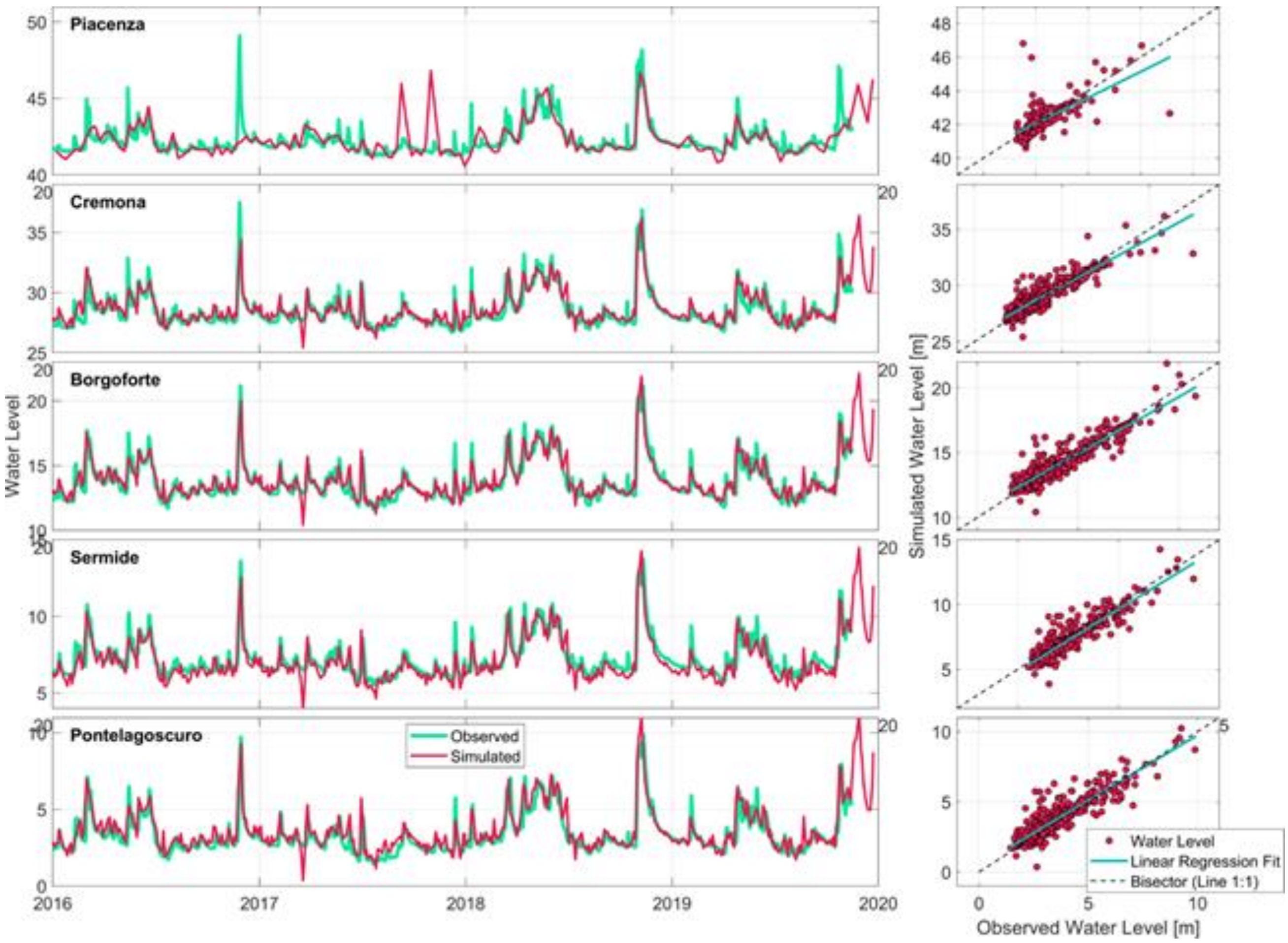

Figure 12*:* Comparison between the altimetry-derived and the ground observed water levels for the five selected stations.

The validation of the NIR sensor product is evaluated in the reproduction of the flow velocity. Generally, the performances in **Table 1** are good with correlation greater than 0.72, and RMSE relatively low, except for Piacenza station, in which evident disagreements are found between the simulated and observed flow velocity. This is attributed to the specific sensor of MODIS Aqua that for Piacenza does not follow the variation of the river. By the analysis of the temporal series in **Figure 13** displacements are found above all for high discharges, mostly due to the missing of satellite data during the flood events. The presence of clouds during rain events prevents the optical sensor from seeing the river. Despite the known limitation of the NIR sensors, the multi-mission allows to better densify the time series, reaching a time-step around 1.62 days on average, almost the double of the altimetry.

Table 1: Performance metrics for the comparison between the satellite-derived and the ground observed variables (water level for altimetry and flow velocity for the NIR sensors) for the five selected stations (Pearson correlation, R, Root Mean Square Error, RMSE, Nash Sutcliffe Efficiency, NSE). The frequency of the temporal series is indicated as time-step in days.

Station	***R*** **[-]**	***RMSE*** **[m or m/s]**	***NSE*** **[-]**	***Time-step*** **[day]**
		ALTIMETRY (water level)		
Piacenza	0.67	0.81	0.22	8.6
Cremona	0.91	0.64	0.81	2.9
Borgoforte	0.92	0.61	0.84	2.9
Sermide	0.91	0.61	0.76	2.9
Pontelagoscuro	0.9	0.65	0.76	2.9
		NIR (flow velocity)		
Piacenza	0.56	0.18	0.31	1.6
Cremona	0.79	0.09	0.62	1.62
Borgoforte	0.76	0.1	0.58	1.59
Sermide	0.72	0.08	0.52	1.68
Pontelagoscuro	0.76	0.13	0.58	1.63

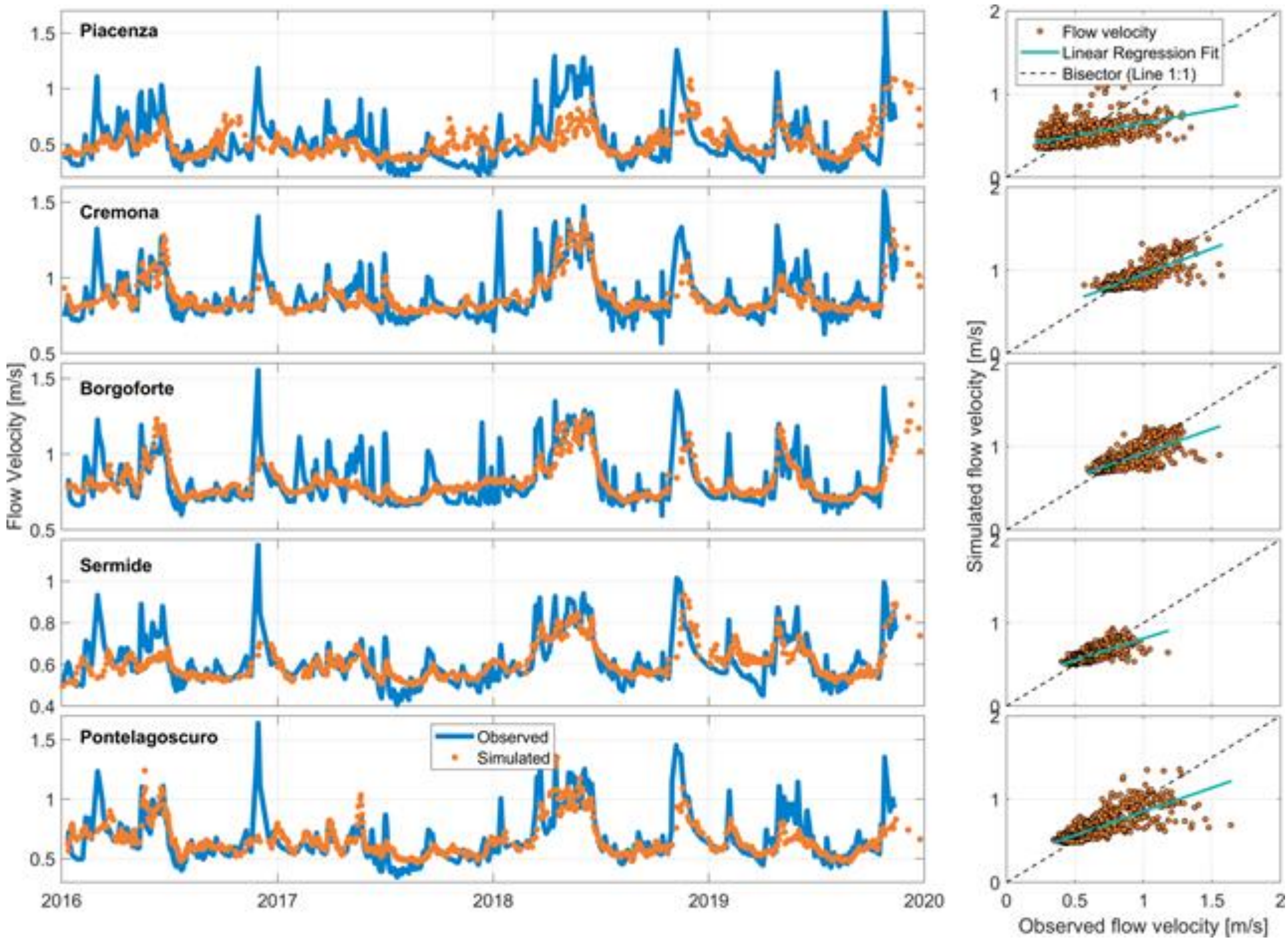

Figure 13*:* Comparison between the NIR-derived and the ground observed flow velocity for the five selected stations.

The river discharge estimated by the combination of satellite products (altimetry and NIR) is validated against the observations recorded at the five stations along the Po River. The temporal series of river discharge are calculated with respect to the NIR product time-step, considering the linear interpolation between two consecutive values of altimetry-derived water level. **Table 2** reports the performances of the comparison between the multi-mission product (altimetry+NIR) and the observations. In order to underline the added value of the multi-mission approach, in brackets the performances obtained by the only use of altimetry for the estimation of river discharge, based on the traditional rating curve between water height and discharge, are also shown.

Table 2: Performance metrics for the comparison between the simulated and ground observed river discharge for the five selected stations (Pearson correlation, *R*, Root Mean Square Error, *RMSE*, Relative RMSE, *rRMSE*, Nash Sutcliffe Efficiency, *NSE*, Kling-Gupta Efficiency, *KGE*)

Station	***R*** [-]	***RMSE*** [-]	***RRMSE*** [%]	***NSE*** [-]	***KGE*** [-]
Piacenza	0.75 (0.68)	315 (344)	45 (48)	0.55 (0.47)	0.66 (0.55)
Cremona	0.93 (0.92)	188 (195)	21 (22)	0.85 (0.84)	0.91 (0.91)
Borgoforte	0.92 (0.92)	224 (226)	21 (21)	0.85 (0.85)	0.91 (0.91)
Sermide	0.92 (0.92)	243 (248)	22 (22)	0.85 (0.85)	0.91 (0.91)
Pontelagoscuro	0.91 (0.90)	272 (284)	24 (25)	0.82 (0.81)	0.89 (0.87)

Despite the altimetry product is highly performing, the rating curve built with the water level derived by altimetry and observed discharge provides lower performances as compared with the proposed approach in which also the contribution of NIR bands is included. This result is particularly evident at Piacenza, where the altimetry product is less efficient and the multi-mission approach provides a substantial improvement. **Figure 14** shows the temporal series of the simulated discharge, both with multi-mission approach and only altimetry rating curve, compared to the ground observations.

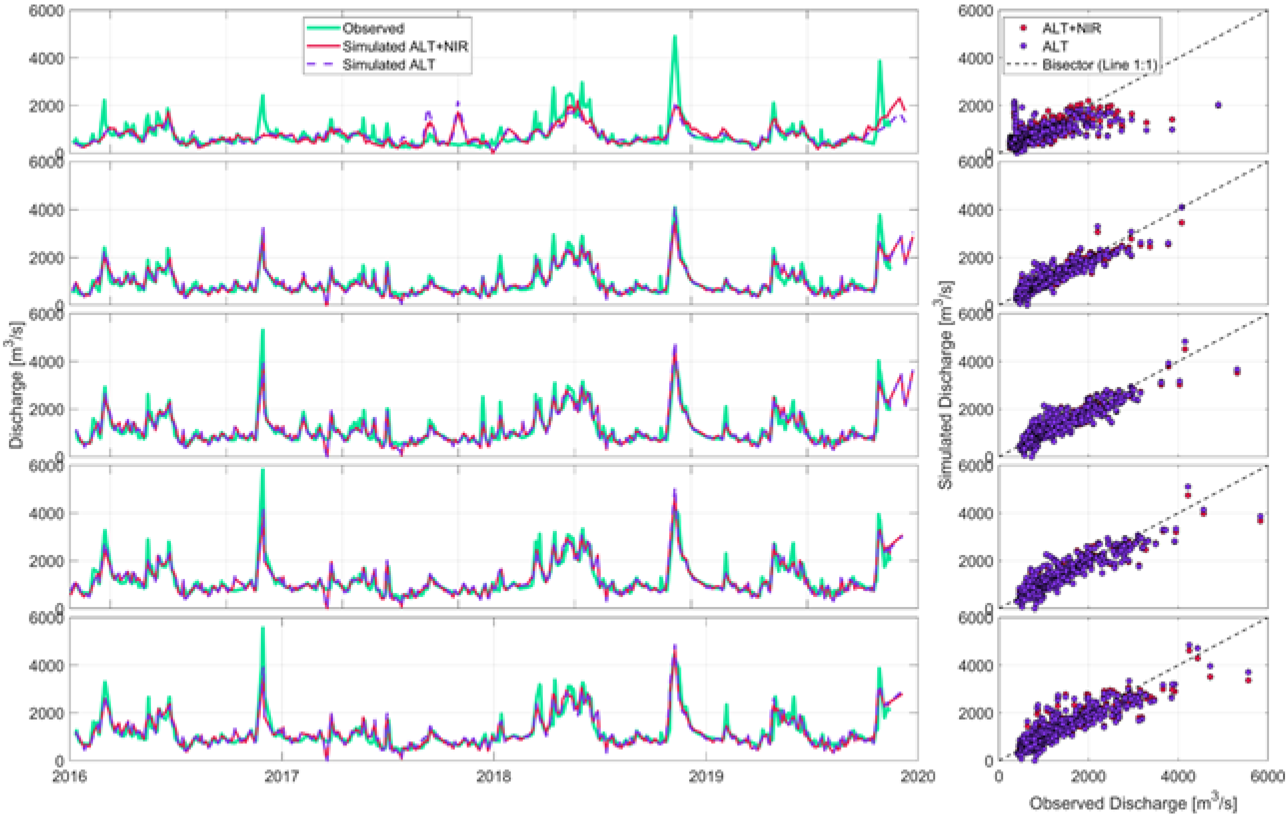

Figure 14*:* Comparison between the discharge simulated by the two approaches, rating curve (ALT) and multi-mission approach (ALT+NIR) and the observed discharge for the five selected stations.

2.5. Snow

Snow-depth data were obtained from the Sentinel-1-based product proposed by **Lievens et al. (2019)**. The data product comes at 1-km spatial resolution and (nominal) daily granularity and is available through the public repository of the C-SNOW project (https://ees.kuleuven.be/project/c-snow/index.html). These maps are likely one of the most resolved, EO-based snow-depth products available on the market, with promising skills in capturing processes that are essential to snow modelling (e.g., slope-scale snow accumulation). The mapping algorithm is based on a change-detection approach and has been shown to provide reasonable performances across the whole northern Hemisphere. Available data cover the period September 2016 - April 2020.

In the context of this project, C-SNOW data were evaluated by comparing their estimates of snow depth with co-located readings across 172 ultrasonic snow-depth sensors across the Po river basin (**Figure 15**). Most of these data belongs to the Italian administrative regions Valle d'Aosta, Piemonte, Lombardia, Liguria, Veneto, and Emilia Romagna and were accessed, downloaded, and processed by CIMA Research Foundation thanks to bilateral agreements between CIMA and the Italian Civil Protection Agency. The spatial distribution of this dataset homogeneously covers all mountain regions of the Po river basin, with the exception of the Swiss Canton of Ticino (**Figure 15**). In terms of elevation distribution, on the other hand, the bulk of the evaluation dataset is located between 1000 m Above Sea Level (ASL) and 2500 m ASL (**Figure 16**). This means that the highest elevations in this region (say, areas above 3000 m ASL) are largely undersampled by this evaluation dataset, a frequent condition in the Alps (Avanzi et al., 2020). Also, note that snow-depth sensors are generally installed in flat and open sites, which may miscapture the spatial distribution and the amount of snow depth across the landscape (Malek et al., 2017). Still, the comparison of C-SNOW snow depth with measurements of snow-depth sensors for the same pixel are unaffected by the potential bias of snow-depth sensors at landscape scale.

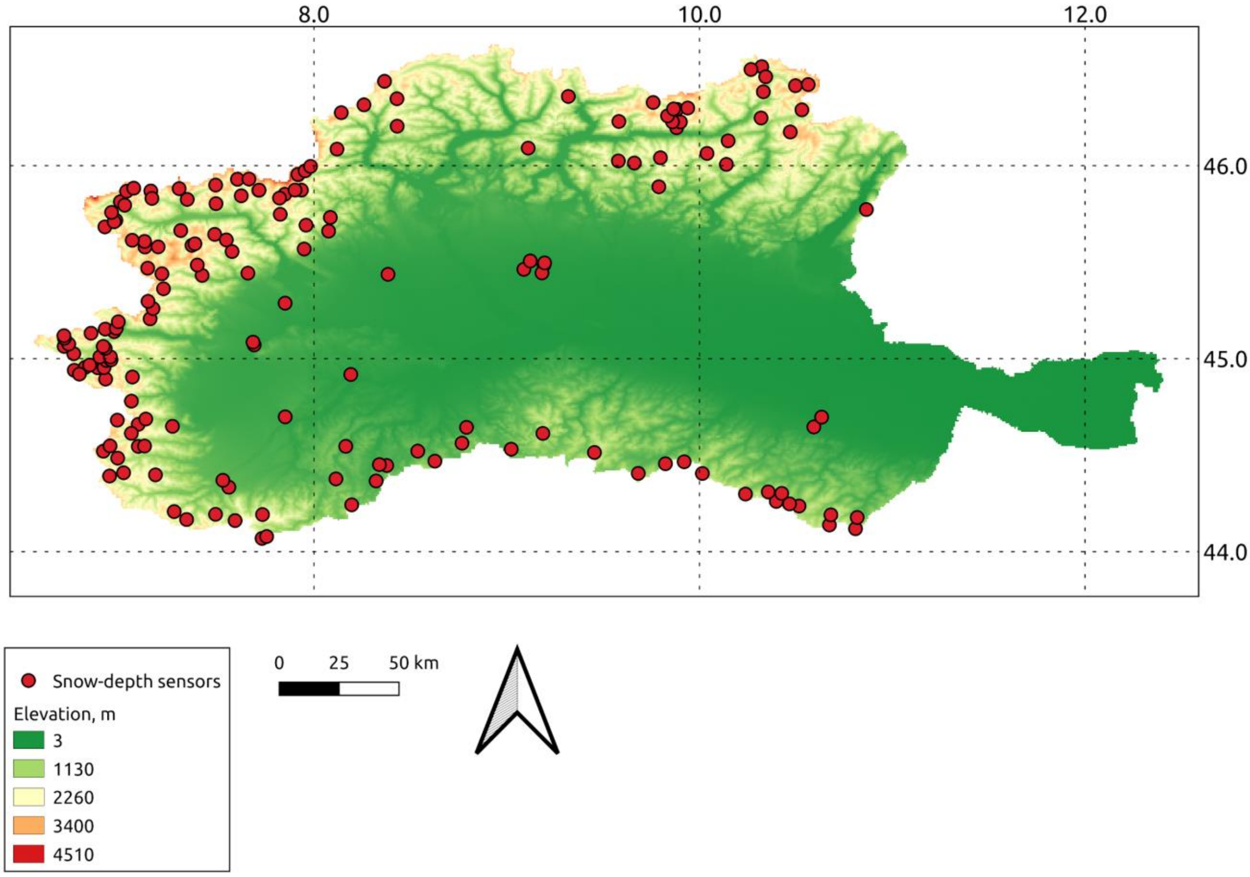

Figure 15: Spatial distribution of the 172 ultrasonic snow-depth sensors across the Po river basin used for C-SNOW evaluation. The background map is a Digital Elevation Model of the Po river basin.

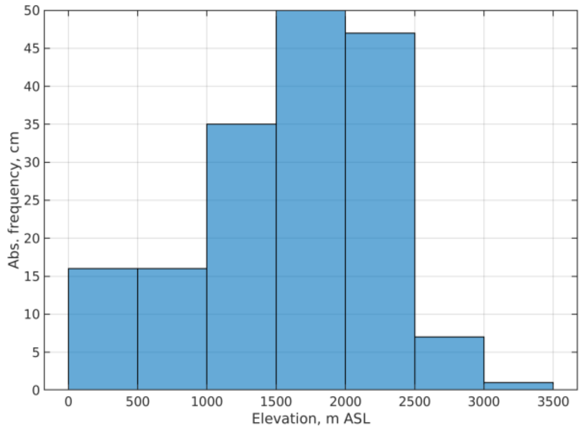

Figure 16: Elevation distribution of the 172 ultrasonic snow-depth sensors across the Po river basin used for C-SNOW evaluation.

The evaluation period was September 1, 2016 to March 31, 2020, the available period of record for the C-SNOW dataset. Raw snow-depth-sensor data from the 172 ultrasonic snow-depth sensors across the Po river basin were processed using semi-automatic filters and were aggregated at daily resolution for consistency with the granularity of C-SNOW data. Time-series of sensor-based daily average snow depth were then compared with daily estimates from C-SNOW, which were extracted from northern-Hemisphere maps using a nearest-neighbouring approach.

Root Mean Square Errors (RMSE) for C-SNOW snow depth increase with elevation (**Figure 17**, left), ranging from less than 20 cm below 1000 m ASL to 60 cm or more above 2000 m ASL. This result agrees with statistics reported in **Lievens et al. (2019)** and is clearly related to snow depth increasing with elevation. Importantly, bias shows no significant trend with elevation besides an increase in variability (**Figure 17**, right). This robustness in bias is particularly important for snow modelling as it ensures that predictions at large scales will not consistently over- or underestimate snow water resources. This finding again agrees with previous results in **Lievens et al. (2019)**.

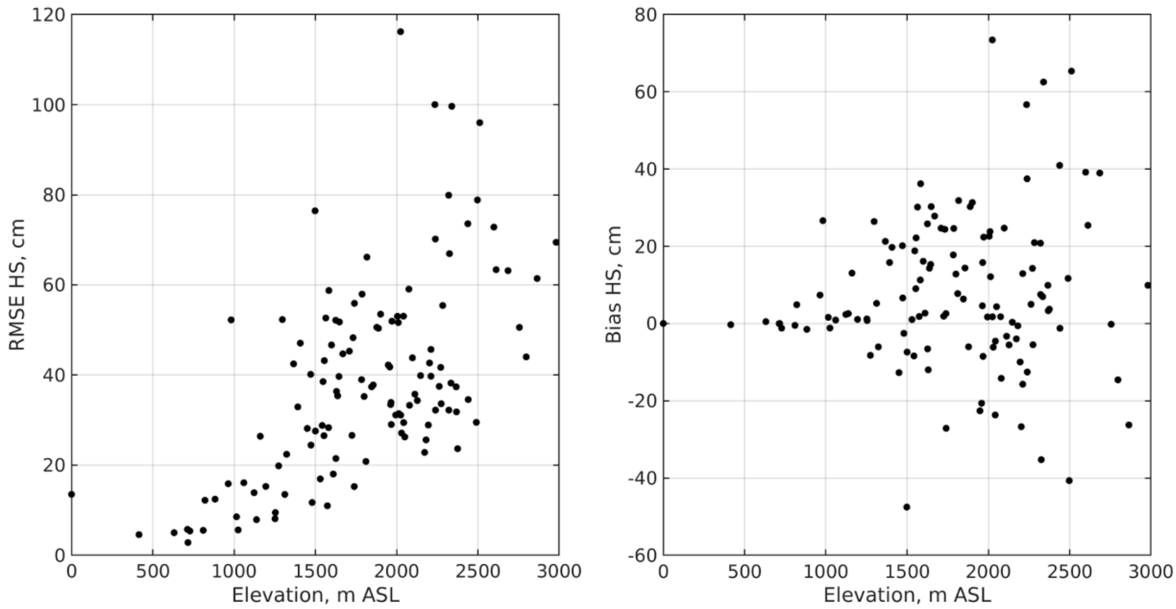

Figure 17: Root Mean Square Error (RMSE, left) and bias of C-SNOW snow depth compared to 172 ultrasonic snow-depth sensors across the Po river basin.

C-SNOW daily snow-depth values are highly correlated with co-located snow-depth-sensor measurements (Pearson's correlation coefficient r = 0.76, p-value = 1, not reported for brevity). This correlation increases with elevation, with r = 0.25 below 1000 m ASL, r = 0.55 between 1500 and 1000 m ASL, r = 0.66 between 2000 and 1500 m ASL, and r = 0.76 above 2000 m ASL (**Figure 18**) This increase in correlation with elevation is likely because low-elevation snow depth is much more ephemeral than that at high elevations, while low elevations also overlap with forests and this may both increase spatial variability in snow depth and hamper satellite retrieval. On the other hand, high elevations are generally forest-free. An increase in correlation with elevation is another asset of C-SNOW for snow modelling because it implies that the product will be more accurate where the snowpack is higher, that is, where the bulk of snow water resources is accumulated.

C-SNOW successfully captures spatial statistics of accumulation timing and amount, with an -- expected -- degradation in accuracy during spring (**Figure 19** and **Figure 20**). Importantly, accuracy of C-SNOW holds across all elevation bands, although some variability across snow seasons emerges (e.g., C-SNOW showed a drop in performance for snow season 2019 and elevations between 2000 and 2500 m ASL). From a data-assimilation standpoint, correctly capturing peak snow-depth at the end of the accumulation season is a valuable result because it drives modelling accuracy for the spring freshet and the consequent summer dry period. The expected drop in accuracy of C-SNOW during spring is evident when looking at monthly bias (**Figure 21**), since April and May are the months with the highest (absolute) values.

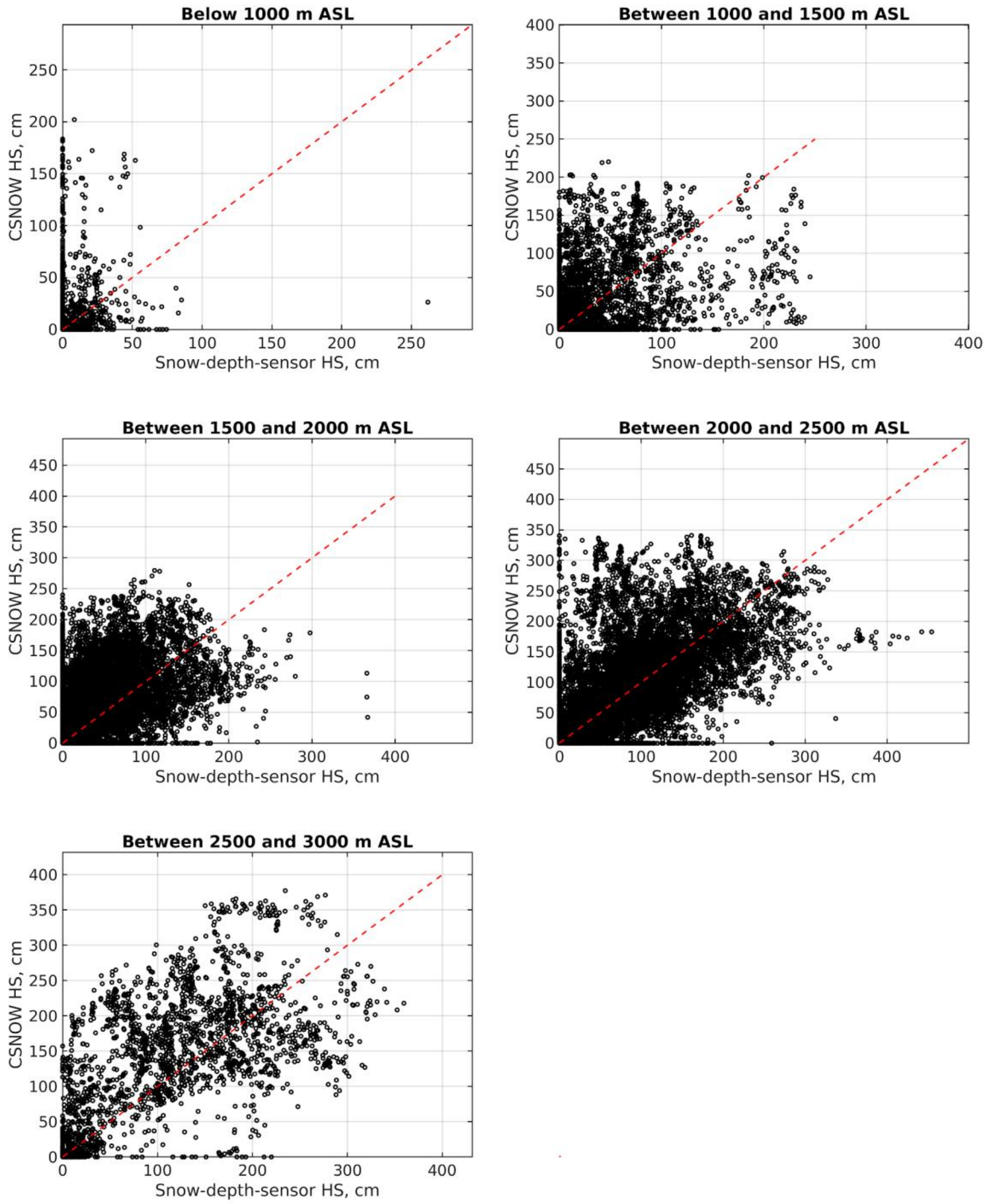

Figure 18: Sensor-based vs. C-SNOW based daily snow depth for all 172 snow depth sensors across the Po river basin, binned in five elevation bands.

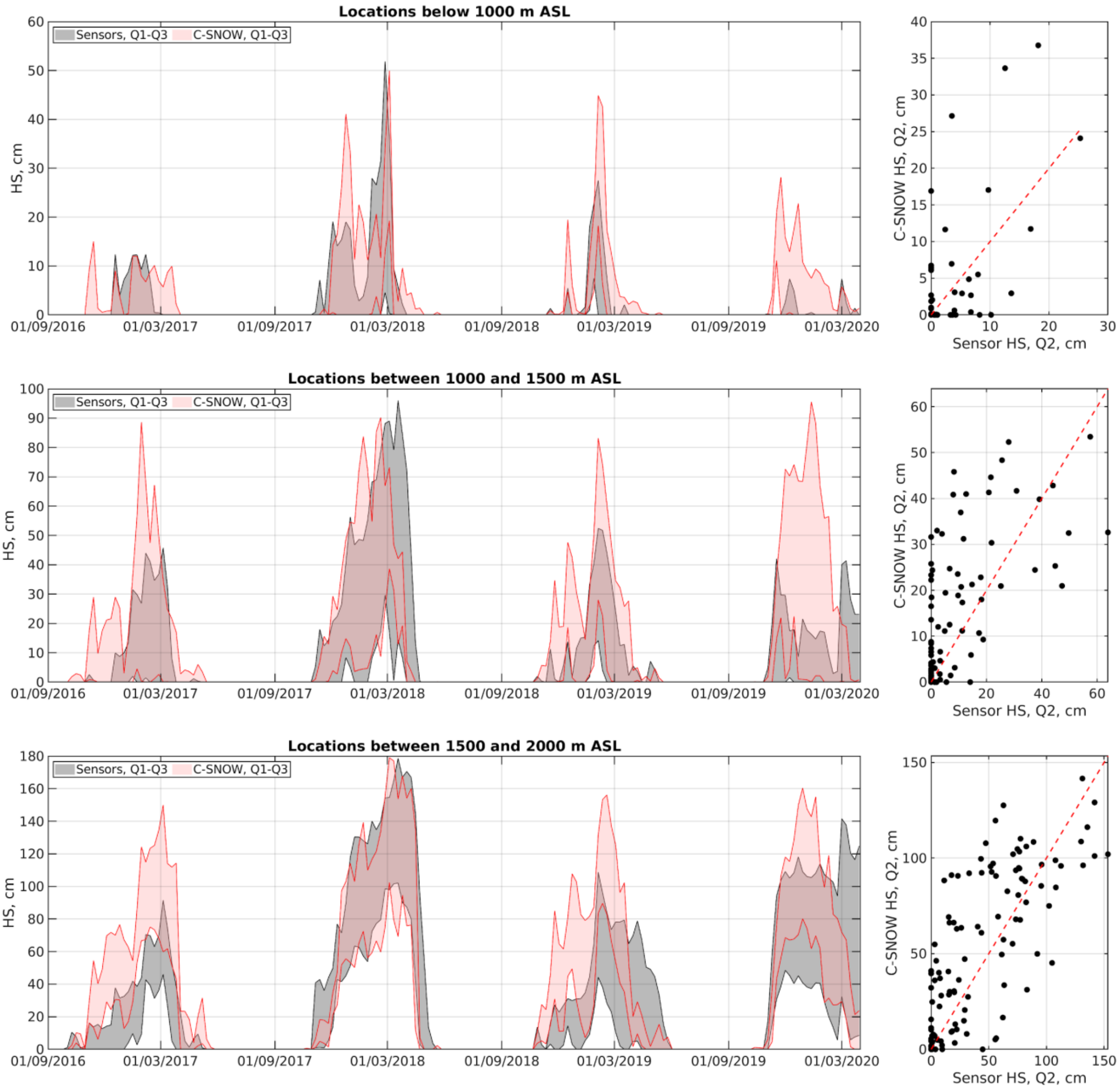

Figure 19: Sensor-based vs. C-SNOW based quartiles of daily snow depth for all 172 snow depth sensors across the Po river basin, binned in three elevation bands (see plot titles). The scatter plot on the right side compares sensor-based vs. C-SNOW based median snow depth for all sensors within that elevation band. Q1, Q2, and Q3 are the first, second, and third quartiles, respectively.

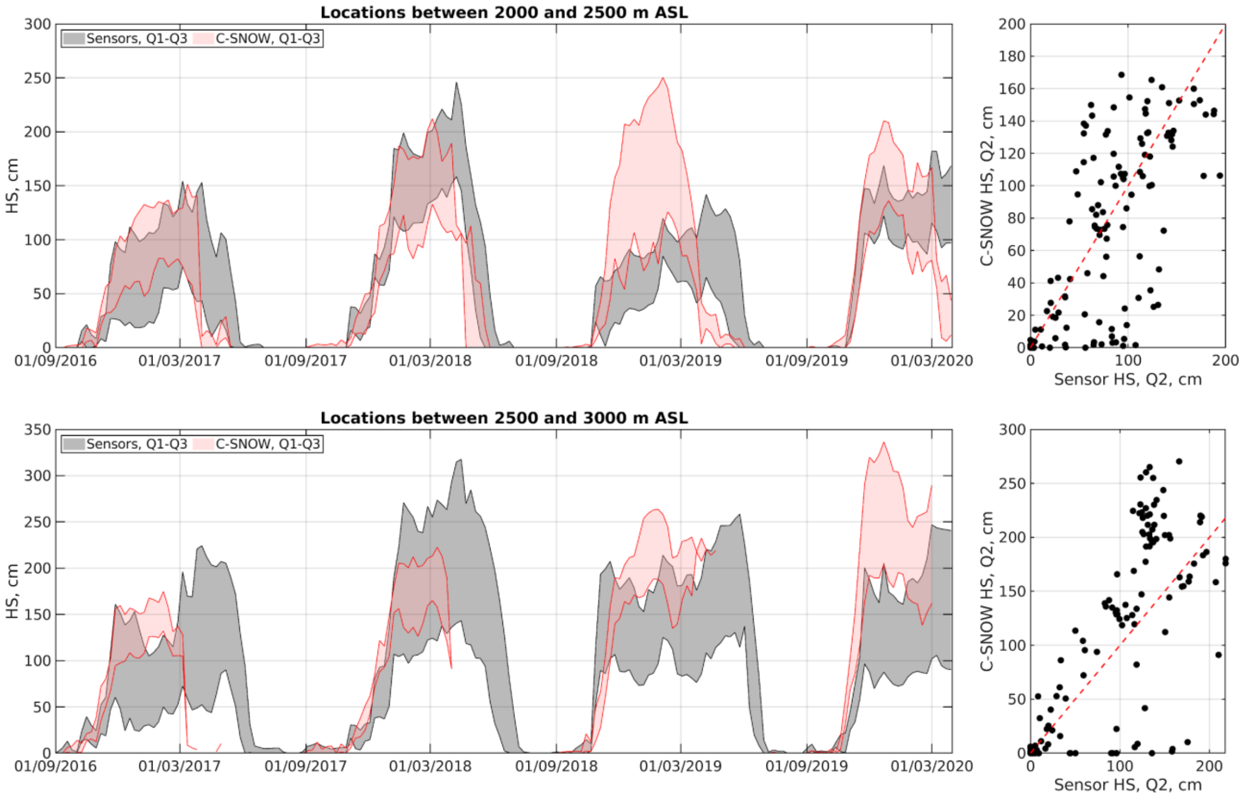

Figure 20: Sensor-based vs. C-SNOW based quartiles of daily snow depth for all 172 snow depth sensors across the Po river basin, binned in two elevation bands (see plot titles). The scatter plot on the right side compares sensor-based vs. C-SNOW based median snow depth for all sensors within that elevation band. Q1, Q2, and Q3 are the first, second, and third quartiles, respectively.

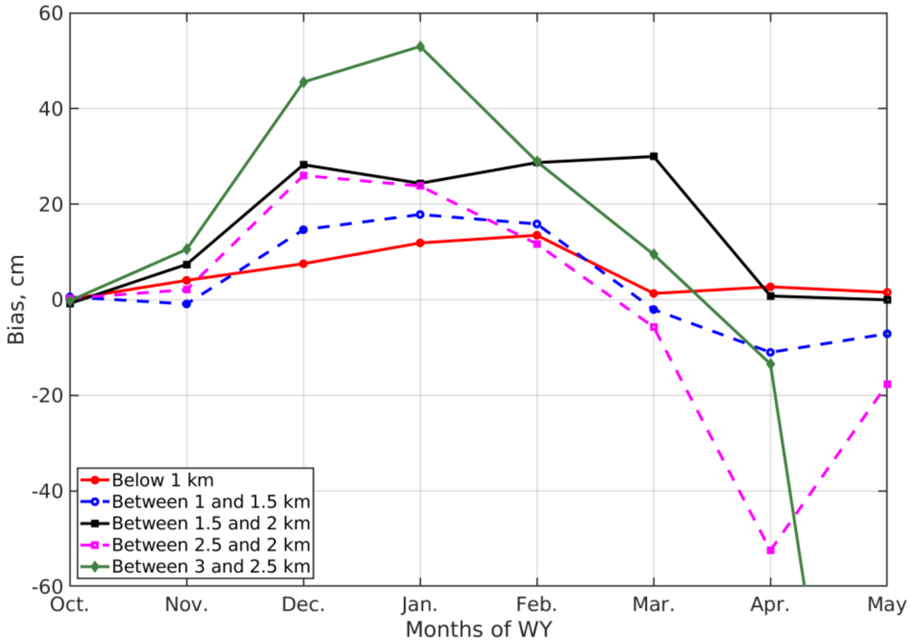

Figure 21: Monthly bias of C-SNOW snow depth for all 172 snow depth sensors across the Po river basin, binned by elevation bands.

3. Modelling system

3.1. Hydrological Modelling

Hydrological modeling activities of WP210 were performed with Continuum, CIMA's in-house model operatively used for flood forecasting by the Italian Civil Protection Department within the suite FloodPROOFS. In WP210 Continuum was used to simulate the dynamics of discharge and of other key hydrological variables in the Po river and in its tributaries. Continuum was set-up, calibrated, and then used to run different input configurations of conventional and remote-sensing data to assess the differences and potential added value of state-of-the-art satellite products, including data assimilation.

3.1.1. Data

Static data

Most input maps for the Continuum hydrological model are derived from a Digital Elevation Model (DEM), hence its choice is evaluated carefully among the available products. For this work, we chose the global USGS Hydrologic Derivatives for Modeling and Analysis (HDMA, **Verdin, 2017**) DEM with 3 arc-second spatial resolution (about 90 m at the equator), as it also provides computed and corrected hydrological derivatives including channel network and macro basins.

We used GRASS GIS to derive static layers including flow accumulation, drainage direction, channel network from the DEM. First, they were extracted at 90 m resolution. Then, the DEM was upscaled at the 1 km resolution chosen for the model domain and carved with a high-resolution stream network of the main rivers. Dikes were manually placed at specific locations to improve the matching of the 1 km resolution river network with the actual one. GRASS GIS was then applied on the upscaled DEM to produce the final static land data for all layers.

To produce the Curve Number map used in Continuum to model direct runoff or infiltration from rainfall excess, we combined information on the land use, land cover and land hydrological behaviours. In detail, we extracted land use and land cover information at the 300 m resolution grid from the global dataset ESA-CCI 2018 Land Cover map (**ESA, 2017**). The hydrologic soil type map was extracted from the HYSOGs250m (**Ross et al., 2018**) map, a globally consistent, gridded dataset of hydrologic soil groups (HSGs) with a geographical resolution of 1/480 decimal degrees, corresponding to a projected resolution of 250 m.

For the static data related to the soil capacity, we applied the USDA method for the soil texture identification using the ISRIC SoilGrids (**Hengl et al., 2017**) global maps of the soil fraction in Sand and Clay with a 250 m spatial resolution, combined with the ESA CCI SoilMoisture (**Dorigo et al., 2017**) global map of soil porosity. Standard USDA conversion tables were adopted to convert the soil texture class to the field capacity under different conditions. Glacier areas used in the cryospheric model S3M were taken from the Randolph Glacier Inventory (RGI) v6 (**Raup et al., 2007**).

To produce the static layers related to the vegetation coverage we used the global land cover map ECOCLIMAP (**Faroux et al., 2013**) with 1 km spatial resolution, as it provides a set of detailed parameters on the vegetation features.

Point data

A set of 99 reservoirs and 3 natural lakes (Maggiore, Como and Garda) have been included in the model setup (**Figure 21**). Information on the dams and the corresponding reservoirs were provided by the Italian Civil Protection Department (DPC) and from the GranD database (**Lehner et al., 2011**). Data ingested for each dam by the Continuum model include geographic coordinates, maximum stored volume, initial volume, maximum non-damaging discharge at the outflow gates, weir length, maximum storage level, outflow coefficient, and coordinates of the release point. For lakes, required metadata are the outlet coordinates, minimum volume inducing outflow discharge, initial volume, and emptying coefficient.

Hydrological data

Discharge data at 27 river gauging stations with hourly sampling frequency for the years 2016-2019 were extracted from the CIMA database, which gathers data transmitted from the Regional Centres of the DPC. 22 stations were selected for model calibration, while 5 were retained for validation only (**Figure 22**).

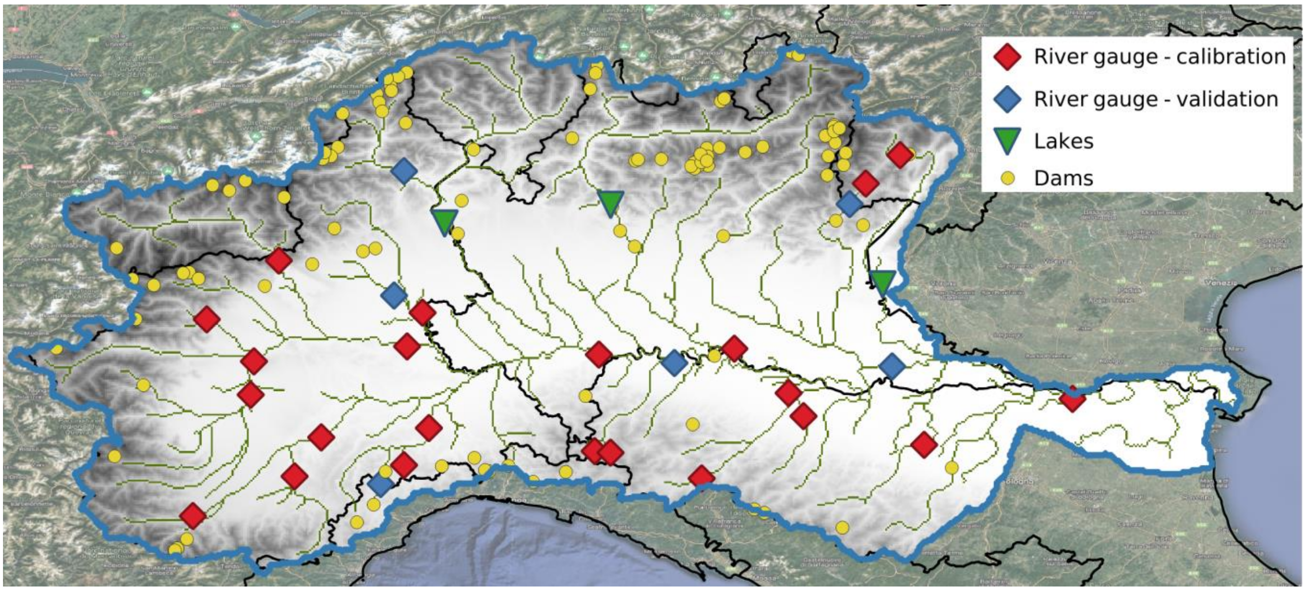

Figure 22*:* Simulated domain (blue line) and river network (dark green) of the Po river basin. Symbols show the point features implemented in the hydrological model.

Meteorological data

The hydrological model Continuum requires, as input, maps of precipitation, air temperature, humidity, wind speed and incoming solar radiation, typically at hourly resolution. The baseline hydrological simulation uses conventional meteorological data as input, which is produced by spatially interpolating point observations collected through the Regional Centres of the DPC. Hourly maps of the weather variables needed by Continuum for the Po river basin ultimately include 1258 temperature stations, 608 for relative humidity, 460 for wind speed and 278 for solar radiation. Temperature maps include an altitude correction algorithm with temperature gradients estimated at every time step by linearly interpolating available data at different elevations. Furthermore, it includes an outlier removal algorithm which discards station data with a deviation of more than 20°C from the corresponding temperature-elevation interpolating line (**Figure 23**).

Precipitation fields were estimated with the Modified Conditional Merging (MCM) technique (**Pignone et al., 2015**), which incorporates rain gauges and radar estimates. MCM is an improvement of the Conditional Merging proposed by **Sinclair and Pegram (2005)** which estimates the structure of covariance and the length of spatial correlation λ at every raingauge, taking it from the cumulated radar rainfall fields. For the Po River basin, MCM is based on 1377 rain gauges and on the mosaic of Italian weather radars.

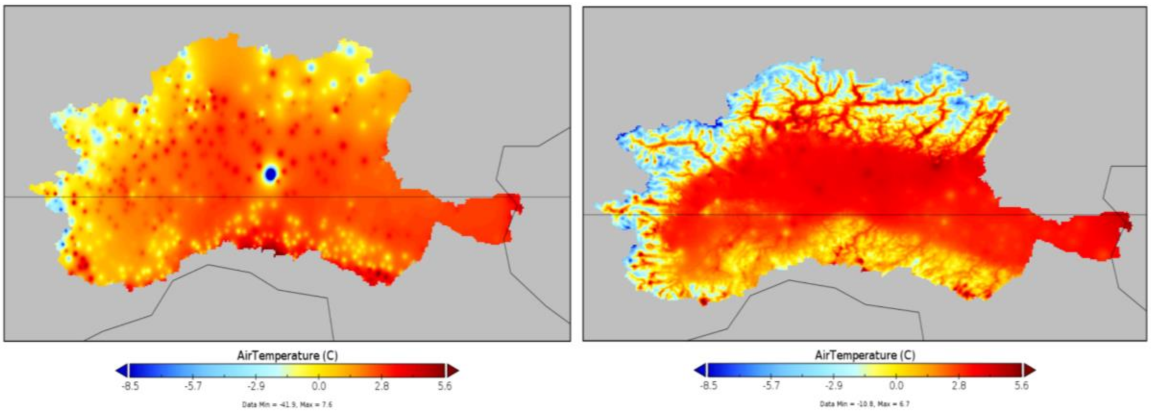

Figure 23*:* Temperature map for a sample time stamp. Interpolated map without (left) and with (right) the altitude correction and outlier removal.

3.1.2. Methods

The Continuum hydrological model

Continuum (Silvestro et al., 2013) is a distributed hydrological model relying on a morphological approach based on the identification of the drainage network components (Giannoni et al., 2000). Continuum is a tradeoff between empirical models, which are easier to implement but sometimes lack realistic features, and complex physically based models, which try to reproduce all the hydrological processes in detail, heavily relying on parameterisation. The main drawback of the latter type is that such parameterisations are likely to introduce considerable uncertainties, especially when observations are sparse, which results in a non-robust estimate of the parameters.

The Continuum model was developed keeping the physical description of the hydrological processes as simple as possible. This resulted in good performance comparable to existing models, with an increased computational efficiency. In particular, the reduced complexity of the mathematical modelling and the relatively small number of parameters lead to a considerably lower calibration effort, increasing model robustness and portability to data-scarce environments. Thanks to the increased efficiency of the code, Continuum can be easily implemented in an ensemble configuration, enabling the modeller to directly estimate the prediction uncertainties.

Continuum is able to reproduce the spatio-temporal evolution of runoff, soil moisture, energy fluxes, surface soil temperature, snow accumulation and melting, and evapotranspiration. Moreover, it can account for the vegetation seasonal variability in terms of interception and evaporation. Deep flow and water table evolution are modelled with a simple scheme that reproduces the main physical characteristics of the processes, while a distributed interaction between water table and soil surface is represented with a simple parameterisation. The introduction of the so-called force-restore equation for the surface energy balance allows the calculation of the land surface temperature, which can be used for calibration and/or assimilation of remote sensing data. In this project, Continuum was set up over the entire Po River basin (drainage area of 74,000 km^2), with a constant grid spacing of 1 km and a time resolution of 1 h.

In this project, the Continuum model was coupled with S3M, a one-layer snow model accounting for precipitation-phase partitioning (rainfall vs. snowfall), snowpack accumulation and melt, snow rheology and hydraulics, as well as glacier melt (**Boni et al., 2010**; **Terzago et al., 2019**, **Avanzi et al. 2020**). With its hybrid approach to snowmelt that decouples the radiation- and temperature-driven contributions, S3M combines a parsimonious approach with a medium-level degree of physical realism. All parameters of S3M were set based on previous validations of this model in Aosta Valley, Italy.

S3M was run using the same set of input as those described above for Continuum. After the model run, S3M yields hourly spatial fields of equivalent precipitation, which is the sum of snowpack runoff and glacier melt, plus rainfall if no snowpack is on the ground. This equivalent precipitation is used to feed Continuum *in lieu* of precipitation to account for cryospheric processes. S3M also outputs a snow mask, which is optionally used by Continuum to inhibit evapotranspiration where snow is on the ground.

Model calibration

The hydrological model requires an initial tuning phase to improve the representation of the hydrological states in the focus region. We deployed a calibration procedure that iteratively searches the combination of model parameterization to best match the available discharge observations over the calibration period at the 22 considered calibration stations. Hydrological simulations run for the model calibration cover the 2 years starting on 2018-01-01, while the calibration period starts on 2018-07-01, leaving the initial 6 months for model warm-up. The calibration tool perturbs 6 model parameters related to 4 physical hydrologic features:

1. infiltration velocity at saturation (ct)
2. field capacity (cf)
3. Curve Number (CN)
4. water sources (ws)

where the calibrated value of ws is a constant for the entire region of interest, while for ct, cf and CN, the calibration consists in a rescaling of their default maps to the best value, thus preserving their spatial patterns, which depends on geographic spatial datasets of the soil characteristics.

The cost function, based on the Kling-Gupta Efficiency, computes an error between the duration curves (described as a set of pre-selected quantiles) weighted with the logarithm of the upstream area, to give more weight to the downstream stations, without neglecting the contribution of the most upstream ones.

The calibration procedure was performed through the implementation of a parallel search algorithm. The algorithm performs an iterative exploration of the 6-dimensional parameter space: the exploration is started with N initial points values sampled with a Gaussian Latin Hypercube Sampling (here N was set to 20). For each of these N parameter sets, a hydrological simulation is performed on the calibration period, and the cost function J is computed to map the error hypersurface. The point that minimizes J is used as the centre for the following iteration, until the algorithm converges to an optimal solution (see e.g., **Figure 24**).

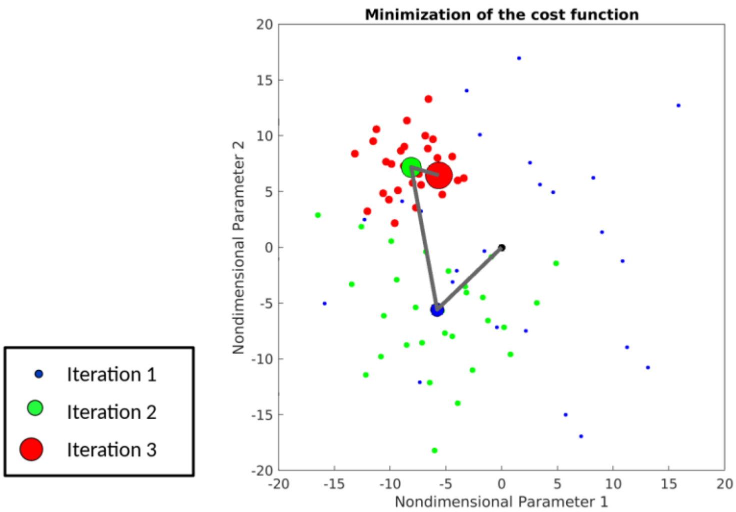

Figure 24*:* Representation of the search algorithm (in a 2-dimension space). The optimal value of each gaussian exploration is used as the centre of the next one.

Data assimilation

Satellite derived soil moisture from the Sentinel 1 RT1 product was assimilated into the Continuum model through a nudging technique **(Stauffer and Seaman, 1990, Brocca et al., 2010, Lakshmivarahan and Lewis, 2013)**. Although the nudging scheme is not optimal in a statistical sense, it is a computationally inexpensive approach to be applied in an operational framework to simulate flood predictions. The update was carried out only when the satellite data were available (once a day for soil moisture and 24 times per day for LST as the higher update frequency) following this equation:

$$X^{+}_{\mathrm{MOD}}(t) = X^{-}_{\mathrm{MOD}}(t) + G \times \left[X_{\mathrm{OBS}}(t) - X^{-}_{\mathrm{MOD}}(t)\right]$$

where X^{+}_{MOD} represents the updated modelled variable (here X denotes soil moisture), which was calculated by adding a correction term to the background-modelled variable X^{-}_{MOD}. The correction term represents the difference between observed (X_{OBS}) and modelled variable multiplied by a gain (G) that takes into account the uncertainties of both the model and the satellite observations.

Similarly, the assimilation of satellite-derived C-SNOW maps into S3M was performed using a Newtonian-relaxation approach:

$$SWE_{S3M,post} = SWE_{S3M,prior} + K\left(SWE_{obs} - SWE_{S3M,prior}\right),$$

where $SWE_{S3M,post}$ and $SWE_{S3M,prior}$ are a-posteriori and a-priori snow water equivalent (SWE), while K is a Kernel function (here assumed equal to 0.5 to mimic direct insertion).

C-SNOW maps come as snow depths, while S3M supports assimilation in the form of SWE, which is a more suitable variable to assimilate to control the water balance. Thus, snow depths from C-SNOW were converted in SWE using simulated snow density, following well established procedures at CIMA Foundation that rely on predictive uncertainty for snow density being much less than for snow depth.

Data assimilation was performed to compute a correction factor U, defined as:

$$U_{SWE} = \frac{SWE_{S3M,post}}{SWE_{S3M,prior}}$$

and then applying this U to correct the dry and the wet phases of snow:

$$SWE_{D,S3M,post} = U_{SWE} \times SWE_{D,S3M,prior}$$

$$SWE_{W,S3M,post} = U_{SWE} \times SWE_{W,S3M,prior}.$$

Along with snow depth information, we leveraged on C-SNOW to determine snow-covered and snow-free areas, and then assimilated this information into S3M to clip modeled snow cover according to satellite snow-covered regions.

More information regarding the theoretical background of SWE assimilation in S3M can be found in **Avanzi et al. (2021)**.

Model improvement

The code of the Continuum model was improved to run the scenarios with satellite derived input data. In detail, the code was adapted to allow evaporation data to be taken as model input, instead of producing it internally through a fully resolved energy balance. An option was inserted in the configuration file allowing to switch off the energy balance. In such a case, it requires both potential and actual evaporation as additional model input. These two variables are used in the updating of retention volume and total volume. All subsequent processes are then updated accordingly, including the water balance in the basin and the updating of the mass balance in lakes and reservoirs.

3.2. Hydraulic modelling

3.2.1. Methods

The flow routing along the river network is modelled adopting the software package HEC-RAS (**Hydrologic Engineering Center, 2001**) that numerically solves the Saint-Venant equations through the implicit four-point finite difference scheme (**Preissman, 1961**). In particular, the numerical model adopts a quasi-2D (quasi-two-dimensional) approach. Although less computational demanding than a full 2D scheme, the quasi-2D structure enables the reproduction of the mutual interactions among the main river channel, depicted through a series of cross-sections, and the lateral dike-protected floodplains modelled as storage areas connected to each other and/or the main channel by means of weirs mimicking the system of minor levees (**Domeneghetti et al., 2015**; **Castellarin et al., 2011b**).

The hydraulic simulation considers the middle-lower reach of River Po, which goes from Ponte Spessa (downstream the confluence with Ticino river) to the beginning of the river Delta (nearly 400 km), crossing the large flat alluvial plain named Pianura Padana (Po Valley), which is a very important agricultural region and industrial heart of Northern Italy. Topographic information adopted for the implementation of the model combines a LiDAR (2 m resolution) and multi-beam sonar survey carried out in 2005, together with traditional ground survey of about 200 cross-sections. Storage areas adopted to reproduce the behaviour of the dike-protected floodplains are simulated adopting volume-level curves extracted from the LiDAR imagery.

The model development followed the general criterion of parsimony: the model uses only one friction coefficient for the entire unprotected floodplain and nine friction coefficients associated with nine hydromorphologically homogeneous sub-reaches identified for the study reach. The subdivision into morphologically homogeneous sub-reaches originates from previous studies and has been updated in the light of the LiDAR survey (**Castellarin et al., 2011a**).

The calibration of the hydraulic models is typically carried out referring to past events for which hydrometric data (i.e., hydrographs at internal streamgauges, inundation dynamics, flood marks) are available. Previous studies carried out on the same river portion calibrated the roughness coefficients referring to ground-surveyed data collected during the major flood event occurred in 2020 (**Castellarin et al., 2010, 2011**; **Domeneghetti et al., 2015**), while other recent studies tested the potential of different single and multi-mission satellite altimetry series for this purpose (**Domeneghetti et al., 2014, 2015, 2021**).

Within this project, the hydraulic model will adopt the discharge series estimated at the upstream station of the main river and considered tributaries in order to simulate the flow routing along the middle-lower portion of the Po river and simulate the hydraulic dynamic of the river in the period of interest (2017-2019). Hydraulic loads at the boundary conditions will be provided by the hydrological simulation carried out over the Po basin by CIMA. Although the quasi-2d model has already been calibrated, alternative procedure for calibrating the model by using recent altimetry information (e.g., Cryosat, Sentinel 3A and 3B) will be eventually tested.

The simulation period covers three years, from January 2017 to December 2019. During this period, the quasi-2D model will provide time series of water levels, flowing discharges, flow velocities and many other hydraulic parameters obtained from the hydrodynamic simulation. These series can be extracted at any cross-section of interest along the study area, enabling the comparison with ground-observed series where available. The spatial and temporal availability of these variables will enable additional investigation in terms of water availability, river dynamics and critical scenarios. Furthermore, the investigations on the use of satellite data for the calibration may provide useful insight on the river parameter setting currently used for the model.

3.2.2. Discussions

Linking the flow routing simulation with the hydrological model will offer the possibility to evaluate the potential of the overall system under different perspectives, with impacts on water management issues that may concern water availability, flowing dynamics, droughts and floods as well as environmental, economic and social impacts. In particular, the modelling chain will provide insights on the usefulness of detailed satellite data in terms of:

- flood genesis: how spatial and temporal hydrological variability concur to flood generation and propagation along the river network. This also implies the capability to provide more accurate estimation of critical inundation scenarios that may be simulated with other modelling solution (e.g., 2D model);
- discharge and water level dynamics: evidence on the modelling chain capability to reproduce flow regime (e.g., flow duration curve) and water level at a given river cross-section in time. This information has potential implication for optimal water usage management (in agricultural, civil, industrial applications, etc.);
- modelling calibration: referring to additional satellite data (e.g., altimetry data) for model calibration can ensure the possibility to extend the modelling chain implemented in this study to regions where in-situ data normally used for this task are lacking.

3.3. 2D Hydraulic modelling

3.3.1. Methods

The flood hazard map delineation is the result of a chain of hydrologic and hydraulic models. In the DTE-Hydrology Project, a 2D hydraulic model is employed for flooding analysis. The model is named WEC-Flood and is suitable for flood hazard maps estimation in areas characterized by high urbanization and complex topography (Sinagra et al., 2020). The first step of the analysis is characterized by a procedure to discretize spatially the entire basin through the use of the Hydronet tool. This component generates a Triangulated Irregular Network (TIN) covering the urban and not urban areas, serving likewise for the topographic model and for supporting the spatial discretization of the governing flow and momentum equations. The method leverages topographical data coming from a digital terrain model (DEM), integrated by other available information, and leads to a TIN, also taking hydraulic infrastructure elevations into account. The last step deals with applying a 2D hydraulic model to estimate the flooded area using the same discretization of the TIN model and using as input data the discharge hydrographs estimated by the hydrological modelling.

The application of a 2D model for simulating flooding events allows one to consider the effects due to the floodplains' topography complexity and to calibrate in a detailed way the domain parameter, mainly the roughness properties. The model requires as input data: 1) a detailed DEM of the area to be investigated; 2) additional topographic information representing hydraulic singularities as culverts, levees and bridges, to consider their impact on the flow dynamics; 3) upstream and downstream boundary conditions, i.e. discharge hydrographs from the hydrological modelling, water levels at the confluence, rating curve relationships, etc.

The model solves the diffusive form of the Saint Venant Equations using the same spatial discretization provided by the TIN computed by the first Hydronet component. The model adopts the diffusive wave approximation of the Saint Venant Equations to obtain a system of differential equations in the 1D and 2D computational domains, that has several advantages compared to dynamic modelling. Among these: 1) with the same simulated time and computational capacity, guarantees the solution in much faster times than the complete modelling; 2) the simplicity of the boundary conditions required by diffusive modelling and the hardness of the diffusive solution, in terms of water height, against the topographical error present in the input data. The two equations are solved in the piezometric head unknown. To solve the Equations, an unstructured hybrid mesh is used. 1D channels are discretized using quadrilateral elements, with one couple of opposite edges overlapping the trace of two river sections and the other couple connecting their ends. The trace of each river section is extended up to the minimum topographic elevation where 1D flow conditions are expected. The 2D computational domain is given by the whole area of the catchment basin and is discretized by triangular elements satisfying the Generalized Delaunay conditions. The use of the diffusive model in the 2D domain, instead of the fully dynamic one, is mainly motivated by the smaller sensitivity of the computed water depth with respect to the topographic error. The model is solved in the context of the MAST (MArching in Space and Time) approach (**Aricò and Tucciarelli, 2007**), where the solution at the end of each time step is sought after through a fractional time step procedure, splitting the original problem in a prediction plus a correction sub-problem.

The WEC-Flood model application is finalized to perform a two-dimensional analysis to define the flood-prone areas. The expected results are hydraulic hazard maps identifying the area affected by flooding, the water depth value at the different nodes of the computational grid and also the discharge hydrograph at different sections selected along the main channel including the outlet section.

The model calibration can usefully take advantage of the mapping of flooded areas provided by high resolution satellites (Sentinel-1). Specifically, past flood events for which satellite mapping of flooded areas are available can be used as case studies, considering the high resolution observed areas as the benchmark for the model calibration. The use of the high-resolution satellite data represents a significant improvement for the 2D model calibration compared with using as benchmark the information of the extension of the flooded areas that can be derived by fragmentary ground/remote data (e.g. pictures, videos, direct testimonies, indications derived from videos recorded during helicopter flights, etc.). Specifically, the case study selected for the project activity concerns the analysis of the inundation process for the flood event that occurred along the Enza river, a right tributary of the Po river, in December 2017. The model application is addressed to reconstruct the dynamic of this inundation using the output of the hydrological model as input discharge and the flooded area depicted by the satellite for the parameter values calibration.

3.3.2. Discussions

The application of the WEC-Flood two-dimensional model allows to assess the impact of a flood event on a flood-prone area. During the DTE-Hydrology project, the distributed hydrological model Continuum is used to simulate the discharge in the Po river and its tributaries considering two different scenarios: for a first analysis, the model uses ground and weather radars meteorological data; a second study includes the use of satellite precipitation and evapotranspiration as input and the assimilation of satellite soil moisture and snow depth. Therefore, two different hydrological inputs will be available to be used as boundary conditions for WEC-Flood whose results' comparison would allow to identify the effect of using high resolution satellite data in the analysis.

Moreover, once the hydraulic model is calibrated considering a past flooding, further investigations on possible scenarios can be analysed. For example, during the selected case study (flood occurred on December 2017 along the Enza river) the flooding was mainly due to a significant levee failure. The analysis of the flood could be developed also assuming the levee undamaged in order to investigate if the inundation of the floodplains would have occurred in any case and with what characteristics.

3.4. Landslide modelling

3.4.1. Methods

Within the DTE-Hydrology project, a slope stability module will be linked to the hydrological modelling chain. In this way, the simulated soil moisture time series over the study area will be used to force the slope stability module. The physically-based approach is based on the infinite slope approach (**Skempton, 1957**), thus it is particularly suited for shallow landslides, as the investigated depth of the landslide is negligible (or very small) compared to the length of the unstable area. On the other hand, this approach limits the needed input data and the modelling of forces and stresses in play within the soil layer. In order to develop a system able to estimate the soil stability conditions under different soil saturation degrees, the formulation proposed in **Lu and Likos, 2004** and **Lu et al., 2010** will be implemented to directly use the output of the distributed high-resolution hydrological model and the satellite soil moisture estimates developed during the project.

The stability module is based on the relationship between soil moisture and suction stress. This stress refers to the force acting between the particles of an unsaturated soil due to effects of negative pore water pressure and surface tension that tend to pull the grains toward one another (**Song, 2014**). In this way, the Factor of Safety (FS) over the study area through time will be estimated as a function of soil saturation conditions.

Usually, a physically-based approach is highly demanding in terms of input parameters (angle of internal friction, cohesion, volume weight), and the application is limited to the slope scale due to the knowledge of soil characteristics and its high variability in space. In the framework of DTE-Hydrology, the module will be tested within the Oltrepo Pavese area, close to Pavia city, over three catchments with detailed information in terms of soil type and characteristics and with a substantial landslide events catalogue during the analysis period (2016-2019).

Moreover, it will be tested for the first time the use of high resolution DTE-Hydrology satellite soil moisture products as direct input for the slope stability module. In this way, the stability analysis will be performed over larger areas, without the need of high-resolution modelled data, saving computational time and resources in the perspective of an operational use also for Civil Protection purposes.

The expected results of the slope stability analysis will be maps of low stability conditions at high spatial and temporal resolution, obtained through the use of satellite and modelled soil moisture data over the study area.

The model will be at first tested and calibrated over the Oltrepo Pavese area by evaluating its performance in terms of identification of past landslide events during the analysis period. The use of high-resolution data will overcome the limitations related to the spatial interpolation of input variables generally used for such applications, i.e. rainfall, and will help a better definition of the model itself. Specifically, the case study selected for the project activity will be related to the analysis of the past events that occurred over three catchments (Versa, Scuropasso and Ardivestra) located in the Oltrepo Pavese area, during two intense rainfall storms that triggered more than 100 landslides.

3.4.2. Discussions

The outcome of the slope stability module will define the risk level over the study area after a rainfall event. Within the DTE-Hydrology project, the slope stability module will be tested and forced with the soil moisture output of the hydrological model Continuum and with the high-resolution satellite soil moisture products developed during the project. The comparison of the FS provided by the module will highlight the impact of using the two different input sources. In the perspective of developing an operational tool for landslide risk assessment, the output of the model can be used to define “landslide guidance” and to evaluate the risk of a certain area in the future by using rainfall (or soil moisture) weather forecast.

4. DTE Hydrology Case study

For DTE Hydrology, based on the interactions with stakeholders in the meeting on 20th January, 2021, and based on the internal discussion with project partners, three case studies have been finally selected addressing: 1) water resources management, 2) river flow and flooding, 3) landslides (see **Figure 1**).

4.1. Water resources management

For the water resources management, two case studies of interest for stakeholders have been identified.

- **Water scarcity monitoring and management at basin scale**

  The knowledge of the different components of the water cycle at basin scale, even aggregated at weekly and monthly time scale, would allow a better understanding of the water availability (storages and fluxes) to be used for optimizing water distribution for agricultural, civil and industrial purposes. The DTE Hydrology system will allow the large-scale assessment of the different components of the water cycle at basin scale, i.e., water fluxes (precipitation, evaporation, runoff, river discharge) and storages (soil moisture and snow), in the different parts of the Po valley and particularly over the mountain areas (alps as water towers).

  For this application, the new capabilities of the DTE Hydrology system, with respect to the state-of-the-art, are: (1) expected improved estimation of water fluxes, precipitation and evaporation, thanks to the integration of high-resolution satellite products, and (2) expected improved estimation of snow water storages over the Alps and Apennines thanks to the snow depth satellite observations provided by Sentinel-1 (observations plus data assimilation).

  The expected output of the DTE Hydrology system will be monthly (weekly) estimates of water fluxes and storages aggregated at basin scale (identified from stakeholders) for the period 2017-2019. The analysis of such data with respect to water scarcity/drought periods occurred in the basin will allow us to identify the potential benefits of the system and its limitations.

- **Irrigation water management at plot scale and consortium scale**

  The knowledge of water availability at field and consortium scale is mostly unknown, particularly over irrigated areas in which the knowledge of the amount of water applied for irrigation is extremely important. The availability of high-resolution soil moisture and evaporation observations from satellites coupled with high resolution simulation of soil moisture and evaporation from hydrological modelling will allow us to identify the areas in which irrigation occurs, and also to quantify the amount of water applied for irrigation. The success of this challenging task is related to the quality of satellite and modelled data, but it can provide invaluable information for the correct management and optimization of water resources. Moreover, the availability of high-resolution precipitation would allow us to distinguish between areas affected by localised storms (e.g., during summer) from areas in which rainfall has not occurred. For the areas affected by thunderstorms crops might be damaged, instead for the non-affected areas irrigation would be needed for maintaining crop conditions in a good status. This information has been required by stakeholders.

For this application, the new capabilities of the DTE Hydrology modelling system are: (1) the possibility to detect and quantify the amount of water applied for irrigation at 1 km scale thanks to the availability of 1 km satellite and modelled soil moisture and evaporation data, (2) the possibility to identify areas affected by localised storms (and potential damages) thanks to the availability of 1 km resolution rainfall data.

The expected output of the DTE Hydrology system will be 1km/hourly soil moisture and evaporation maps obtained from hydrological modelling and the corresponding maps as obtained from satellite products. From the differences between the maps irrigation detection and quantification will be estimated, as well as the available water storages for agricultural water management.

4.2. River flow and flooding prediction

The enhanced simulation of the water cycle components at large scales (e.g., the overall Po river basin) expected by DTE Hydrology will provide, among other hydrological variables, a better estimation of the water fluxes (i.e., river discharge) expected along the superficial river network. The high spatial resolution of the hydrological analysis will enable a better estimation of basin dynamics, thus highlighting the different behaviours and contributions of sub-basins in forming flow hydrographs along the main channel. This detailed information represents the boundary conditions for the hydraulic modelling (1D and 2D) of flow routing dynamics along the rivers, which in turn ensures a more proficient evaluation of the water availability (e.g., simulation of the hydrologic regime at a given section) and potentially hazardous scenarios (e.g., extreme floods and severe droughts). In addition, the 1D hydraulic model of the main course of the Po river will be calibrated exploiting the added values of dense altimetry measurements, while the calibration of the 2D model developed to simulate the flooding events (e.g., Enza river flood, December 2017; **Figure 25**) will take advantage of Sentinel-1 images of the flooded areas.

For this application, the new capabilities of the DTE Hydrology system, with respect to the state-of-the-art, are: (1) enhanced understanding of basin dynamics in the determination of flow hydrographs at different locations over the basin (i.e., sub-basins contribution depending on hydrological boundary conditions); (2) better estimation of flow rates at the sections of interest for a more accurate evaluation of water availability and flowing conditions. These could also benefit the evaluation of the interactions among superficial flows with water tables, as well as the definition of water management policies for social and agricultural uses; (3) enhanced model calibration for large rivers by using satellite altimetry and NIR products; (4) accurate simulation of flood-prone areas by using satellite images for 2D hydraulic model calibration.

The expected output of the DTE Hydrology system will be hourly (or even sub-hourly) estimates of discharge and water level along the Po river for the period 2017-2019. Those series will be used to evaluate water availability (e.g., in terms of flow duration curves) or critical scenarios, such as droughts or flood events. Concerning the latter, the analysis will provide inundation maps for the flood event occurred along the Enza river in December 2017 that caused extensive flooding mainly due to a levee failure that will be included in the hydraulic simulation.

Figure 25*:* Enza flood event. Left) aerial image of flooding during the event, right) simulated flooded area for the event by Emilia Romagna region.

4.3. Landslide hazard prediction

Currently, landslide hazard is assessed by means of physically-based models over limited areas, due to the large amount of data and information needed, or by means of empirical relationships using triggering factors such as rainfall intensity and duration, for instance, for large areas. The use of remote sensing information is very limited, despite the great availability of products with ever increasing spatial and temporal resolution. Up to now, the highest temporal (daily) and spatial (kilometres) resolution provided by state-of-the-art rainfall and soil moisture products are considered still very coarse for geo-hydrological hazard assessment, due to the limited size of the landslides that normally impact society.

The DTE-Hydrology project will provide improved input variables characterized by both high temporal (hourly) and spatial (1km) resolutions that will foster their use within a slope stability module over large areas. The use of 1 km soil moisture (obtained through Continuum model or through satellite retrievals) will allow us to recognize wetter zones and to better identify small areas prone to landslides.

For this application, the new capabilities of the DTE Hydrology system, with respect to the state-of-the-art, are: (1) expected improved estimation of slope stability conditions, thanks to the use of high-resolution modelled and satellite soil moisture and precipitation products within a physically-based approach, and (2) expected better model formulation and calibration over the case study area.

The expected output of the DTE Hydrology system will be daily (hourly) estimates of Factor of Safety over the case study area for the period 2016-2019 (**Figure 26**). The analysis of past landslide events triggered over this area will allow us to identify the potential added-value of the system and its limitations. Moreover, the joint use of satellite and modelled data will provide a comparison of the two methodologies, highlighting the possibility of merging the two sources of information.

Figure 26*:* Case study location for landslide hazard assessment

5. DTE Hydrology Prototype description

Increasing accessibility to the results of the hydrological modeling for water resource management, flood risk, landslide risk, and drought risk is achievable via an interactive visualization tool. The development of this tool also increases the ability for non-scientific decision makers to familiarize themselves directly with the results of the hydrological modeling. The following will provide a description of the current dashboard functionality, and a review of the current microservice solution to support the dashboard functionality, and the testing carried out against it.

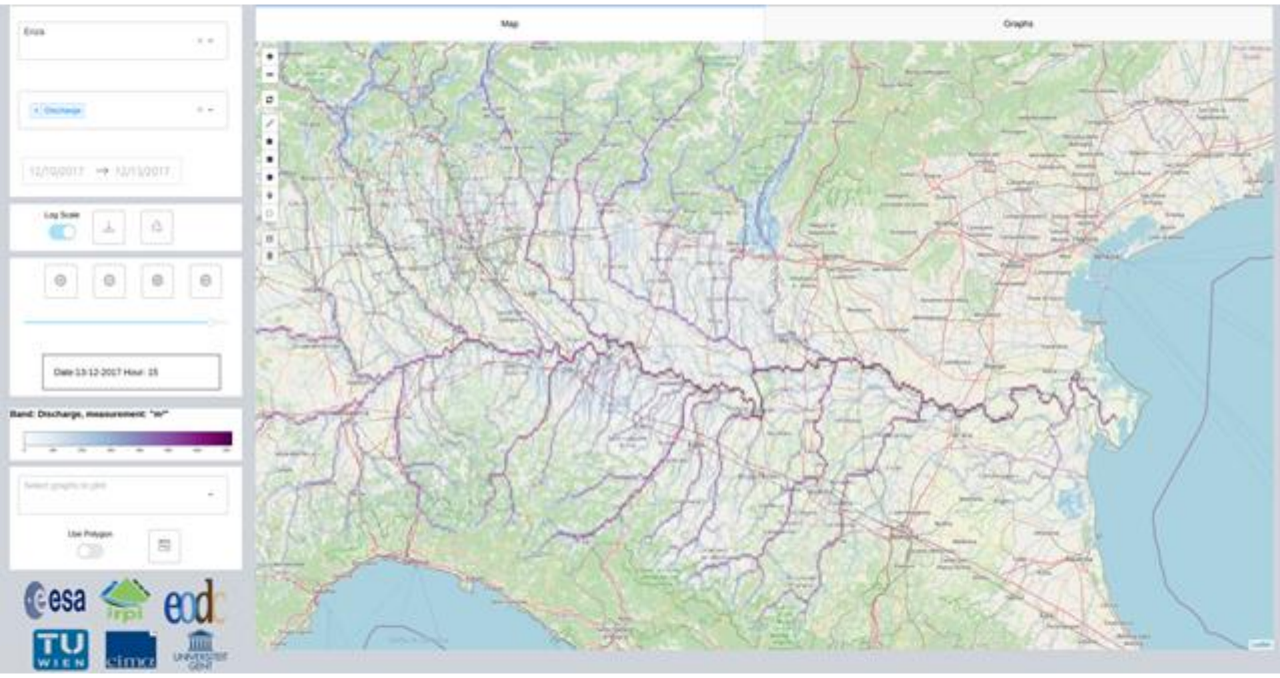

Figure 27: Dashboard Illustration

The dashboard has been written using the plotly dash library, an open source python library that makes analytical dashboard development possible solely in python. Having this development purely in python provides a single point for code management and increases the speed at which future patching or failure investigation can occur. This does come at an initial cost at implementing additional functionality to the dashboard if it does not exist yet. However, it is possible to tailor solutions in javascript for additional functionality, and implement them in python using the plotly boilerplate. The current scope of this library is sufficient for fulfilling the functional requirements of the dashboard, and implementing any additional functions in the future.

The current functional capabilities of the dashboard are; let the user browse the variable of discharge, soil moisture, precipitation, and evaporation, to allow the user to define temporal extents within the dashboard, to allow the user to generate various graphs for their chosen variable, and to allow the user to specify custom spatial extents for graph generation. These capabilities are all met by a micro-service solution, utilizing open-data cube and DASK.

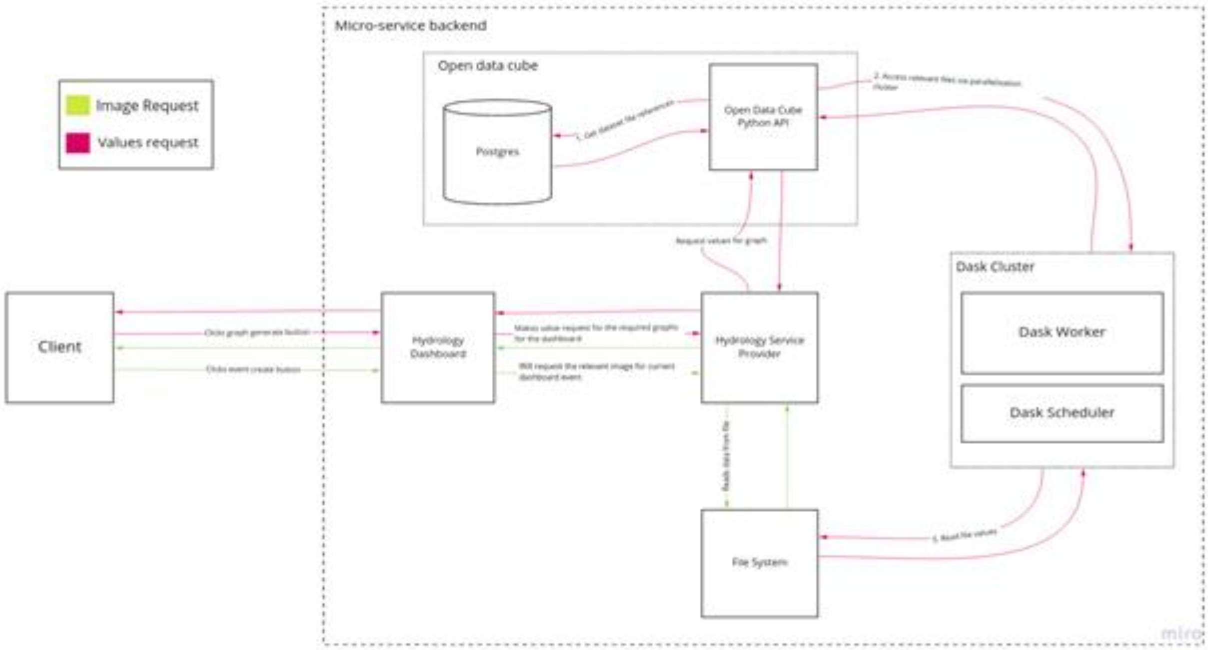

Figure 28: Dashboard Functional Diagram

The current micro-service supports low scale deployments of the application, but further development and refactoring would improve the deployments ability to function for higher workloads, and improve the applications scalability. Currently, the dashboard does not support user defined spatial extents for requesting images, so the solution for image writing was to write from file, as this can be done quickly.

However, load tests were carried out to stress the efficacy of this approach. One round of testing required the service to process 1500 image requests, this lasted for 3 rounds. In round 1 they were requested in single order (avg. request time 0.153s), in round 2 requests were made 15 at a time (avg. request time 1.121s), and in round 3 requests were made 50 at a time (avg. request time 3.619s). Increasing the load horizontally allows for some evaluation of the current architecture setup. The rate at which users can request images from the dashboard using the play function is 1.25s, so the current microservice deployment only fractionally provides a usable service for 15 people with regards to image browsing. Testing was only carried out directly on the core service for the visual data exploration. So writing the images from the file is limited as the service load increases.

The solution to reducing service time in this instance, would be to increase the usage of the dask cluster, this would remove the direct reading of the file system from the Hydrology Service Provider (Fig. 28). In addition, code is not optimized and loads values externally from the parallelization environment. This creates an increase in CPU and memory usage while non-optimal services load the data values. Manipulation of the data values is required for the dashboard, but this can be improved by ensuring it is carried out within the dask cluster. This would improve the rate at which graphs and image values can be retrieved and returned. Additionally, the dask cluster can be used for writing images, this would make it possible to parallelize the rendering as well as the data resampling. Lastly, this change would also make it easy to support rendering for user defined spatial extents, in the same way that graphs can be prepared for these extents.

The current deployment supports the current functional requirements with a low-scale deployment in mind. However, with moderate refactoring and optimization, it would be possible to serve the needs of the dashboard to a higher volume of users.

6. References

Avanzi, F., Gabellani, S., Delogu, F., Silvestro, F., Cremonese, E., Morra di Cella, U., Ratto, S., and Stevenin, H.: S3M 5.1: a distributed cryospheric model with dry and wet snow, data assimilation, glacier mass balance, and debris-driven melt, Geosci. Model Dev. Discuss. [preprint], https://doi.org/10.5194/gmd-2021-92, in review, 2021.

Avanzi, F., Ercolani, G., Gabellani, S., Cremonese, E., Pogliotti, P., Filippa, G., Morra di Cella, U., Ratto, S., Stevenin, H., Cauduro, M., and Juglair, S.: Learning about precipitation lapse rates from snow course data improves water balance modeling, Hydrol. Earth Syst. Sci., 25, 2109–2131, https://doi.org/10.5194/hess-25-2109-2021, 2021.

Blunden J., Arndt D.S., editors (2020). State of the Climate in 2019, Bulletin of the American Meteorological Society. 1;101(8):S1–429.

Boni, F. Castelli, S. Gabellani, G. Machiavello and R. Rudari (2010). Assimilation of MODIS snow cover and real time snow depth point data in a snow dynamic model. 2010 IEEE International Geoscience and Remote Sensing Symposium, Honolulu, HI, USA, pp. 1788-1791, doi: 10.1109/IGARSS.2010.5648989.

Brocca, L., Melone, F., Moramarco, T., Wagner, W., Naeimi, V., Bartalis, Z., and Hasenauer, S.: Improving runoff prediction through the assimilation of the ASCAT soil moisture product, 14, 1881–1893, https://doi.org/10.5194/hess-14-1881-2010, 2010.

Brocca, L., Filippucci, P., Hahn, S., Ciabatta, L., Massari, C., Camici, S., Schüller, L., Bojkov, B., Wagner, W. (2019). SM2RAIN-ASCAT (2007-2018): global daily satellite rainfall from ASCAT soil moisture. Earth System Science Data, 11, 1583–1601, doi:10.5194/essd-11-1583-2019.

Brocca, L., Massari, C., Pellarin, T., Filippucci, P., Ciabatta, L., Camici, S., Kerr, Y.H., Fernández-Prieto, D. (2020). River flow prediction in data scarce regions: soil moisture integrated satellite rainfall products outperform rain gauge observations in West Africa. Scientific Reports, 10, 12517, doi:10.1038/s41598-020-69343-x.

Camici, S, Massari, C., Ciabatta, L., Marchesini, I., Brocca, L. (2020). Which rainfall metric is more informative about the flood simulation performance? A comprehensive assessment on 1318 basins over Europe. Hydrology and Earth System Sciences, 24, 4869–4885, doi:10.5194/hess-24-4869-2020.

Castellarin, A, Di Baldassarre, G., Brath, A. (2011). Floodplain management strategies for flood attenuation in the river Po. River Res. Appl. 27, 1037–1047. doi:10.1002/rra.1405

Castellarin, Attilio, Domeneghetti, A., Brath, A. (2011). Identifying robust large-scale flood risk mitigation strategies: A quasi-2D hydraulic model as a tool for the Po river. Phys. Chem. Earth, Parts A/B/C 36, 299–308. doi:10.1016/j.pce.2011.02.008

Domeneghetti, A., Carisi, F., Castellarin, A., Brath, A. (2015). Evolution of Flood Risk Over Large Areas: Quantitative Assessment for The Po River. J. Hydrol. 527, 809–823. doi:10.1016/j.jhydrol.2015.05.043

Domeneghetti, A., Molari, G., Tourian, M.J., Tarpanelli, A., Behnia, S., Moramarco, T., Sneeuw, N., Brath, A. (2021). Testing the use of single- and multi-mission satellite altimetry for the calibration of hydraulic models. Adv. Water Resour. doi:https://doi.org/10.1016/j.advwatres.2021.103887

Domeneghetti, A., Tarpanelli, A., Brocca, L., Barbetta, S., Moramarco, T., Castellarin, A., Brath, A. (2014). The use of remote sensing-derived water surface data for hydraulic model calibration. Remote Sens. Environ. 149, 130–141. doi:10.1016/j.rse.2014.04.007

Dorigo, W., Wagner, W., Albergel, C., Albrecht, F., Balsamo, G., Brocca, L., Chung, D., Ertl, M., Forkel, M., Gruber, A., Haas, E., Hamer, P. D., Hirschi, M., Ikonen, J., de Jeu, R., Kidd, R., Lahoz, W., Liu, Y. Y., Miralles, D., Mistelbauer, T., Nicolai-Shaw, N., Parinussa, R., Pratola, C., Reimer, C., van der Schalie, R., Seneviratne, S. I., Smolander, T. and Lecomte, P. (2017). ESA CCI Soil Moisture for improved Earth system understanding: State-of-the art and future directions, Remote Sensing of Environment, 203, 185–215, https://doi.org/10.1016/j.rse.2017.07.001.

ESA (2017) Land Cover CCI Product User Guide Version 2. Tech. Rep. Available at: maps.elie.ucl.ac.be/CCI/viewer/download/ESACCI-LC-Ph2-PUGv2_2.0.pdf.

ESA (2017) Land Cover CCI Product User Guide Version 2. Tech. Rep., 2017.

Faroux, S., Kaptué Tchuenté, A. T., Roujean, J.-L., Masson, V., Martin, E. and Le Moigne, P. (2013) ECOCLIMAP-II/Europe: a twofold database of ecosystems and surface parameters at 1 km resolution based on satellite information for use in land surface, meteorological and climate models, Geoscientific Model Development, 6(2), 563–582, https://doi.org/10.5194/gmd-6-563-2013.

Giannoni, F., Roth, G. and Rudari, R. (2000) A semi-distributed rainfall-runoff model based on a geomorphologic approach, Physics and Chemistry of the Earth, Part B: Hydrology, Oceans and Atmosphere, 25(7–8), 665–671, https://doi.org/10.1016/s1464-1909(00)00082-4.

Hengl, T., Jesus, J. M. de, Heuvelink, G. B. M., Gonzalez, M. R., Kilibarda, M., Blagotić, A., Shangguan, W., Wright, M. N., Geng, X., Bauer-Marschallinger, B., Guevara, M. A., Vargas, R., MacMillan, R. A., Batjes, N. H., Leenaars, J. G. B., Ribeiro, E., Wheeler, I., Mantel, S. and Kempen, B. (2017). SoilGrids250m: Global gridded soil information based on machine learning, PLOS ONE, 12(2), e0169748, https://doi.org/10.1371/journal.pone.0169748.

Hydrologic Engineering Center (2010). HEC-RAS hydraulic reference manual. US Army Corps of Engineers, Davis.

Kling, H., Fuchs, M., and Paulin, M. (2012). Runoff conditions in the upper Danube basin under an ensemble of climate change scenarios, Journal of Hydrology, 424–425, 264–277, https://doi.org/10.1016/j.jhydrol.2012.01.011.

Lakshmivarahan, S. and Lewis, J. M.: Nudging Methods: A Critical Overview, in: Data Assimilation for Atmospheric, Oceanic and Hydrologic Applications (Vol. II), edited by: Park, S. K. and Xu, L., Springer, Berlin, Heidelberg, 27–57, https://doi.org/10.1007/978-3-642-35088-7_2, 2013.

Lehner, B., Liermann, C. R., Revenga, C., Vörösmarty, C., Fekete, B., Crouzet, P., Döll, P., Endejan, M., Frenken, K., Magome, J., Nilsson, C., Robertson, J. C., Rödel, R., Sindorf, N. and Wisser, D. (2011). High-resolution mapping of the world's reservoirs and dams for sustainable river-flow management, Frontiers in Ecology and the Environment, 9(9), 494–502, https://doi.org/10.1890/100125.

Lu, N., Godt, J.W., Wu, D.T., (2010). A closed-form equation for effective stress in unsaturated soil. Water Resour. Res., 46, p. W05515

Lu, N., Likos, W.J. (2004). Unsaturated soil mechanics. John Wiley & Sons Inc., New York.

Malek, S.A.; Avanzi, F.; Brun-Laguna, K.; Maurer, T.; Oroza, C.A.; Hartsough, P.C.; Watteyne, T.; Glaser, S.D. (2017).Real-Time Alpine Measurement System Using Wireless Sensor Networks. Sensors, 17, 2583. https://doi.org/10.3390/s17112583

Martens, B., De Jeu, Richard A.M., Verhoest, N.E.C., Schuurmans, H., Kleijer, J., and Miralles, D.G. (2018). Towards estimating land evaporation at field scales using GLEAM, Remote Sens. 10, no. 11: 1720.

Martens, B., Miralles, D.G., Lievens, H., van der Schalie, R., de Jeu, R.A.M., Fernández-Prieto, D., Beck, H.E., Dorigo, W.A., and Verhoest, N.E.C. (2017) GLEAM v3: Satellite-based land evaporation and root-zone soil moisture, Geoscientific Model Development, 10, 1903–1925.

Massari, C., Brocca, L., Pellarin, T., Abramowitz, G., Filippucci, P., Ciabatta, L., Maggioni, V., Kerr, Y., Fernández-Prieto, D. (2020). A daily/25km short-latency rainfall product for data scarce regions based on the integration of the GPM IMERG Early Run with multiple satellite soil moisture products. Hydrology and Earth System Sciences, 24, 2687–2710, doi:10.5194/hess-24-2687-2020.

Massari, C., Crow, W., Brocca, L. (2017). An assessment of the accuracy of global rainfall estimates without ground-based observations. Hydrology and Earth System Sciences, 21, 4347-4361, doi:10.5194/hess-21-4347-2017.

Massari, C., Maggioni, V., Barbetta, S., Brocca, L., Ciabatta, L., Camici, S., Moramarco, T., Coccia, G., Todini, E. (2019). Complementing near-real time satellite rainfall products with satellite soil moisture-derived rainfall through a Bayesian inversion approach. Journal of Hydrology, 573, 341-351, doi:10.1016/j.jhydrol.2019.03.038.

Miralles, D. G., Jiménez, C., Jung, M., Michel, D., Ershadi, A., McCabe, M. F., Hirschi, M., Martens, B., Dolman, A. J., Fisher, J. B., Mu, Q., Seneviratne, S. I., Wood, E. F., and Fernández-Prieto, D. (2016). The WACMOS-ET project – Part 2: Evaluation of global terrestrial evaporation data sets, Hydrol. Earth Syst. Sci., 20, 823–842.

Muñoz-Sabater, Joaquín, Emanuel Dutra, Anna Agustí-Panareda, Clément Albergel, Gabriele Arduini, Gianpaolo Balsamo, Souhail Boussetta, et al. (2021). ERA5-Land: A State-of-the-Art Global Reanalysis Dataset for Land Applications. Earth System Science Data Discussions, March, 1–50. https://doi.org/10.5194/essd-2021-82.

Pignone, F., Rebora, N. and Silvestro, F. (2015). Modified Conditional Merging technique: a new method to estimate a rainfall field combining remote sensed data and raingauge observations, 17, 3013.

Preissmann, A. (1961). Propagation of translatory waves in channels and rivers, in: First Congress of French Association for Computation. pp. 433–442.

Rains et al. (in preparation). European-scale 1 km evaporation and soil moisture data based on Sentinel observations.

Rains, D., Lievens, H., De Lannoy, G. J. M., McCabe, M. F., De Jeu, R. A. M., and Miralles, D. G. (in review) Sentinel-1 backscatter assimilation using Support Vector Regression or the Water Cloud model at European soil moisture sites, IEEE Geoscience and Remote Sensing Letters, in review.

Raup, B., Racoviteanu, A., Khalsa, S. J. S., Helm, C., Armstrong, R. and Arnaud, Y.: The GLIMS geospatial glacier database (2007) A new tool for studying glacier change, Global and Planetary Change, 56(1), 101–110, https://doi.org/10.1016/j.gloplacha.2006.07.018.

Ross, C. W., Prihodko, L., Anchang, J., Kumar, S., Ji, W. And Hanan, N. P. (2018). Global Hydrologic Soil Groups (HYSOGs250m) for Curve Number-Based Runoff Modeling, ORNL Distributed Active Archive Center..

Silvestro, F., Gabellani, S., Delogu, F., Rudari, R. and Boni, G. (2013). Exploiting remote sensing land surface temperature in distributed hydrological modelling: the example of the Continuum model, Hydrology and Earth System Sciences, 17(1), 39–62, https://doi.org/10.5194/hess-17-39-2013.

Sinclair, S. and Pegram, G. (2005).Combining radar and rain gauge rainfall estimates using conditional merging, Atmospheric Science Letters, 6(1), 19–22.

Song, Y.S. (2014). Suction stress in unsaturated sand at different relative densities. Engineering Geology, Volume 176, 1-10.

Stauffer, D. R. and Seaman, N. L.: Use of four-dimensional data assimilation in a limited-area mesoscale model. Part I: experiments with synoptic-scale data, 118, 1250–1277, https://doi.org/10.1175/1520-0493(1990)118<1250:UOFDDA>2.0.CO;2, 1990.

Terzago, S., Andreoli, V., Arduini, G., Balsamo, G., Campo, L., Cassardo, C., Cremonese, E., Dolia, D., Gabellani, S., von Hardenberg, J., Morra di Cella, U., Palazzi, E., Piazzi, G., Pogliotti, P., and Provenzale, A. (2020). Sensitivity of snow models to the accuracy of meteorological forcings in mountain environments, Hydrol. Earth Syst. Sci., 24, 4061–4090, https://doi.org/10.5194/hess-24-4061-2020.

Verdin, K. L. (2017). Hydrologic Derivatives for Modeling and Analysis—A new global high-resolution database, Hydrologic Derivatives for Modeling and Analysis—A new global high-resolution database, U.S. Geological Survey, Reston, VA, https://doi.org/10.3133/ds1053.

Technical Note 3: Simulation and impact assessment report

1. Introduction

1.1. The DTE Hydrology Project

The objective of DTE Hydrology is to develop and demonstrate a prototype of Digital Twin Earth with focus on water cycle and hydrological processes and their impacts. In DTE Hydrology we aim to highlight the huge potential of high-resolution ESA satellite products for describing the water cycle, for predicting hydrology extremes (floods, landslides and drought) and for monitoring and managing water resources.

The activity comprises four sequential steps: 1) building the 4D DTE Hydrology dataset, a high resolution (1 km, hourly, 2016-2019) EO-based dataset, also integrating in situ observations, 2) develop a high resolution modelling system ingesting the 4D DTE Hydrology dataset and able to provide a 4D reconstruction of the water cycle, 3) integrating the modelling system in the cloud-based DTE Hydrology simulation and visualization tool, and 4) exploiting the DTE Hydrology tool to develop user-oriented case studies focusing on flood and landslide risk, and water resources management.

The area of focus of DTE Hydrology is the Po River Basin (northern Italy). In this area high quality ground observations are available, which are useful to calibrate and test the modelling system. Floods and landslides occur in the area due to the complex topography and meteorological conditions. The large agricultural area in the Po River Valley ("Pianura Padana") makes water resources management fundamental, as crop production is largely dependent on rainfall and on water availability from the Po River.

DTE Hydrology builds on the expertise of the consortium members. Within the project EO datasets of rainfall, soil moisture, evaporation, river discharge, snow depth and land cover will be used. Soil moisture, rainfall, snow depth and evaporation datasets are provided by partners with well-established algorithms from satellite observations, TU Wien, CNR-IRPI, CIMA and UGent respectively. Expertise in hydrological and hydraulic modelling at high resolution is brought in by CNR-IRPI, CIMA and UNIBO. High performance computing is pivotal in DTE Hydrology and is managed and hosted by EODC. Outreach and visualization of the project outcomes is done by CNR-IRPI, CIMA, EODC and UNIBO.

1.2. Scope of this Report

This report describes the activities performed in WP400 related to the evaluation of the results of the hydrological and hydraulic modelling systems and to the impact assessment in terms of flooding, landslides and water resources management.

1.3. Applicable Documents

- [D1.1] - Deliverable D1.1: 4D DTE Hydrology underlying data reconstruction
- [D1.2] - Deliverable D1.2: DTE Hydrology data set
- [PR1] - Progress report October 2020-January 2021

- [D2.1] - Deliverable D2.1 v2.0: Technical Note 2: DTE-Hydrology consistent end-to-end integrated framework description and validation

1.4. Reference Documents

- [RD-01] - DTE Hydrology Technical Proposal - V1.0

2. Hydrological modelling

In this section the results of the two hydrological modelling systems (CONTINUUM and MISDc) tested in the DTE Hydrology project have been described.

2.1. CONTINUUM model

2.1.1. In situ baseline run

The calibrated model version for the Po Basin was first run for the entire focus period 2016-2019 at hourly resolution, to produce a simulation based on conventional data as input. Hereafter it is referred to as "baseline run". Performance scores for the 27 stations over the years 2017-2019 are summarized in **Table 2.1**, including the Kling-Gupta Efficiency (**Kling et al., 2012**) and its decomposition into its three components of correlation, bias and variability, while five sample hydrographs are shown in **Figure 2.1** for a visual representation.

2.1.2. EO configurations

In the second phase of the WP210, the baseline run is used as reference for comparison versus model runs forced by combinations of satellite-derived input. By using the same model setup, we then run a number of additional scenarios by replacing one or more input data with alternative satellite products provided by the project partners, according to the following scheme (labels in parenthesis will be used in the following for simplicity).

1. P-SM2RAIN (GPM+ASCAT+Sentinel-1) (**SM2RAIN**)
2. ET-GLEAM (**GLEAM**)
3. SWE-C_SNOW_As (**C-SNOW**)
4. SM-RT1_As (**RT1**)
5. P-GPM_SM2RAIN + ET-GLEAM + SWE-C_SNOW_As + SM-RT1_As (**All EO**)

Note that the naming is taken after the satellite input used in place of the conventional one. A leading string is used to indicate the corresponding input variable name among P=precipitation, ET=evaporation, SWE=snow water equivalent and SM=soil moisture. Also, an ending "_As" indicates assimilation of the satellite derived product.

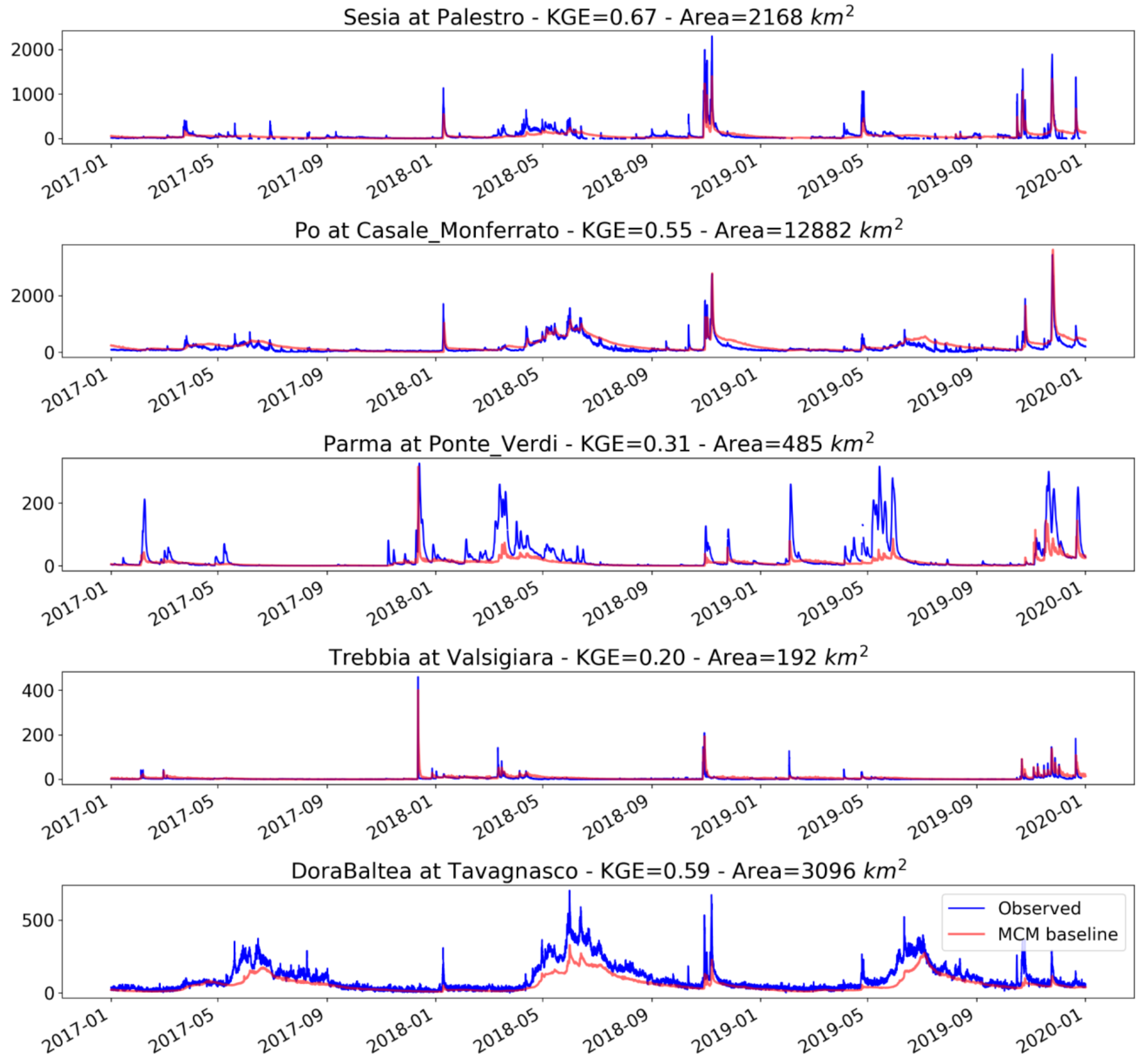

Figure 2.1*:* Observed versus simulated (baseline) discharge for the years 2017-2019 at five river gauging stations.

Table 2.1: Skill scores including RMSE, Kling-Gupta Efficiency (KGE) and its decomposition terms over 2017-2019 for the 27 gauging stations. Results for the 5 validation stations are in bold.

n°	Station	Area [km²]	KGE	r	Bias rate	CV rate	RMSE [m³/s]
1	Gaiola	515	0.61	0.89	0.71	1.23	9
2	Cassine	1364	-0.12	0.82	1.88	0.34	59
3	Carignano	3649	0.88	0.89	0.97	1.05	38
4	Torino_Murazzi	6134	0.73	0.88	1.24	1.03	61
5	Lanzo	541	0.74	0.83	0.81	1.02	16
6	Ponte_Alto	1077	0.60	0.82	1.12	0.67	24
7	S_Secondo	1422	0.46	0.71	0.94	0.55	74
8	Ostia_Parmense	387	0.62	0.65	0.96	0.86	26
9	**Candoglia**	**1480**	**0.56**	**0.86**	**0.60**	**1.14**	**47**
10	Palestro	2168	0.67	0.88	0.81	0.76	93
11	Casale_Monferrato	12882	0.55	0.83	1.33	0.75	156
12	Ponte_Verdi	485	0.31	0.71	0.43	0.74	41
13	Valsigiara	192	0.20	0.77	1.71	0.71	10
14	Tavagnasco	3096	0.59	0.90	0.61	0.94	64
15	Spessa	35976	0.80	0.90	0.87	1.11	333
16	**Piacenza**	**39195**	**0.76**	**0.89**	**0.83**	**1.13**	**384**
17	Pontelagoscuro	67487	0.69	0.88	0.91	1.28	565
18	Cremona	47616	0.69	0.89	0.83	1.23	427
19	**Borgoforte**	**59169**	**0.68**	**0.88**	**0.85**	**1.26**	**521**
20	Farigliano	1379	0.80	0.84	0.95	0.88	23
21	Alba_Q_A	3180	0.75	0.81	1.12	0.90	45
22	Salsominore	171	0.06	0.61	1.85	1.10	12
23	Ragoli	504	0.19	0.27	0.95	0.67	11
24	**Ponte_dei_Tedeschi**	**361**	**0.15**	**0.41**	**0.41**	**0.82**	**14**
25	Cimego	233	-0.03	0.00	1.00	0.75	4
26	**Piana_Crixia**	**229**	**0.17**	**0.66**	**0.76**	**0.28**	**18**
27	Cartosio	180	0.69	0.78	1.05	0.78	11

2.1.3. Results

Results for the 5 simulations driven by remote sensing derived input are summarized in **Table 2.2** (KGE), **Table 2.3** (correlation) and **Table 2.4** (bias rate), together with a comparison with the baseline simulation. Simulations including GLEAM and C-SNOW produce a benefit in the overall scores, with average KGE increasing by 0.01 and 0.02 respectively, which even become 0.07 and 0.04 if only validation stations are considered. In addition, these model runs show relatively few stations where the model performance has deteriorated. Simulations including RT1 soil moisture and SM2RAIN produced an average worsening of the model results (-0.04 for RT1 and -0.10 for SM2RAIN). The model run driven by all four satellite derived products (All EO) shows a similar behaviour as that of SM2RAIN, with average loss in KGE of 0.11. As expected, the run “All EO” shows the lowest correlation to the observed values, as it includes all the deviations of the satellite based products, though it retains an overall mean value with considerable skills (mean rAllEO=0.61), proving that satellite based products are a skilful alternative in regions where ground data is not available. Larger absolute bias is seen in the runs driven by SM2RAIN, RT1 and All EO, in all cases due to an average underestimation of river discharges, (between -0.24 in RT1 and -0.31 in AllEO). Runs including GLEAM and C-SNOW improve the bias rate compared to the baseline run by reducing the slight underestimation of the latter.

Figure 2.2 and **Figure 2.3** show examples of observed versus simulated time series for some of the stations that benefited by the use of GLEAM and C-SNOW respectively. GLEAM evaporation shows the largest benefits in the lower part of the Po River, thanks to an increase in the mean runoff and in turn a reduction of the underestimation of discharges (**Figure 2.2**). As expected, the C-SNOW dataset produces the largest benefits in smaller catchments with significant contribution of the snow accumulation and melting on the hydrological cycle, as shown in **Figure 2.3**.

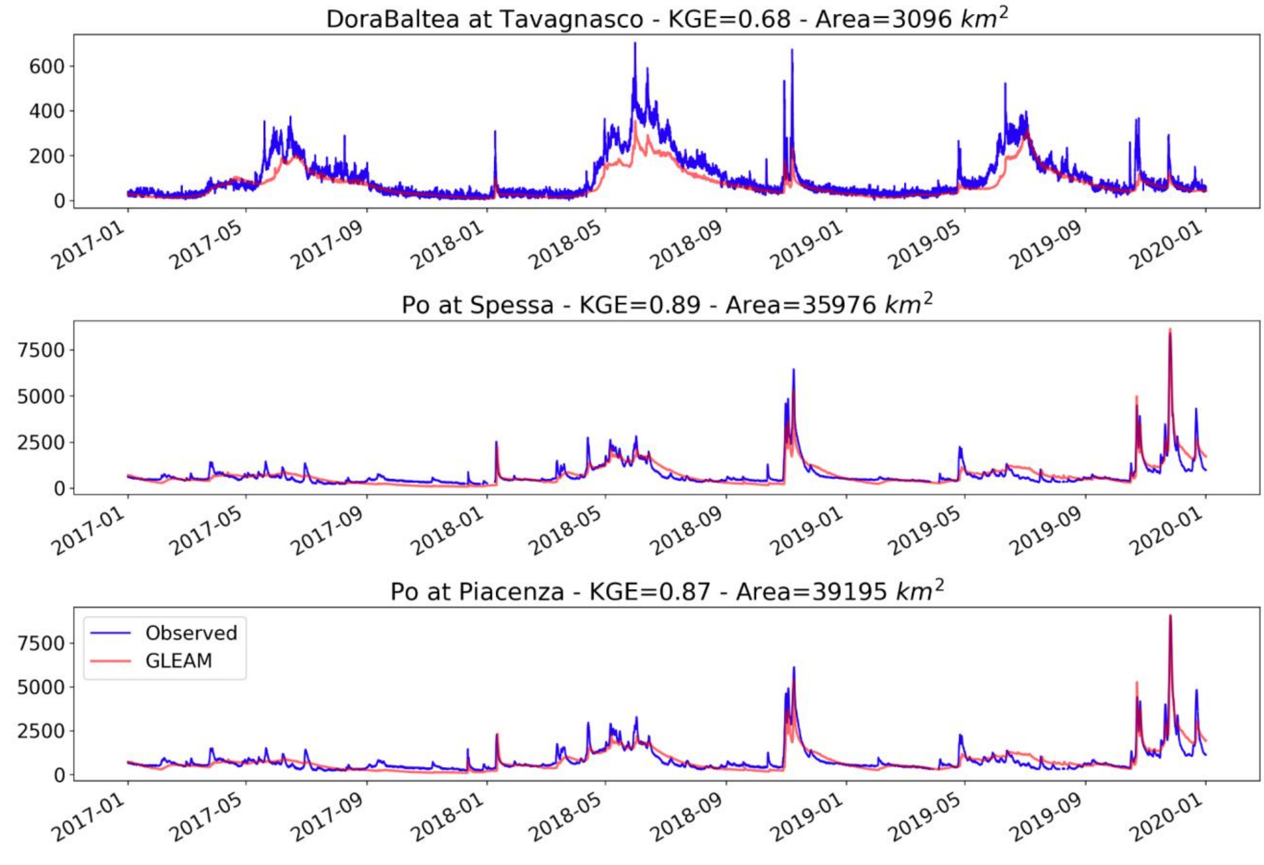

Figure 2.2*:* Observed versus simulated (GLEAM) discharge for the years 2017-2019 at three river gauging stations where satellite based evaporation improved the simulated discharges.

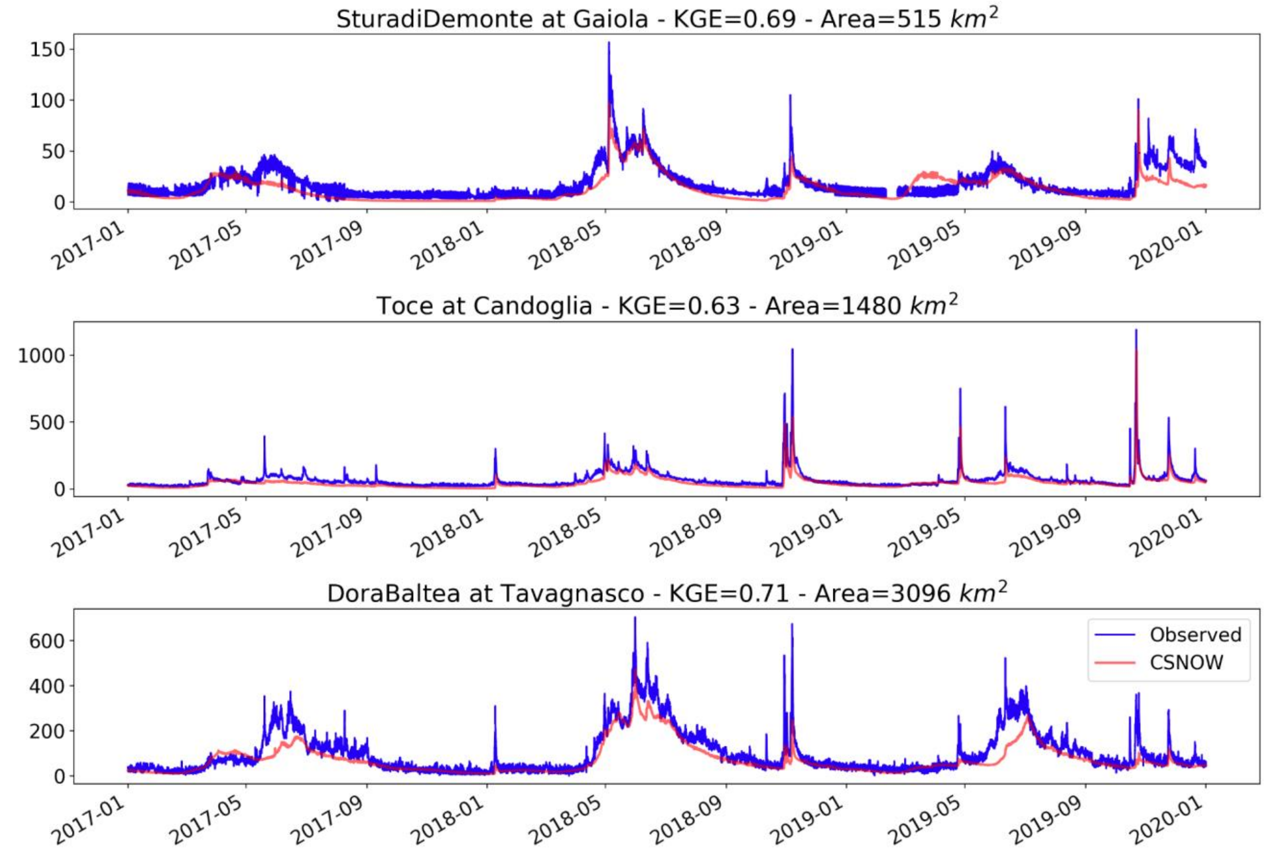

Figure 2.3*:* Observed versus simulated (C-SNOW) discharge for the years 2017-2019 at three of the river gauging stations where satellite based snow water equivalent improved the simulated discharges.

One must note that all simulations tested have skills (mean KGE ≥ 0.40) considerably larger than the no-skill threshold value ($KGE_0=1-2^{1/2} \approx -0.41$), thus proving the value of satellite derived products, which are thus to be considered particularly valuable in ungauged regions. Overall, results show that the Continuum hydrological model is capable of reproducing the observed discharges at a number of stations including a set of independent stations not used in calibration, which performances are in line with those of the calibration stations. This was possible thanks to an efficient multi-site calibration strategy that can infer parameter sets for optimal reconstruction of the hydrological processes also in areas relatively far from the calibration points. We found that the bias of the satellite products used as input or as assimilation datasets is among the key factors to investigate when running this type of analysis driven by remote sensing products. Such an effect can be attenuated or removed altogether if an accurate observational dataset is available for bias correction, though this is often not the case, considering the large proportion of ungauged regions of the world where satellite products are the only available source. However, we suggest that the bias correction is performed on the original product rather than at the stage of hydrological model calibration, so as to avoid pushing the calibrated parameters (which in Continuum have physical meaning) to unrealistic levels.

Table 2.2: KGE in the baseline run (column 3) for the 27 stations and related differences in the following model runs (columns 4-8) driven by satellite derived data. Green (red) shades indicate improvement (worsening) compared to the baseline run. Results for the 5 validation stations are in bold.

Station	UpsArea [km²]	Baseline	SM2RAIN	GLEAM	C-SNOW	RT1	All EO
Gaiola	515	0.61	-0.14	-0.01	0.07	-0.22	-0.25
Cassine	1364	-0.12	0.21	-0.03	0.07	0.28	0.29
Carignano	3649	0.88	-0.29	-0.01	0.00	-0.24	-0.35
Torino_Murazzi	6134	0.73	0.00	-0.15	-0.10	0.02	-0.02
Lanzo	541	0.74	-0.25	0.06	-0.01	-0.14	-0.28
Ponte_Alto	1077	0.60	-0.21	-0.18	0.05	0.04	-0.23
S_Secondo	1422	0.46	-0.12	-0.03	0.02	0.06	-0.11
Ostia_Parmense	387	0.62	-0.26	-0.01	0.01	0.00	-0.30
Candoglia	**1480**	**0.56**	**-0.09**	**0.06**	**0.08**	**-0.14**	**-0.12**
Palestro	2168	0.67	-0.21	-0.04	0.00	-0.03	-0.23
Casale_Monferrato	12882	0.55	0.13	-0.23	-0.10	0.20	0.06
Ponte_Verdi	485	0.31	-0.14	0.02	-0.01	-0.06	-0.19
Valsigiara	192	0.20	0.12	-0.01	0.10	0.41	0.23
Tavagnasco	3096	0.59	-0.13	0.09	0.11	-0.19	0.03
Spessa	35976	0.80	-0.17	0.09	0.05	-0.20	-0.15
Piacenza	**39195**	**0.76**	**-0.16**	**0.11**	**0.04**	**-0.19**	**-0.15**
Pontelagoscuro	67487	0.69	-0.08	0.15	0.04	-0.20	-0.06
Cremona	47616	0.69	-0.12	0.16	0.06	-0.20	-0.07
Borgoforte	**59169**	**0.68**	**-0.10**	**0.17**	**0.05**	**-0.19**	**-0.07**
Farigliano	1379	0.80	-0.16	-0.03	-0.02	-0.12	-0.36
Alba_Q_A	3180	0.75	-0.05	-0.04	0.01	-0.03	-0.21
Salsominore	171	0.06	0.27	0.01	0.12	0.17	0.14
Ragoli	504	0.19	-0.19	0.09	-0.07	-0.05	-0.10
Ponte_dei_Tedeschi	**361**	**0.15**	**0.00**	**0.04**	**0.03**	**-0.04**	**0.04**
Cimego	233	-0.03	-0.04	0.01	-0.08	-0.03	-0.01
Piana_Crixia	**229**	**0.17**	**-0.14**	**0.00**	**0.00**	**0.00**	**-0.15**
Cartosio	180	0.69	-0.26	-0.02	0.03	0.05	-0.26
Mean KGE		**0.51**	**0.42**	**0.52**	**0.53**	**0.47**	**0.40**
Δ(mean KGE)			**-0.10**	**0.01**	**0.02**	**-0.04**	**-0.11**

Table 2.3: Correlation (r) in the baseline run (column 3) for the 27 stations and related differences (columns 4-8) in the following model runs driven by satellite derived data. Green (red) shades indicate improvement (worsening) compared to the baseline run. Results for the 5 validation stations are in bold.

Station	UpsArea [km²]	Baseline	SM2RAIN	GLEAM	C-SNOW	RT1	All EO
Gaiola	515	0.89	-0.09	-0.01	-0.05	-0.04	-0.28
Cassine	1364	0.82	-0.30	0.00	0.01	-0.01	-0.28
Carignano	3649	0.89	-0.12	0.00	-0.01	-0.03	-0.21
Torino_Murazzi	6134	0.88	-0.07	0.00	0.00	-0.03	-0.13
Lanzo	541	0.83	-0.17	0.01	0.00	-0.02	-0.18
Ponte_Alto	1077	0.82	-0.20	0.01	0.01	-0.05	-0.22
S_Secondo	1422	0.71	-0.10	0.00	0.01	0.00	-0.14
Ostia_Parmense	387	0.65	-0.11	0.00	0.00	0.00	-0.13
Candoglia	**1480**	**0.86**	**-0.05**	**0.00**	**0.00**	**-0.03**	**-0.10**
Palestro	2168	0.88	-0.19	0.01	0.00	-0.01	-0.19
Casale_Monferrato	12882	0.83	-0.04	0.00	0.01	-0.02	-0.02
Ponte_Verdi	485	0.71	-0.13	0.00	-0.01	-0.08	-0.28
Valsigiara	192	0.77	-0.32	0.00	0.00	-0.03	-0.28
Tavagnasco	3096	0.90	-0.05	0.01	0.00	-0.10	-0.05
Spessa	35976	0.90	-0.05	0.00	0.00	0.00	-0.06
Piacenza	**39195**	**0.89**	**-0.04**	**0.00**	**0.00**	**0.00**	**-0.05**
Pontelagoscuro	67487	0.88	-0.03	0.01	0.00	0.00	-0.06
Cremona	47616	0.89	-0.03	0.00	0.00	0.00	-0.07
Borgoforte	**59169**	**0.88**	**-0.02**	**0.00**	**0.00**	**0.01**	**-0.08**
Farigliano	1379	0.84	-0.15	0.00	-0.01	-0.04	-0.40
Alba_Q_A	3180	0.81	-0.09	0.01	0.00	-0.05	-0.34
Salsominore	171	0.61	-0.24	0.00	0.01	-0.04	-0.22
Ragoli	504	0.27	-0.04	0.09	-0.01	0.00	-0.02
Ponte_dei_Tedeschi	**361**	**0.41**	**0.09**	**0.02**	**0.05**	**0.07**	**0.16**
Cimego	233	0.00	0.07	0.02	-0.01	0.03	0.17
Piana_Crixia	**229**	**0.66**	**-0.21**	**0.00**	**0.00**	**0.02**	**-0.13**
Cartosio	180	0.78	-0.20	0.00	0.01	-0.01	-0.13
Mean r		**0.75**	**0.64**	**0.75**	**0.75**	**0.73**	**0.61**
Δ(mean r)			**-0.11**	**0.01**	**0.00**	**-0.02**	**-0.14**

Table 2.4: Bias rate in the baseline (column 3) and in the model runs driven by satellite products (columns 4-8), for the 27 stations considered. Red shades denote worsening compared to the optimal value Br=1 (i.e., no bias). Results for the 5 validation stations are in bold.

Station	UpsArea [km²]	Baseline	SM2RAIN	GLEAM	C-SNOW	RT1	All EO
Gaiola	515	0.71	-0.19	-0.02	0.03	-0.19	-0.22
Cassine	1364	1.88	-0.50	0.03	-0.08	-0.33	-0.71
Carignano	3649	0.97	-0.29	0.08	0.06	-0.24	-0.34
Torino_Murazzi	6134	1.24	-0.34	0.16	0.10	-0.32	-0.40
Lanzo	541	0.81	-0.17	0.09	-0.01	-0.13	-0.15
Ponte_Alto	1077	1.12	-0.28	0.24	-0.10	-0.22	-0.41
S_Secondo	1422	0.94	-0.24	0.07	-0.06	-0.13	-0.33
Ostia_Parmense	387	0.96	-0.34	-0.01	-0.07	-0.11	-0.43
Candoglia	**1480**	**0.60**	**-0.08**	**0.04**	**0.06**	**-0.10**	**-0.07**
Palestro	2168	0.81	-0.12	0.12	-0.01	-0.09	-0.15
Casale_Monferrato	12882	1.33	-0.28	0.22	0.10	-0.30	-0.21
Ponte_Verdi	485	0.43	-0.08	0.08	-0.03	-0.06	-0.11
Valsigiara	192	1.71	-0.45	0.00	-0.09	-0.42	-0.79
Tavagnasco	3096	0.61	-0.09	0.10	0.12	-0.17	0.06
Spessa	35976	0.87	-0.18	0.10	0.04	-0.16	-0.19
Piacenza	**39195**	**0.83**	**-0.18**	**0.10**	**0.03**	**-0.15**	**-0.18**
Pontelagoscuro	67487	0.91	-0.17	0.12	0.03	-0.15	-0.18
Cremona	47616	0.83	-0.15	0.10	0.04	-0.14	-0.15
Borgoforte	**59169**	**0.85**	**-0.15**	**0.11**	**0.03**	**-0.14**	**-0.15**
Farigliano	1379	0.95	-0.13	0.03	-0.06	-0.21	-0.31
Alba_Q_A	3180	1.12	-0.22	0.04	-0.07	-0.26	-0.39
Salsominore	171	1.85	-0.75	-0.01	-0.15	-0.30	-0.95
Ragoli	504	0.95	-0.25	0.11	0.30	-0.23	0.01
Ponte_dei_Tedeschi	**361**	**0.41**	**-0.03**	**0.04**	**0.04**	**-0.11**	**0.00**
Cimego	233	1.00	0.00	0.08	0.25	-0.27	0.21
Piana_Crixia	**229**	**0.76**	**-0.22**	**0.02**	**-0.02**	**-0.13**	**-0.26**
Cartosio	180	1.05	-0.33	0.02	-0.05	-0.11	-0.35
Mean Bias rate		**0.95**	**0.73**	**1.02**	**0.97**	**0.76**	**0.69**
Δ(mean Br)		**-0.05**	**-0.27**	**0.02**	**-0.03**	**-0.24**	**-0.31**

2.2. MISDc model

This paragraph presents the results of an additional hydrological validation carried out through the "Modello Idrologico SemiDistribuito in continuo" MISDc", MISDc (**Brocca et al., 2011**) over the Po river basin. Specifically, the simulations performed with MISDc have been addressed to test multiple satellite and ground-based rainfall products being MISDc less computational demanding with respect to Continuum and likely more flexible to ingest satellite rainfall products as carried out in multiple previous studies (e.g., **Camici et al., 2020**; **Brocca et al., 2020**).

2.2.1. Short description of the model

MISDc is a continuous semidistributed hydrological model and it consists of three main components: (1) a snow module to simulate snowmelt and glacier melt (2) a soil module to simulate the soil moisture temporal pattern, and (3) a routing module to transfer the water through the channels and through the rivers for flood simulation. The MISDc model includes 12 model parameters: the initial condition of soil water content, $W(t_0)$; the maximum water capacity of the soil layer, W_{max} (i.e. field capacity term); the initial abstraction coefficient, λ; the parameter of the relationship between the saturation degree and the soil retention, *a*; the correction factor for actual evapotranspiration *b*; the saturated hydraulic conductivity Ks; the exponent of drainage component, *m*; the fraction of drainage that transforms into subsurface runoff, *θ*; the degree-day coefficients, Cm-snowpack and Cm-glaciers for the melting process of snowpack and glaciers; the coefficient of lag–area relationship, *η;* the celerity *C* and the diffusivity, *D*. Each model parameter can vary within a range of admissible values derived by other applications of MISDc over many catchments worldwide (**Camici et al., 2018**; **Massari et al., 2015**; **Masseroni et al., 2017**). The calibration of the MISDc model parameters requires rainfall, air temperature and streamflow time series as input data. The calibration process consists in adopting a standard gradient based automatic optimization method implemented in the MATLAB software package ('fmincon' function; MATLAB R2016b, The MathWorks, Inc., Natick, Massachusetts, United States). This algorithm is particularly suitable and efficient for a limited number of model parameters and enables one to maximize an objective function. In this case, the objective function is the difference between the unity and the modified Kling-Gupta efficiency statistic dimensionless, KGE, proposed by **Gupta et al. (2009)**.

2.2.2. In situ and EO configurations

In the following the results of the hydrological validation are illustrated. Specifically, three groups of precipitation products considered in the analysis:

1. In situ data. Pobs, i.e. in situ observed precipitation data and MCM, i.e. precipitation data obtained through a modified conditional merging (MCM) by blending data from national radar and rain-gauge networks are included in this group;

2. Single satellite precipitation data. This group includes GPM, i.e. precipitation data from Global Precipitation Measurement, Final Run and $SM2R_{ASC,}$ i.e., the precipitation data obtained by applying the SM2RAIN algorithm to ASCAT soil moisture data;

3. Integrated satellite precipitation data. In this group are included GPM+SM2R$_{ASC}$, i.e. the precipitation obtained by merging GPM and SM2R$_{ASC}$ precipitation data and DTE, i.e. the precipitation obtained by merging GPM, SM2R$_{ASC}$ and SM2R$_{S1}$ precipitation data. SM2R$_{S1}$ is a precipitation product obtained by applying the SM2RAIN algorithm to S1 soil moisture data.

To evaluate the reliability of each product for flood simulation, the following procedure has been adopted. For each product, MISDc model has been calibrated over the period 2016-2019 and the simulated river discharge time series has been compared against the in situ observed data. For simplicity, only 18 out 27 in situ gauging stations available over the Po basin have been considered for this analysis (see **Figure 2.4**). Through a sequential calibration (De Lavenne et al., 2019), MISDc model has been calibrated over 11 sections (in bold in the **Table 2.5**). The remaining 7 sections have been used for validation.

The location of the gauging stations and the raingauges over the Po river basin is illustrated in **Figure 2.4**. The name of the gauging stations are reported in **Table 2.5**.

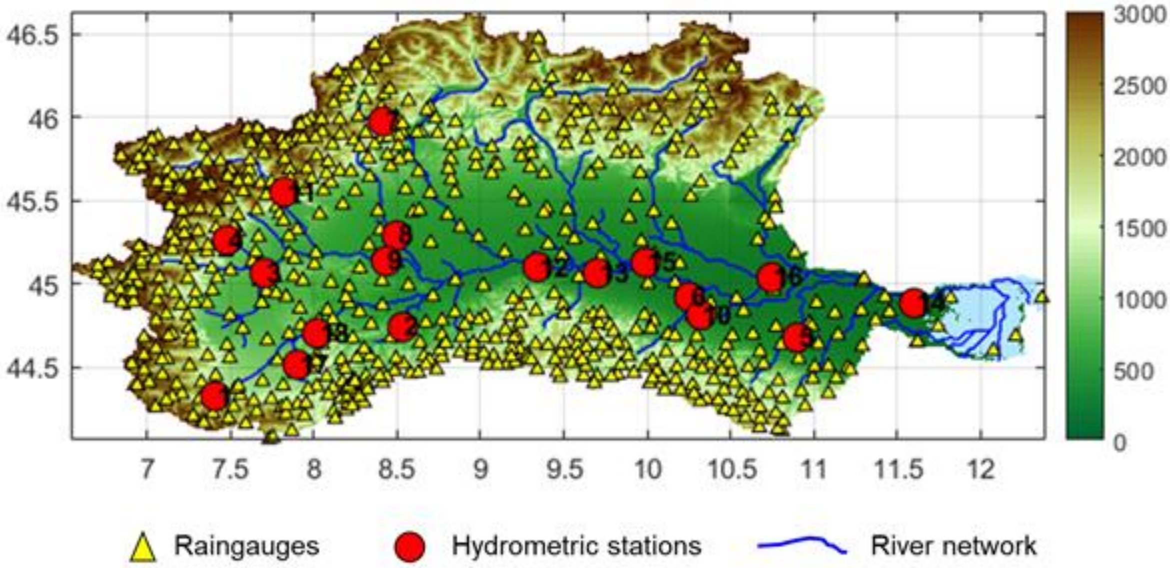

Figure 2.4. Location of the gauging stations and the raingauges over the Po river basin. The numbers in the figure are associated with the locations of **Table 2.5**.

2.2.3. Results

Results in terms of KGE are illustrated in **Figure 2.5** and in **Table 2.5** for each product and for the 18 sections. It can be noted that the overall performances of the in situ data are very good. Even if Pobs and MCM show similar median values, MCM performs slightly better for some sections (i.e., 1, 6-7, 11-17, see **Table 2.**) and worst for others (**5**i.e., 3 to 5, 8-10, 18, see **Table 2.5**). The single satellite precipitation data underperforms the observed data. In particular, among the investigated precipitation products, GPM shows the lowest median KGE value (KGE$_{med}$= 0.66) whereas better performances are obtained by using SM2R$_{ASC}$ (KGE$_{med}$= 0.77). The performances in terms of flood modelling improves by using the integrated products. In particular, by using the DTE product the median KGE value increases up to 0.82, a value higher than the one obtained by using the observed data (KGE_{med}= 0.79).

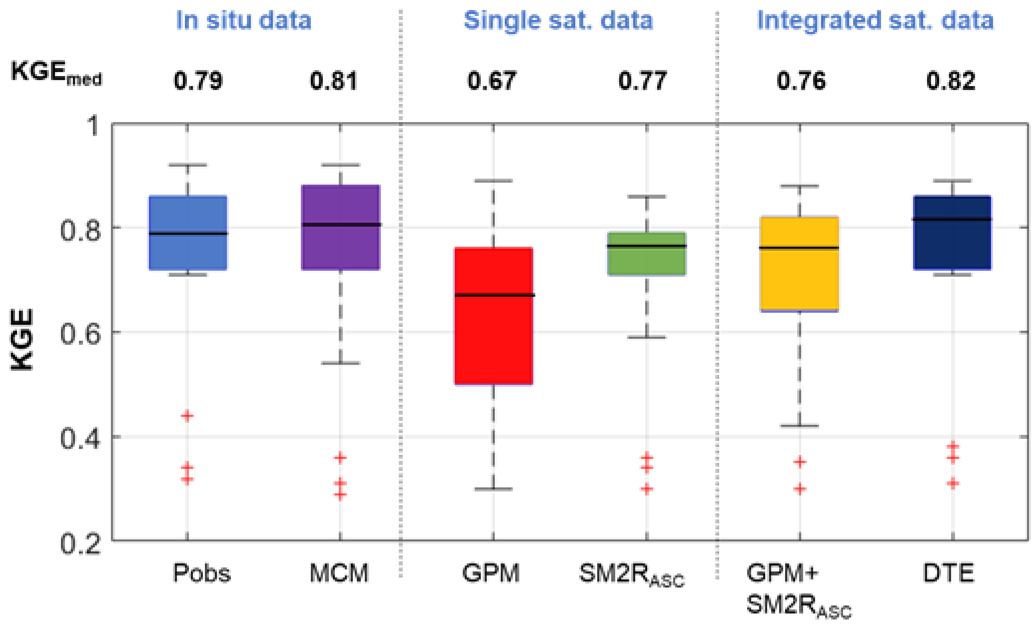

Figure 2.5. Boxplot of KGE scores for the different rainfall products. The numbers over each boxplot indicate the median KGE value. For each boxplot the buffers indicate the minimum and maximum value, 25th 50th and 75th percentiles are indicated by the three lines in the rectangle.

Table 2.5: Skill scores in terms of Kling-Gupta Efficiency (KGE) over 2017-2019 for the 19 gauging stations. Results for the 8 validation stations are in bold.

ID station	Name station	Pobs	MCM	GPM	$SM2R_{ASC}$	$SM2R_{ASC}$ + GPM	DTE 1km_hourly
1	Stura di Demonte@Gaiola	0.75	0.82	0.66	0.73	0.64	0.78
2	Bormida@Cassine	0.92	0.92	0.50	0.74	0.73	0.77
3	**Po@Torino Murazzi**	0.32	0.29	0.33	0.36	0.30	0.31
4	Stura di Lanzo@Lanzo	0.72	0.54	0.71	0.71	-0.17	0.80
5	**Secchia@Ponte Alto**	0.44	0.31	0.30	0.34	0.42	0.38
6	**Taro@S. Secondo**	0.34	0.36	0.37	0.30	0.35	0.36
7	Toce@Candoglia	0.89	0.92	0.68	0.79	0.82	0.85
8	Sesia@Palestro	0.76	0.72	0.35	0.59	0.80	0.71
9	Po@Casale Monferrato	0.89	0.87	0.79	0.82	0.77	0.87
10	Parma@Ponte Verdi	0.79	0.77	0.53	0.75	0.64	0.72
11	Dora Baltea@Tavagnasco	0.86	0.88	0.89	0.78	0.85	0.86
12	Po@Spessa	0.85	0.89	0.77	0.86	0.88	0.89
13	**Po@Piacenza**	0.81	0.85	0.76	0.85	0.86	0.88
14	Po@Pontelagoscuro	0.71	0.78	0.76	0.78	0.80	0.84
15	**Po@Cremona**	0.79	0.84	0.75	0.82	0.84	0.87
16	**Po@Borgoforte**	0.73	0.78	0.74	0.79	0.80	0.83
17	Tanaro@Farigliano	0.88	0.92	0.54	0.79	0.75	0.85
18	**Tanaro@Alba Q.A.**	0.82	0.79	0.53	0.75	0.70	0.77

The same considerations can be drawn by looking at the scatterplots in **Figure 2.6**, where the KGE values obtained for the different precipitation products (i.e., MCM, GPM, SM2RASC, GPM+SM2RASC, and DTE, in the y-axis) are plotted against the ones obtained by using the Pobs data as input to MISDc model. By looking at the figure it can be noted that, among the satellite products, DTE overperforms the in situ data for 9 sections out 18 sections (dots above the 1:1 line). This aspect is better illustrated in **Figure 2.7** where the difference between the performances of DTE and Pobs data is computed. The improvements are more evident for the sections located along the Po valley. This might be linked to the irrigation signal included into the DTE satellite precipitation data (through Sentinel-1).

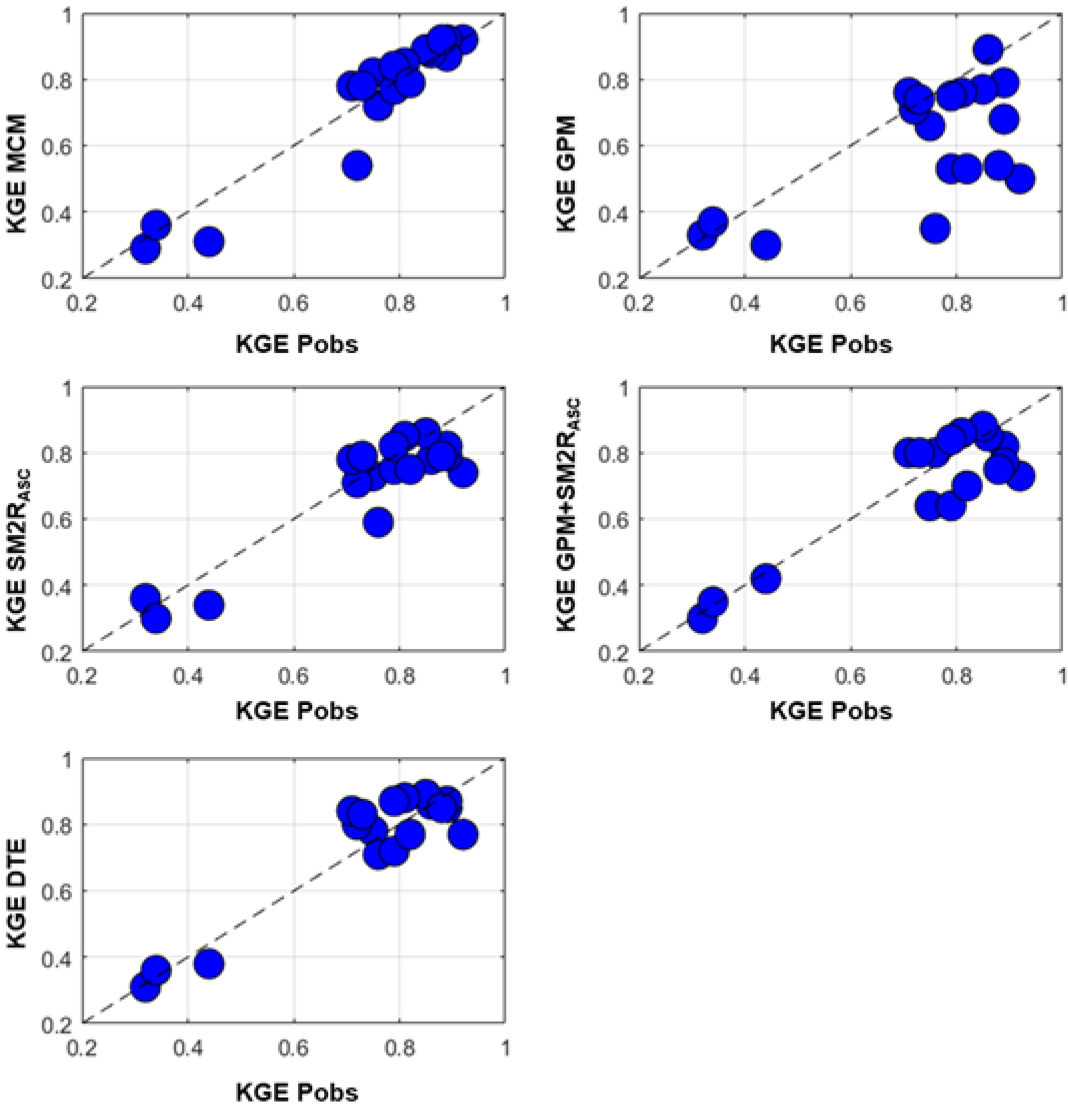

Figure 2.6. Scatterplots of KGE values obtained for different precipitation products (MCM, GPM, SM2R$_{ASC}$, GPM+SM2R$_{ASC}$, and DTE, in the y-axis) against the ones obtained by using the Pobs (x-axis) as input to MISDc model.

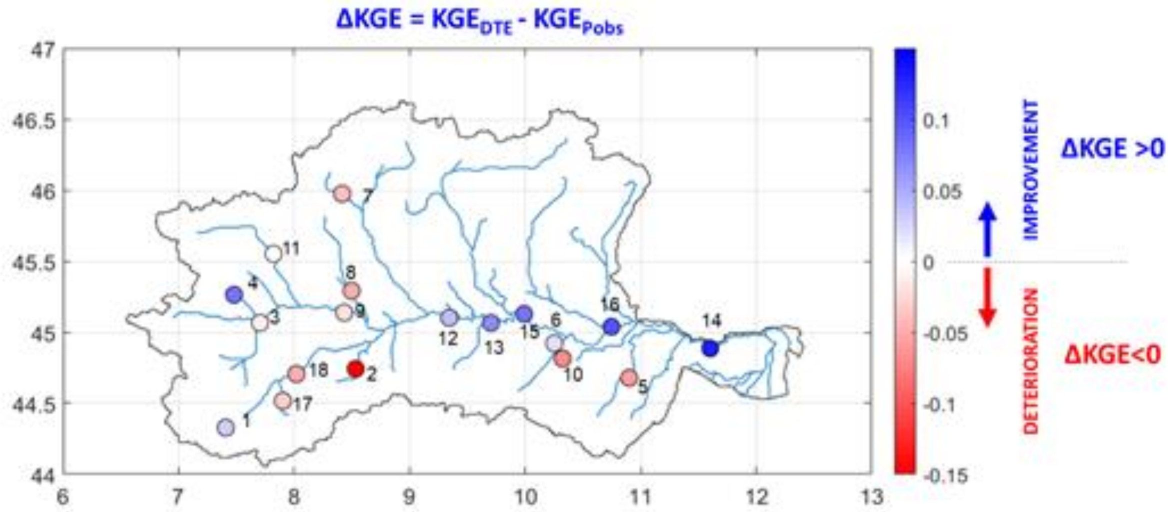

Figure 2.7. Difference between the KGE values obtained by using DTE and Pobs precipitation data over the Po river. Blue/red dots indicate the improvement/deterioration on flood simulation when the MISDc model is forced with DTE precipitation product. The numbers in the figure are associated with locations of **Table 2.5**.

The comparison between the observed and the simulated river discharge time series for some sections over the Po basin is illustrated in **Figures 2.8-2.10**.

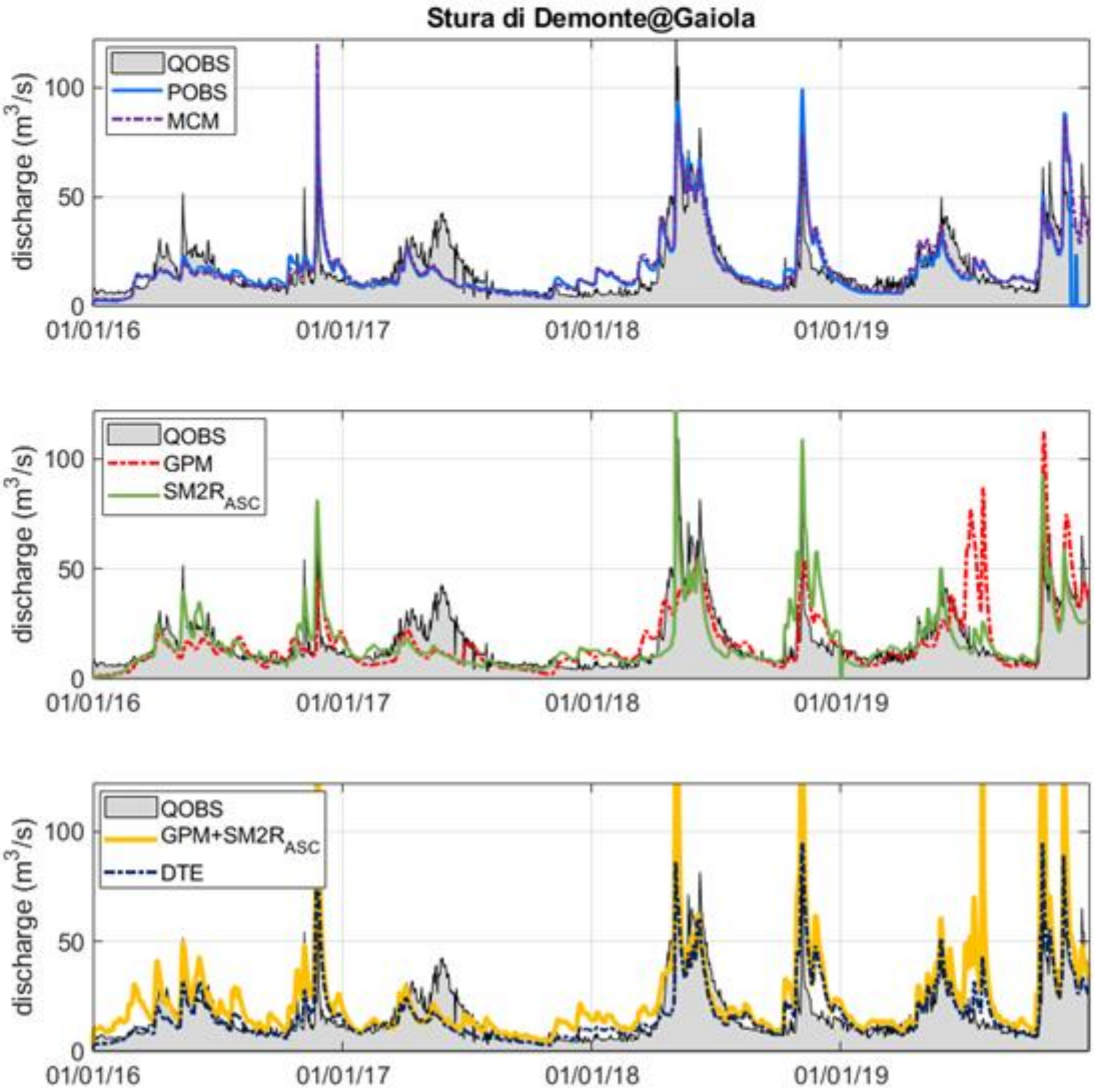

Figure 2.8. Comparison between observed and simulated river discharge time series for the Stura di Demonte river at Gaiola station. The first plot illustrates the results obtained by forcing the MISDc model with in situ data. Results for the single and integrated satellite rainfall data are presented in the second and third plot, respectively.

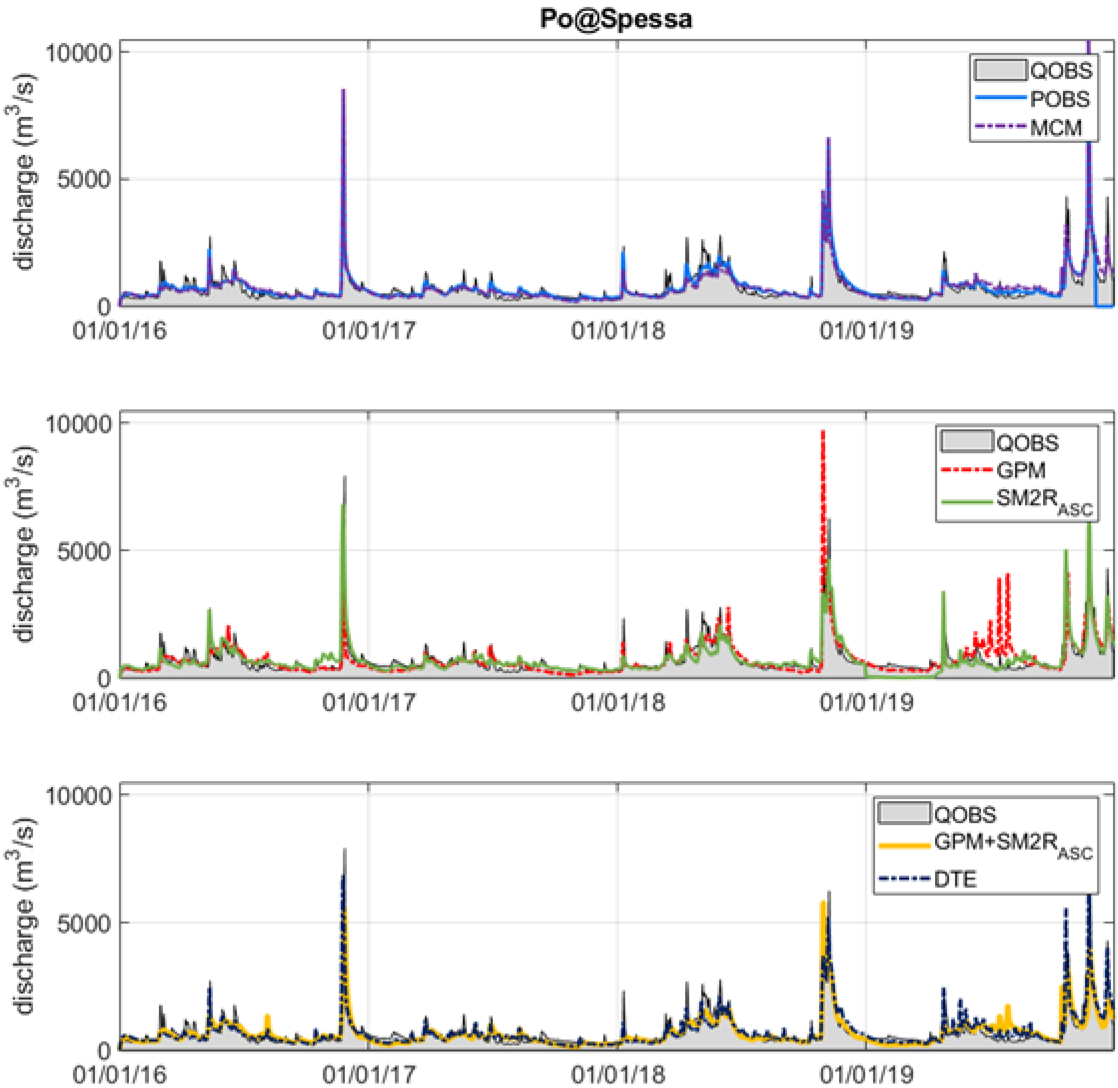

Figure 2.9. As in **Figure 2.8** but for the Po River at Spessa station.

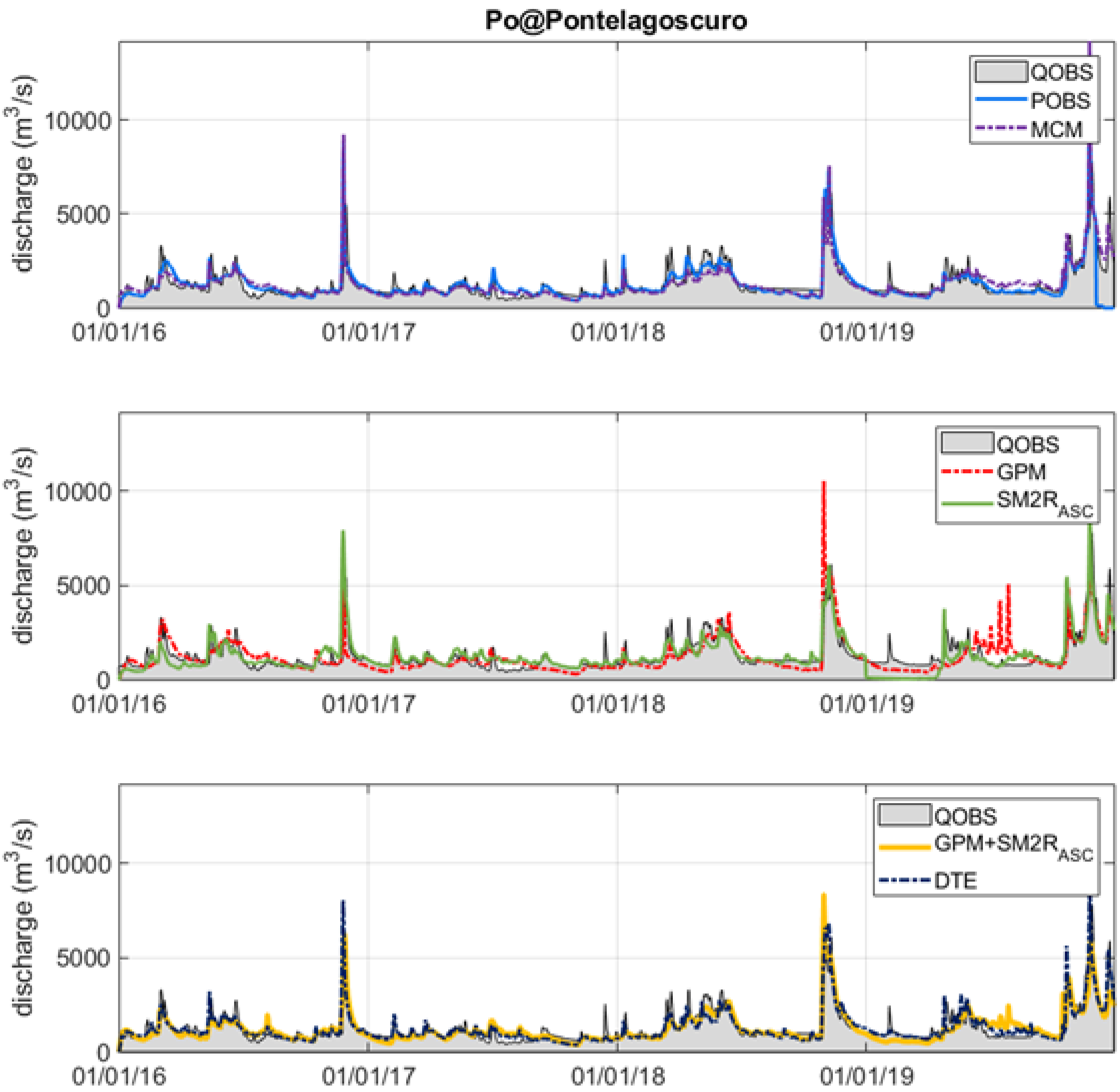

Figure 2.10. As in **Figure 2.8** but for the Po River at Pontelagoscuro station.

3. Hydraulic modelling

3.1. Method

The hydraulic modelling within the DTE-Hydrology project aims at simulating the flow routing dynamic of the main stream of the Po river, nearly 400 km, from Ponte Spessa (downstream the confluence with Ticino river) to the beginning of the river Delta. As detailed on Deliverable 2.1 [D2.1], the hydraulic modelling has been implemented adopting a quasi-2D schematization (**Domeneghetti et al., 2015**; **Castellarin et al., 2011b**), settled with the use of the software HEC-RAS (**Hydrologic Engineering Center, 2001**) and taking advantage of most recent topographic surveys of the river (i.e., river bathymetry) and flood-prone areas. **Figure 3.1** provides an example of river cross-sections and of the quasi-2D numerical scheme adopted for simulating the interaction among the main river and the dike-protected floodplains.

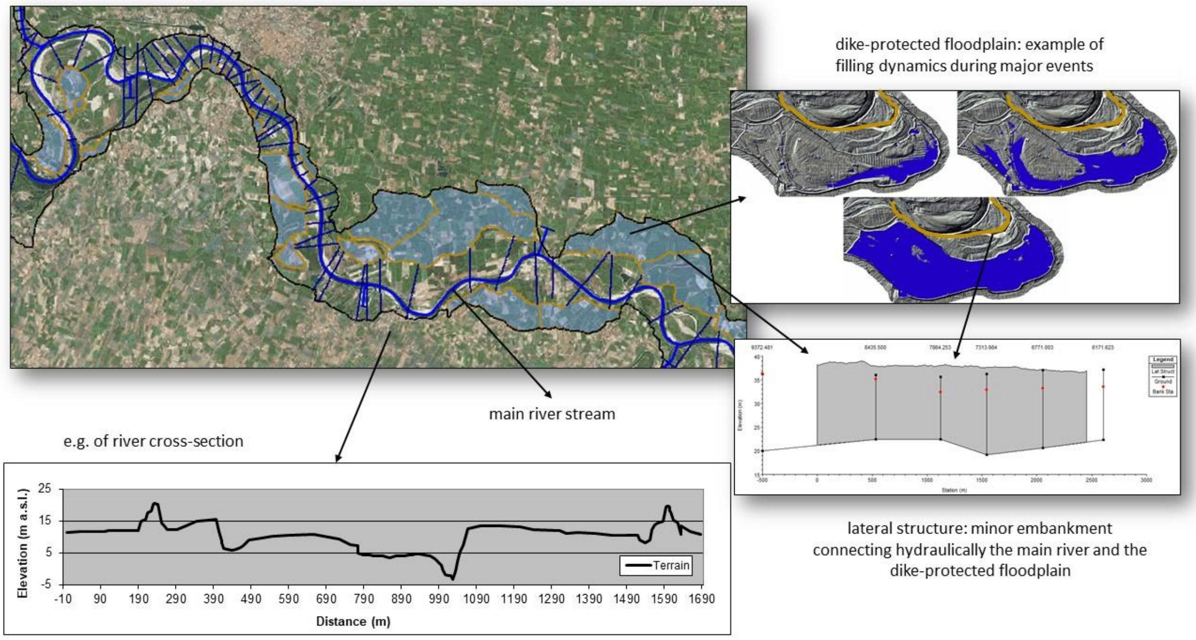

Figure 3.1: Modelling scheme: example of river cross-section, storage areas and later structure adopted in the quasi-2D hydraulic model.

The hydraulic simulation of the Po river has been conceived in order to route the discharge series simulated at the upstream stations of the main river and considered tributaries for the period of interest (2017-2019) by the hydrological modelling settled over the Po basin by CIMA (CONTINUUM, see **Section 2.1**). Thus, this report presents the results obtained by performing the hydraulic simulation considering as input the outcomes of the hydrological model, which in turn has been driven by adopting several satellite products. In according to hydrological simulations, hydraulic scenarios refer to the following input configurations:

1. P-SM2RAIN (GPM+ASCAT+Sentinel-1) (**SM2RAIN**)
2. ET-GLEAM (**GLEAM**)

3. SWE-C_SNOW_As (**C-SNOW**)
4. SM-RT1_As (**RT1**)
5. P-GPM_SM2RAIN + ET-GLEAM + SWE-C_SNOW_As + SM-RT1_As (**All EO**)

Note that the naming is taken after the satellite input used in place of the conventional one. A leading string is used to indicate the corresponding input variable name among P=precipitation, ET=evaporation, SWE=snow water equivalent and SM=soil moisture. Also, an ending "_As" indicates assimilation of the satellite derived product.

3.2. Model calibration

The overall river portion simulated with the quasi-2D hydraulic model is shown in **Figure 3.2**. The model has been calibrated taking advantage of both traditionally observed and remotely sensed data.

Specifically, the calibration was carried out in order to accurately reproduce:

- daily mean discharge and water level series recorded at the gauging stations located within the studied portion (yellow dots in **Figure 3.2**); observations are available for the overall period considered in the project (January 2017-December 2019).
- Sentinel 3A and Sentinel 3B altimetry series available at few locations along the river (triangles in **Figure 3.2**);
- multi-mission satellite altimetry time series (i.e., obtained merging Cryosat-2, Saral/Altika and Sentinel-3 observations; RIDESAT project; https://eo4society.esa.int/projects/ridesat/; http://hydrology.irpi.cnr.it/projects/ridesat/) provided from previous studies at the gauging stations.

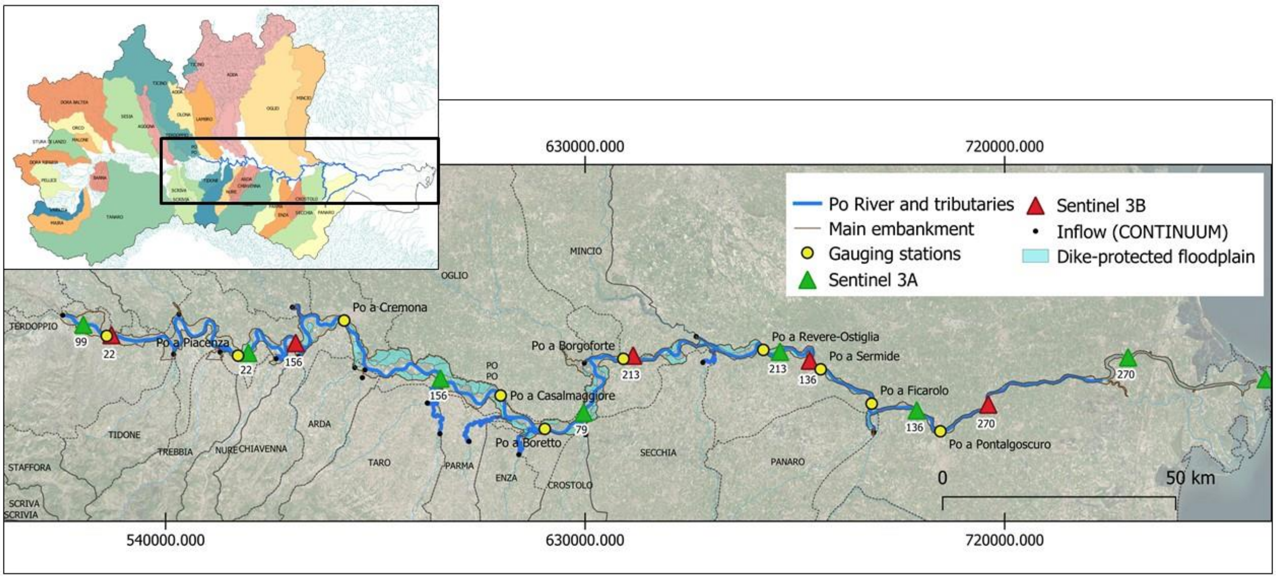

Figure 3.2 : Middle-lower Po river portion considered for the hydraulic modelling.

The calibration has been performed over the period March 2018- February 2019, which experienced both high and low flow conditions, adopting as hydraulic boundary conditions observed discharges at the gauging stations. The calibration focused on the identification of proper Manning's friction coefficients for all the homogeneous sub-reaches identified in relation to river characteristics, as well as in relation to the spatial distribution of the available observations (both traditional and remotely sensed data; see **Figure 3.2**). The values of the Manning's friction coefficients obtained in this study for the main channel fall in the range 0.041-0.025 $sm^{-1/3}$, while for the lateral floodplains, according to previous investigations, has been fixed to 0.1 $sm^{1/3}$. Those values agree with what reported in the scientific literature and observed in previous studies carried out over the same river (Domeneghetti et al., 2015; Castellarin et al. 2011).

Table 3.1 summarizes the scores for the 5 gauging stations for the calibration considering the observed water level and discharge series. Performances are evaluated in terms of KGE (Kling-Gupta Efficiency; Kling et al., 2012), MAE (Mean Absolute Error) and NSE (Nash-Sutcliffe Efficiency) considering both variables. For a visual inspection of the calibration performances, **Figure 3.3** and **Figure 3.4** report the simulated and the observed flow and water level hydrographs at the gauging stations, respectively.

Table 3.1: Calibration results (KGE, MAE and NSE) at the gauging stations over the calibration period.

	Discharge [m^3/s]			Water level [m a.s.l.]		
	MAE [m^3/s]	NSE [-]	KGE [-]	MAE [m]	NSE [-]	KGE [-]
Piacenza	120.13	0.92	0.92	0.16	0.94	0.93
Cremona	122.58	0.89	0.87	0.23	0.95	0.97
Boretto	144.15	0.87	0.85	0.3	0.94	0.95
Borgoforte	125.92	0.91	0.91	0.37	0.93	0.94
Pontelagoscuro	162.24	0.85	0.81	0.25	0.93	0.94

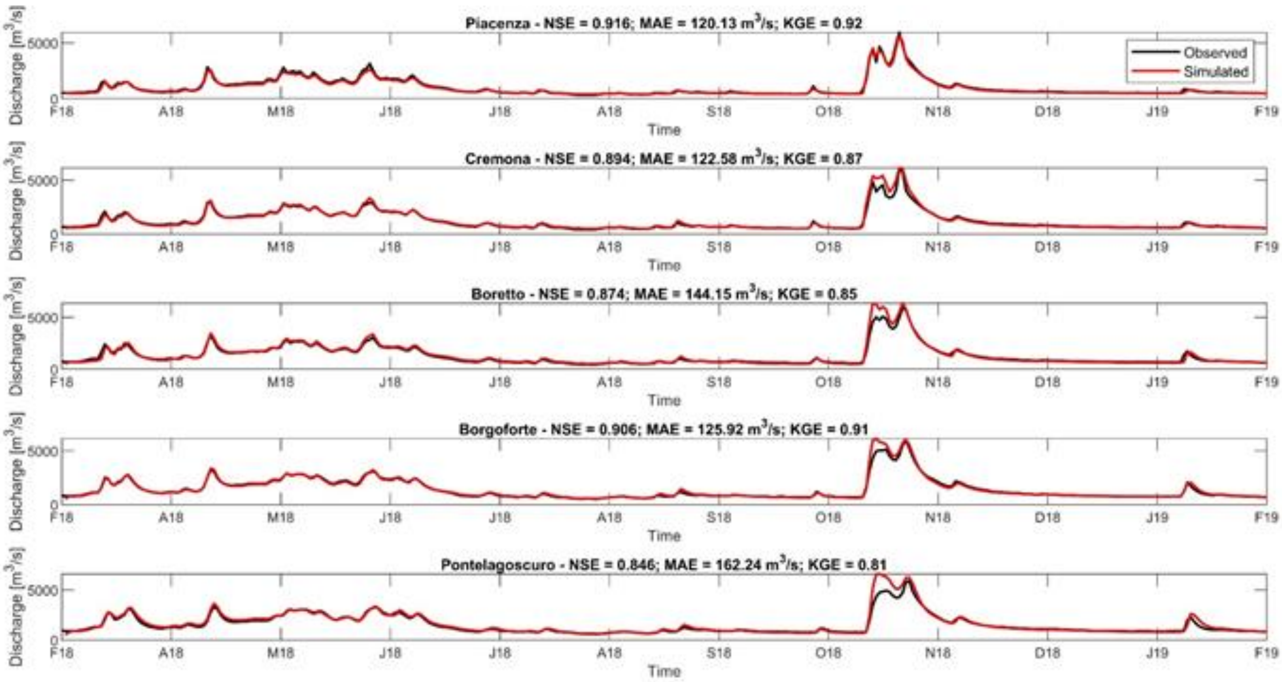

Figure 3.3: Observed versus simulated discharge at the gauging stations over the calibration period.

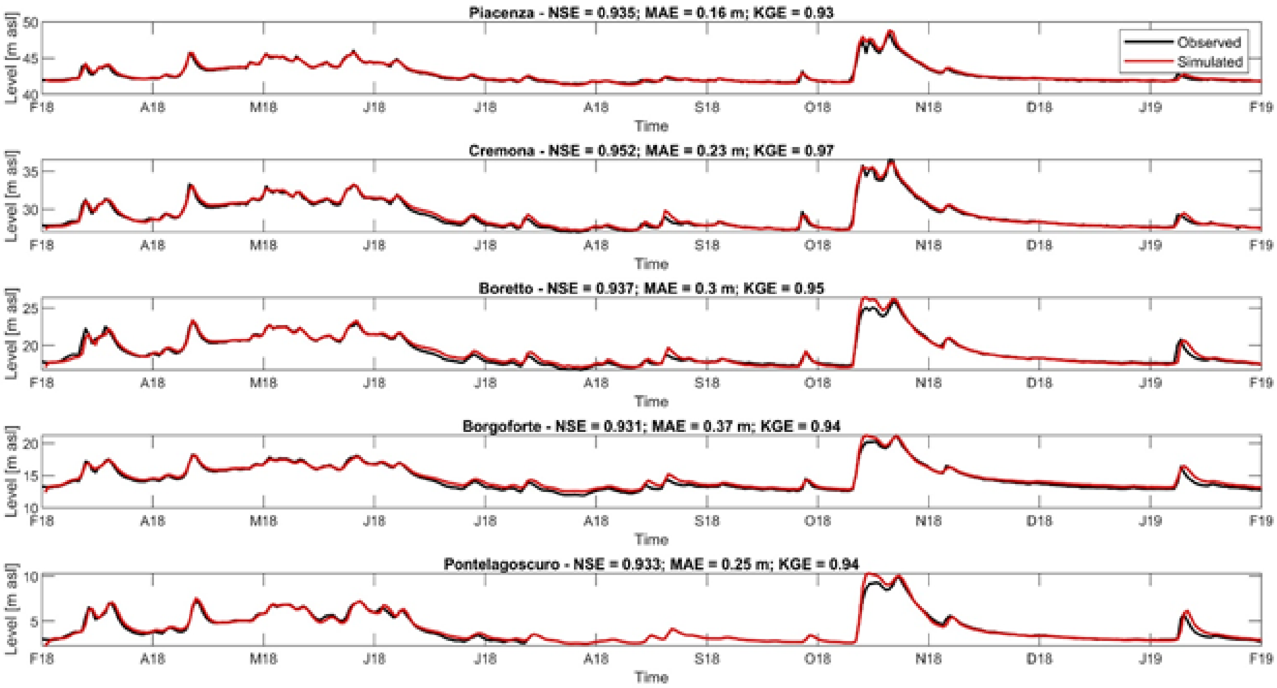

Figure 3.4: Observed versus simulated water level at the gauging stations over the calibration period.

Figure 3.5 and 3.6 report the calibration results referring to water levels retrieved from Sentinel 3A and 3B, respectively. Scores vary within locations. Despite few significant errors, water levels retrieved from Sentinel 3A appear realistic and are in line with water levels reproduced by the model adopting observed discharges. Scores confirm that with KGE varying between 0.58 and 0.95. Slightly worse performances are observed considering Sentinel 3B data (**Figure 3.6**), in particular for the virtual station (VS) S3B-156, where simulated and remotely-sensed water levels disagree. Despite this bias, performances are good at all other VS, with maximum KGE equal to 0.87.

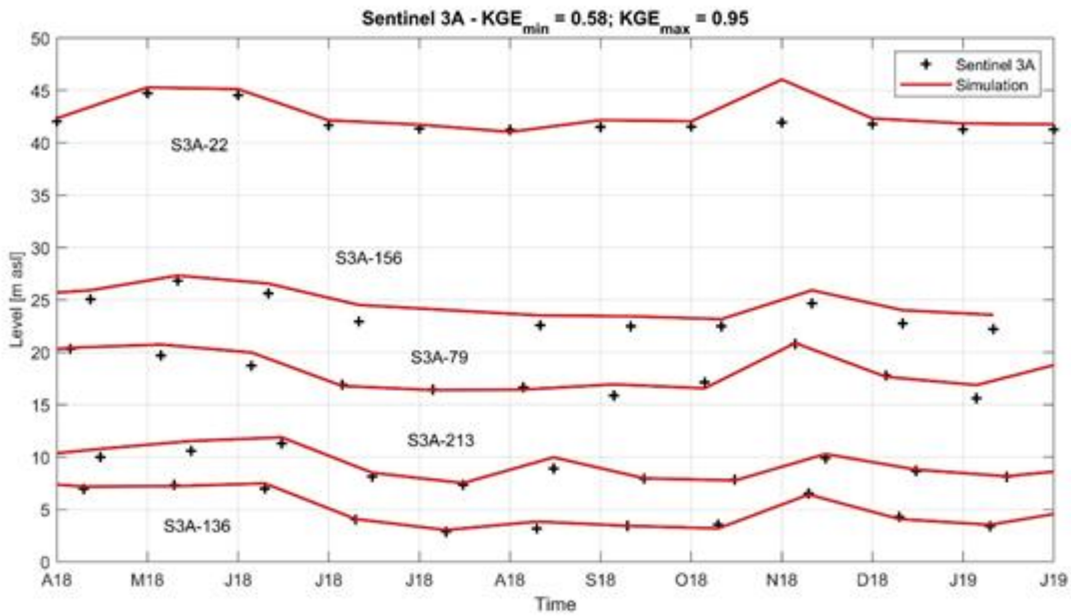

Figure 3.5: Sentinel 3A versus simulated water level at the VS over the calibration period.

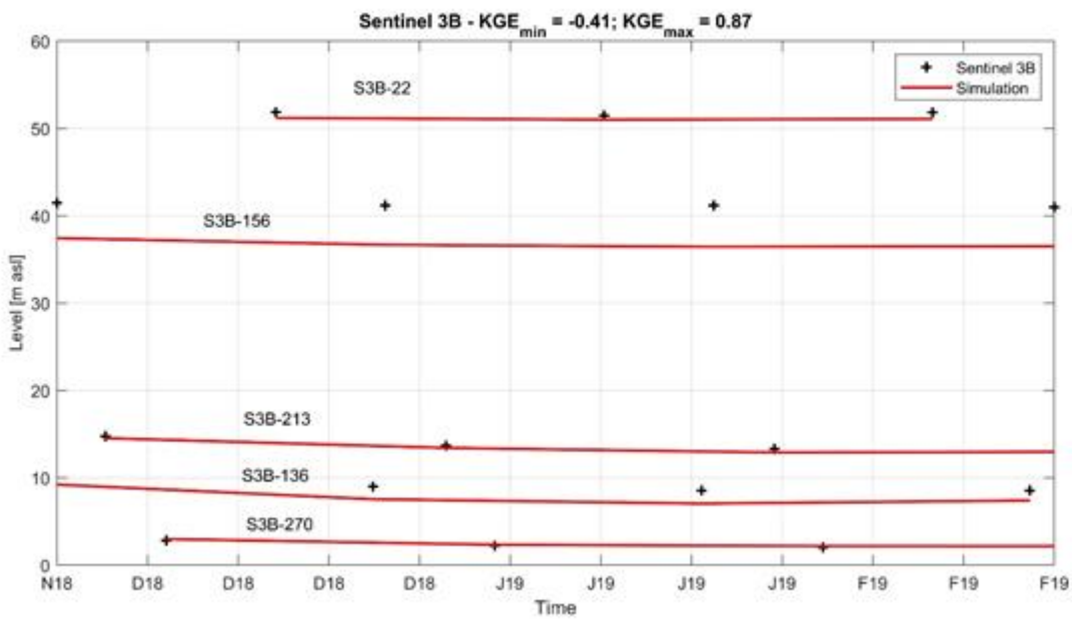

Figure 3.6: Sentinel 3B versus simulated water level at the VS over the calibration period.

Finally, **Figure 3.7** shows the comparison among simulated and multi-mission altimetry series obtained by merging Cryosat-2, Saral/Altika and Sentinel-3 dataset at the gauging stations. **Table 3.2** summarizes the scores at the gauging stations, enabling the comparison with those obtained considering observed water levels (**Table 3.1**).

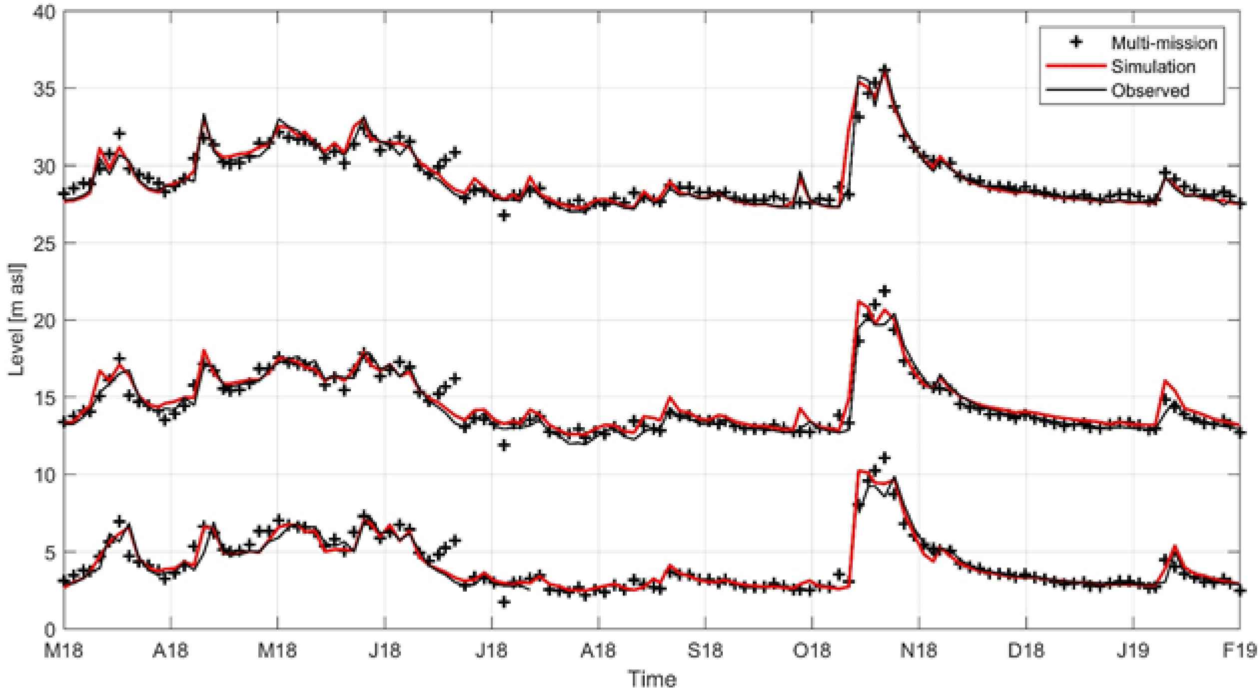

Figure 3.7: Multi-mission version simulated water levels over the calibration period at the gauging stations (Cremona, Borgoforte and Pontelagoscuro; from top to down).

Table 3.2: Calibration results (MAE, NSE and KGE) at the gauging stations over the calibration period considering multi-mission series. Comparison from simulation and traditional observations are recalled from **Table 3.1** for an easier comparison.

	Simulation Vs. Multi-mission			Simulation Vs. Observation		
	MAE [m]	NSE [-]	KGE [-]	MAE [m]	NSE [-]	KGE [-]
Cremona	0.46	0.85	0.88	0.23	0.95	0.97
Borgoforte	0.44	0.89	0.94	0.37	0.93	0.94
Pontelagoscuro	0.37	0.89	0.94	0.25	0.93	0.94

Multi-mission proved to be valuable products for hydraulic model calibration, confirming the results of previous studies carried out in the literature (Domeneghetti et al., 2021). In general, MAE adopting Multi-mission data are higher than those obtained using traditional data; however, a part for few remarkable biases observed during specific events (see for example mid of June 2018), remote series properly capture the water level dynamics in time, appearing a valuable alternative to traditionally recorded data typically missing in sparse and ungauged areas.

3.3. Numerical simulations

The calibrated hydraulic model is run adopting as input the outcomes of the hydrological model performed using different satellite-derived hydrological products (see **Section 2.1**). In particular, a first simulation was run for the entire study period 2017-2019 at hourly resolution adopting as input to the hydrological model the conventional data (see **Section 2.1**). According to what was done for hydrological investigations, the numerical results of this simulation is hereafter referred to as "baseline" and adopted as reference for comparison with other simulations carried out considering different satellite input. **Figure 3.8** reports the flow hydrographs at the gauging stations reproduced for the baseline comparing the simulated and the observed series. Each plot also reports the score performances in terms of MAE, NSE and KGE. **Figure 3.9** reports the same comparison (observed vs simulated baseline configuration) in terms of water levels.

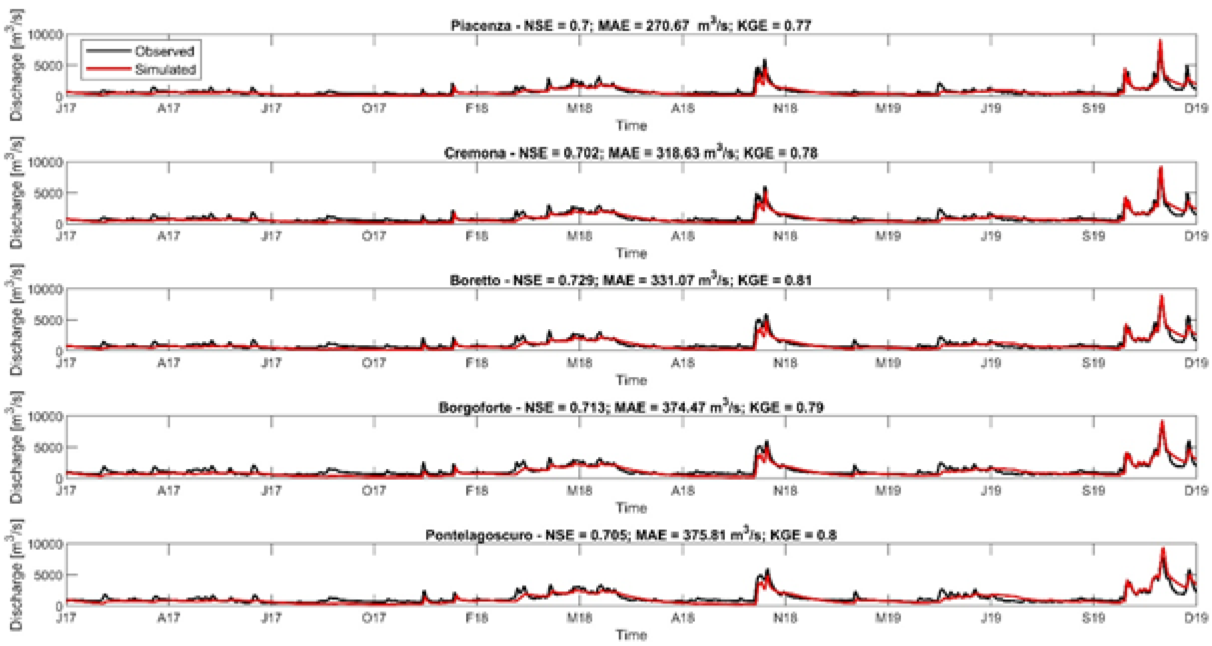

Figure 3.8: Observed vs Simulated (baseline) discharge at the gauging stations. Performance scores (NSE, MAE and KGE) are reported in the plot title.

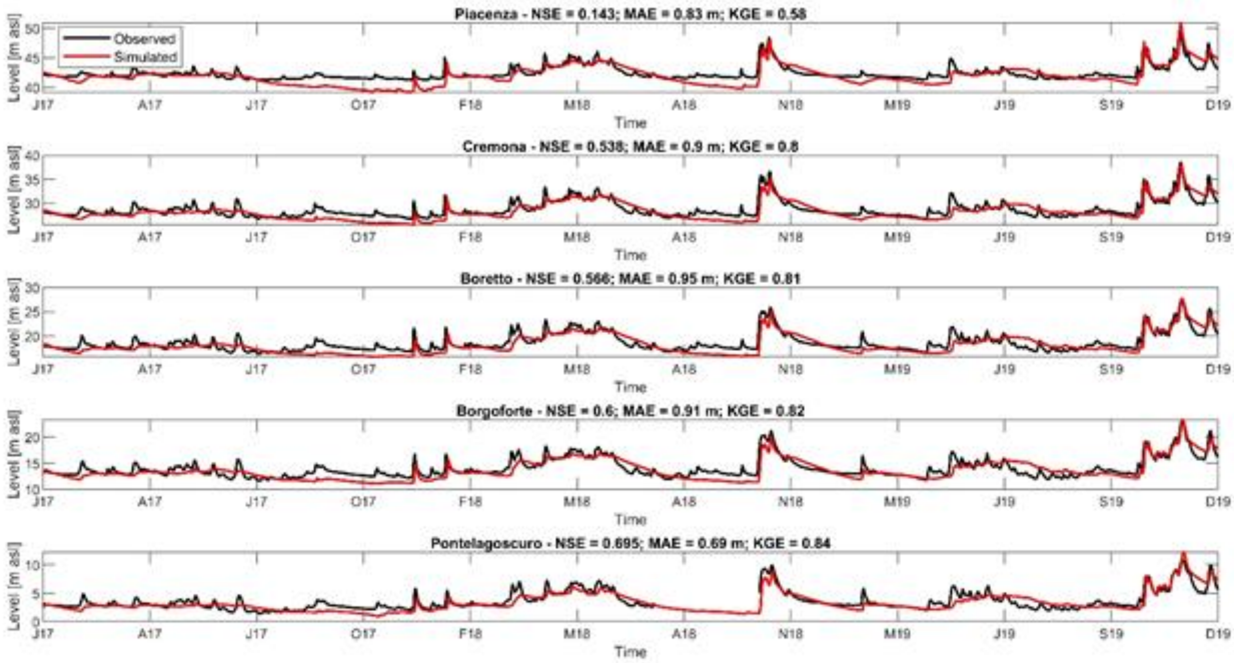

Figure 3.9: Observed vs Simulated (baseline) water levels at the gauging stations. Performance scores (NSE, MAE and KGE) are reported in the plot title.

The following are the different input settings tested in the analysis:

1. SM2RAIN
2. GLEAM
3. C-SNOW
4. RT1
5. All EO

Results obtained for the 5 hydraulic simulations are summarized in terms of KGE in **Table 3.4** and **Table 3.5**, for discharge and water level, respectively. For a better evaluation of satellite-derived settings, the table also reports skill scores for the calibration (see also **Table 3.1**) and for the baseline. Concerning the calibration performance, although these values are referred to a shorter period (i.e., calibration period: March 2018-February 2019), the performance obtained extending the simulation with the calibrated settings to the overall period of interest (2017-2019) provide scores of the some order of magnitude of those achieved for the calibration, and thus not shown for brevity. Shades in tables denote better performance (the darker, the better), while values in bold denote performances better than the baseline.

Table 3.4: KGE for the hydraulic model calibration (column 2), for the baseline (green) and for the 5 different runs driven by satellite data (blue shades) in reproducing the observed discharges at the gauging stations. Performances better than those of the reference simulation (baseline) are in bold. The last row reports the mean performance along the overall river stretch.

	Calibration	Baseline	SM2RAIN	C-SNOW	GLEAM	RT1	All EO
Piacenza	0.92	0.77	0.39	**0.8**	**0.82**	**0.63**	**0.62**
Cremona	0.87	0.78	0.38	**0.81**	**0.84**	0.64	0.62
Boretto	0.85	0.81	0.61	0.81	0.81	**0.83**	0.6
Borgoforte	0.91	0.79	0.44	0.81	**0.86**	0.66	0.62
Pontelagoscuro	0.81	0.8	0.36	0.82	**0.85**	0.71	0.54
Mean	0.87	0.79	0.44	**0.81**	**0.84**	0.694	0.6

Table 3.5: KGE for the hydraulic model calibration (column 2), for the baseline (green) and for the 5 different runs driven by satellite data (blue shades) in reproducing the observed water levels at the gauging stations. Performances better than those of the reference simulation (baseline) are in bold. The last row reports the mean performance along the overall river stretch.

	Calibration	Baseline	SM2RAIN	C-SNOW	GLEAM	RT1	All EO
Piacenza	0.93	0.58	0.34	0.58	**0.63**	**0.64**	0.58
Cremona	0.97	0.8	0.6	0.8	0.8	**0.82**	0.6
Boretto	0.95	0.81	0.61	0.81	0.81	**0.83**	0.6
Borgoforte	0.94	0.82	0.65	0.81	0.82	**0.83**	0.59
Pontelagoscuro	0.94	0.84	0.6	**0.85**	**0.86**	0.78	0.62
Mean	0.95	0.77	0.56	0.77	**0.78**	**0.78**	0.60

The comparison between the calibration and baseline scenarios denotes an overall good performance of the hydraulic simulation driven with results of the hydrological model settled adopting traditional data set (baseline). Although KGEs for the baseline are in general lower than those ensured with the model driven adopting observed data, these differences can be attributed to the difficulties of the hydrological model in reproducing small flood events ascribable to minor basins. This appears evident looking at **Figure 3.8**, and in particular for the upper part of the basin (e.g., Piacenza). Major events, such as those on Oct. 2018 and Oct-Nov. 2019 are instead reproduced in a more satisfying way.

As expected, results obtained from the hydraulic simulations confirm the findings emerged from the hydrological simulations. In particular, focussing on discharges (**Table 3.4**), simulations including GLEAM and C-SNOW are those ensuring better performances. GLEAM, more than others, ensures increasing KGE, with an average improvement of 0.07, that locally can rise up to scores similar or better than the baseline. Performances on discharge estimation in this case are very close to those obtained during the calibration phase, thus further sustaining the potential of using satellite products in hydrological and hydraulic modelling.

Simulations including RT1 soil moisture, SM2RAIN as well as the one adopting all four satellite derived products (All EO) produced an average worsening of the model performances (-0.08, -0.17 and -0.33 for RT1, All EO and SM2RAIN, respectively). The worsening for All EO and SM2RAIN configurations are due to biases on reproducing major events, with in general an overestimation of peak flows and events duration. Nevertheless, all configurations guarantee valuable mean performances (KGE positive and generally higher than 0.6), which prove the potential of satellite-based products as alternatives in regions where ground data is not available.

Results in terms of water level (**Table 3.5**) confirm previous consideration though performances appear slightly worse than for discharge. This is attributed due to the additional uncertainties and biases introduced with the river schematization and hydraulic settings. Nevertheless, mean scores are of the same order of magnitude of the baseline and slightly worse in case of adopting all satellite products (All EO).

Figure 3.10 and **Figure 3.11** show examples of observed versus simulated discharge time series at the gauging stations obtained for GLEAM and All EO settings, respectively.

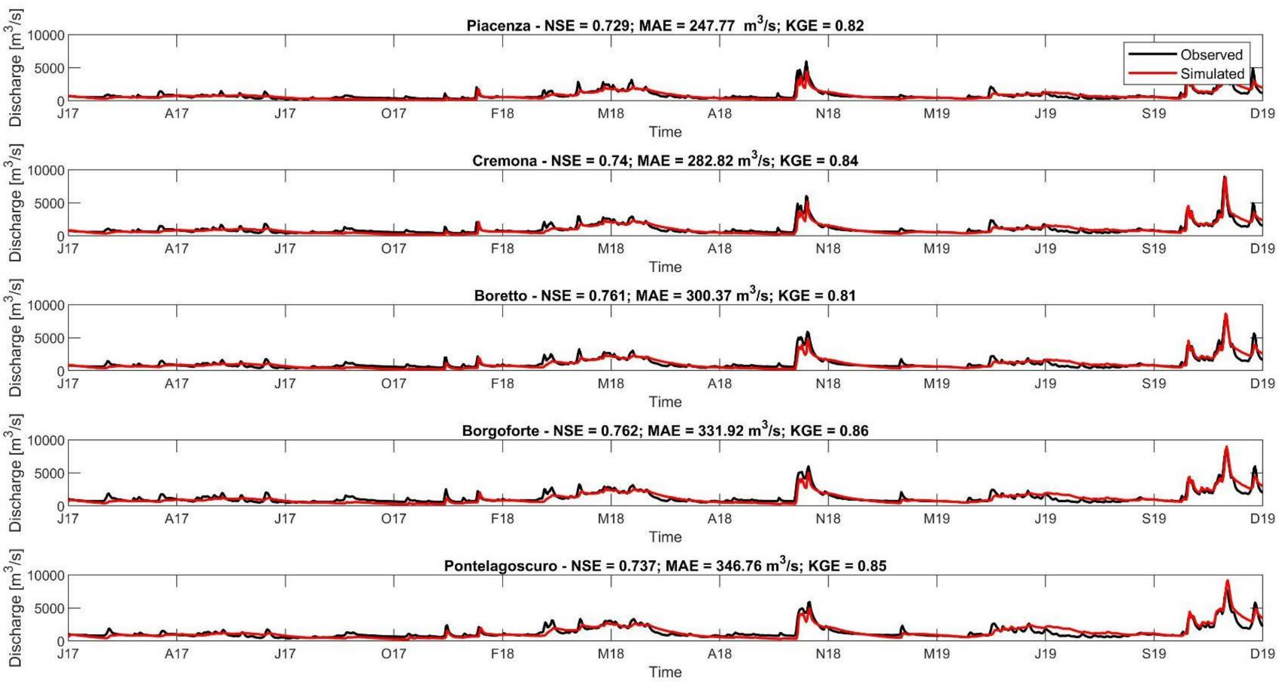

Figure 3.10: Observed vs Simulated (GLEAM) discharge at the gauging stations. Performance scores (NSE, MAE and KGE) are reported in the plot title.

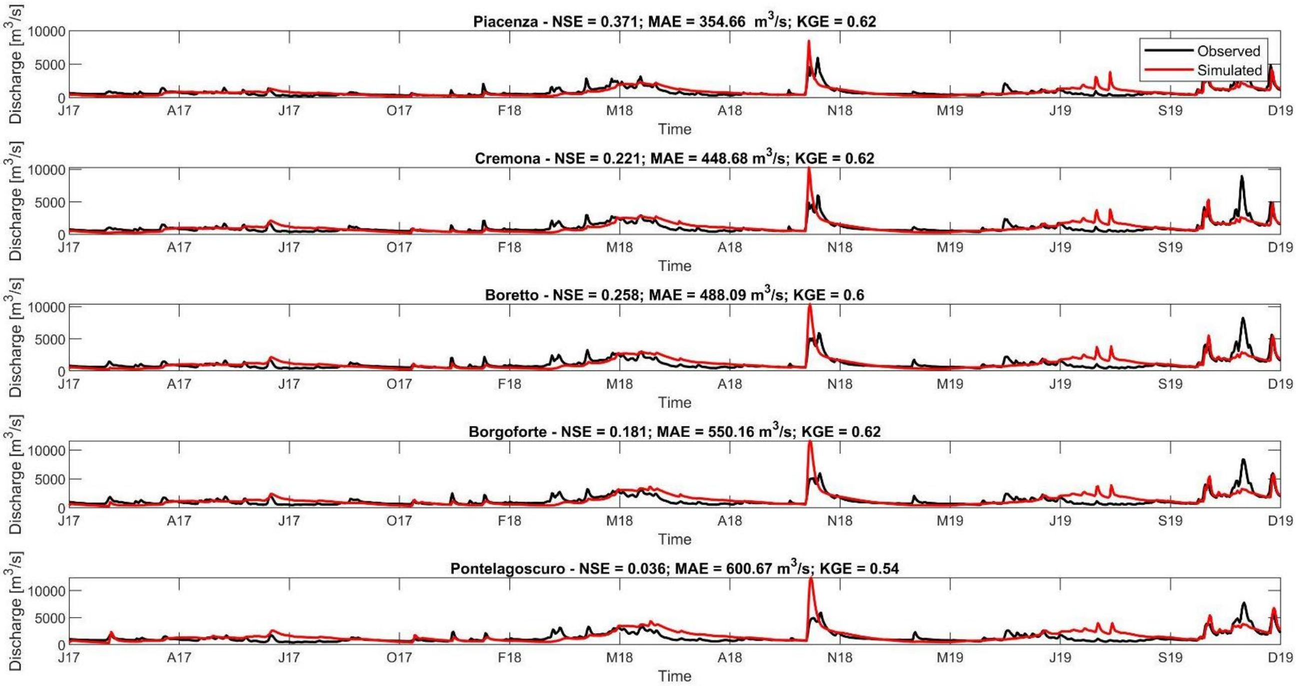

Figure 3.11: Observed vs Simulated (All EO) discharge at the gauging stations. Performance scores (NSE, MAE and KGE) are reported in the plot title.

In addition to the simulation of the flow hydrographs (i.e. water level and discharge series can be retrieved at any location of interest along the river), the use of hydrological and hydraulic models can potentially be profitable for many water management applications. For example, the model can provide information concerning the water volume dynamics within specific areas (es. within minor dike-protected floodplains, where such knowledge is useful for the evaluation of the impacts on side activities eventually planned in the areas - e.g., agriculture, recreative initiatives, etc.), provide insights concerning the water availability and thus on the functionality of water intake plant, agriculture planning, environmental conditions, etc.

Concerning information on water availability, a key information is typically represented by the flow duration curve (FDC), which graphically represents the relationship between river discharges expected at a given cross-section and the duration (i.e., the percentage of time) they are exceeded, or equal, during a given reference period (e.g., a year, or longer, periods). FDCs provide a general overview of the hydrological regime of a catchment, thus, they are widely and routinely used in many water resource investigations, such as water resource management, hydropower generation, design and management of water supply systems, irrigation planning, and eco-hydrological studies (**Domeneghetti et al., 2018**).

Figure 3.12 and **Figure 3.13** report two examples of FDC retrieved at two of the gauging stations (Cremona and Pontelagoscuro) available along the studied river, providing a comparison between observed FDCs and those constructed based on hydrological and hydraulic simulations.

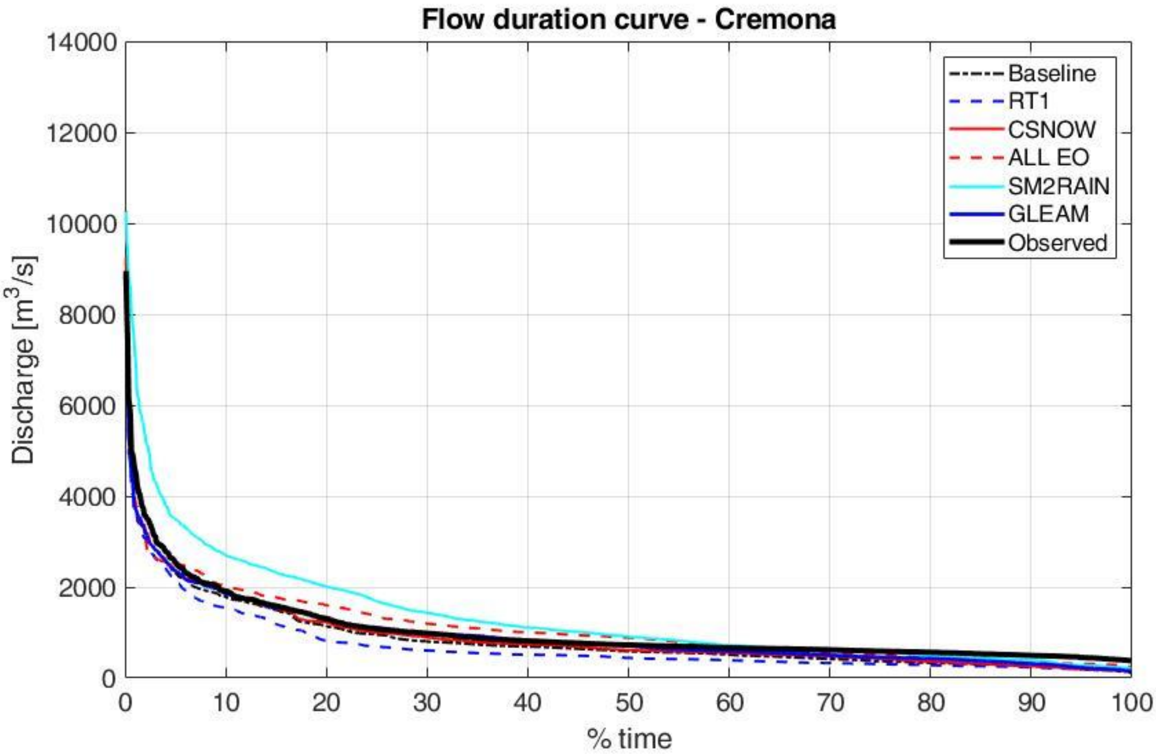

Figure 3.12: Observed vs simulated FDCs at Cremona.

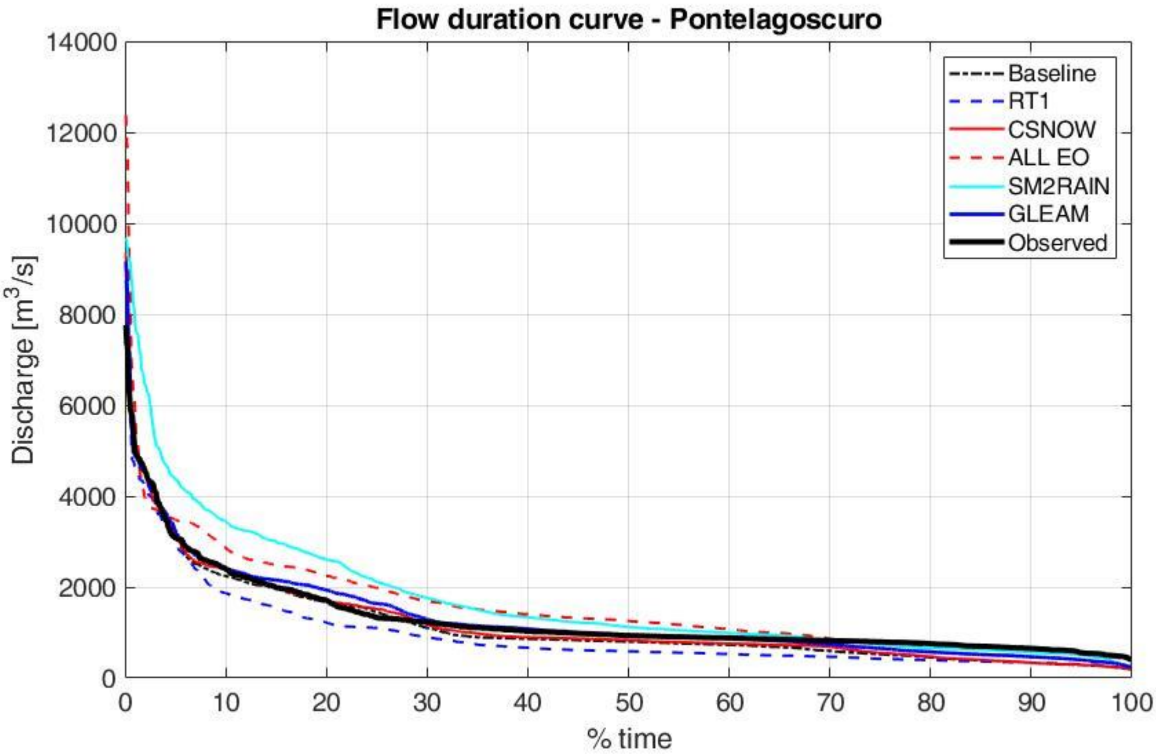

Figure 3.13: Observed vs simulated FDCs at Pontelagoscuro.

As expected, results show a general agreement between observed, GLEAM and C-SNOW FDCs, whereas a general underestimation (overestimation) on discharge values is obtained in case of RT1 (ALL EO and SM2RAIN). That said, the comparison between observed and satellite-derived FDCs provide encouraging results and demonstrates the potential of hydrological and hydraulic model driven by satellite data in estimating the flow regime of the river at different locations.

4. Flood prediction: Enza River (2D flooding modelling)

For the 2D flooding modelling analysis of the DTE-Hydrology Project the WEC-Flood model (**Sinagra et al., 2020**) is employed. The proposed model is able to generate, through a mesh-generator application and a GIS interface, a computational domain composed of cells of variable size, which correspond the geometric parameters of the areas investigated, on which to study the unsteady flow in the two dimensions. It is composed by two components.
The first, named *Hydronet*, generates a Triangulated Irregular Network (TIN) covering all the computational domains (urban and not urban areas) and a set of nodal topographic elevations performing two different tasks - to be a suitable computational mesh for the shallow water hydraulic model, and - to form with some of its edges a hydrographic network of previously assigned density. The method leverages topographical data coming from a digital elevation model (DEM), integrated by other available information, and leads to a TIN, also taking hydraulic infrastructure elevations into account.
The second component is a *2D hydraulic model* aimed to efficiently estimate the flooded area using the same spatial discretization of the TIN model, leveraging the heterogeneity of the computational mesh density inside the urban and the upstream basin area.
The proposed model requires as input the Digital Elevation Model (DEM) of a basin, additional topographic information representing hydraulic singularities as culverts, levees and bridges, as well as observed/forecasted precipitation, upstream and downstream boundary conditions and is able to provide the flood maps automatically.

4.1. In situ and satellite data

The flood event occurred along the Enza River in December 2017 has been analysed by using the WEC-Flood model. The selected event caused extensive flooding mainly due to a levee failure close to Lentigione di Brescello. The Enza River is one of the right tributaries of the Po river. It has a drainage area of about 890 km^2 and a total length of about 100 km (**Figure 4.1a**).
The study was aimed at the reproduction of the flooded areas as shown by three available satellite images during the flood event period in the area located downstream the Sorbolo hydrometric station (see **Figure 4.1b**). The input data used for running the WEC-Flood model are:

- the Digital Elevation Model (DEM) at 1 m resolution (**Figure 4.2**). It has to be underlined that the available DEM is characterized by some areas (identified by the brown colour in **Figure 4.2**) with zero elevation data. These areas were not included in the hydraulic simulations;
- the upstream boundary condition represented by the discharge hydrograph recorded at Sorbolo gauged station (**Figure 4.3**);
- the location and geometric characteristics of the levee breach occurred on 12/12/2017 at 5.27 am.

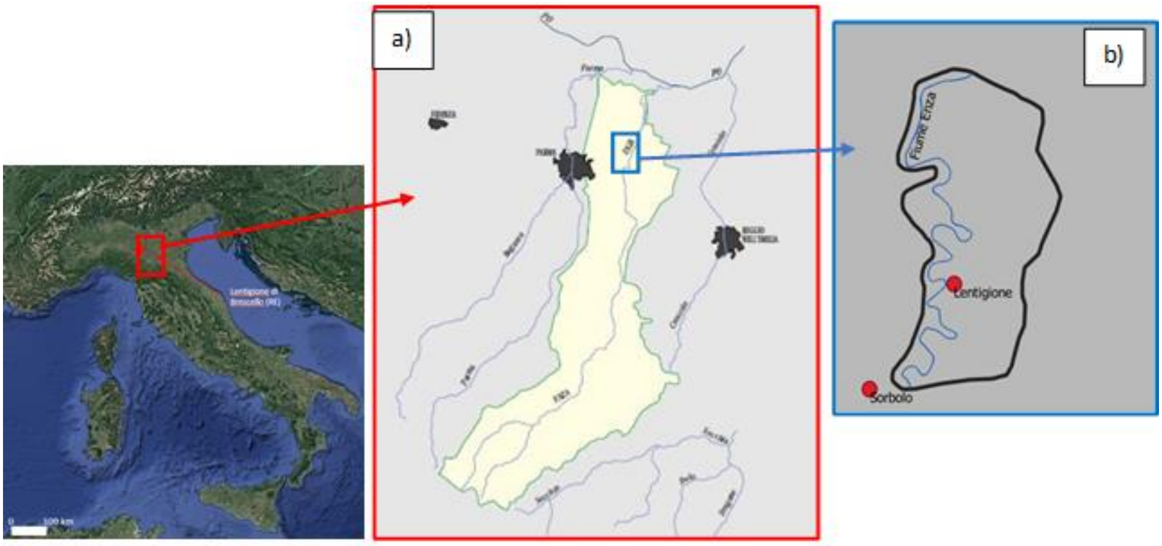

Figure 4.1 – Case study location: a) Enza river basin; b) investigated area.

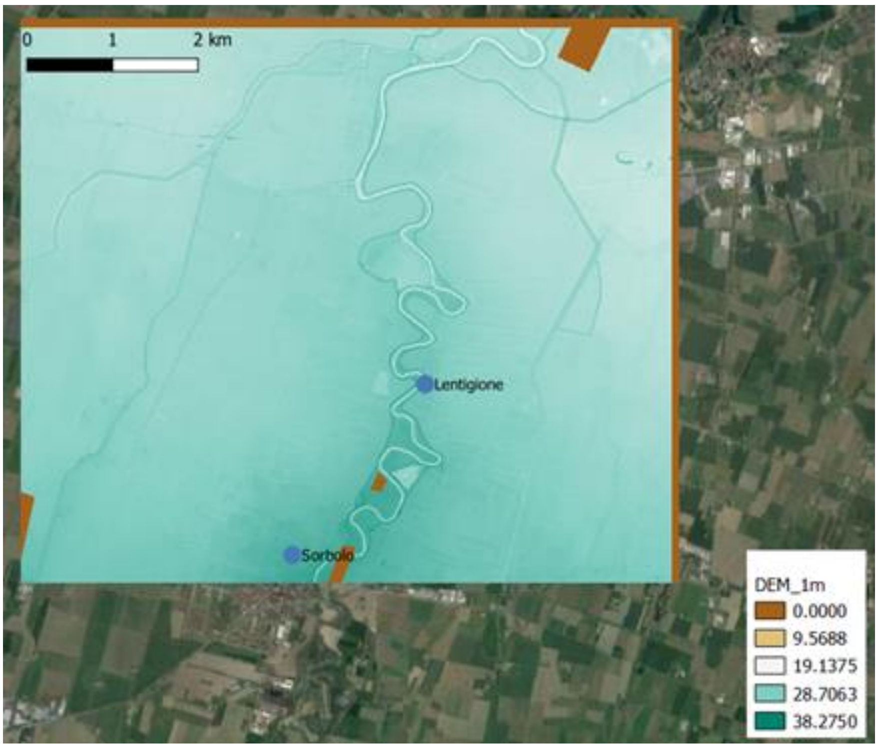

Figure 4.2 - Digital Elevation Model (DEM) at 1 m resolution.

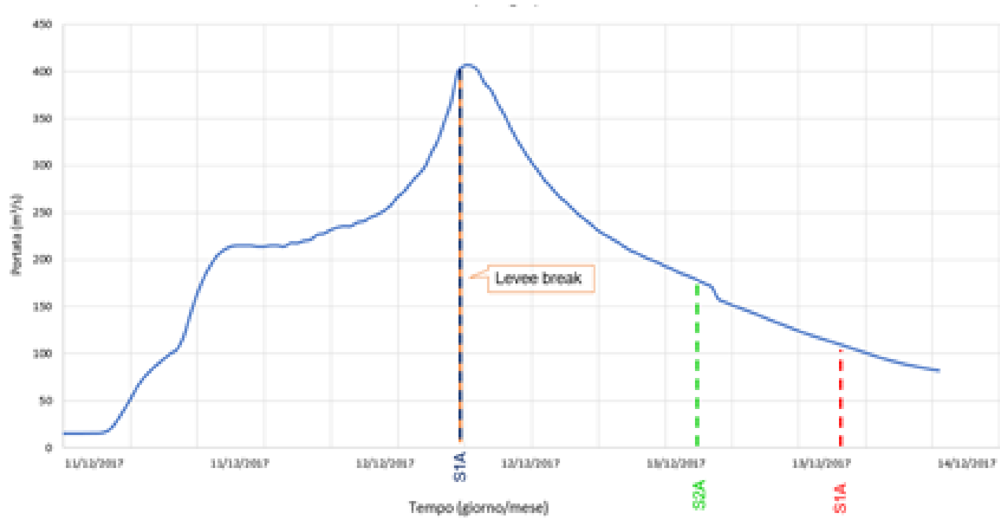

Figure 4.3 – Discharge hydrograph recorded at Sorbolo gauged section. The occurrence time of the levee breach and of the three used satellite images is also shown.

The use of the high-resolution satellite data represents a significant improvement for the 2D hydraulic model calibration, if compared with using as benchmark the information of the extension of the flooded areas that can be derived by fragmentary ground/remote data (e.g. pictures, videos, direct testimonies, indications derived from videos recorded during helicopter flights, etc.). For the selected case study, three high resolution satellite images have been used to map the flooded area at different times during the evolution of the flood event. Specifically, the following satellite images were used:

1) Sentinel-1A GRD in VV polarization descending, acquired on 12th December, 2017 at 5:27 am. This image shows the area condition just before the levee breach occurrence (**Figure 4.4**);
2) Sentinel-2A descending, acquisition date 13th December, 2017 at 10:24 am. This image shows the area condition about 29 hours after the levee breach occurrence (**Figure 4.5**);
3) Sentinel-1A VV ascending, acquisition date 13th December, 2017 at 5:15 pm. This image shows the area condition about 36 hours after the levee breach occurrence (**Figure 4.6**).

The acquisition time of each satellite image is also indicated in **Figure 4.3**.

Figure 4.4 – Satellite imagine: Sentinel 1A GRD VV descending (12 December 2017 5:27 am).

Figure 4.5 – Satellite image: Sentinel 2A [NGB] descending (13 December 2017 10:24 am).

Figure 4.6 - Satellite imagine: Sentinel 1A VV ascending (13 December 2017 5:15 pm).

4.2. Simulations and Results

The flood event simulation by using the WEC-Flood was carried out after the model setup. First, the boundary of the computational domain was identified, as well as the internal discontinuities (e.g. levees longitudinal systems and river network). The computational mesh was developed by setting a spatial resolution equal to 5 meters.

The discharge hydrograph observed at Sorbolo gauged station (shown in **Figure 4.3**) identified the upstream boundary condition. The levee breach occurrence was simulated in the model. WEC-Flood allows to modify the topographical elevation of selected nodes of the mesh during the simulation. Therefore, starting from the time of the breach occurrence, the lower elevation of the levee crest was considered simulating the known geometrical characteristics of the breach, i.e. 160 meters long and 3 meters deep (**Figure 4.7**, right).

The roughness parameter *n* (i.e. Manning coefficient) assessment is the main focus of the calibration analysis based on the comparison between the model results (flooded maps) and the evidence provided by the satellite images. To this end, some simulations were carried out by using different roughness parameter values. The different values of the roughness Manning coefficient were assumed in a feasible range (0.06, 0.08, 0.09, 0.10, 0.11, 0.12, 0.13 $m^{-1/3}s$). The roughness characteristics were considered uniform for all the computational domain. It is worth noting that preliminary simulations were carried out in order to test the effects of using different values of *n* parameter for the main channel elements and the elements of the floodplains and levees; the results clearly showed that no significant modifications were introduced by the parameter differentiation.

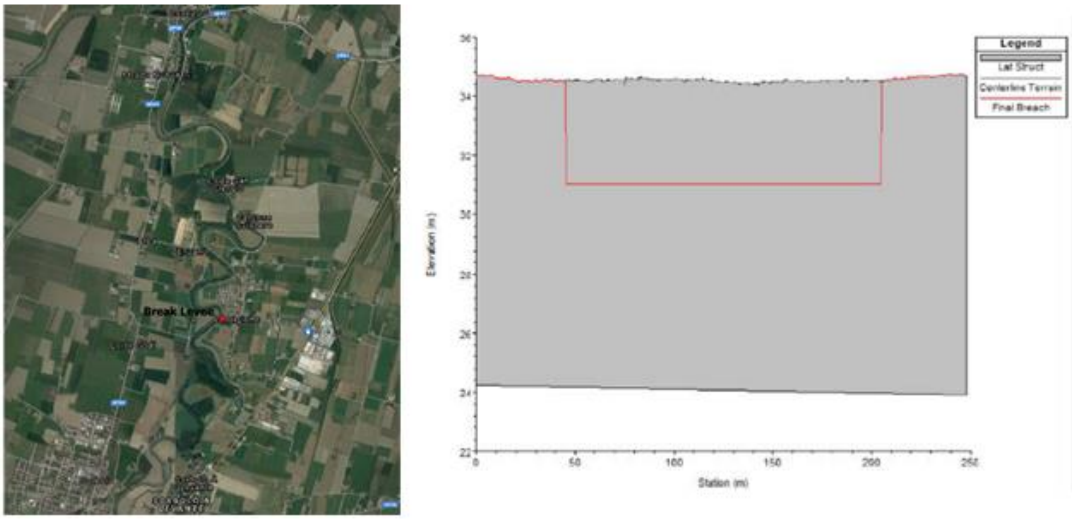

Figure 4.7 – Levee breach along the Enza river: left) location and right) geometry used in the model.

Figure 4.8 - Flooded area simulated by the hydraulic model for different Manning coefficients (hydraulic simulation frame corresponding to the satellite image acquired on 13/12/2017 at 5:15 pm).

In order to identify the optimal value of the roughness coefficient, the results obtained by applying different Manning coefficients were compared with the observed satellite images. By way of example, **Figure 4.8** shows, for the hydraulic simulation frame corresponding to the satellite image acquired on 13 December 2017 at 5:15 pm, the flooded areas estimated by the model with different roughness properties. It can be easily seen that when the Manning coefficient is low (i.e. equal to 0.06 $m^{-1/3}s$) the extent of the flooded area is limited, while when the Manning coefficient is higher (0.10 or 0.12 $m^{-1/3}s$) the flooded area is more extended.

The extraction of the flooded areas from the satellite images was carried out following the well consolidated methods available in literature. Specifically, for the optical image, several spectral indices were calculated:

AWEI = 4* (GREEN - SWIR1) - (0.25 * NIR + 2.75 * SWIR2) (**Feyisa et al., 2014**)

$AWEI_{sh}$ = BLUE + 2.5 * GREEN - 1.5 * (NIR + SWIR1) - 0.25 * SWIR2 (**Feyisa et al., 2014**)

NDWI = (GREEN - NIR) / (GREEN + NIR) (**Mc Feeters et al., 1996**)

NDVI = (NIR - RED) / (NIR + RED)

mNDWI = (GREEN - SWIR1) / (GREEN + SWIR1) (**Xu, 2006**)

NDFI = (RED - SWIR2) / (RED + SWIR2) (**Boschetti et al., 2014**)

WRI = (GREEN + RED) / (NIR + SWIR1) (**Shen and Li, 2010**)

Based on these spectral indices and assuming a threshold equal to zero for all the indices, except for NDFI that is equal to 0.32 and WRI equal to 1, the flooded areas were derived and are shown in **Figure 4.9**. By the comparison with the image in false colour of **Figure 4.5**, the water map extracted by the use of mNDWI seems to be the most reliable and it is used for the successive analysis of calibration.
For the SAR images, the histogram threshold (**Hostache et al., 2009**) is a common approach used to distinguish between flooded and non-flooded areas by the analysis of the radiometric distributions of water bodies and other land use types. Considering that it is difficult to identify a single threshold value that permits to detect water bodies only, it is necessary to check the estimated flooded boundaries through several observed control points. In the case of the two images acquired on 12th December, 2017 at 5:27 am and on 13th December 2017 at 5:15 pm, the flooded areas cover different surfaces and the histogram are deeply different as represented in **Figure 4.10a** and **Figure 4.10b**. However, a common threshold is identifiable looking at the minimum value between the two distributions and it is fixed equal to -18.1 dB. The resulting flooded areas are illustrated in **Figure 10c** and **Figure 10d**.
In order to objectively identify the optimal value of the roughness coefficient, each simulated flooding scenario was compared against the one observed by the satellite images by applying the procedure proposed by **Aronica et al. (2002)**, which is based on the index *F* representing the measure of how much overlap there is between the observed and the computed flooded areas:

$$F = A/(A + B + C)$$

where A is the size of the wet area correctly predicted by the hydraulic model, B is the area predicted as wet that is instead observed dry (overprediction), and C is the wet area not predicted by the model (underprediction). *F* ranges from 0 to 1; when it is equal to 1, observed and predicted areas coincide exactly, and when it is equal to 0, no overlap between predicted and observed areas exists. Therefore, the maximization of *F* allows one to estimate the optimal value of *n* for which the flooded area estimated by the model is as close as possible to the observed one (Tarpanelli et al. 2013).

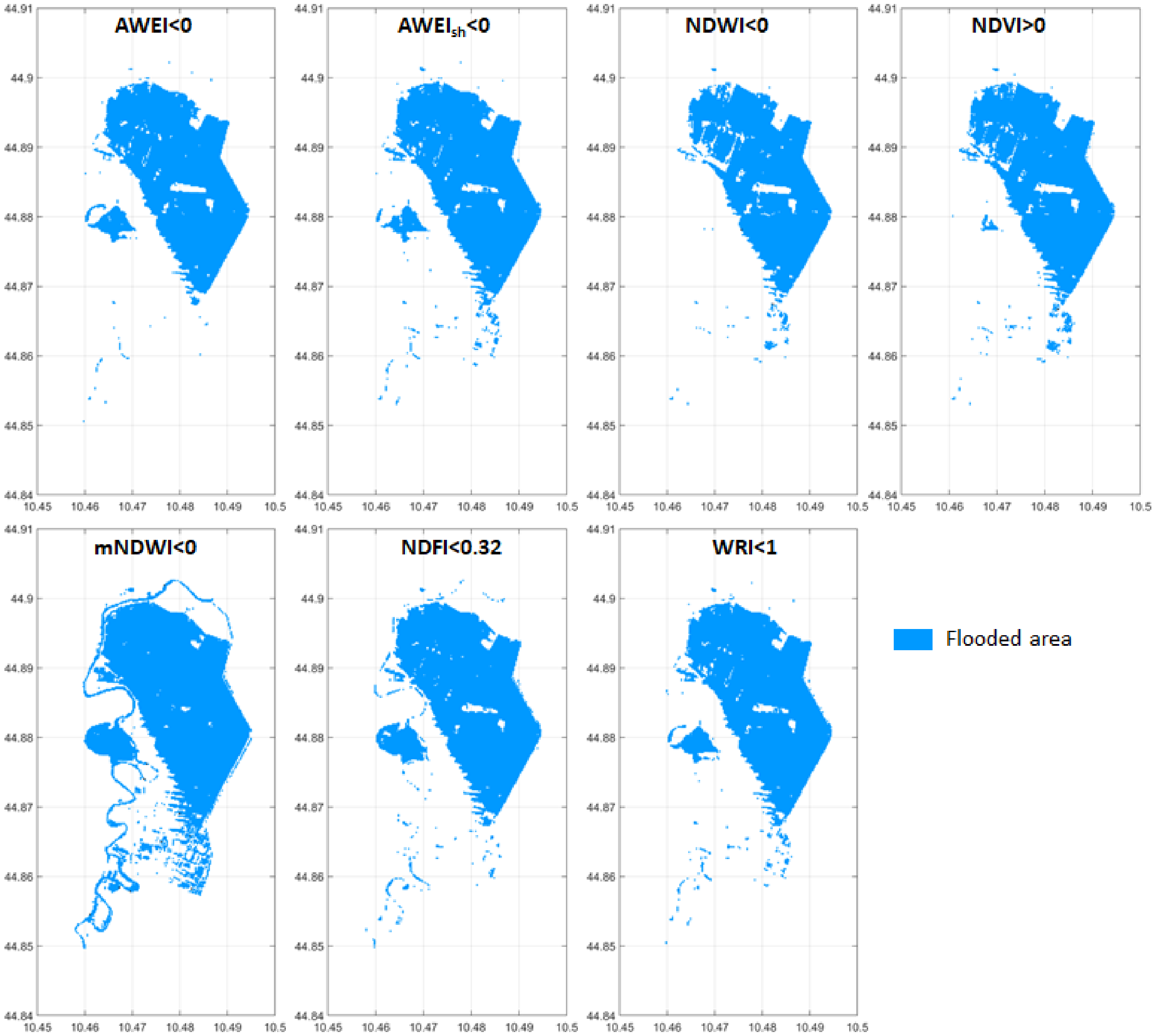

Figure 4.9 - Flooded area retrieved by the optical images through the use of seven spectral indices.

Specifically, the index estimation was carried out for the two selected satellite images by considering the corresponding frames of the hydraulic simulations. Indeed, the S1 image acquired just before the levee breach occurrence highlights small areas covered by inundation; therefore, a calibration of the Manning parameter with this image could not be optimal for the analysis. The S1 and S2 images available after some hours from the levee breach occurrence, cover better the downstream part of the area, where the water accumulated close to the SP41. Therefore, both the images are considered for the comparison with the hydraulic model simulations.

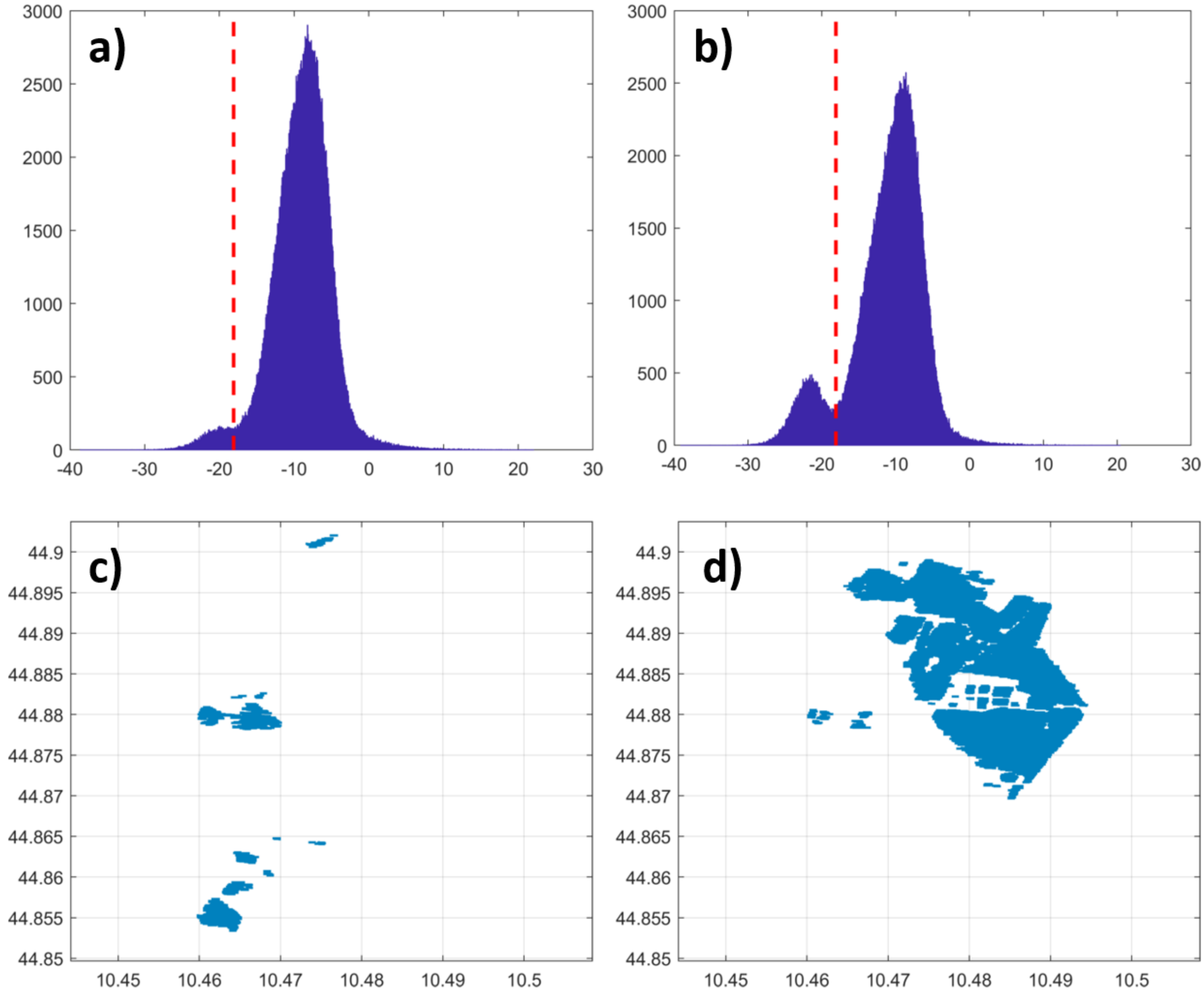

Figure 4.10 - Histogram of the backscatter (a and b) and flooded areas (c and d) below the threshold shown in dashed red line of the two SAR images acquired on 12th December, 2017 at 5:27 am (a and c) and 13th December 2017 at 5:15 pm (b and d).

The results of the analysis are summarized in **Figure 4.11** in terms of *F* for both the optical and SAR image. The two plots show a difference both in the value (for optical *F* values are greater than those of SAR image) and in the optimal Manning roughness coefficient. Specifically, the hydraulic model is able to represent more accurately the edge extracted by the optical image. Concerning the comparison with the SAR image, the hydraulic model shows flooded areas in the upstream part that are completely neglected by the SAR image and this provides a lower number of pixels in agreement (and consequently a lower value of A and a larger value of B in the *F* formulation). Therefore, the analysis of the WEC-Flood hydraulic model results indicates that the roughness coefficient equal to 0.11 $m^{-1/3}s$ is the one providing a better reproduction of the area condition as shown in the Sentinel 2A image acquired on 13th December 2017 at 10:24 am, about 29 hours after the levee breach formation. **Figure 4.12** shows the comparison between the flooded area simulated by setting n=0.11 $m^{-1/3}s$ and the flooded area depicted in the optical satellite image.

The comparison of the hydraulic model results with the last image Sentinel 1A image acquired on 13 December 2017 at 5:27 pm, about 36 hours after the levee breach occurrence, indicates that the roughness coefficient equal to 0.09 $m^{-1/3}s$ is the one providing a better reproduction of the flooded area. **Figure 4.13a** shows the comparison between the flooded area simulated by setting n=0.09 $m^{-1/3}s$ and the flooded area depicted in the satellite image. It is evident the large overestimation of the model to reproduce the flooded area depicted by the satellite and a consequent low value of Manning coefficient. For a sake of comparison **Figure 4.13b** shows the comparison with the n=0.11 $m^{-1/3}s$ optimized for the optical image. The comparison between the two maps demonstrates no overestimation of the model, and the flooded area extracted by the SAR image is completely mapped by the model. This means that the simulation was not able to accurately represent the dry conditions occurred after some hours from the inundation.

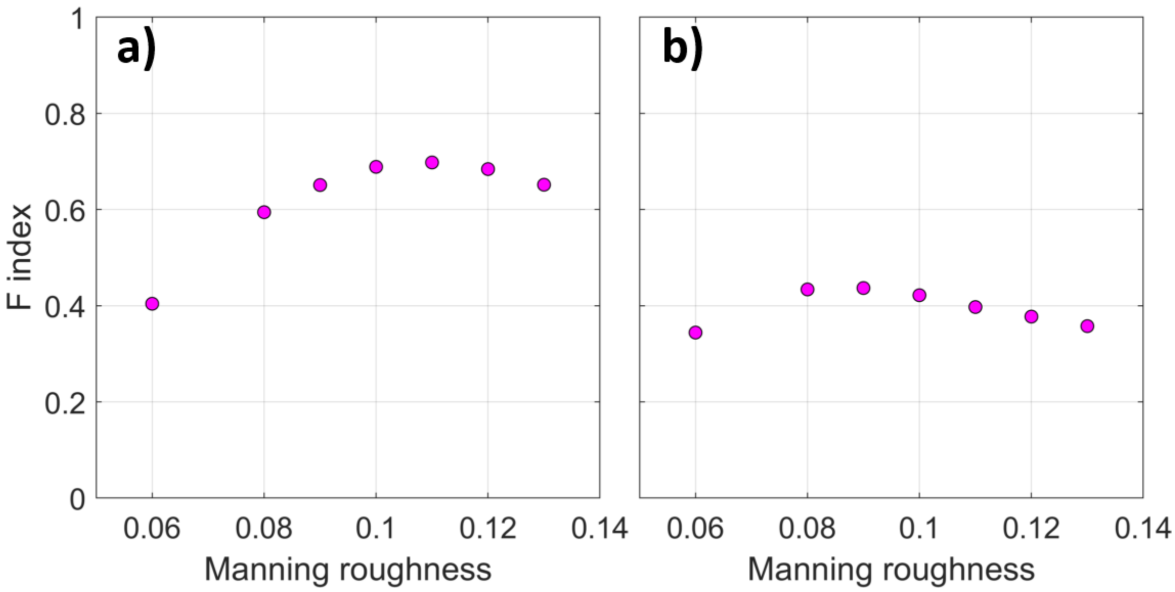

Figure 4.11 – Flooded areas analysis: variability of the measure of fit F as a function of the Manning roughness coefficient for two satellite images: a) Sentinel 2A (13/12/2017 10:24 am); b Sentinel 1A (13/12/2017 5:15 pm).

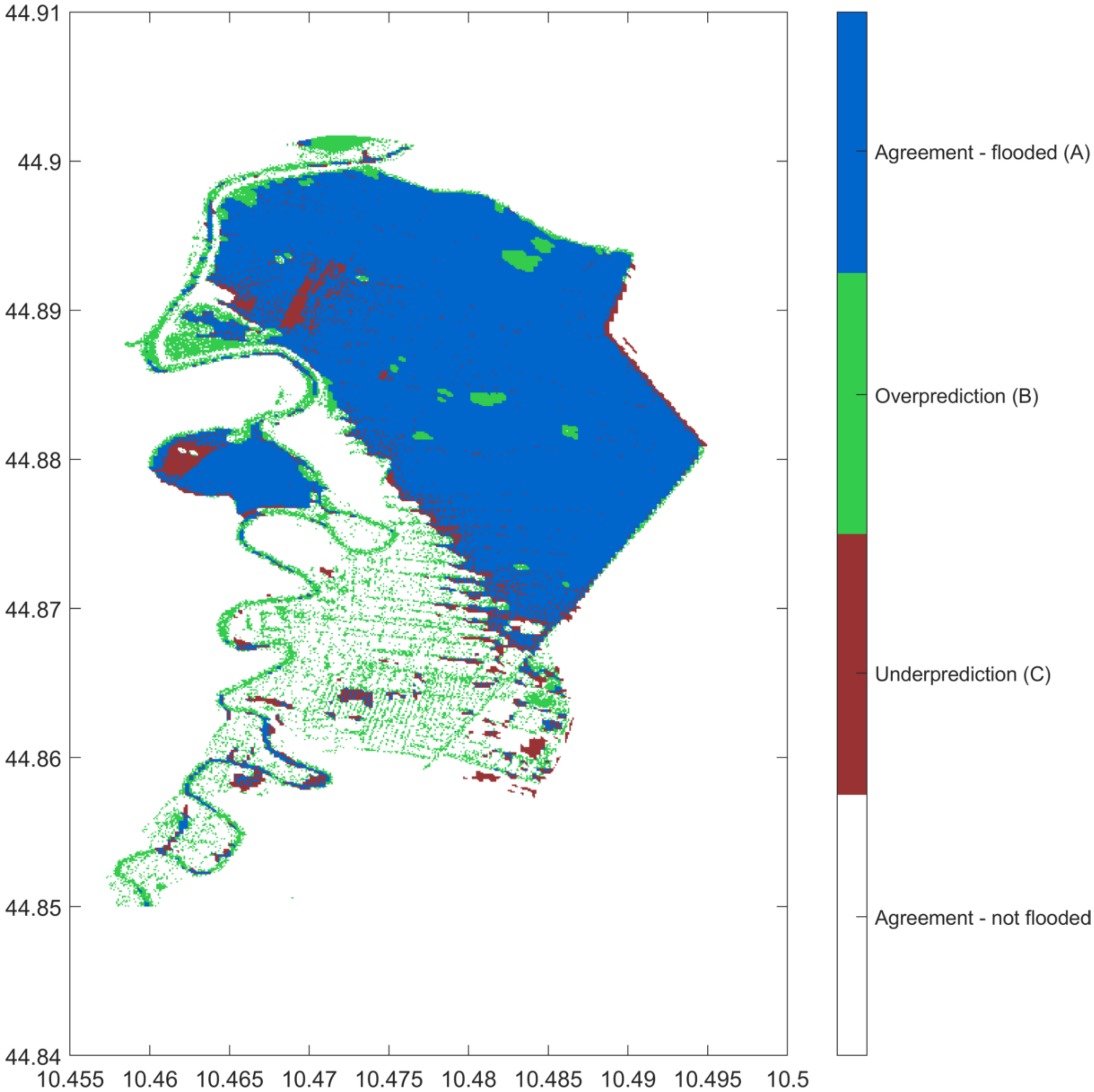

Figure 4.12 – Flooded area on 13/12/17 at 10.24 am: comparison between the flooded areas extracted by the satellite image Sentinel 2A and those derived by Wec-Flood model simulation with n=0.11 $m^{-1/3}s$.

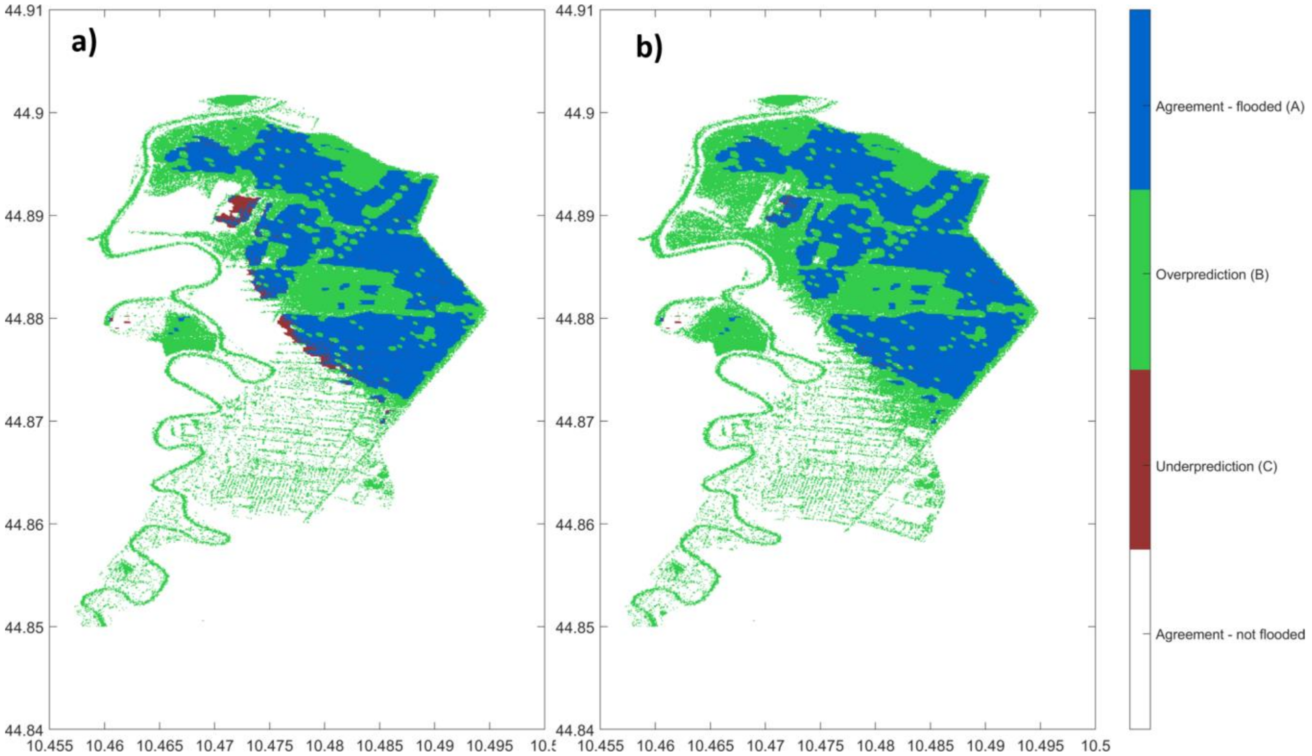

Figure 4.13 – Flooded area on 13/12/17 at 5.15 pm: comparison between the flooded areas extracted by the satellite image Sentinel 1A and those derived by Wec-Flood model simulation with n=0.09 $m^{-1/3}s$ (a) and n=0.11 $m^{-1/3}s$ (b).

5. Landslide prediction: Oltrepò Pavese

5.1. The slope stability model

The implemented slope stability model is based on the infinite slope approach (**Skempton and De Lory, 1957**). The model is based on the following assumptions:

- slope extent is undefined or much larger than the depth of potential slip surface;
- slope angle is constant;
- soil characteristics are homogeneous along the slope direction;
- failure or slip surface is parallel to the slope's ground surface;
- rigid-perfectly plastic constitutive law;
- Mohr-Coulomb's failure criterion on the slip surface.

The infinite slope geometry here considered is drawn in **Figure 5.1** where β is the slope angle, γ is the soil volume weight, H_{ss} is the depth of the sliding surface and H_{wt} is the depth of the water table.

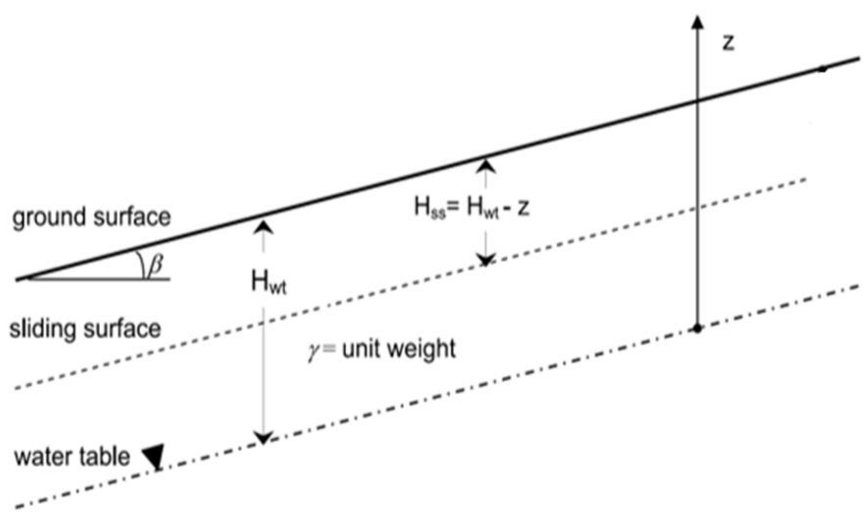

Figure 5.1. Infinite slope schematization (from **Lu and Godt, 2008**)

In the limit equilibrium approach the slope stability conditions are estimated through an index called Factor of Safety (FS), defined as the ratio of the resisting forces over the mobilizing forces acting on the slope. When FS reaches 1, we are at the equilibrium and an instability is likely to occur. **Lu and Godt (2008)** proposed a method to evaluate stability conditions for different saturation degrees. In this way it is possible to estimate the FS as a function of the soil moisture and its variations in time.

Through the use of the following equation, the impact of soil saturation is taken into account:

$$FS = \frac{tan\varphi}{tan\beta} + \frac{2c}{H_{ss}\gamma sin2\beta} - \frac{\sigma^s}{H_{ss}\gamma}(tan\beta + cot\beta)tan\varphi$$

Where β is the slope angle, φ is the angel of internal friction, c is the soil cohesion, H_{ss} is the depth of the sliding surface, γ is the unit weight of soil and σ^s is the soil suction, defined as:

$$\sigma^s = Se(u_a - u_w)$$

Where Se is the relative soil saturation, u_a and u_w are the air the water pore pressures, respectively.

In order to test the capabilities of the high resolution products developed within DTE Hydrology, the proposed methodology has been applied to two rainfall events localized in the Oltrepo Pavese area (North Italy) that triggered about 100 shallow landslides.

5.2. Case study

The analysis carried out within DTE Hydrology involved two rainfall events that occurred in February 2016 and November 2019 over the Ardivestra catchment in North Italy (**Figure 5.2**).

Figure 5.2 - Localization of the study area.

The two rainfall events triggered about 100 shallow landslides within the Ardivestra catchment, as drawn in **Figure 5.3**.

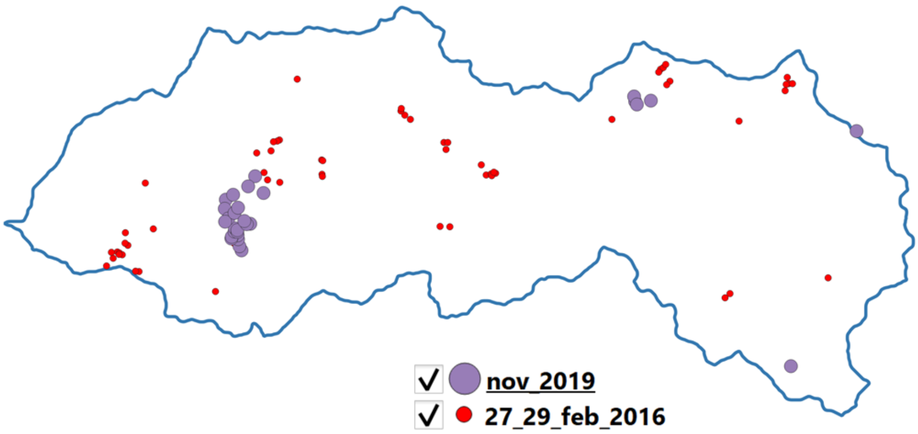

Figure 5.3 - Spatial distribution of the considered landslides within the catchment.

The soil mechanics and hydraulics parameters have been obtained by field surveys, laboratory tests and literature analysis. In this way, the soil parameters values vary among the different lithologies, defining for each landslide a set of parameters values related to the geological setting. For each landslide a common value of 2 m for the depth of the sliding surface has been chosen according to field campaign data.

The hourly rainfall product that integrates raingauges and ground radar data has been used as driving input. In order to test the added value of using high resolution soil saturation data for slope stability purposes, three different soil moisture products have been tested:

1) RT1 (**Quast et al., 2019**);
2) Integration between S1 and ASCAT data (hereinafter S1ASCAT);
3) DIREX SAR product (hereinafter DIREX).

In order to match the temporal resolution of the input datasets, the daily temporal scale has been used. The surface soil moisture data have been considered at such depth by applying the same filter to the raw observations. In this case we applied an exponential filter with a characteristic time length (T) of 20 days. The parametrized model has been run over a 1 km grid, the same used for providing the input data, during all the analysis period, i.e. 2016-2019. In **Figure 5.4** it can be observed the time series of soil saturation, rainfall and FS in a time period including the February 2016 event.

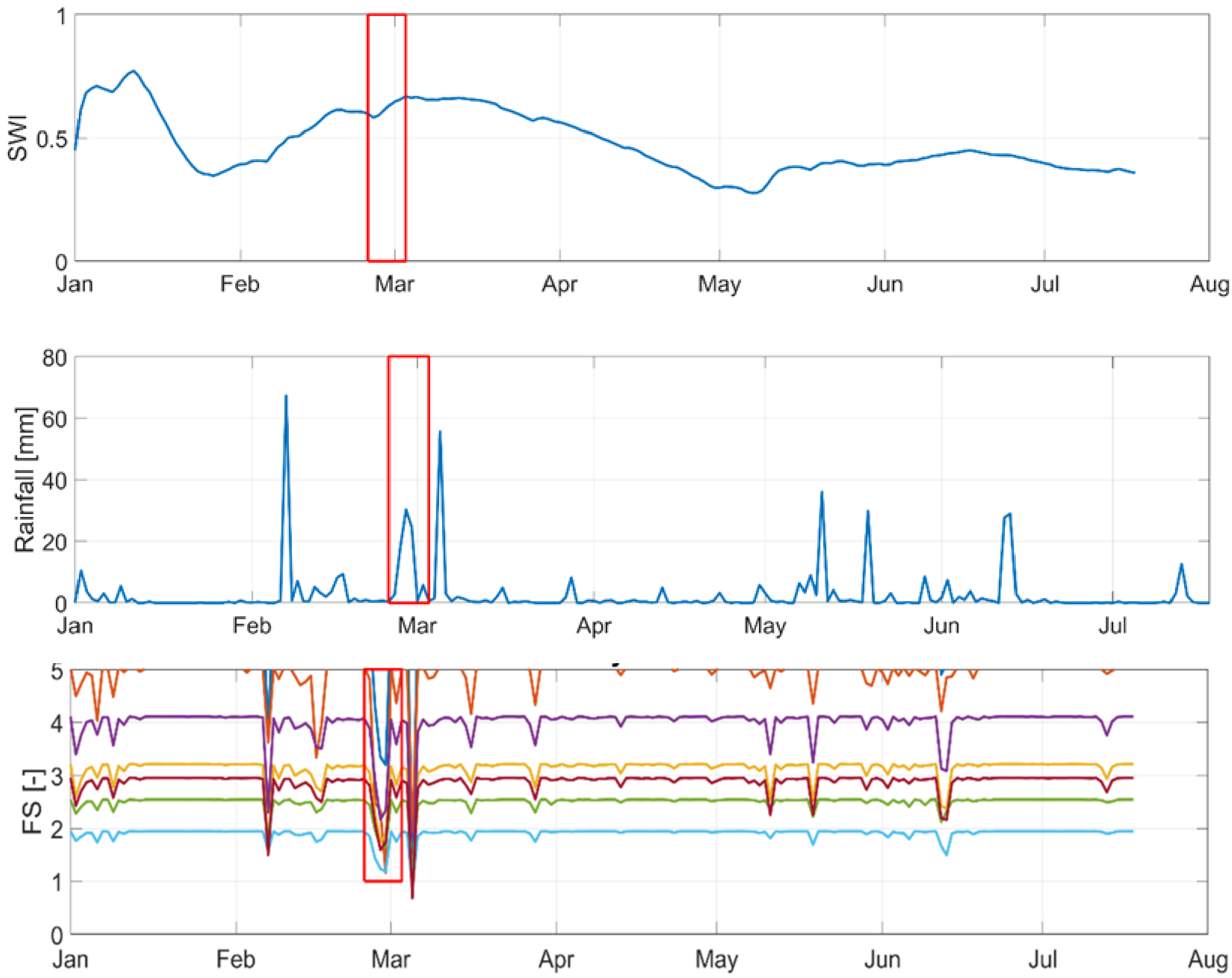

Figure 5.4 - Soil saturation (upper panel), rainfall (middle panel) and FS (lower panel). The red boxes highlight the rainfall events that likely triggered the landslides. The time period is from January to August 2016.

Overall, the high resolution soil saturation data provided important information and allowed the model to identify when and where the landslide occurred. With respect to the February 2016 event, the model correctly identified 51, 56 and 26 landslides out of 68 when forced with S1ASCAT, DIREX and RT1, respectively. If we look at the November 2019 event, similar results can be observed. The model forced with S1ASCAT and DIREX identified 29 out 31 landslides, while with RT1, 28 events.

Despite the very good performance provided by the model in identifying the soil saturation/rainfall conditions that triggered the landslides, there are a non-negligible number of false alarms issued by the stability module. As it can be seen in **Figure 5.5**, the FS values obtained for each grid point reached instability conditions (values close to 1) without any triggering of landslides. This is may be caused by the uncertainties related to the model parametrization.

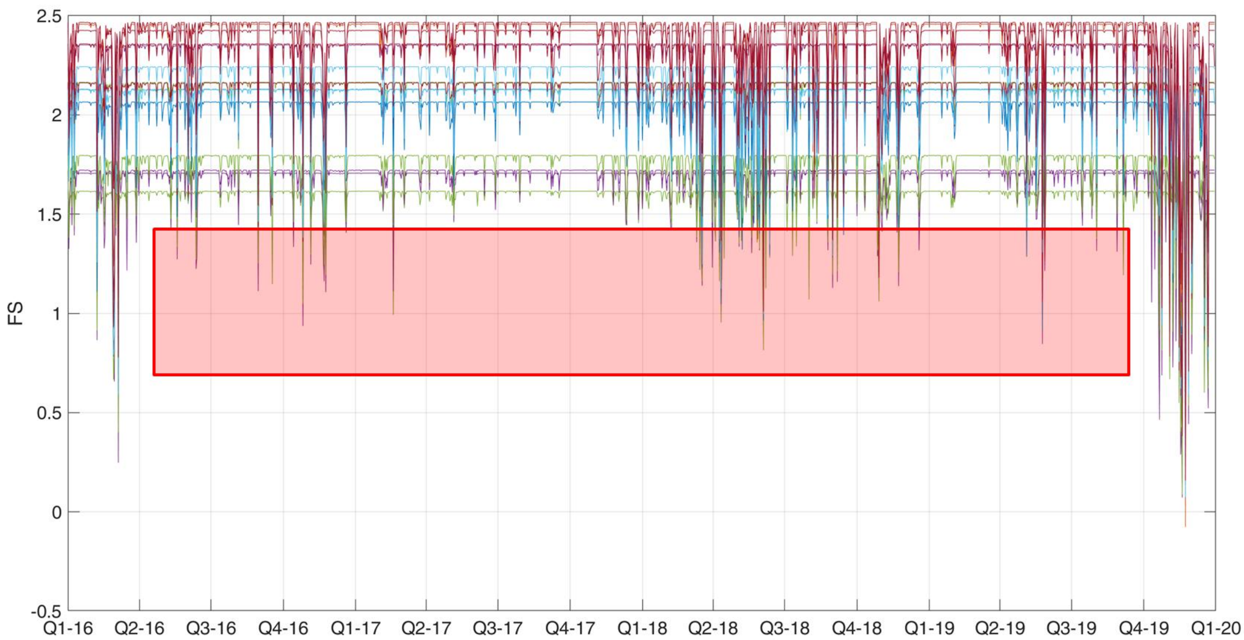

Figure 5.5 - FS timeseries over the entire analysis period. The red box identifies the area of false alarms issued by the model.

If we look more in detail at the spatial distribution of false alarms within the study area (**Figure 5.6**), we can observe how the largest amount of false alarms are localized in those areas characterized by high values of slope angle. This can be explained by two main reasons:

1) high slope angles are associated with high susceptibility areas, in which it is expected that landslides occur more easily;
2) In complex topography areas the satellite retrieval is characterized by higher uncertainties that may lead to wrong soil moisture values used as input for the model.

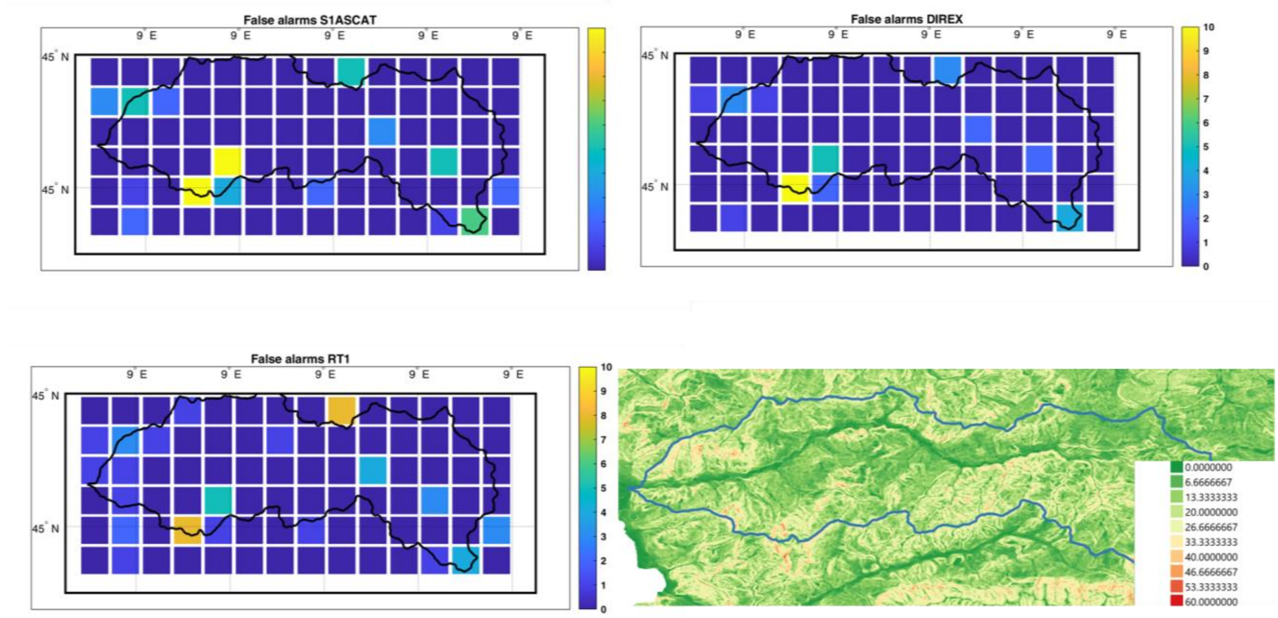

Figure 5.6 - Spatial distribution of false alarms over the study area for S1ASCAT, DIREX and RT1. In the lower right corner is reported a map showing the slope angels within the Ardivestra catchment.

6. Water management: Irrigation water quantification

6.1. The SM-based inversion approach

The approach is an evolution of the SM2RAIN algorithm (Brocca et al., 2014), originally developed to estimate rainfall from soil moisture observations. In the new configuration, the method allows to retrieve irrigation amounts by inverting the soil water balance (Brocca et al., 2018; Dari et al., 2020), expressed as:

$$nZdS(t)/dt \ = \ i(t) + r(t) - g(t) - sr(t) - e(t) \qquad (6.1)$$

in which n [-] indicates the soil porosity, Z [mm] is the depth of the soil layer. $S(t)$ [-] is the relative soil moisture, $i(t)$ [mm/day] indicates the irrigation rate, $r(t)$ [mm/day] is the rainfall rate, $g(t)$ [mm/day] is the drainage rate, $sr(t)$ [mm/day] represents the surface runoff, and $e(t)$ [mm/day] is the actual evapotranspiration rate. Eq. (5.1.1) can be alternatively written as:

$$Win(t) \ = \ nZdS(t)/dt + g(t) + sr(t) + e(t) \qquad (6.2)$$

where $Win(t)$ indicates the algorithm output, i.e., the sum of irrigation and rainfall rates. By assuming the surface runoff negligible (Brocca et al., 2015) and by linking the drainage term to soil moisture through the power law $g(t) = aS(t)^b$, with a [mm] and b drainage parameters, the solving equation can be expressed as:

$$Win(t) \ = \ Z^*dS(t)/dt + aS(t)^b + e(t) \qquad (6.3)$$

with $Z^* = nZ$[mm] indicating the water capacity of the soil layer. In order to represent the actual evapotranspiration term, a soil-moisture-limited approach is used. Hence, the $e(t)$ term is expressed as the potential evapotranspiration rate, $e_0(t)$, multiplied by the available water content. In addition, and adjustment factor, F, ranging between 0.6 and 1.4 is adopted. As a result, Eq. (6.3) can be written as follows:

$$Win(t) \ = \ Z^*dS(t)/dt + aS(t)^b + F * S(t) * e_0(t) \qquad (6.4)$$

with Z^*, a, b, and F parameters to be calibrated. In principle, the calibration procedure can be carried out through two alternative configurations: (i) by using the total amount of water entering the soil or (ii) rainfall only as a benchmark. The parameters are calibrated through the minimization of the root mean square difference between the algorithm output and the reference value. In the approach (i), the sum of irrigation and rainfall rates is considered, while in the configuration (ii) rainfall only is taken into account. In order to do this, the potentially irrigated days (i.e., summer days in which rainfall rates are equal to zero) are masked out. Such a configuration does not require the a priori knowledge of irrigation, allowing to generalize the method and to apply it over any agricultural area. In the performed analysis the configuration (ii) has been adopted. Once the parameters are calibrated, the Eq. (6.3) allows to estimate the total amount of water entering the soil. Hence, irrigation is estimated by removing rainfall rates from the output. Negative irrigation rates (if any) are set equal to zero and winter periods are masked out. In order to remove negligible irrigation rates attributable to random errors, the results are discarded if the ratio between weekly estimated irrigation and weekly rainfall is lower than 1.2.

6.2. Case study and performed analysis

The approach has been applied over a 15 km x 30 km tile North of the Reggio Emilia city (see **Figure 6.1**), in the Po river valley. The year 2018 has been considered. Soil moisture data from RT1 (Quast et al., 2019), potential evapotranspiration rates from GLEAM, and rainfall data from MCM have been used as input data. The calibration step has been carried out considering a group of pilot agricultural fields in the San Michele-Fosdondo area (marked in blue in Figure 5.1b); the performances in retrieving rainfall obtained in this phase are shown in **Figure 6.2**. A satisfactory reproduction of rainfall rates is found, quantified by a RMSE equal to 16.66 mm/7-days, a Pearson correlation coefficient, r, equal to 0.68, and a BIAS equal to 0.51 mm/7-days.

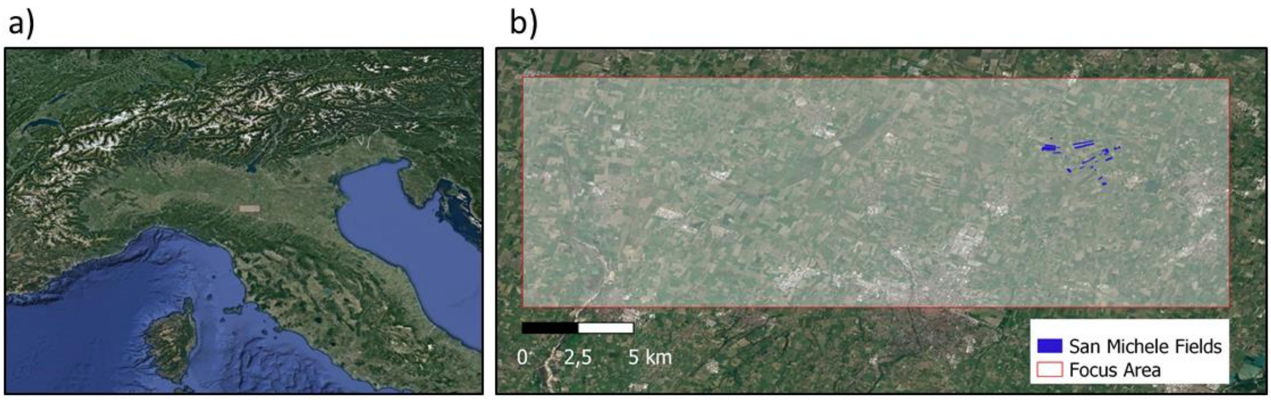

Figure 6.1: Pilot area for the irrigation water quantification analysis.

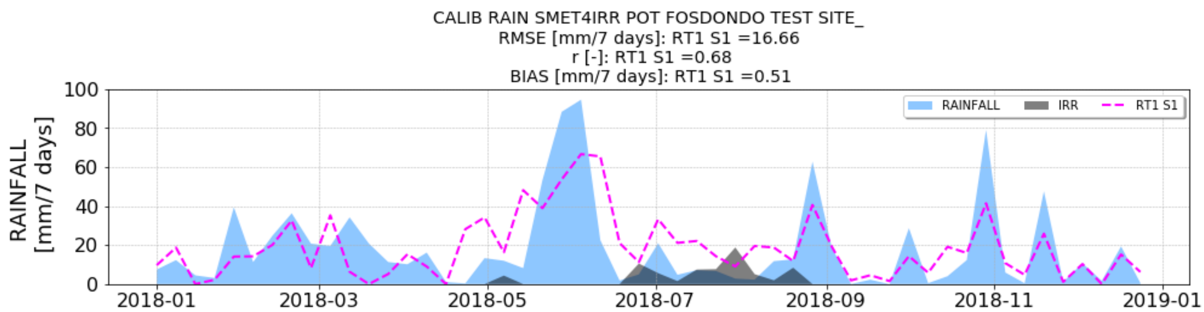

Figure 6.2: Results of the calibration step carried out over the San Michele-Fosdondo pilot fields. RT1 S1-derived estimates and the benchmark rainfall are represented by the dashed magenta line and the blue shaded area, respectively. Irrigation rates are also provided (grey shaded area).

The resulting calibrated parameters are a= 12.67 mm, b = 5.70, Z^*= 91.25 mm and F = 0.98. Such values have been assumed for each pixel of the area over which irrigation estimates have been carried out. The maps of the irrigation amounts averaged and cumulated during summer 2018 are provided in **Figure 6.3**. The cities are masked out and the San Michele-Fosdondo pilot fields are represented in red to highlight their location with respect to the considered box. The highest irrigation rates are detected in the Northeast portion of the pilot area, with cumulated values during the whole irrigation season higher than 250 mm.

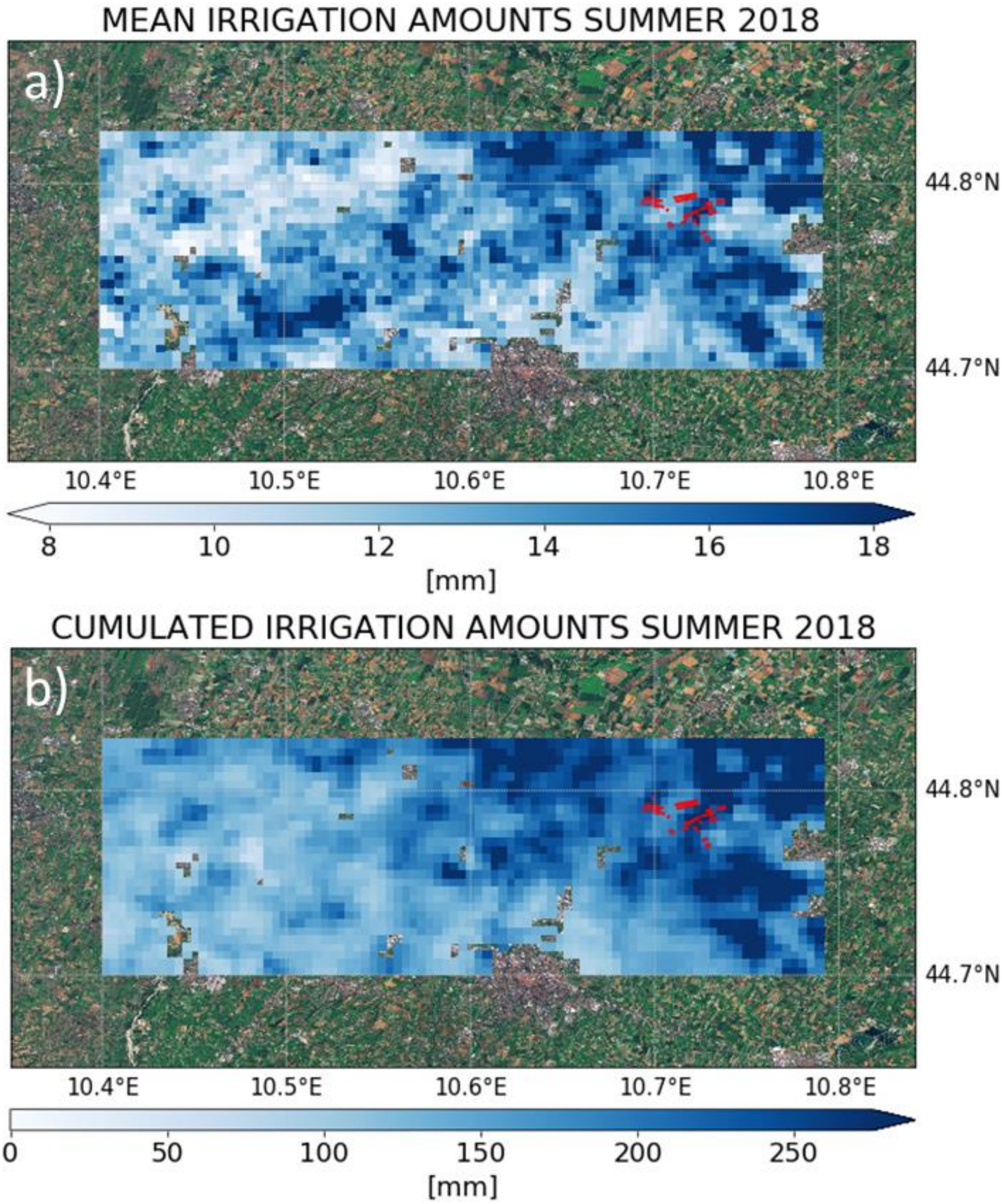

Figure 6.3: Mean (upper panel) and cumulated (lower panel) estimated irrigation amounts during summer 2018. The San Michele-Fosdondo pilot fields are represented in red to highlight their location.

Unfortunately, a comprehensive evaluation of the irrigation estimates is not possible. Nevertheless, a comparison between the irrigation water supplied to the San Michele-Fosdondo pilot sites and the irrigation estimates averaged over their area is provided in **Figure 6.4**. The benchmark irrigation amounts are represented in grey, while the estimates provided by the SM-based inversion approach are indicated in magenta. It can be observed that the proposed method overestimates the actual irrigation amounts, especially during the beginning of the irrigation season. This issue can be likely attributed to the spatial mismatch between the resolution of the remotely sensed soil moisture data and the scale at which irrigation occurs (**Dari et al., 2021**; **Massari et al., 2021**). In fact, the spatial resolution of the RT1-derived data set is probably too coarse to properly capture the irrigation dynamics occurring over the pilot agricultural fields and the contamination between estimates coming from adjacent pixels can introduce uncertainties in the comparison with the benchmark amounts. It is noteworthy that, within the ESA IRRIGATION+ project framework, RT1 soil moisture provided better results over areas of the Po river valley where irrigation occurs at the small-district scale, which is closer to the data spatial resolution.

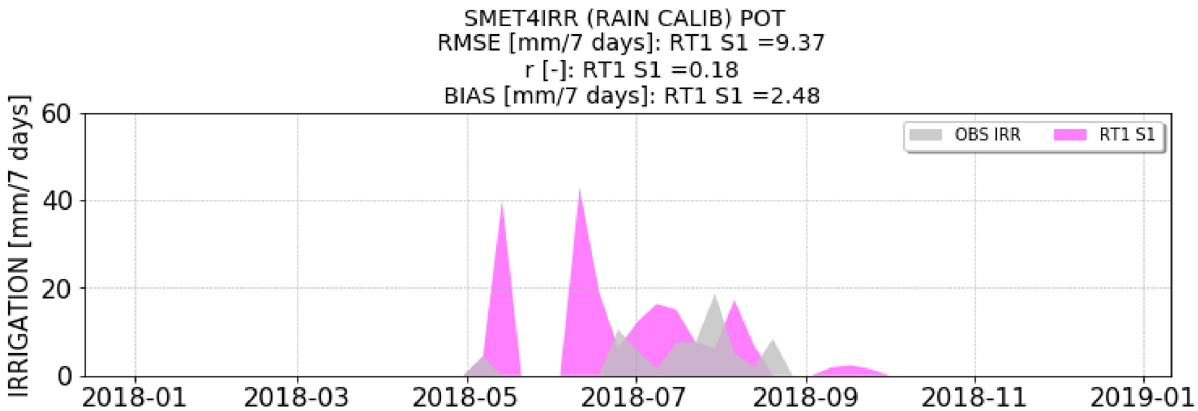

Figure 6.4: Weekly time series of estimated (magenta) and benchmark (light grey) irrigation amounts over the San Michele-Fosdondo pilot sites.

A qualitative assessment of the reliability of the spatial distribution of the irrigation water use can be carried out by comparing the maps of **Figure 6.3** with iColt data (produced by the Agenzia Prevenzione AMbiente Energia Emilia-Romagna, ARPAE, and available at: https://sites.google.com/drive.arpae.it/servizio-climatico-icolt/icolt2018?authuser=0) referring to year 2018, provided in **Figure 6.5**; iColt is a crop type data set produced at the plot scale. The map shown in **Figure 6.5** is obtained by aggregating the data at the same spatial scale at which the analysis has been performed (i.e., ~500 m) and by assigning to each pixel the irrigation attribute if the predominant crop type is a summer crop (likely irrigated during summer) or the non-irrigation attribute in the opposite case, i.e., if the predominant class is a winter crop or a non-agricultural area. Patterns of evenly irrigated domains matching with areas showing the highest mean irrigation rates (see **Figure 6.3a**) can be observed in the Eastern and Southwestern (to a lesser extent) portions of the box. Lower summer-averaged irrigation rates are estimated at Northwest of the area, where iColt-derived irrigated and non-irrigated pixels are more mixed together.

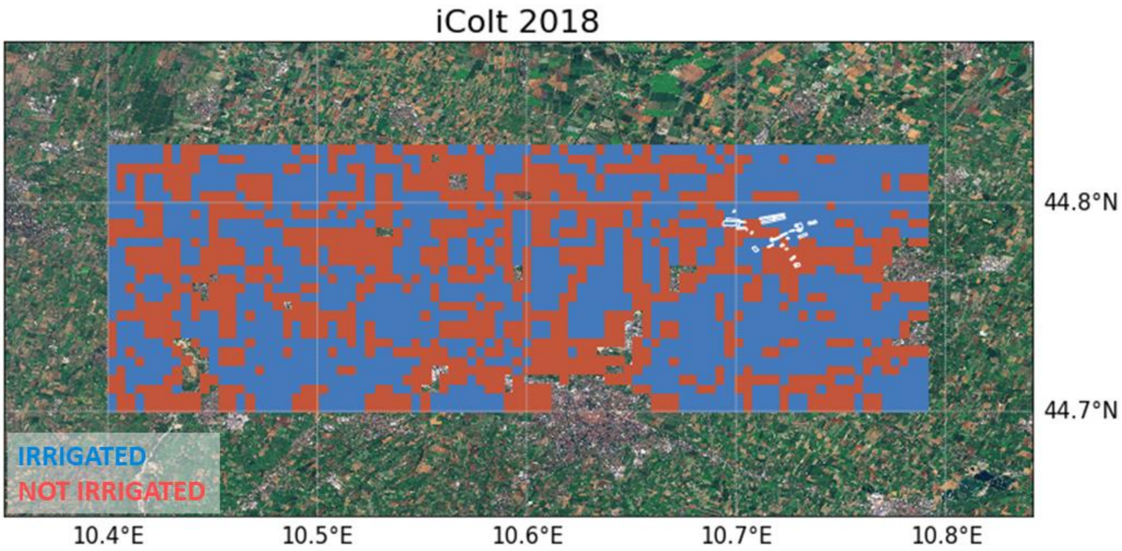

Figure 6.5: iColt-derived data referring to the year 2018.

7. References

Aronica, G., Bates, P. D., and Horritt, M. S. (2002). "Assessing the uncertainty in distributed model predictions using observed binary pattern information within GLUE." Hydrol. Processes, 16(10), 2001–2016.

Avanzi, F., Gabellani, S., Delogu, F., Silvestro, F., Cremonese, E., Morra di Cella, U., Ratto, S., and Stevenin, H.: S3M 5.1: a distributed cryospheric model with dry and wet snow, data assimilation, glacier mass balance, and debris-driven melt, Geosci. Model Dev. Discuss. [preprint], https://doi.org/10.5194/gmd-2021-92, in review, 2021.

Avanzi, F., Ercolani, G., Gabellani, S., Cremonese, E., Pogliotti, P., Filippa, G., Morra di Cella, U., Ratto, S., Stevenin, H., Cauduro, M., and Juglair, S.: Learning about precipitation lapse rates from snow course data improves water balance modeling, Hydrol. Earth Syst. Sci., 25, 2109–2131, https://doi.org/10.5194/hess-25-2109-2021, 2021.

Blunden J., Arndt D.S., editors (2020). State of the Climate in 2019, Bulletin of the American Meteorological Society. 1;101(8):S1–429.

Boni, F. Castelli, S. Gabellani, G. Machiavello and R. Rudari (2010). Assimilation of MODIS snow cover and real time snow depth point data in a snow dynamic model. 2010 IEEE International Geoscience and Remote Sensing Symposium, Honolulu, HI, USA, pp. 1788-1791, doi: 10.1109/IGARSS.2010.5648989.

Boschetti, M., Nutini, F., Manfron, G., Brivio, P.A., Nelson, A., 2014. Comparative analysis of normalised difference spectral indices derived from MODIS for detecting surface water in flooded rice cropping systems. PLoS One 9. https://doi.org/10.1371/journal.pone.0088741.

Brocca, L., Ciabatta, L., Massari, C., Moramarco, T., Hahn, S., Hasenauer, S., Kidd, R., Dorigo, W., Wagner, W., Levizzani, V., 2014. Soil as a natural rain gauge: Estimating global rainfall from satellite soil moisture data. J. Geophys. Res., 119, 5128–5141.

Brocca, L., Massari, C., Ciabatta, L., Moramarco, T., Penna, D., Zuecco, G., Pianezzola, L., Borga, M., Matgen, P., Martínez-Fernández, J., 2015. Rainfall estimation from in situ soil moisture observations at several sites in Europe: an evaluation of the SM2RAIN algorithm. J. Hydrol. Hydromechanics 63, 201–209. https://doi.org/10.1515/johh- 2015-0016

Brocca, L., Melone, F., Moramarco, T., Wagner, W., Naeimi, V., Bartalis, Z., and Hasenauer, S.: Improving runoff prediction through the assimilation of the ASCAT soil moisture product, 14, 1881–1893, https://doi.org/10.5194/hess-14-1881-2010, 2010.

Brocca, L., Melone, F. and Moramarco, T. (2011). Distributed rainfall-runoff modelling for flood frequency estimation and flood forecasting. Hydrological Processes, 25(18), 2801–2813.

Brocca, L., Filippucci, P., Hahn, S., Ciabatta, L., Massari, C., Camici, S., Schüller, L., Bojkov, B., Wagner, W. (2019). SM2RAIN-ASCAT (2007-2018): global daily satellite rainfall from ASCAT soil moisture. Earth System Science Data, 11, 1583–1601, doi:10.5194/essd-11-1583-2019.

Brocca, L., Massari, C., Pellarin, T., Filippucci, P., Ciabatta, L., Camici, S., Kerr, Y.H., Fernández-Prieto, D. (2020). River flow prediction in data scarce regions: soil moisture integrated satellite rainfall products outperform rain gauge observations in West Africa. Scientific Reports, 10, 12517, doi:10.1038/s41598-020-69343-x.

Brocca, L., Tarpanelli, A., Filippucci, P., Dorigo, W., Zaussinger, F., Gruber, A., Fernández-Prieto, D., 2018. How much water is used for irrigation? A new approach exploiting coarse resolution satellite soil moisture products. Int. J. Earth Obs. Geoinformation, 73, 752-766.

Camici, S, Massari, C., Ciabatta, L., Marchesini, I., Brocca, L. (2020). Which rainfall metric is more informative about the flood simulation performance? A comprehensive assessment on 1318 basins over Europe. Hydrology and Earth System Sciences, 24, 4869–4885, doi:10.5194/hess-24-4869-2020.

Camici, S., Ciabatta, L., Massari, C. and Brocca, L. (2018). How reliable are satellite precipitation estimates for driving hydrological models: a verification study over the Mediterranean area. Journal of Hydrology, 563, 950–961. doi:10.1016/j.jhydrol.2018.06.067

Castellarin, A, Di Baldassarre, G., Brath, A. (2011). Floodplain management strategies for flood attenuation in the river Po. River Res. Appl. 27, 1037–1047. doi:10.1002/rra.1405

Castellarin, Attilio, Domeneghetti, A., Brath, A. (2011). Identifying robust large-scale flood risk mitigation strategies: A quasi-2D hydraulic model as a tool for the Po river. Phys. Chem. Earth, Parts A/B/C 36, 299–308. doi:10.1016/j.pce.2011.02.008

Dari, J., Brocca, L., Quintana-Seguí, P., Casadei, S., Escorihuela, M.J., Stefan, V., Morbidelli, R., 2021. Double-scale analysis on the detectability of irrigation signals from remote sensing soil moisture over an area with complex topography in central Italy. Under review in Adv. Water Res.

Dari, J., Brocca, L., Quintana-Seguí, P., Escorihuela, M.J., Stefan, V., Morbidelli, R., 2020. Exploiting high-resolution remote sensing soil moisture to estimate irrigation water amounts over a Mediterranean region. Remote Sens., 12, 2593.

De Lavenne, A., Andréassian, V., Thirel, G., Ramos, M. H., & Perrin, C. (2019). A regularization approach to improve the sequential calibration of a semidistributed hydrological model. Water Resources Research, 55(11), 8821-8839.

Domeneghetti, A., Carisi, F., Castellarin, A., Brath, A. (2015). Evolution of Flood Risk Over Large Areas: Quantitative Assessment for The Po River. J. Hydrol. 527, 809–823. doi:10.1016/j.jhydrol.2015.05.043.

Domeneghetti, A., Tarpanelli, A., Grimaldi, L., Brath, A., Schumann, G., Flow duration curve from satellite: potential of lifetime SWOT mission, Remote Sens. 2018, 10(7), 1107; https://doi.org/10.3390/rs10071107.

Domeneghetti, A., Molari, G., Tourian, M.J., Tarpanelli, A., Behnia, S., Moramarco, T., Sneeuw, N., Brath, A. (2021). Testing the use of single- and multi-mission satellite altimetry for the calibration of hydraulic models. Adv. Water Resour. doi:https://doi.org/10.1016/j.advwatres.2021.103887.

Domeneghetti, A., Tarpanelli, A., Brocca, L., Barbetta, S., Moramarco, T., Castellarin, A., Brath, A. (2014). The use of remote sensing-derived water surface data for hydraulic model calibration. Remote Sens. Environ. 149, 130–141. doi:10.1016/j.rse.2014.04.007.

Domeneghetti, A., Molari, G., Tourian, M. J., Tarpanelli, A., Behnia, S., Moramarco, T., Sneeuw, N., & Brath, A. (2021). Testing the use of single-and multi-mission satellite altimetry for the calibration of hydraulic models. Advances in Water Resources, 151, 103887.

Dorigo, W., Wagner, W., Albergel, C., Albrecht, F., Balsamo, G., Brocca, L., Chung, D., Ertl, M., Forkel, M., Gruber, A., Haas, E., Hamer, P. D., Hirschi, M., Ikonen, J., de Jeu, R., Kidd, R., Lahoz, W., Liu, Y. Y., Miralles, D., Mistelbauer, T., Nicolai-Shaw, N., Parinussa, R., Pratola, C., Reimer, C., van der Schalie, R., Seneviratne, S. I., Smolander, T. and Lecomte, P. (2017). ESA CCI Soil Moisture for improved Earth system understanding: State-of-the art and future directions, Remote Sensing of Environment, 203, 185–215, https://doi.org/10.1016/j.rse.2017.07.001.

ESA (2017) Land Cover CCI Product User Guide Version 2. Tech. Rep. Available at: maps.elie.ucl.ac.be/CCI/viewer/download/ESACCI-LC-Ph2-PUGv2_2.0.pdf.

ESA (2017) Land Cover CCI Product User Guide Version 2. Tech. Rep., 2017.

Faroux, S., Kaptué Tchuenté, A. T., Roujean, J.-L., Masson, V., Martin, E. and Le Moigne, P. (2013) ECOCLIMAP-II/Europe: a twofold database of ecosystems and surface parameters at 1 km resolution based on satellite information for use in land surface, meteorological and climate models, Geoscientific Model Development, 6(2), 563–582, https://doi.org/10.5194/gmd-6-563-2013.

Feyisa, G.L., Meilby, H., Fensholt, R., Proud, S.R., 2014. Remote sensing of environment automated water extraction index: a new technique for surface water mapping using Landsat imagery. Remote Sens. Environ. 140, 23–35. https://doi.org/10.1016/j.rse.2013.08.029

Giannoni, F., Roth, G. and Rudari, R. (2000) A semi-distributed rainfall-runoff model based on a geomorphologic approach, Physics and Chemistry of the Earth, Part B: Hydrology, Oceans and Atmosphere, 25(7–8), 665–671, https://doi.org/10.1016/s1464-1909(00)00082-4.

Gupta, H. V., Kling, H., Yilmaz, K. K. and Martinez, G. F. (2009). Decomposition of the mean squared error and NSE performance criteria: Implications for improving hydrological modelling. Journal of Hydrology, 377(1–2), 80–91. doi:10.1016/j.jhydrol.2009.08.003.

Hengl, T., Jesus, J. M. de, Heuvelink, G. B. M., Gonzalez, M. R., Kilibarda, M., Blagotić, A., Shangguan, W., Wright, M. N., Geng, X., Bauer-Marschallinger, B., Guevara, M. A., Vargas, R., MacMillan, R. A., Batjes, N. H., Leenaars, J. G. B., Ribeiro, E., Wheeler, I., Mantel, S. and Kempen, B. (2017). SoilGrids250m: Global gridded soil information based on machine learning, PLOS ONE, 12(2), e0169748, https://doi.org/10.1371/journal.pone.0169748.

Hydrologic Engineering Center (2010). HEC-RAS hydraulic reference manual. US Army Corps of Engineers, Davis.

Kling, H., Fuchs, M., and Paulin, M. (2012). Runoff conditions in the upper Danube basin under an ensemble of climate change scenarios, Journal of Hydrology, 424–425, 264–277, https://doi.org/10.1016/j.jhydrol.2012.01.011.

Lakshmivarahan, S. and Lewis, J. M.: Nudging Methods: A Critical Overview, in: Data Assimilation for Atmospheric, Oceanic and Hydrologic Applications (Vol. II), edited by: Park, S. K. and Xu, L., Springer, Berlin, Heidelberg, 27–57, https://doi.org/10.1007/978-3-642-35088-7_2, 2013.

Lehner, B., Liermann, C. R., Revenga, C., Vörösmarty, C., Fekete, B., Crouzet, P., Döll, P., Endejan, M., Frenken, K., Magome, J., Nilsson, C., Robertson, J. C., Rödel, R., Sindorf, N. and Wisser, D. (2011). High-resolution mapping of the world's reservoirs and dams for sustainable river-flow management, Frontiers in Ecology and the Environment, 9(9), 494–502, https://doi.org/10.1890/100125.

Lu, N., Godt, J.W. (2008). Infinite slope stability under steady unsaturated seepage conditions. WATER RESOURCES RESEARCH, VOL. 44, W11404, doi:10.1029/2008WR006976

Malek, S.A.; Avanzi, F.; Brun-Laguna, K.; Maurer, T.; Oroza, C.A.; Hartsough, P.C.; Watteyne, T.; Glaser, S.D. (2017).Real-Time Alpine Measurement System Using Wireless Sensor Networks. Sensors, 17, 2583. https://doi.org/10.3390/s17112583

Martens, B., De Jeu, Richard A.M., Verhoest, N.E.C., Schuurmans, H., Kleijer, J., and Miralles, D.G. (2018). Towards estimating land evaporation at field scales using GLEAM, Remote Sens. 10, no. 11: 1720.

Martens, B., Miralles, D.G., Lievens, H., van der Schalie, R., de Jeu, R.A.M., Fernández-Prieto, D., Beck, H.E., Dorigo, W.A., and Verhoest, N.E.C. (2017) GLEAM v3: Satellite-based land evaporation and root-zone soil moisture, Geoscientific Model Development, 10, 1903–1925.

Massari, C., Brocca, L., Pellarin, T., Abramowitz, G., Filippucci, P., Ciabatta, L., Maggioni, V., Kerr, Y., Fernández-Prieto, D. (2020). A daily/25km short-latency rainfall product for data scarce regions based on the integration of the GPM IMERG Early Run with multiple satellite soil moisture products. Hydrology and Earth System Sciences, 24, 2687–2710, doi:10.5194/hess-24-2687-2020.

Massari, C., Brocca, L., Tarpanelli, A. and Moramarco, T. (2015). Data assimilation of satellite soil moisture into rainfall–runoff modelling: a complex recipe? Remote Sensing, 7(9), 11403– 11433. doi:10.3390/rs70911403

Massari, C., Crow, W., Brocca, L. (2017). An assessment of the accuracy of global rainfall estimates without ground-based observations. Hydrology and Earth System Sciences, 21, 4347-4361, doi:10.5194/hess-21-4347-2017.

Massari, C., Maggioni, V., Barbetta, S., Brocca, L., Ciabatta, L., Camici, S., Moramarco, T., Coccia, G., Todini, E. (2019). Complementing near-real time satellite rainfall products with satellite soil moisture-derived rainfall through a Bayesian inversion approach. Journal of Hydrology, 573, 341-351, doi:10.1016/j.jhydrol.2019.03.038.

Massari, C., Modanesi, S., Dari, J., Gruber, A., De Lannoy, G.J.M., Girotto, M., Quintana-Seguí, P., Le Page, M., Jarlan, L., Zribi, M., Ouaadi, N., Vreugdenhil, M., Zappa, L., Dorigo, W., Wagner, W., Brombacher, J., Pelgrum, H., Jaquot, P., Freeman, V., Volden, E., Fernandez Prieto, D., Tarpanelli, A., Barbetta, S., Brocca, L., 2021b. A review of irrigation information retrievals from space and their utility for users. Under review in Remote Sens.

Masseroni, D., Cislaghi, A., Camici, S., Massari, C. and Brocca, L. (2017). A reliable rainfall–runoff model for flood forecasting: review and application to a semi-urbanized watershed at high flood risk in Italy. Hydrology Research, 48(3), 726–740. doi:10.2166/nh.2016.037.

McFeeters, S.K., 1996. The use of the normalized difference water index (NDWI) in the delineation of open water features. Int. J. Remote Sens. 17, 1425–1432. https://doi.org/10.1080/01431169608948714.

Miralles, D. G., Jiménez, C., Jung, M., Michel, D., Ershadi, A., McCabe, M. F., Hirschi, M., Martens, B., Dolman, A. J., Fisher, J. B., Mu, Q., Seneviratne, S. I., Wood, E. F., and Fernández-Prieto, D. (2016). The WACMOS-ET project – Part 2: Evaluation of global terrestrial evaporation data sets, Hydrol. Earth Syst. Sci., 20, 823–842.

Muñoz-Sabater, Joaquín, Emanuel Dutra, Anna Agustí-Panareda, Clément Albergel, Gabriele Arduini, Gianpaolo Balsamo, Souhail Boussetta, et al. (2021). ERA5-Land: A State-of-the-Art Global Reanalysis Dataset for Land Applications. Earth System Science Data Discussions, March, 1–50. https://doi.org/10.5194/essd-2021-82.

Pignone, F., Rebora, N. and Silvestro, F. (2015). Modified Conditional Merging technique: a new method to estimate a rainfall field combining remote sensed data and raingauge observations, 17, 3013.

Preissmann, A. (1961). Propagation of translatory waves in channels and rivers, in: First Congress of French Association for Computation. pp. 433–442.

Quast, R., Albergel, C., Calvet, J.-C., Wagner, W., 2019. A Generic First-Order Radiative Transfer Modelling Approach for the Inversion of Soil and Vegetation Parameters from Scatterometer Observations. Remote Sens., 11(3), 285.

Rains et al. (in preparation). European-scale 1 km evaporation and soil moisture data based on Sentinel observations.

Rains, D., Lievens, H., De Lannoy, G. J. M., McCabe, M. F., De Jeu, R. A. M., and Miralles, D. G. (in review) Sentinel-1 backscatter assimilation using Support Vector Regression or the Water Cloud model at European soil moisture sites, IEEE Geoscience and Remote Sensing Letters, in review.

Raup, B., Racoviteanu, A., Khalsa, S. J. S., Helm, C., Armstrong, R. and Arnaud, Y.: The GLIMS geospatial glacier database (2007) A new tool for studying glacier change, Global and Planetary Change, 56(1), 101–110, https://doi.org/10.1016/j.gloplacha.2006.07.018.

Ross, C. W., Prihodko, L., Anchang, J., Kumar, S., Ji, W. And Hanan, N. P. (2018). Global Hydrologic Soil Groups (HYSOGs250m) for Curve Number-Based Runoff Modeling, ORNL Distributed Active Archive Center..

Shen, L., Li, C., 2010. Water body extraction from landsat ETM+ imagery using adaboost algorithm. 2010 18th Int. Conf. Geoinformatics. https://doi.org/10.1109/GEOINFORMATICS.2010.5567762. Geoinformatics 2010 1–4.

Silvestro, F., Gabellani, S., Delogu, F., Rudari, R. and Boni, G. (2013). Exploiting remote sensing land surface temperature in distributed hydrological modelling: the example of the Continuum model, Hydrology and Earth System Sciences, 17(1), 39–62, https://doi.org/10.5194/hess-17-39-2013.

Sinagra M., Nasello C., Tucciarelli T., Barbetta S., Massari C., Moramarco T. (2020) 'A self-contained and automated method for flood hazard maps prediction in urban areas', Water 2020, 12, 1266; doi:10.3390/w12051266, https://www.mdpi.com/2073-4441/12/5/1266/htm.

Sinclair, S. and Pegram, G. (2005).Combining radar and rain gauge rainfall estimates using conditional merging, Atmospheric Science Letters, 6(1), 19–22.

Skempton A.W., DeLory, F.A. (1957). Stability of Natural Slopes in London Clay. Proc. Intern. Conf., 4th Soil Mech., Lond., 2, pp. 378-381

Song, Y.S. (2014). Suction stress in unsaturated sand at different relative densities. Engineering Geology, Volume 176, 1-10.

Stauffer, D. R. and Seaman, N. L.: Use of four-dimensional data assimilation in a limited-area mesoscale model. Part I: experiments with synoptic-scale data, 118, 1250–1277, https://doi.org/10.1175/1520-0493(1990)118<1250:UOFDDA>2.0.CO;2, 1990.

Tarpanelli, A., Brocca, L., Melone, F., and Moramarco, T. (2013). "Hydraulic modelling calibration in small basins by using coarse resolution synthetic aperture radar imagery." Hydrol. Process., 27(9), 1321–1330.

Terzago, S., Andreoli, V., Arduini, G., Balsamo, G., Campo, L., Cassardo, C., Cremonese, E., Dolia, D., Gabellani, S., von Hardenberg, J., Morra di Cella, U., Palazzi, E., Piazzi, G., Pogliotti, P., and Provenzale, A. (2020). Sensitivity of snow models to the accuracy of meteorological forcings in mountain environments, Hydrol. Earth Syst. Sci., 24, 4061–4090, https://doi.org/10.5194/hess-24-4061-2020.

Verdin, K. L. (2017). Hydrologic Derivatives for Modeling and Analysis—A new global high-resolution database, Hydrologic Derivatives for Modeling and Analysis—A new global high-resolution database, U.S. Geological Survey, Reston, VA, https://doi.org/10.3133/ds1053.

Xu, H., 2006. Modification of normalised difference water index (NDWI) to enhance open water features in remotely sensed imagery. Int. J. Remote Sens. 27, 3025–3033. https://doi.org/10.1080/01431160600589179.

DTE Hydrology Community Roadmap

1. Introduction

1.1.The DTE Hydrology Project

The objective of DTE Hydrology is to develop and demonstrate a prototype of Digital Twin Earth with focus on water cycle and hydrological processes and their impacts. In DTE Hydrology we aim to highlight the huge potential of high-resolution ESA satellite products for describing the water cycle, for predicting hydrology extremes (floods, landslides and drought) and for monitoring and managing water resources.

DTE Hydrology builds on the expertise of the consortium members. Within the project EO datasets of rainfall, soil moisture, evaporation, river discharge, snow depth and land cover will be used. Soil moisture, rainfall, snow depth and evaporation datasets are provided by partners with well-established algorithms from satellite observations, TU Wien, CNR-IRPI, CIMA and UGent respectively. Expertise in hydrological and hydraulic modelling at high resolution is brought in by CNR-IRPI, CIMA and UNIBO. High performance computing is pivotal in DTE Hydrology and is managed and hosted by EODC. Outreach and visualisation of the project outcomes is done by CNR-IRPI, CIMA, EODC and UNIBO.

1.2.Scope of this Report

This document summarises the main achievements obtained during the DTE Hydrology project and outlines the future steps that should be carried out in this activity.

1.3.Applicable Documents

- [D1.1] - Deliverable D1.1: 4D DTE Hydrology underlying data reconstruction
- [D1.2] - Deliverable D1.2: DTE Hydrology data set
- [PR1] - Progress report October 2020-January 2021
- [D2.1] - Deliverable D2.1 v2.0: Technical Note 2: DTE-Hydrology consistent end-to-end integrated framework description and validation
- [D4.1] - Deliverable D4.1: Technical Note 3: Simulation and impact assessment report

1.4. Reference Documents

- [RD-01] - DTE Hydrology Technical Proposal - V1.0

2. DTE Requirement Baseline and Preliminary Definition Report

2.1. Theme definition and overall objectives

In recent years, the availability of high-resolution observations (<1km, sub-daily) from remote sensing, in situ monitoring networks and new sensors/techniques (drones, citizen science), in addition to the increased computational and storage capacity, and the development of advanced machine learning techniques, have fostered the development of modelling systems at **high resolution for hydrological applications**. The European Commission (EC) is promoting these developments through the EU's digital strategy, the Green Deal, and specifically the Destination Earth initiative. The development of digital twins of the Earth System is currently in the EC agenda as one of the most pressing activities to be accomplished to build a resilient society able to cope with adverse extreme events (flood, drought, heatwaves, landslides), exacerbated by global and climate change.

The overall objective of the DTE Hydrology project has been the 4D reconstruction of the water cycle at high resolution through the integration of the most recent satellite observations and advanced hydrological modelling (see **Figure 1**). The Po River basin in northern Italy has been selected as a case study.

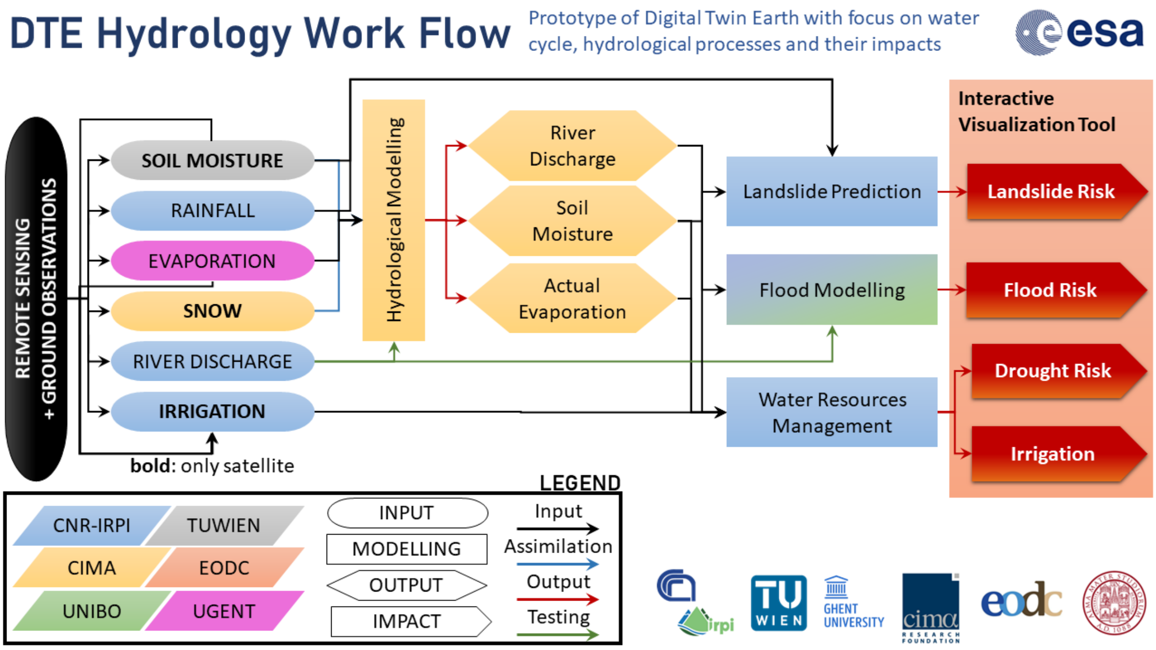

Figure 1: Work flow of the DTE Hydrology project.

2.2. Stakeholders and overarching needs (policy, science, public/private users, citizens)

On 20 January 2021 a virtual meeting with a group of stakeholders working over the Po River Basin was carried out. Specifically, the following agencies/authorities were present:

- Dipartimento Nazionale di Protezione Civile: Multi-risk Italian Center of civil protection
- Regione Emilia Romagna: Regional Center for emergency management and civil protection
- Centro Funzionale Valle d'Aosta: Regional Center for geo-hydrological and hydraulic risk assessment
- Autorità di bacino distrettuale del fiume Po: Multi-regional Center for the implementation of water management, flood and landslide risk plan
- ARPA Lombardia: Regional Center for water resources management and hydrological monitoring
- ARPA Emilia Romagna: Multi-risk regional Center for civil protection, emergency management, geo-hydrological risk, and relationship with the scientific community
- Consorzio di Bonifica del Canale Emiliano Romagnolo: Management of irrigation at regional and national scale
- Consorzio bonifica Emilia Centrale: Regional Center for irrigation network management, drainage area management, floods risk prevention

Therefore, the participants are involved in different sectors related to the water cycle including: (1) hydrological and hydraulic risk prediction and prevention, (2) geo-hydrological (landslide) risk prediction and prevention, (3) water resources management, and (4) irrigation management and planning. All Italian regions (except Piemonte Region) belonging to the Po River Basin area were represented.

2.3. Overall DTE vision and high-level design

Despite the high-resolution hydrology being an important opportunity for future research and operation applications, the challenges to be addressed are quite a lot and non-trivial. The increased computational capabilities are far from being sufficient to develop high resolution hydrological systems at a continental or a global scale. The four most important high-level challenges are the following:

1) **Observations** (e.g., precipitation, evaporation, soil moisture, river discharge, snow) have to be available not only at **high spatial and temporal resolution**, but also with sufficient **accuracy** and **uncertainty** characterisation.
2) The **representation of physical processes at high resolution is significantly different from processes at coarse resolution** (20km), currently modelled by continental and global scale land surface and hydrological models.
3) The **human impact on the water cycle** (e.g., irrigation, reservoir management, river water diversion) acting at very high resolution, challenges the current attempts of reproducing a digital replica of the Earth.
4) An **ICT infrastructure** allowing the users (scientists, stakeholders, citizens) to easily interact with data and models needs to be properly designed, scaled and implemented. The infrastructure needs to ingest open data following the FAIR (Findability, Accessibility, Interoperability, and Reusability) principles, should be interoperable, modular, and seamlessly working on the cloud as a web service.

In the following, further details on these challenges are provided.

3. State of the art, latest developments

3.1. Existing capabilities

The 4D reconstruction of the water cycle at high resolution has been attempted in the last 10 years through land surface modelling and global scale hydrological modelling (Bierkens et al., 2015). However, as explained below, the number of challenges to be addressed are still far from being resolved.

3.2. EO data aspects: towards full 4D reconstruction

Earth Observation is able to provide different products for describing the water cycle, but most of these products are available at coarse resolution. For instance, satellite soil moisture products at coarse resolution (>10km) can be obtained from different satellite platforms and sensors (e.g., SMOS, SMAP, ASCAT) but high resolution (<=1km) soil moisture products have been made available only recently. The same applies for other variables such as evaporation, precipitation, snow, and river discharge. Evaporation cannot be directly measured from space and thus it’s estimation often includes modelling. The modelling approach can however be adjusted to make the most optimal use of available observations.

In DTE Hydrology we have developed and tested for the first time the following high-resolution satellite products:

1) **Precipitation**: a first of its kind satellite precipitation product at hourly time scale and 1km spatial resolution has been obtained through the integration of GPM IMERG late run product (10km, hourly), SM2RAIN (Brocca et al., 2019) applied to ASCAT soil moisture (10km, daily) and SM2RAIN applied to Sentinel-1 (1km, 3day). The resulting product (1km, hourly) has been tested for the first time in the project [D4.1].
2) **Evaporation**: the high resolution (1km, daily) version of the well-established global GLEAM product (25km, daily) has been obtained by making use of high-resolution static and dynamic datasets describing the land surface, e.g. MODIS fractional vegetation cover (DiMiceli et al., 2015) and the 3D soil hydraulic database (Tóth et al., 2017) (see **Figure 2**). Furthermore, datasets from DTE-Hydrology are used: Sentinel-1 based soil moisture retrievals (Quast et al., 2019) are assimilated through a Newtonian Nudging scheme and the merged precipitation product (see above) is used as input into GLEAM. Further advances being explored in making use of high-resolution observations in GLEAM are the use of Sentinel 3 land surface temperature retrievals for creating high-resolution and gap-free temperature and net radiation inputs (Rains et al., in prep.) as well as the assimilation of Sentinel-1 backscatter observations (Rains et al., 2021).

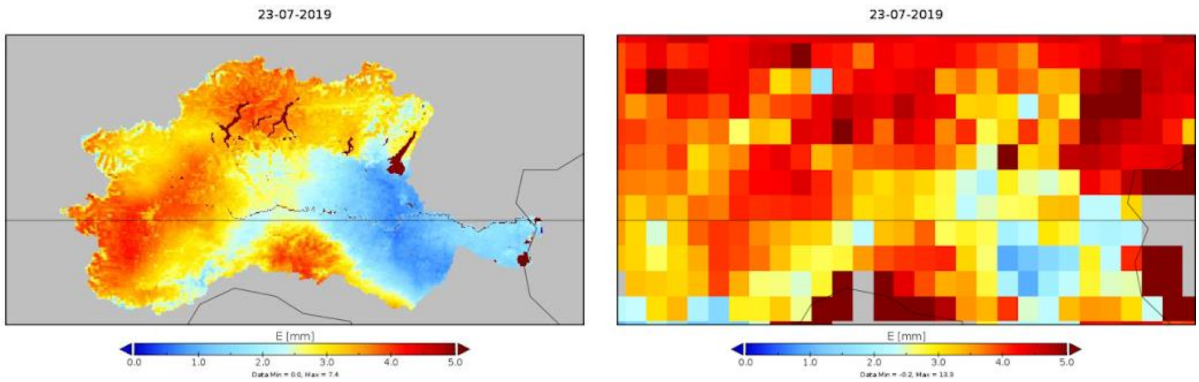

Figure 2: Evaporation across the Po river basin on 23th July 2019 with the GLEAM high-resolution simulations at 1 km (left) and with GLEAM v35b at the global 0.25 resolution (right).

3) **Soil Moisture**: an improved high resolution (1km) soil moisture product has been obtained from the application of RT1 algorithm (Quast et al., 2019) to Sentinel-1 observations.
4) **Snow**: the high-resolution snow depth product developed by Lievens et al. (2019) has been successfully tested and compared with 172 ground stations over the Alps [D2-1].
5) **River Discharge**: the integrated river discharge product first developed under the ESA RIDESAT project has been further improved in the project and tested along the Po River at 5 stations. The product has a temporal resolution of 1-2 days thanks to the integration of multiple altimetry tracks and near infrared observations from MODIS and OLCI sensors.

In the longer term, new satellite-based products might be available that will further improve our potential to reproduce the water cycle at high resolution. Specifically, the following missions\products are expected to be developed:

- **L-band future missions**: By integrating Sentinel-1 with the upcoming L-band ROSE-L SAR mission, the spatiotemporal sampling and accuracy of soil moisture, water body, and other hydrological data products (e.g., flooded areas) could be significantly improved. This would directly lead to major improvements in derived rainfall and root zone soil moisture data sets.
- **High resolution thermal missions**: Within the Copernicus program, the Land Surface Temperature Mission (LSTM) will complement Sentinel observation capabilities with high spatial-temporal resolution TIR (Thermal Infrared) observations over land and coastal regions in support of agriculture management services, and possibly a range of additional applications and services. The primary objective is to enable monitoring the evapotranspiration (ET) rate at European field scale by capturing the variability of Land Surface Temperature (LST) (and hence derived ET) allowing more robust estimates of field-scale.
- **Global Navigation Satellite System (GNSS) Reflectometry**: The technique of Global Navigation Satellite System (GNSS) Reflectometry is increasingly seen as a valuable alternative to SMOS and SMAP to collect L-band data for the monitoring of soil moisture, water bodies, freeze/thaw status etc. For example, ESA has recently approved the Scout Mission HydroGNSS. However, the development of robust data products will probably be more challenging for this bi-static active measurement technique than for both passive (SMOS, SMAP) and mono-static active (ASCAT, Sentinel-1, etc.) sensing techniques.
- **Terrestrial water storage and groundwater dynamic**: The next generation gravity missions (currently named MAGIC) are expected to significantly improve the spatial and temporal resolution of water

storage measurements from space (weekly, <100km), thus providing new observations for hydrological modelling and prediction in medium scale basins.

- **Geosynchronous radar missions**: Geosynchronous radar missions would have a huge potential to study dynamic hydrological processes at sub-daily time intervals. Unfortunately, after the deselection of Hydroterra mission, which was one of the candidate missions for ESA's 10th Earth Explorer, there are no concrete plans for such a mission in Europe (a Chinese mission seems to be under development, but little is known about it).
- **High-resolution optical platforms**: Further advances in the field of global terrestrial evaporation monitoring may involve developments in high-resolution optical platforms (McCabe et al. 2017), and ongoing and future thermal missions such as ECOSTRESS (Fisher et al. 2020) and TRISHNA (Lagouarde et al. 2018). Moreover, the use of cubesat data from the Planet constellation has already demonstrated a high potential for monitoring evaporation at agricultural field scales (Aragon et al., 2020). The question of whether current evaporation models (e.g., GLEAM) are suited to extract the intrinsic value of these high-resolution observations, or whether models of plant water use employed in agricultural science are more suitable for this task, is still unanswered.
- **Snow**: Sentinel 3 satellite should soon provide snow covered area at 300 m resolution and daily granularity. This is a step change compared to the revisit time of Sentinel-2. Moreover, the assimilation of CSNOW data (from Sentinel-1) into hydrological modelling has shown the potential not only of Snow Covered Area (SCA) but also snow depth. CSNOW is not operational, but products like that are extremely valuable for next-generation mountain hydrology.

3.3. Earth science and modelling aspects, process understandings

When moving from the common resolution of 0.25° (order of 25 km at the equator) down to 1 km and smaller, many concepts that have been designed to resolve small-scale processes at the sub-grid scale are not appropriate. In order of importance, we provide here the most important steps to be carried out to develop a high-resolution reconstruction of the water cycle.

First, **simple cell fractionation has to be replaced by explicit dynamics**. Lateral fluxes at the surface and in the sub-surface need to be explicitly modelled. At coarse scale (>25km), several processes are conceptualised through simplifications such as the fraction of saturated soil assumed as a function of surface elevation (or predefined empirical distribution) or the modelling of surface fluxes separately for the different subgrid surface fractions (or "tiles"). However, when moving to higher resolutions, the explicit spatial juxtaposing of saturated soils with time has to be accounted for. Similarly, the assumption that vertical gradients of water and energy fluxes are much larger than horizontal gradients (valid at coarse scale) may be not valid as horizontal advection becomes important, particularly over fractionated agricultural fields where irrigation is applied. The accurate estimation of river discharges in the entire river network is made difficult by the wide range of values to be represented (several orders of magnitudes). Improving process representation and model parameterization is key to achieve skilful modelling in the entire domain, though a number of factors involved are known to bias the choice in favour of specific classes of basins (e.g., the objective function used in calibration, the data quality, the station locations, their runoff regimes and their relative weights compared to the others). We also note that the explicit representation of lateral fluxes is an issue for code parallelization as it introduces the explicit spatial and temporal dependence between the modelling cells of the domain.

Second, in 0.5° models, water stress assessments are based on the assumption that water demand is satisfied by available surface water and groundwater within the same grid cell. This assumption works well because most regional water redistribution works fit within a 50 × 50 km area around the location where water is consumed. However, at resolutions of 10 km and finer, inter-cell redistribution of water from abstraction points to hotspots of water consumption, or from lateral groundwater flow, need to be considered. **Relating local water demand and water abstraction at high resolution requires knowledge of local water redistribution systems** that is not available globally.

Third, it is well-known that moving to higher resolutions will pose a huge challenge as epistemic uncertainties will become very large because of **lack of process and parameter knowledge at such high resolutions** (Beven and Cloke, 2012). Recent EO products can be used to fill the current gaps, particularly for static maps of soil types and land use/land cover. However, high resolution dynamic variables such as precipitation, which contribute to a large part of the uncertainty in model output, are not available on a global scale.

Additional processes that are currently not well modelled and hence assessed by global scale land surface and hydrological modelling are related to:

- **surface water-groundwater interaction**: modelling the interactions between the unsaturated zone and the groundwater dynamics on a large scale is an important challenge mainly due to missing observations on groundwater storage variability and subsurface soil characteristics. The novel gravity missions to be launched in cooperation between ESA and NASA (MAGIC mission) could provide gravity measurements at improved spatial (<50km) and temporal (<3-7 days) scales that can be used to constrain and test groundwater modelling for medium to large river basins.
- **Plant phenology and roots dynamics** are also other processes which impact the hydrological cycle especially under water stress and that are generally very difficult to model with significant impact on evaporation estimation. The suboptimal representation of evaporation by Earth system models is not rare. For example, many models do not include stomatal response to dry periods, hydrologic regulation of plant rooting depth, correct representation of the plant hydraulics as well as coevolution mechanisms such as vegetation mortality and expansion. Remote sensing can provide important information on the plant phenology and canopy structure and temperature which can help to overcome model limitations. Particular benefit is expected from the new mission ECOSTRESS and the future TRISHNA and ESA LSTM missions thanks to the enhanced high spatial-temporal resolution measurements they will provide.

3.4. Artificial Intelligence (AI)

In recent years, the development of new Artificial Intelligence (AI) / Machine Learning (ML) techniques is growing steadily and at a high rate. In the DTE Hydrology project AI/ML techniques have not been considered mainly due to time constraints and to the team expertise. It is expected that AI/ML techniques can be used to improve the outcomes of the DTE Hydrology project, and it will be tested in future developments.

Future developments exploiting AI/ML techniques will be developed in future projects, in section 5 some preliminary suggestions for exploiting these approaches in the DTE Hydrology framework have been listed.

3.5. Technology aspects

In the last years the operationally available EO data streams increased significantly. The European Copernicus programme has launched a wide range of Earth Observation (EO) satellites, named Sentinels. The ever-increasing amount of acquired data makes Copernicus the largest EO data provider and the third biggest data provider in the world. Currently the daily generated data volume is more than 10 TB per day and the satellite data achieved by the Sentinels from their start in 2015 already exceeds several 10ths of PB. Therefore, large IT infrastructures are required to store and process these data volumes. An example of this kind of IT infrastructure is developed by EODC that has set up a dedicated EO focused IT infrastructure to tackle the problem. Next to large scale processing with a High Performance Computing (HPC) System, i.e. the Vienna Scientific Cluster (https://vsc.ac.at/), it includes a cloud computing environment as well as a dedicated processing cluster for near-real time data analysis. Furthermore, high performance internet connectivity is essential. Therefore, the EODC IT infrastructure is embedded in the European GÉANT network via the Austrian ACOnet access provider.

In the long-term, we believe that the Open DTE Hydrology Platform is best built on a **federated infrastructure** (**Figure 3**) that functionally connects a number of powerful data centres that each have a clearly identified expertise and focus. This focus could be on specific modelling capabilities or expertise with specific satellite data processing lines. As each data centre should be capable of serving users with matching interests (via the Open Platform in an agnostic way or for power-users via user-tailored accounts), selected higher-level data sets should be shared among several or all participating data centres so that data download does not become a bottleneck in the analysis of the data. Data exchange should go via a standard suitable for working with satellite and climate data cubes, as e.g. implemented via the **openEO API** (Schramm et al. 2021). The federation should be built hand in hand with the role out of the European Open Science Cloud, with protocols and tools developed by supranational organisations such as EGI (https://www.egi.eu/). One practical example where this concept is realised is the ESA openEO Platform activity (see https://openeo.cloud/).

The core of the DTE Hydrology infrastructure would be a data centre capable of running a global high-resolution hydrological land surface model, assimilating various data sets coming from the other federated centres. **ECMWF** would be well versed to host this system component, but in principle, it could be another data centre given that - technically - the atmosphere and the land surface will be run independently, as e.g. already done by ECMWF in the case of ERA5 and ERA5-Land (Muñoz-Sabater et al., 2021). This DTE Hydrology core facility should be connected to a number of expert data centres that contribute relevant data to the system. Amongst others this could be EUMETSAT, EODC, the facility planned for replacing the four ESA DIASes, and various national centres such as SURFsara.

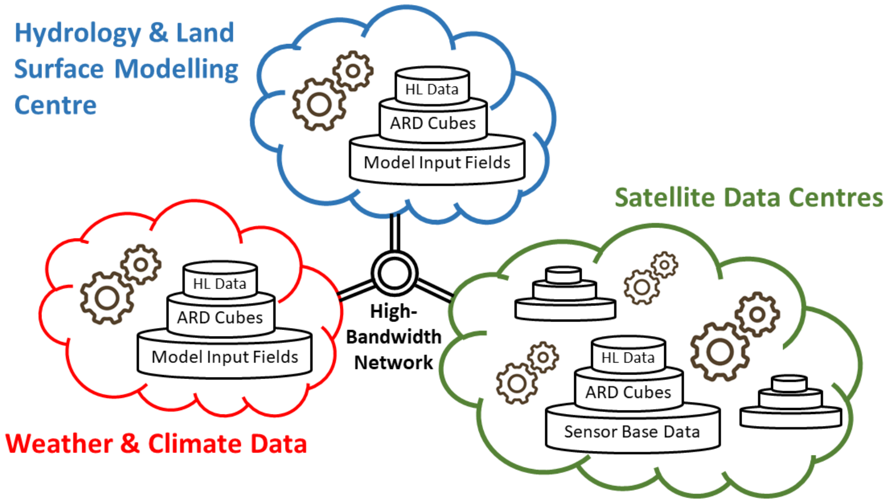

Figure 3: Building the DTE Hydrology Open Platform on a federated infrastructure.

From the **satellite side**, the goal should be to develop a network of functionally connected expert data centres with a focus on specific satellites, sensor lines and applications. This is to be seen in contrast to the vision of creating one big EO data centre serving all European satellites systems. The fact is that not even the Google Earth Engine (Gorelick et al., 2017) should be regarded as such a one-can-do-it-all platform but rather as a thematic platform with a focus on the land surface, an extensive data archive built mostly by harvesting existing free and open data sets, and powerful user interfaces.

For the DTE Hydrology infrastructure one of the most important contributing facilities will be **EUMETSAT** that has, amongst other initiatives in this direction, started to open up its data archives and processing capabilities to SAF (Satellite Application Facility) partners via the EUMETSAT Cloud. This has e.g. enabled TU Wien to start processing high-resolution ASCAT Level 1 data directly in Darmstadt, obviating the need for transferring the large-volume Level 1 data to Vienna. A possible scenario therefore is that the EUMETSAT Cloud becomes a key platform where European meteorological satellite data needed for DTE Hydrology are processed from the raw sensor recordings (Level 0) to the sequence of higher-level data sets without ever leaving Darmstadt. Selected meteorological satellite data sets would then be shared with other data centres, with automatic updating and synchronisation, user management etc.

Given that there will be several contributing data centres, the DTE Hydrology infrastructure must in the end be a well-designed federated system with numerous data dependencies. For example, the quality of Sentinel-1 and ASCAT higher-level data sets (soil moisture, water bodies, vegetation, etc.) would benefit significantly from integrating ECMWF forecasts in the processing (e.g. for dynamic masking of snow and frost-affected backscatter measurements). At the same time, ECMWF already assimilates various satellite-based soil moisture data (ASCAT, SMOS, …) and might consider doing the same for high-resolution Sentinel-1 soil moisture retrievals. So, it will be fundamental to have powerful "connections" between ECMWF, EUMETSAT and all of the other contributing facilities. Here, "Connection" not just means the internet cables, but the overall system of IT resources, software and contractual agreements (IPRs, etc.).

3.6. Interface aspects (visualisation and interaction)

The DTE Hydrology online data portal should be interactive, enabling not only data and scenario visualisation, but also the interaction with the data such as the download of data and georeferenced maps for selected regions/time periods. Ideally one should be able to upload ancillary products and dataset to complement or compare the DTE Hydrology output with local information and enhance the system to become an effective decision support tool. A key requirement for a common visualisation platform is a flexible framework, able to read different data formats and display various types of products including gridded and polygon maps, time series, and geo-located information, among others.

Products and services should be built on open geospatial data standards (such as implemented by the OGC) that enable full interoperability. Hazard data is especially useful when combined with local information on vulnerability and exposure. Hazard data platforms that are interoperable and easily combined with local information are much more likely to be used to prevent major impacts (Alfieri et al., 2018). Current hazard-oriented DTE Hydrology implementation should evolve towards metrics that are relevant for the citizens and their activities, such as the number of people potentially affected by a hazard, estimated economic losses, bridges or road sections at risk of closure, hectares of crops or livestock hit by water shortage, etc. Ultimately, the system should be able to assess the additive and often non-linear impacts of multiple interconnected events, e.g., intense low-pressure systems inducing extreme precipitation and flash floods upstream, cascading to riverine floods and compound floods at river estuaries due to storm surge and backwater effects inland, with the possible complication of precipitation-triggered landslides and windstorms. On the other hand, precipitation deficits are often interconnected with streamflow droughts and heat waves, which combined impacts should be assessed jointly, to evaluate more accurately the level of response needed to cope with the emergency and identify worst affected areas and prioritise emergency operations. Catastrophic events in vulnerable societies contribute to triggering conflicts and mass migration, hence the anticipation of such dynamics would be of utmost importance.

4. DTE Demonstration

4.1. DTE Demonstration Exercise Description

DTE Hydrology has developed a prototype of Digital Twin Earth with focus on water cycle and hydrological processes and their impacts (Alfieri et al., 2021). The activity has comprised four sequential steps:

1. building of the 4D DTE Hydrology dataset, a high resolution (1 km, hourly, 2016-2019) EO-based dataset, also integrating in situ observations;
2. developing of a high-resolution modelling system ingesting the 4D DTE Hydrology dataset and able to provide a 4D reconstruction of the water cycle (see **Figure 4**);
3. integration of the modelling system in the cloud-based DTE Hydrology simulation and visualisation tool;
4. exploitation of the DTE Hydrology tool to develop user-oriented case studies focusing on flood and landslide risk, and water resources management (see **Figure 4**).

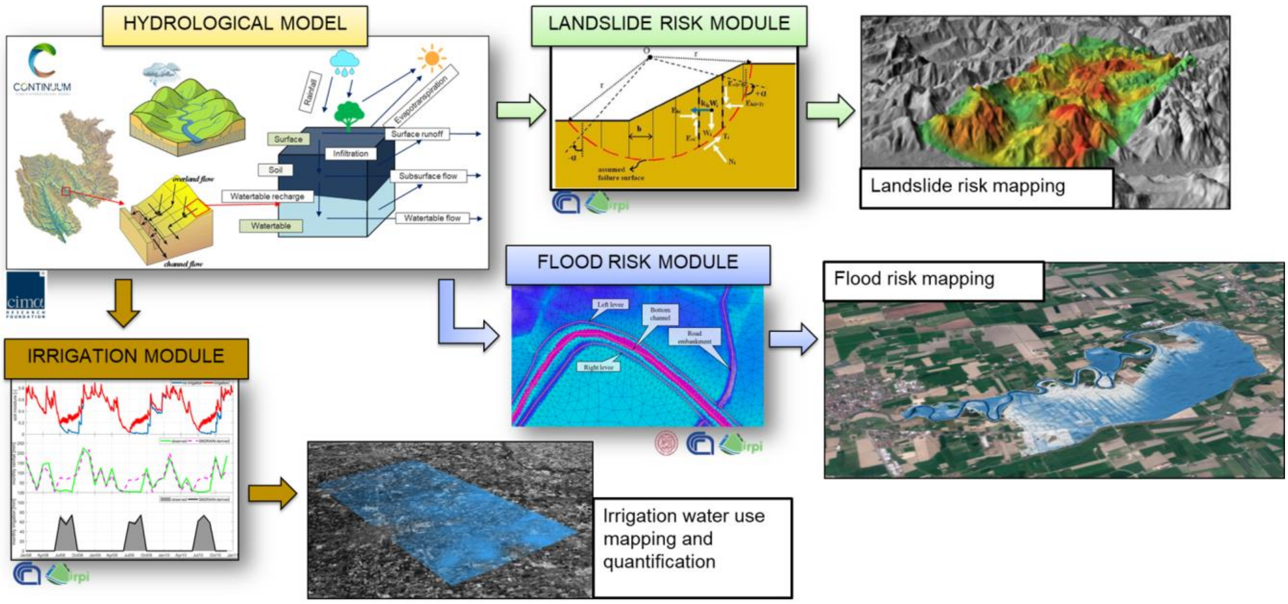

Figure 4: DTE Hydrology Modelling Framework.

The area of focus of DTE Hydrology has been the Po River Basin (northern Italy). In this area high quality ground observations are available, which have been useful to calibrate and test the quality of satellite observations and of the modelling system (Alfieri et al., 2021).

Additional information can be found in the project website at: http://hydrology.irpi.cnr.it/projects/dte-hydrology/

4.2. DTE Demonstration Exercise Output Datasets Description

The first step of the DTE Hydrology project has consisted in the building of the 4D DTE Hydrology dataset (DTE Hydrology Datacube). During the project multiple satellite and in situ products have been tested for the different variables (soil moisture, precipitation and evaporation). Based on the results of the validation and of the modelling simulation, a final version of the Datacube has been selected and it has been available openly to the science community.

The final DTE Hydrology Datacube contains 1km remote sensing and modelled data for the Po River Basin in the period 2016-2019 (see **Table 1** and **Figure 5**):

- the data are structured in NetCDF files longitude x latitude x variable
- the 1km spatial grid is the same for all variables (689 longitude x 309 latitude)
- the temporal grid varies for the different variables (3-day, daily, hourly)

Table 1: DTE Hydrology Datacube.

Variable	Datasource	Temporal coverage	Spatial resolution	Temporal resolution
Soil Moisture	Satellite	2016-2019	1 km	2-4 days
Soil Moisture	Model	2017-2019	1 km	1 hour
Evaporation	Satellite	2019-2019	1 km	1 day
Evaporation	Model	2017-2019	1 km	1 hour
Precipitation	Satellite	2016-2019	1 km	1 hour
River Discharge	Model	2017-2019	1 km	1 hour
Snow depth	Satellite	2016-2019	1 km	2-4 days

In addition to the DTE Hydrology Datacube, the project has also developed experimental datasets for landslide risk assessment over the Oltrepo area, for flooding during the levee break of the Enza River, and for irrigation water assessment in the agricultural area surrounding Modena city. These experimental datasets have been made available for developing the DTE Hydrology Video: https://www.esa.int/ESA_Multimedia/Videos/2021/10/Digital_Twin_Hydrology

Additional details on the ESA Phi-Week presentation can be found here: https://www.esa.int/Applications/Observing_the_Earth/Working_towards_a_Digital_Twin_of_Earth

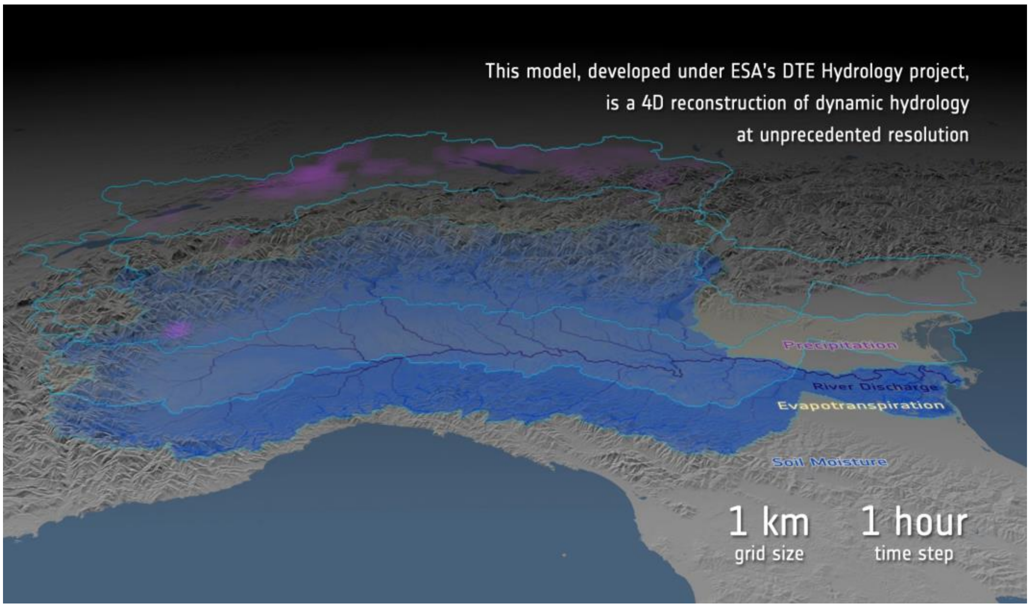

Figure 5: Visualisation of the DTE Hydrology Datacube.

4.3. DTE Prototype Performance and Validation Report

The validation of satellite data products against in situ observations are fully described in [D2.1], modelling results and their performance are reported in [D4.1]. Here a short summary of the results is given.

The **satellite soil moisture** product obtained from the application of RT1 algorithm to Sentinel-1 observations is found to outperform previous products over the Po River basin if compared with in situ observations (1 station) and modelled data (ERA5 Land). However, a more comprehensive test and validation of the product is ongoing and will be explored under the future 4DMed-Hydrology ESA project starting in November 2021.

The **satellite evaporation** product has been compared with a few stations in Europe showing similar performance than the well-established GLEAM product at 25km resolution. However, performances are evaluated only over time and a spatial assessment of the product is still missing. The same applies to satellite soil moisture data, for both products a spatial assessment is mandatory for future activities (to be performed under the future 4DMed-Hydrology ESA project).

The DTE Hydrology **satellite precipitation product** has been tested for the first time in the project both as compared with ground data (rain gauges and meteorological radar) and for hydrological simulation (MISDc and Continuum). The product is found reliable in reproducing spatial-temporal precipitation at high resolution, particularly at daily time scale. The more important results are obtained in the hydrological validation of the DTE Hydrology satellite precipitation product. Indeed, the performances are slightly better than those obtained with ground station data using MISDc and they are good also by using the Continuum model even if slightly lower than the performances of the run with ground data. By considering the high density of stations in the Po River Basin (640 stations), these results are very promising for obtaining a satellite-based high resolution (1km, 1 hour) precipitation product in Europe (also this activity will be explored under the future 4DMed-Hydrology ESA project).

The **satellite snow depth** product developed by Lievens et al. (2019) is compared with 172 ground stations throughout the Alps with good performances both in terms of bias and of temporal variability. Further testing of the product is clearly needed but the promising results open new possibilities for improving snow assessment and modelling at high resolution as needed over the Alps.

The **satellite river discharge product** is compared with several stations along the main Po River highlighting its capability to reproduce daily variations in river discharge with good accuracy.

Satellite products are integrated into the **S3M snow model** and into **Continuum hydrological model** to reproduce snow water equivalent, snow water content, soil moisture, actual evaporation, runoff and river discharge at high spatial (1km) and temporal (1hour) resolution continuously in time and space. The model simulations are compared with river discharge observations at 27 stations in different configurations. Indeed, model simulations have been carried out by using as input: (1) only ground observations, (2) only satellite precipitation data, (3) only satellite evaporation data, (4) assimilation of snow depth, (5) assimilation of soil moisture, (6) all satellite observations. The results of the different configurations are analysed and compared with important insights on the quality of satellite products, on the possibility to integrate such high-resolution observations into hydrological modelling, and on the limitations to be filled to optimally integrate model and satellite products in a data assimilation framework.

4.4. DTE Prototype Impact and Benefit Assessment

Increasing accessibility to the results of the hydrological modelling for water resource management, flood risk, landslide risk, and drought risk is achievable via an interactive visualisation tool. In the project we have developed the DTE Hydrology dashboard to increase the ability for non-scientific decision makers to familiarise themselves directly with the results of the hydrological modelling, and the visualisation/exploration of satellite observations.

The current functional capabilities of the DTE Hydrology dashboard are:

- let the user browse the variable of discharge, soil moisture, precipitation, and evaporation;
- allow the user to define temporal extents within the dashboard;
- allow the user to generate various graphs for their chosen variable;
- allow the user to specify custom spatial extents for graph generation.

These capabilities are all met by a micro-service solution, utilising open-data cube and DASK.

In the DTE Hydrology dashboard it's possible to explore and visualise also the results of the case studies investigating the impact assessment of irrigation water estimation, landslide risk, and flood risk assessment [D4.1]. For specific events occurred in the study period, the dashboard allows the user to visualise in space and time the project results and specifically:

- **Irrigation water estimation**: the case study shows the irrigation water use for an area 30x50 km centred on Modena city in the Po Plain. Monthly values of irrigation for the year 2018 can be visualised, at a spatial resolution of 1km. Thus, the differences in the irrigation water use for different fields can be explored and the understanding of irrigation water use variability can be investigated (see **Figure 6**).

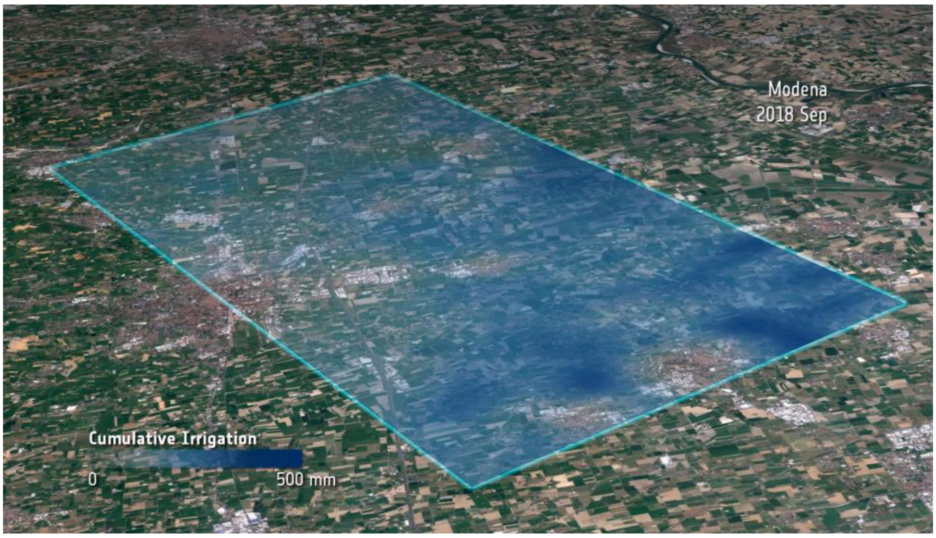

Figure 6: Cumulative irrigation for the year 2018 as estimated from remote sensing observations in the DTE Hydrology project.

- **Landslide risk analysis**: the case study shows the landslide risk for an area 10x20 km in the Oltrepò Pavese during November 2019, a period in which several landslide events occurred as testified by ground surveys post event. The user can interact with the landslide risk map for understanding how the landslide risk varies in time and space (see **Figure 7**).

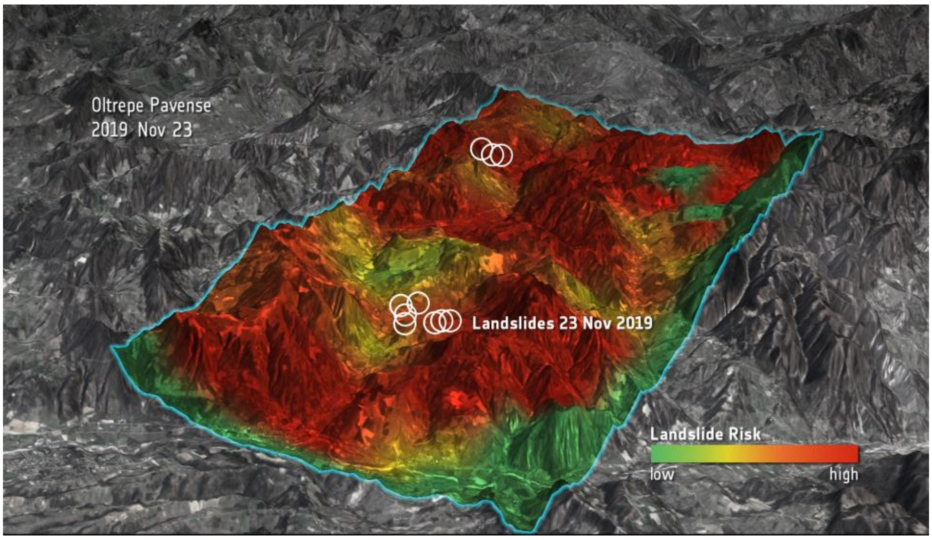

Figure 7: Landslide risk map as obtained from modelled and satellite soil moisture observations in the DTE Hydrology project.

- **Flood risk analysis**: the case study visualises the flooding of Enza river during the event occurred in

December 2017 for which the break of the levee happened. The flood depth map is obtained through the integration of the hydrological modelling system with a very high resolution (5m) digital elevation model and 2D hydraulic modelling. Results are available at a 15 min time scale and can be explored to see the variability in water depth over time and space and hence to identify, for instance, the areas most affected by the flood event (see **Figure 8**).

Figure 8: Map of flooded areas during the event in December 2019 for the Enza river. The flooded area map is obtained through the integration of hydrological and hydraulic modelling at high resolution in the DTE Hydrology project.

5. DTE scientific and technological opportunities, current gaps/limitations and roadmap

5.1. User needs

At the Stakeholder meeting the overall DTE Hydrology project was presented and the expected results were shown. All stakeholders actively participated to the discussion and the following main suggestions were drawn:

- The high spatial and temporal resolution of the developed datasets and simulations (1km, 1hour) is the resolution needed for performing decision making, there's high expectations on exploring and assessing project's results.
- The Po River Basin is a highly complex system and multiple case studies (if feasible) should be considered to assess the project impact on different sectors (floods, landslides, agriculture, water management).
- The system should be targeted to different users and applications. It is not possible to develop a system satisfying the needs of all users. A targeted approach should be developed.
- The assessment of the different water storages (soil moisture, groundwater, snow) in the Po River Basin is needed for water resources management, particularly for monitoring resources under water scarcity. The system can be used to perform different what-if scenarios and thus provide detailed information for planning.
- The system can be used for policy applications and as an insurance tool. Thus, the system can have a significant impact both in the public and in the private sector.

5.2. Overall community high level roadmap and timeline

The DTE Hydrology project has successfully tested and implemented the integration of Earth Observation, advanced hydrological, hydraulic and geo-hydrological modelling, for the 4D reconstruction of the water cycle over the Po River Basin, and for assessing its potential in operational applications such as flood and landslide risk assessment and water resources management. For the continuation of DTE Hydrology, the following steps are foreseen:

- Extension of the experiments at regional and continental scale. Specifically, both the EO-based products and the modelling simulations should be assessed on a larger scale, and on different climatic, morphological, land use/ land cover, and soil type conditions. Moreover, the system testing over data scarce regions needs to be implemented.
- Development of an Open Science Platform in which the DTE Hydrology results, i.e., EO and modelled datasets, are stored. The Open Platform should allow full access to data and modelling simulations to the users, and also the capabilities to implement modelling and algorithms within the platform thus providing the direct access to the data in a cloud system working seamlessly as a web service.
- Continuous and full involvement of stakeholders and end users for better framing the system's objectives and for developing an architecture that will maximise the usability from non-experts.
- Development of interfaces for the integration with other Digital Twins (Ocean, Atmosphere, Antarctica, …) and thus for building the constituent blocks of the Digital Twin of the Earth.

Figure 9 shows the high-level description of the potential extension of the DTE Hydrology project. Specifically, there's the need to fully exploit the potential of AI and ML techniques (see section 5.5). Moreover, the development of an open science platform will allow multiple users (scientists, stakeholders) to work on the data and on the modelling results thus potentially to steadily improve the platform capabilities and advances. The high-level technical requirements for the extension of the project at Italian, European and Global scale is also reported, in terms of data storage and number of GPU.

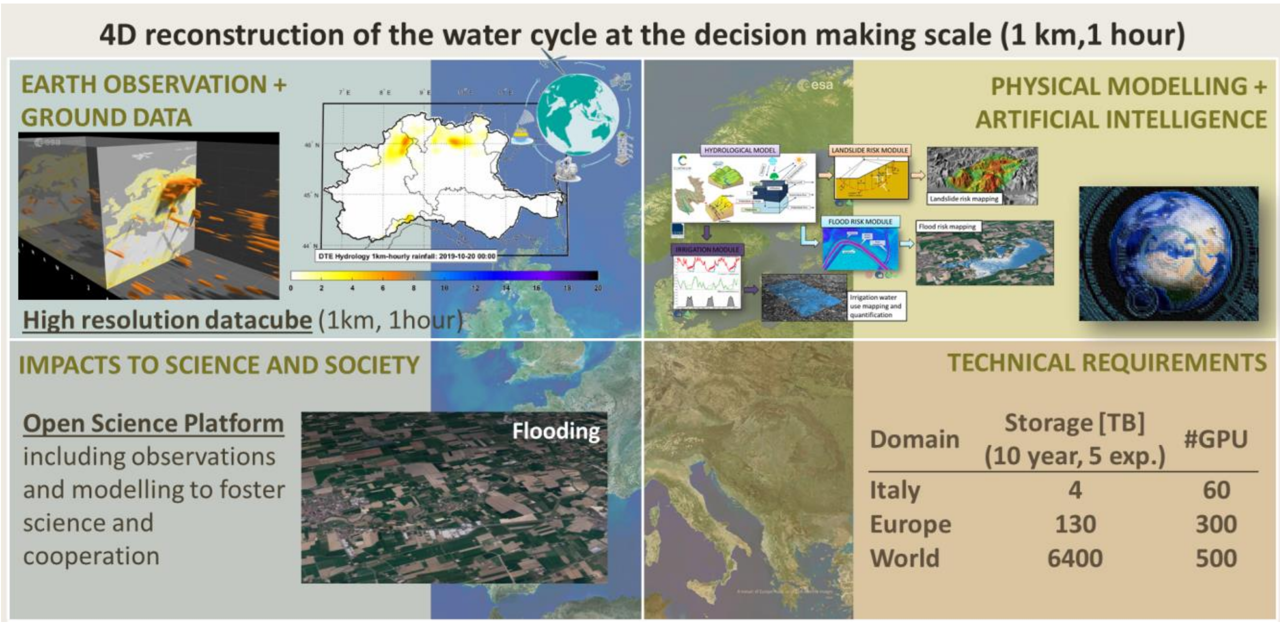

Figure 9: High level description of potential future extension of DTE Hydrology project at the European scale including technical requirements and the exploitation of artificial intelligence.

5.3. Science needs and required developments

In our opinion, **hydrological science lags behind technological advances**. Today it is technically and computationally feasible to perform hydrological simulations at continental and global scales at high resolution of 1km (or finer), and we can also ingest high resolution observations from remote sensing, ground data and other sources (e.g., citizen science). However, moving at such resolutions, the quality and reliability of modelling systems and observations (both in situ and remote sensing) is not known, and we are also not aware if we are describing the physical processes correctly. Last but not least, the human intervention on the water cycle (irrigation, reservoirs management, groundwater management, …) is mostly unknown as not observed.

Therefore, the development of DTE Hydrology on a global scale needs a **strong involvement of the science community** working together to solve the science challenges ahead (see below for more details). This involvement should consider not only hydrologists, but their close collaboration with remote sensing specialists, meteorologists, and likely also sociologists to incorporate the human "component" in the system.

5.4. Data needs and required developments

The most important variables needed for performing hydrological simulations are: precipitation (including rainfall and snowfall), evaporation, soil moisture, snow, groundwater storage and river discharge. It is evident that the quality and usability of satellite-based hydrological products is growing in the very recent period, also thanks to the Sentinel constellation providing a wealth of new data sources. Indeed, beside the products used in the DTE Hydrology project, we want to underline that alternative products for soil moisture (e.g., THEIA, VANDERSAT) and evaporation (e.g., Sen-ET) at high resolution are available and a large-scale and comprehensive comparison of their characteristics and accuracy is surely needed (part of this activity is foreseen in the future 4DMed-Hydrology ESA project).

It should be clearly underlined that the **high-resolution products** developed under the DTE Hydrology project are among the **most advanced satellite-based hydrological products currently available** and have been **developed very recently** (in the past couple of years). Some of the products have been validated during the DTE Hydrology project, but, due to time constraints, over a limited region and temporal period (4-year). Therefore, all products need to be further tested in different regions and climates to assess comprehensively their quality, reliability and usability for high resolution hydrological applications. The most stringent test of the developed EO-based products should be carried out for assessing their performance at high spatial and temporal resolutions. For instance, it needs to be assessed if a 1km soil moisture or evaporation product is able to distinguish water variability among neighbouring agricultural fields that can reflect irrigation practices. It is highly challenging to test the capability of the products to reproduce spatial patterns at high resolution due to the unavailability of ground observations at such spatial scales within the study region and period.

An important issue for all **high-resolution satellite data products** is the fact that it is not enough to just scale up computer power and apply algorithms developed at coarse spatial scales to the new satellite generation. Instead, one needs to advance the algorithms to make them fit to deal with the **increased physical complexity** at the finer scales. This in turn implies that the algorithms become even more data hungry. Therefore, there is a strong need to work towards the integration of satellite data streams, combining data from different spectral bands, measurement techniques and different processing levels. To facilitate working with the data it is important to create multi-dimensional datacube systems that allow to develop advanced satellite data retrieval algorithms and connect the different data streams with the models. To move towards global applications of high-resolution Copernicus data, an obvious need would be to build systems connecting existing analysis-ready datacubes for Sentinel-1 (Wagner et al. 2021) and Sentinel-2 (Frantz 2019).

5.5. Models and data assimilation needs and required developments

In the DTE Hydrology project, the CIMA's hydrological model (Continuum), has successfully shown applications of assimilating a range of satellite products, including river discharges, snow depth and soil moisture. Specifically, we have shown applications of Continuum with data assimilation of high-resolution soil moisture from RT1 and snow water equivalent from C-SNOW (see Deliverable 3.1), showing several cases of improvement over a baseline run driven by conventional ground-based observations. The data assimilation scheme used is based on nudging techniques which, despite being a relatively simple approach, yields skilful results at very moderate computational expenses, hence suitable for operational applications. On the other hand, the testing of multiple ground-based and satellite-based precipitation dataset into the CNR-IRPI's hydrological model has demonstrated the potential of these products to obtain highly accurate predictions of river discharge. The use of two different hydrological models has also demonstrated that the integration of EO-based products and hydrological models is dependent on the modelling structure, and more research on this aspect is needed.

As also described in section 3.3, several challenges need to be addressed for global-scale application of hydrological modelling at high resolution. The main limitations can be summarised in:

- **Lack of static and time-variant data\observations at high resolution**, needed for characterising the land surface and sub-surface (static data), and as input forcing of the modelling system (time variant observations).
- **Lack of understanding of physical processes at high resolution**, particularly for large scale (continental, global) modelling systems.
- **Lack of observations of the human impact** on the water cycle.

On this basis, we have foreseen a number of steps to be carried for improving modelling simulations:

- Development of **flexible and dynamic modelling systems** able to adapt and to integrate in an optimal framework the newly developed high-resolution observations obtained from remote sensing, newly ground sensors (e.g., drones) and citizen science. Some modelling systems have carried out the first steps for such an integration, but we are far from the target. For instance, in the DTE Hydrology project we have found that a simpler model is more suitable to integrate satellite precipitation data with respect to a more complex and distributed modelling system. On the other hand, the distributed model is found more ready to ingest distributed soil moisture and snow depth observations, and to provide a more consistent spatial pattern of the variables of interest. Therefore, in relation to the scale/resolution of application, as well as of users' interests (depending on the application/user, some hydrological processes can be omitted or considered in a simpler way; or neglected in given regions due to their characteristics) there's the need to evaluate and test different modelling schemes and frameworks.
- A fundamental issue in hydrological and land surface modelling is related to their **capability to reproduce the spatial variability of physical variables**, such as soil moisture, evaporation and runoff. Typically, the modelled spatial variability is significantly lower than ground-based and in situ observations and the actual reproduction of spatial patterns is rarely obtained (Brocca et al., 2017). The lack of spatial data used for modelling assessment is one of the issues to be addressed, but also improvements in modelling parameterization and physical processes description should be carried out.

5.6. AI needs and required developments

Artificial Intelligence (AI) and Machine Learning (ML) techniques can be used to improve the outcomes of the DTE Hydrology project through a number of approaches. Specifically, the following implementation of AI/ML techniques is foreseen:

- Improve parameterization of satellite retrieval algorithms and modelling, including bridging the gap between modelled variables and satellite measurements, e.g. backscatter, for data assimilation applications. In the case of snow, for example, AI is currently being tested as a way to improve Snow Water Equivalent (SWE) estimates across the landscape, and so come up with improved data-driven products that could then be assimilated in models.

- Replace modelling components for which we have lack of understanding, i.e., through the development of surrogate or hybrid modelling in which physically-based and AI/ML techniques are optimally integrated.
- Improve the parameterization of the hydrological and hydraulic modelling systems, particularly for the areas in which uncertainties are larger (e.g., soil hydraulic and groundwater dynamic parameterization).
- Emulate complex modelling components to decrease the simulation time and the computational costs.
- Perform uncertainty analysis, i.e., characterization of the error in satellite products and modelling outputs.
- Develop diagnostic tools through AI/ML techniques for assessing the performance of the modelling systems.
- Using AI/ML in assimilation, both as an alternative assimilation technique to nudging or particle/Kalman filter and to improve assimilation sources.

5.7. System integration, ICT and HPC needs

In the DTE Hydrology project, different data sources have been integrated and processed based on different requirements. Therefore, next to a proper data management plan, a detailed planning of the processing requirements has been essential. Moreover, next to the processing of data, IT requirements and adequate software layers have been required to allow interactive visualisation of the project results. Therefore, the ICT requirements for developing a continental\global scale DTE Hydrology system need to be properly designed. For the current activity performed in the DTE Hydrology project, limited process resources have been used. To scale up the service offering towards a continental or even global scale, additional studies for runtime estimation and possible optimisation options are required.

In the following, the benefits that could be gained by using High Performance Computing (HPC) in the DTE Hydrology implementation on continental/global scale are illustrated, subdivided by sectors: (1) modelling, (2) EO-based products, and (3) ICT infrastructure.

For modelling, HPC is crucial for scaling applications to larger domains and increased resolutions. The existing DTE Hydrology setup in the Po River Basin could be extended to near-real time pan-European simulations if HPC resources were made available with suitable storage space for archiving the results. The lateral exchanges of energy and mass within each cell of a river basin force us to have a computation running on the same platform rather than in isolation via several parallel jobs (as in land surface schemes). Ideally the hydrology and hydraulics should be connected, and inundated areas outside river beds should modify the soil moisture profiles as well as the evaporation fluxes, in turn feeding back to the atmosphere. All this strongly supports the development of a fully integrated digital twin of the Earth system, yet at the expense of increased computing requirements.

For EO-based products, the vision for a Digital Twin Earth must include provisions for a regular re-analysis of all involved data sets and models to keep data quality up to date with the state of the art. This can only be done with HPC systems capable of reprocessing Petabyte of data, such as e.g. be demonstrated by Wagner et al. (2021) when creating a worldwide 20 m Sentinel-1 backscatter data cube.

The ICT infrastructure where modelling and observations will be integrated should be properly designed. The users (scientists, stakeholders, citizens) should be able to easily interact with data and models, also in an operational (automatic) context. A “top-down” approach in which a large institution develops a “community” model might be not affordable and will have the effect of losing all the expertise and knowledge gained in the science community (hydrologists, EO experts, meteorologists, soil scientists, socio-hydrologists). A “bottom-up” approach is preferable and should be pursued to build a flexible, interoperable, cloud-based ICT infrastructure addressing the needs of the society as a whole (scientists, stakeholders, citizens). FAIR principles should be understood and implemented.

HPC resources are an important computing environment for non-time critical data processing use cases. Resources on HPC systems are orchestrated by a resource scheduler (e.g., SLURM), providing compute resources on demand via a sophisticated queuing system. In order to run real-time processing of high-resolution products on continental or global scale a dedicated compute infrastructure is needed. Short latency of such products can only be achieved considering stream processing concepts which are contradicting the batch processing concept utilised on HPC systems. The continuous stream of high-resolution EO based hydrological data products is the baseline for further analysis to extract needed information. Furthermore, real-time interactive analysis of such data products requires dedicated infrastructure such as provided by cloud computing services. Those services offer the possibility to instantly scale in real-time depending on the load the system has to deal with.

The openEO Platform, https://openeo.cloud/, offers such a service to users following the cloud computing model “Function as a Service”. Interactive analysis of data is given via a RESTful API, openEO API, utilised by a number of client libraries written in Python, R or JavaScript. Data can be analysed through the REST API remotely following the idea of data cubes allowing for analysis on a per pixel level. This offers the opportunity to compute data when needed only, aiming for reducing any related compute costs. In addition, the openEO API enables decision makers to merge data from various sources (data cubes) supporting their decision making process. On the fly data extraction is supported by providing functionalities to export any requested analysis result to commonly used data formats, supplemented by making those available via dedicated secondary services such as WMS-T, WMTS or xyz.

6. References

Alfieri, L., Avanzi, F., Delogu, F., Gabellani, S., Bruno, G., Campo, L., Libertino, A., Massari, C., Tarpanelli, A., Rains, D., Miralles, D. G., Quast, R., Vreugdenhil, M., Wu, H., and Brocca, L.: High resolution satellite products improve hydrological modeling in northern Italy, Hydrol. Earth Syst. Sci. Discuss. [preprint], https://doi.org/10.5194/hess-2021-632, in review, 2021.

Alfieri, L., Cohen, S., Galantowicz, J., Schumann, G. J.-P., Trigg, M. A., Zsoter, E., Prudhomme, C., Kruczkiewicz, A., Coughlan de Perez, E., Flamig, Z., Rudari, R., Wu, H., Adler, R. F., Brakenridge, R. G., Kettner, A., Weerts, A., Matgen, P., Islam, S. A. K. M., de Groeve, T., and Salamon, P.: A global network for operational flood risk reduction, Environmental Science & Policy, 84, 149–158, https://doi.org/10.1016/j.envsci.2018.03.014, 2018.

Aragon, B., Ziliani, M. G., Houborg, R., Franz, T. E. & McCabe, M. F. CubeSats deliver new insights into agricultural water use at daily and 3 m resolutions. Sci Rep-uk 11, 12131 (2021).

Beven KJ, Cloke HL. (2012). Comment on “Hyperresolution global land surface modeling: Meeting a grand challenge for monitoring Earth's terrestrial water” by Eric F. Wood et al. Water Resources Research 48: W01801.

Bierkens, M. F., Bell, V. A., Burek, P., Chaney, N., Condon, L. E., David, C. H., …, Wood, E. F. (2015). Hyper-resolution global hydrological modelling: what is next? “Everywhere and locally relevant”. Hydrological processes, 29(2), 310-320.

Brocca, L., Ciabatta, L., Massari, C., Camici, S., Tarpanelli, A. (2017). Soil moisture for hydrological applications: open questions and new opportunities. Water, 9(2), 140, doi:10.3390/w9020140.

Brocca, L., Filippucci, P., Hahn, S., Ciabatta, L., Massari, C., Camici, S., Schüller, L., Bojkov, B., Wagner, W. (2019). SM2RAIN-ASCAT (2007-2018): global daily satellite rainfall from ASCAT soil moisture. Earth System Science Data, 11, 1583–1601, doi:10.5194/essd-11-1583-2019.

DiMiceli, C., M. Carroll, R. Sohlberg, D. Kim, M. Kelly, J. Townshend. *MOD44B MODIS/Terra Vegetation Continuous Fields Yearly L3 Global 250m SIN Grid V006*. 2015, distributed by NASA EOSDIS Land Processes DAAC, https://doi.org/10.5067/MODIS/MOD44B.006.

Fisher, J. B., and Coauthors, 2020: ECOSTRESS: NASA’s Next Generation Mission to Measure Evapotranspiration From the International Space Station. Water Resour. Res. 56, doi:10.1029/2019WR026058.

Frantz, D. (2019). FORCE—Landsat+ Sentinel-2 analysis ready data and beyond. Remote Sensing, 11(9), 1124.

Gorelick, N., Hancher, M., Dixon, M., Ilyushchenko, S., Thau, D., & Moore, R. (2017). Google Earth Engine: Planetary-scale geospatial analysis for everyone. Remote sensing of Environment, 202, 18-27.

Lievens, H., Demuzere, M., Marshall, HP. et al. (2019). Snow depth variability in the Northern Hemisphere mountains observed from space. Nat Commun 10, 4629, https://doi.org/10.1038/s41467-019-12566-y.

Lagouarde, J.-P., 2018: The Indian-French Trishna Mission: Earth Observation in the Thermal Infrared with High Spatio-Temporal Resolution. In Proceedings of the IGARSS 2018—2018 IEEE International Geoscience and Remote Sensing Symposium, Valencia, Spain, 22–27 July 2018; pp. 4078–408.

McCabe, M. F. and Coauthors, 2017a: The Future of Earth Observation in Hydrology. Hydrol. Earth Syst. Sci., 21, 3879–3914, doi:10.5194/hess-21-3879-2017.

Muñoz-Sabater, J., Dutra, E., Agustí-Panareda, A., Albergel, C., Arduini, G., Balsamo, G., ... & Thépaut, J. N. (2021). ERA5-Land: A state-of-the-art global reanalysis dataset for land applications. Earth System Science Data, 13(9), 4349-4383.

Quast, R., Albergel, C., Calvet, J. C., and Wagner, W. (2019). A Generic First-Order Radiative Transfer Modelling Approach for the Inversion of Soil and Vegetation Parameters from Scatterometer Observations, Remote Sensing, 11(3), 285, doi:10.3390/rs11030285.

Rains, D., H. Lievens, G. J. M. De Lannoy, M. F. McCabe, R. A. M. de Jeu and D. G. Miralles (2021). Sentinel-1 Backscatter Assimilation Using Support Vector Regression or the Water Cloud Model at European Soil Moisture Sites, *IEEE Geoscience and Remote Sensing Letters*, doi: 10.1109/LGRS.2021.3073484.

Schramm, M., Pebesma, E., Milenković, M., Foresta, L., Dries, J., Jacob, A., ... & Reiche, J. (2021). The openeo api–harmonising the use of earth observation cloud services using virtual data cube functionalities. Remote Sensing, 13(6), 1125.

Tóth, B, Weynants, M, Pásztor, L, Hengl, T. 3D soil hydraulic database of Europe at 250 m resolution. *Hydrological Processes*. 2017; 31: 2662– 2666. https://doi.org/10.1002/hyp.11203.

Wagner, W., B. Bauer-Marschallinger, C. Navacchi, F. Reuß, S. Cao, C. Reimer, M. Schramm, C. Briese (2021) A Sentinel-1 backscatter datacube for global land monitoring applications, Remote Sensing, 13, 4622, 18p.